INVESTIGATIONS OF SPECTRAL LINES FROM HIGH TEMPERATURE PLASMAS USING FABRY-PÉROT INTERFEROMETRY

by

DAVID EDWARD ROBERTS

A Thesis submitted for the Degree of
Doctor of Philosophy of the
University of London

February 1967

Physics Department
Imperial College of Science and Technology

CONTENTS

		page
Abstract		7.
Notation		8.
Chapter 1 : Introduction		
1.1	Content of thesis	9.
1.2	Presentation of material	10.
1.3	Mechanisms which case line broadening and shift	12.
1.4	Convolution of broadening mechanisms	18.
1.5	Previous work on Stark broadening	19.
1.6	Reasons for studying AII	21.
Chapter 2 :	Use of the scanning Fabry-Férot interferometer for recording line profiles.	
2.1	Introduction	23.
2.2	Instrument function of the scanning Fabry-Pérot	23.
2.3	Experimental treatment of finesse	25.
2.4	Effective finesse : Variation with wavelength	31.
2.5	Light gathering power	35.
2.6	Continuous scanning of line profiles	36.
2.7	Single shot scanning of line profiles	38.
2.8	Measurement of line shifts	41.

Chapter 3 : Measurement of Impact broadened widths of AII lines emitted by a linear pinch

3.1	Introduction	43.
3.2	Source used and previous work	43.
3.3	Limits on the required line width	45.
3.4	Choice of working conditions	48.
3.5	Check of optical thinness of plasma	53.
3.6	Measurement of other AII line widths	56.
3.7	Discussion of results	56.

Chapter 4 : Study of AII line broadening using a B_z stabilised, pinched plasma

4.1	Introduction	63.
4.2	Source used	63.
4.3	Initial diagnostics of the B_z pinch	64.
4.4	Optically thin line widths	72.
4.5	Measurement of plasma diameter	75.
4.6	Correction for optical depth	79.
4.7	Estimation of T_e from AII line widths	81.
4.8	AIII line widths	82.
4.9	Measurement of AIII line widths	84.
4.10	Estimation of T_e from AIII line widths	86.
4.11	Discussion of results	89.

Chapter 5 : Calculations on Stark broadening for isolated spectral lines

5.1	Introduction	94.
5.2	Reasons for calculations	94.
5.3	Electron impact broadening of isolated lines	96.

5.4	Calculations on the Stark broadening of AII $\lambda 4806\text{Å}$ and $\lambda 4880\text{Å}$	105.
(i)	General results	105.
(ii)	Treatment of the relevant matrix elements	111.
(iii)	Convergence of the width and shift	114.
(iv)	Strong collision contribution to width	123.
(v)	Validity of straight line classical path approximations	126.
(vi)	Lower level broadening	128.
(vii)	Ion broadening	129.
5.5	L-S coupling approximation	130.
5.6	Line widths within a multiplet	132.
5.7	Summary of results	133.

Chapter 6 : Interferometric measurements of N_e on an unstabilised Z-pinch discharge

6.1	Introduction	135.
6.2	Comparison of luminosities of interferometer systems	136.
6.3	Initial measurements of N_e	138.
6.4	Abel inversion of laser measurements	141.
6.5	Contributions to plasma refractive index	146.
6.6	Experimental investigation of free electron contribution to plasma refractive index	151.
6.7	Discussion	152.

Chapter 7 : Electron temperature measurements

7.1	Choice of diagnostic	155.
7.2	Preliminary measurements of line width and shift	156.
7.3	Intensity ratio measurements	159.
7.4	Validity of L.T.E.	161.
7.5	Estimate of T_e for plasmas not in L.T.E.	168.
7.6	Plasma polarisation shift	172.

Chapter 8 : Further measurements of AII line broadening parameters

8.1	Width measurements	174.
8.2	Distortion of profile due to plasma inhomogeneity	175.
8.3	Measured values of $\Omega(T_e)$	178.

Chapter 9 : Discussion of work on impact broadening

9.1	Discussion of AII results	180.
9.2	Other singly ionised emitters	183.
9.3	General applicability of Stark broadening theory	185.
9.4	Further theoretical work	187.
9.5	Further experimental work	199.

Chapter 10 : Measurement of N_e and T_e in an R-F Induced plasma

10.1	Introduction	201.
10.2	Measurement of T_e	201.
10.3	Measurement of N_e	207.
10.4	Validity of L.T.E.	215.
10.5	Discussion	216.
10.6	Check of $\Omega(T_e)$ for $\lambda 4159\text{Å}$, AI	218.

Chapter 11 : Doppler shift measurements of theta pinch rotation

11.1 Introduction 223.

11.2 Doppler shift measurement of rotation 224.

11.3 Measurement of line shifts using a Fabry-Pérot etalon 225.

11.4 Experimental measurements 229.

11.5 Discussion 244.

Acknowledgements 254.

Appendix I : Description of computor programme for the calculation of electron impact broadened widths, shifts and ion broadening parameters of isolated spectral lines. 255.

Appendix II : Computor programme for calculating the Stark profile emitted by an optically thin, inhomogeneous but cylindrically symmetric plasma. 262.

Appendix III : Further laser measurements on an unstabilised Z-pinch. 264.

References 280.

Publications 286.

ABSTRACT

In this thesis an experimental and analytical investigation of the Stark broadening of spectral lines emitted by singly ionised argon is described.

These lines were broadened by the high electron density produced in transient unstabilised and B_Z stabilised Z-pinch discharges.

The line profiles were recorded using a piezoelectric driven scanning Fabry-Pérot interferometer. The plasma electron density was measured by Fabry-Pérot interferometry using a laser light source.

At a known electron density AII line widths of more than a factor of two times larger than existing theoretical values were observed.

Calculations showed that these discrepancies arose from breakdown of the validity of several assumptions made in the existing theory of the Stark broadening of isolated lines emitted by heavy ions. An improved quantitative treatment of the existing theory gave better agreement with experiment.

The implications of these results on the Stark broadening of lines emitted by other ionised and neutral species is discussed.

Following this, an account of the measurement of electron density in an R-F induced plasma in argon is given. The density was obtained from the Stark broadening of neutral argon lines. The broadening of one line was checked using a plasma of known electron density generated by a conventional shock tube.

These measurements were done primarily to ascertain the extent to which a model of complete Local Thermodynamic Equilibrium could be applied to the R-F plasma.

Finally, a Doppler shift method of determining mass rotational velocities of a thetatron plasma is described. The shifts were recorded by crossing a Haidinger fringe produced by a tilted Fabry-Pérot etalon with an eight channel fibre bundle array. The measured velocities were shown to correspond to a stable mode of rotation.

NOTATION

The following abbreviations and symbols are used frequently throughout this thesis. Wherever possible this conforms with standard practice.

S.F.P.	Scanning Fabry-Pérot
L.T.E.	Local thermodynamic equilibrium
w	$\frac{1}{2}$ width at $\frac{1}{2}$ peak intensity of a dispersive profile
d	Shift of a dispersive profile
g	$\frac{1}{2}$ width at 1/e peak intensity of a Gaussian profile
Ω	w, at $N_e = 10^{16} cm^{-3}$, for electron impact broadening
$T_e (T_i)$	Electron (Ion) temperature
N_e	Electron number density
N_z	Total density of ions in charge state z
$N(z,p)$	Density of ions of charge z in state p
$W_m (W_n)$	Energy of upper (lower) state of a transition
ΔW_z or (ΔW_{oo})	Depression of ionisation limit of charge state z
A_{mn}	Transition probability ($m \rightarrow n$)
f_{nm}	Absorption oscillator strength
$l_>$	The greater of the two l quantum numbers involved in a transition.
σ	Radial integral expression involved in the calculation of matrix elements
u or α	Refers to the upper state on an impact broadened line.
α'	Refers to the corresponding perturbing states.
L or β and β'	are the corresponding subscripts referring to the lower state.

CHAPTER 1
INTRODUCTION

1.1 Content of Thesis

The material presented in this thesis consists of an account of work performed by the author on the study of line profiles emitted by high temperature plasmas. The main diagnostic technique used through out this work was interferometry using A Fabry-Pérot etalon. However the work described consists of three fairly independent topics:-

Firstly, the main content of this thesis is an account of a study of the Stark broadening of lines emitted by singly charged argon ions in a plasma. The plasmas utilised in this study were produced by linear pinches, both unstabilised and with B_Z stabilisation. For the recording of the profiles of lines emitted by these transient sources a rapid scanning Fabry-Pérot interferometer [Ref.1] was employed. The electron number density in the discharges, the main parameter which characterises the Stark broadening, was measured using Fabry-Pérot interferometry with a laser light source.

The outcome of this work was the measurement of line widths deviating from theoretical predictions by factors greater than two. Further calculations of the widths are described which lead to better agreement with experiment. However, more important, the results of the calculations and measurements show up several limitations in the existing theory of Stark broadening as applied to heavy ion lines.

Applications of the conclusions obtained to other species are discussed and suggestions for further work

are presented.

Secondly, some straight-forward diagnostics performed to ascertain the electron number density in an R-F induced plasma are described. N_e was determined from the broadening of neutral argon lines emitted by this plasma, again studied with the S.F.P. The results obtained were checked by width measurements on a source of known N_e i.e. a conventional shock tube.

Thirdly, investigations of plasma rotation in a theta pinch are described. The basis of this work involved measurements of the Doppler shift of an impurity line. A static Fabry-Pérot etalon was used as a dispersive element and an eight channel fibre optic array gave spectral resolution. Rotational velocities were measured at much earlier times in the discharge history than had previously been measured from high speed photographic techniques. These velocities are shown to correspond to a stable mode of rotation.

1.2 Presentation of Material

The three topics, discussed above, comprise the following chapters:-

Topic (1) : Chapters 2 to 9

Topic (2) : Chapter 10

Topic (3) : Chapter 11

The material presented in each chapter can be summerised as follows:-

Chapter 2 : A brief, experimentally biassed, description of the rapid scanning Fabry-Pérot as used for continuous and single shot scanning of line profiles.

Chapter 3 : Time resolved AII line width measurements using a linear pinch as a light source.

Chapter 4 : Further line width measurements using a B_Z stabilised linear pinch. N_e was readily determined, using this source, by means of laser interferometry. Also T_e was deduced from optically thick line widths. Consequently line broadening parameters much larger than predicted by theory were measured for two AII lines.

Chapter 5 : Recalculation of the broadening parameters of the two AII lines for which large discrepancies had been found. Further, an investigation of the validity of various assumptions made in the theory is discussed.

Chapter 6 : Development of a means for obtaining accurate distributions of N_e in an unstabilised pinched discharge.

Chapter 7 : Measurement of electron temperature in the unstabilised and B_Z stabilised pinch discharges using a method independent of that given in Chapter 4.

Chapter 8 : Line width measurements using the unstabilised pinch at conditions under which accurate determinations of N_e and T_e had been made, [as described in Chapters 6 and 7]. The results obtained are then compared with the existing theory.

Chapter 9 : Discussion of the limitations in Stark boradening theory for AII, as found from the results given in Chapters 3 to 8. Application of the results to other species and suggestions for further investigations in this field are described.

Chapter 10 : Measurements of N_e and T_e for an R-F plasma torch to determine the extent to which thermal equilibrium prevails in such a source. N_e was measured

from the widths of AI lines. Broadening parameters were checked using a conventional shock tube source.

Chapter 11 : Measurement of theta pinch plasma rotation using a Doppler shift technique. The velocities determined were checked with those measured by photographic techniques and the results discussed in the light of existing theories.

Appendix I : Brief description of computor programme used for Stark broadening calculations.

Appendix II : Brief description of computor programme used to determine the distortion of a line profile emitted by an inhomogeneous plasma.

Appendix III : Some new results on Z-pinch dynamics which were obtained as a sideline of the results described in Chapter 6.

Due to the relevance of line widths and shifts in this work the various sources of these phenomena in a plasma are briefly presented below. We shall concentrate on Stark broadening as this forms the main topic of this thesis. Further, the main emphasis will be on isolated lines such as are emitted by AII.

Later, reasons for studying AII will be discussed. The object of the investigations described in topics (2) and (3) will be given in the relevant chapters.

1.3. Mechanisms which cause line broadening and shift

For all the lines studied in this work natural broadening and resonance broadening could be completely neglected. This conclusion was reached by applications

of the formulae from reference 2. We shall therefore only consider :-

(a) Doppler broadening and shift

The radiation emitted by atoms or ions moving with a velocity v is shifted by an amount:-

$$\Delta\lambda = \frac{v}{c}\lambda \qquad \ldots 1.1$$

For atoms with a Maxwellian velocity distribution the net effect on a line of wavelength λ is to give a broadened profile of Gaussian shape with $\frac{1}{2} - \frac{1}{e}$ width given by :-

$$g = \left(\frac{2kT}{M_c 2}\right)^{\frac{1}{2}}\lambda \qquad \ldots 1.2$$

Where M is the mass of the emitting species.

(b) Van Der Waals broadening and shift

Perturbations of emitters by neutral particles can cause broadening and shift of a line profile. This boradening effect is most important in weakly ionised gases when, if there is no resonance between emitter and perturber states, it is referred to as Van Der Waals broadening. In this case Griem (ref.2) gives the width and shift respectively of a level α as :-

$$W_\alpha = \pi N \left(\frac{9\pi n^5 \bar{R}_\alpha^2}{16 m^3 E_p^2}\right)^{\frac{2}{5}} \frac{3}{\sqrt{5}} \text{ sec}^{-1} \qquad \ldots 1.3$$

$$\text{and } d_\alpha \sim -\frac{2}{3} W_\alpha \qquad \ldots 1.4$$

Where N is the neutral particle density.

$\bar{R}_\alpha^2$ is the square of the coordinate vector of the radiating electron in state α (in atomic units).

E_p is the excitation energy of the resonance level.

V is the perturber velocity.

The shape of the profile is dispersive.

(c) Stark broadening and shift

The Stark effect is important when the dominant perturbations of emitters are caused by charged particles. Since this case forms the main topic of the thesis it will be considered in some detail.

The interaction between the radiator and perturber can be expressed in a multipole expansion of the form :-

$$V(t) = \frac{Z_1 Z_2 e^2}{r^2} \quad \underline{r} - \underline{d} \cdot \underline{E} + \quad \ldots \; 1.5$$

Where Z_1, Z_2 are the charges on the emitter and perturber respectively.

$\underline{r}$ = position vector of the perturber. (origin at the emitter)

$\underline{d}$ = dipole moment of emitter

$\underline{E}$ = field produced by perturber at r = o.

For a neutral emitter the first term is zero. In practice two limiting approximations can be considered for the perturbers:-

a) The Quasi-static approximation

Here the perturbers do not move appreciably during the times of interest [see below]. We can then assume that the perturbation is fixed so that for a particular perturber (i.e. a particular value of $\underline{E}$) every transition of the emitter splits into a spectrum of sharp lines. The intensities and separations of these lines are defined

by the quantum mechanics of the (static) Stark effect. If we then average over all perturber positions a broadened spectrum is obtained for each unperturbed line.

In line broadening times of interest, i.e. times for which the emitted wavetrain changes its phase appreciably, are $\sim \frac{1}{\Delta\nu}$

Where $\Delta\nu$ is the frequency separation from the line centre.

Thus for this approximation to hold we require a typical perturber collision time, t_c, to be such that

$$t_c \gg \frac{1}{\Delta\nu}$$

Where $t_c \sim \frac{\rho}{v}$

(ρ is the impact parameter and v the velocity of the perturber).

In general it happens that this approximation is good for ions (v small) but is poor for electrons (v large) except in the line wings ($\Delta\nu$ large). Electron perturbations can usually best be treated by :-

b) <u>The impact approximation</u>

Here it is assumed that,

$$t_c \ll \frac{1}{\Delta\nu}$$

The original theory, as developed by Lorentz and Weisskopf [see ref.3] assumed that all perturber collisions were instantaneous and occurred with a frequency γ. Each collision interrupted the light train from the emitter completely. Fourier analysis of these interrupted trains gives a dispersive line shape :-

$$I(\nu) \propto \frac{1}{1+\left(\frac{\nu-\nu_o}{2\gamma}\right)^2} \qquad \ldots 1.6$$

Where ν_o is the unperturbed line frequency.

The $\frac{1}{2}$-$\frac{1}{2}$ width of this dispersive shape is the collision frequency,

$$\gamma = \int_{v=o}^{\infty} dv \int_{\rho=o}^{\infty} 2\pi N \rho \, d\rho \, v f(v) \qquad \ldots 1.7$$

Where N is the number density of perturbers,

f(v) is the distribution of perturber velocities.

The integral over ρ in 1.7 diverges at large ρ and has to be cut off at the 'Weisskopf' radius, ρ_w, giving :-

$$\gamma = \pi N \bar{v} \rho_w^2 \qquad \ldots 1.8$$

ρ_w was defined by considering only those collisions which gave phase shifts of the wavetrain $\gtrsim 1$ as effective.

Lindholm ([see ref.3] considered the amplitude of the emitted wavetrain as remaining constant but that collisions caused phase shifts. The same line shape as in 1.6 was obtained but a shift of the profile from ν_o was also possible.

The above approximations are limiting. In general a perturber can cause any amplitude or phase change of the emitted wavetrain. The former case (non-adiabatic model) means that the perturber can cause transitions of the optical electron to neighbouring ('perturbing') states. The first treatment of such in-elastic collisions was done

by Anderson, [ref.4]. The first extensive calculations of the broadening of isolated lines were performed by Griem [ref.2]. In Griem's theory the broadening is calculated by perturbation theory. The impact approximation allows the calculation to be done assuming the effects of the perturbers are scalarly additive so that the resultant width is proportional to the number of perturbers. For high perturber velocities perturbation theory is exact and at low velocities the calculations reduce to the adiabatic theory of Lindholm.

However, breakdown of perturbation theory for strong interactions sets a lower limit, ρ_s, to the impact parameters that can be considered. Collisions for impact parameters less than this are therefore treated on the 'Strong collision' theory of Lorentz-Weisskopf with $\rho_w = \rho_s$.

The resultant electron impact effect is to give a shifted dispersive profile of $\frac{1}{2}$-$\frac{1}{2}$ width,

$$W = \Omega\ (Te)Ne \qquad \ldots\ 1.9$$

(Where Ω (Te) is generally a rather slowly varying function of Te.)

and shift,

$$d = k(Te)Ne \qquad \ldots\ 1.10$$

The quantities $\Omega(Te)$ and $k/\Omega(Te)$ have been tabulated by Griem for many isolated lines [ref.2].

To obtain the resultant profile of a line broadened by both electrons and ions the Stark components of the line, for a particular ion field $\underline{E}$, are first calculated. The impact approximation is then used to calculate the

electron broadened profiles of these components and then the whole pattern averaged over the statistical distribution of the ion field.

For isolated lines the quadratic Stark effect is operative and the ion broadening is generally small. The resultant line width is then given approximately by [ref.2]:-

$$W_T = [1 + 1.75\ \alpha\ (1 - 0.75\ R)]W \quad \ldots\ 1.11$$

for neutral emitters,

and $W_T = [1 + 1.75\ \alpha\ (1 - 1.2R)]W \quad \ldots\ 1.12$

for singly ionised emitters.

Where, R is the ratio of the mean inter-ion distance to the Debye length and α is the ion broadening parameter [again tabulated in ref.2 for many isolated lines].

1.4 Convolution of broadening mechanisms

For independent broadening mechanisms with profiles A, B, etc. the resultant observed profile is the convolution of these :-

$$I_{OBS} = A^* B^* \cdots$$

We will only consider Gaussian (Doppler) profiles of $\frac{1}{2} - \frac{1}{e}$ width g and dispersive (Stark) profiles of $\frac{1}{2} - \frac{1}{2}$ width W. In addition the instrument profile must be considered. This can usually be approximated to a Voigt profile, with parameters g_1 and W_1, using the tables of Allen [ref.5].

The resultant width of the observed profile as a convolution of instrument, Stark and Doppler broadening effects is then [ref.5] :-

$$B = (W^2 + 2.80G^2)^{\frac{1}{2}} + W \quad \ldots 1.13$$

$$\text{Where } W = W + W_1 \quad \ldots 1.14$$

$$\text{and } G = (g^2 + g_1{}^2)^{\frac{1}{2}} \quad \ldots 1.15$$

We shall assume, unless otherwise stated, that the broadening mechanisms we consider are in fact independent.

1.5 Previous work on Stark broadening

Many checks of the modern quantum mechanical theory of Stark broadening have been made for hydrogen like emitters. The agreement with theory has been typically $\sim$ 10% for hydrogen [see ref.6].

In the case of H_β more detailed calculations were performed by Griem et al [ref.7] and the agreement has been $\sim$ 5% [ref.6].

In these cases the l-degeneracy gives rise to a linear Stark effect so that ion broadening is large. In addition there is the complication of overlapping lines caused by the l-degeneracy [refs 8 and 9].

For heavy element emitters the l-splitting is large and we have isolated lines and small ion broadening so that the relations 1.8 to 1.11 are applicable. The first calculations in this case were done by Griem for HeI [ref.10] and later extended to many neutral and singly ionised species, [ref.2].

Many checks of the theory have also been made for this case. Results for neutral emitters are summarised in Fig.1.1. Since the work on AII, described in this thesis, was started results have also been published for singly

FIG.1.1 VERIFICATIONS OF STARK BROADENING THEORY - ISOLATED LINES FROM NEUTRAL ELEMENTS

Element	Plasma Source	Measurement of W and d	Independent measurement of T_e	Independent measurement of N_e	Worker	Agreement with theory (widths only*)
AI	High current water cooled Arc	Microphotometering of photographic recording	Absolute intensity of AII λ4348Å using a measured A_{mn}	Pressure balance: atmospheric P + T_e + Saha equn. → N_e (LTE)	Gericke [ref.14] N_e corrected by Griem [ref.15]	± 20% However possibility of a systematic error in N_e-see Ch.10
CsI	Parallel geometry Hot cathode Cs diode	Monochrometer scanned with photomultiplier (P.M)	Absolute line intensity	Absolute continuum intensity	Stone and Agnew [ref.16]	± 10%
HeI	T - Tube	Monochrometer scanned with P-M on a multi-shot basis	Relative intensities HeI line to continuum also HeII to HeI line	Absolute continuum intensity	Berg, Ali, Linke and Griem [ref.13]	± 10%
O I	Wall stabilised Arc	Monochrometer scanned with P-M	Absolute intensity of OI, λ6157Å	Arc pressure + T_e + Saha → N_e	Wiese and Murphy [ref.17]	± 6%
OI	Wall stabilised Arc	Monochrometer scanned with P-M	Absolute intensity OI, λ6654Å	Arc pressure + T_e + Saha → N_e	Jung [ref.18]	± 10% to ± 20%
NI	Wall stabilised Arc	Monochrometer scanned with P-M	Absolute Line intensity	Arc pressure + T_e + Saha → N_e	Stampa [ref.19]	± 10% to ± 20%

* The agreement between experiment and theory was typically poorer for shifts - this will be discussed in Chapter 5.

ionised emitters. However discussion of these will more conveniently be left to a later chapter for comparison with the results on AII recorded there.

Generally the results for neutral lines are in poorer agreement with the theoretical widths and shifts calculated by Griem than for the hydrogen like case.

1.6 Reasons for studying AII

Data on AII line broadening was of particular importance at Imperial College since linear pinches, in which AII was the predominant species, had been studied in the Plasma Physics Group for several years. In particular Burgess [ref.11] had scanned some AII lines, emitted by such a pinched discharge, using a photoelectric recording spectrometer on a multi-shot procedure. Burgess thus found excellent fits of the observed line profiles to the dispersive profiles expected from broadening of isolated lines due to electron impacts.

Accurate knowledge of the AII line broadening parameters, $\Omega(T_e)$, could therefore be used in conjunction with line widths to obtain values of Ne in such discharges.

Apart from their use in plasma diagnostics, however, the broadening parameters provide a check on the existing theory of electron impact broadening. Originally the poor agreement with theory for isolated lines emitted by heavy elements was thought to arise mainly from uncertainties in the radial matrix elements connecting transitions from a given upper state to a perturbing level. The results of recent calculations by Statz et al [ref.12] on wavefunctions

for AII could be used to minimize theoretical errors from this source.

In addition the first term in the multi-pole expansion, 1.1, has been omitted in Griem's calculations for ionised emitters, i.e. the electron interaction was assumed to be mainly long range so the perturbers moved along straight line orbits rather than the correct hyperbolic paths. Berg et al [ref.13] suggested that the Coulomb interaction caused a set negative space charge in the neighbourhood of an ion. Consequently this would cause a blue shift of all ion lines. However Burgess has pointed cut (private communication) that inclusion of a correct time dependent potential in the calculation of this so called 'plasma polarisation shift' should lead to an increase in broadening, as well as giving shift, for all singly ionised lines. Investigation of a possible increase in broadening is therefore of interest.

CHAPTER 2

USE OF THE SCANNING FABRY-PÉROT INTERFEROMETER FOR RECORDING LINE PROFILES

2.1 Introduction

Due to the transient nature of the plasma sources used in this work the rapid scanning Fabry-Pérot [ref.1] provided an ideal instrument for recording line profiles. This instrument was fully developed in the Plasma Physics Department by J.Cooper and J.R.Grieg. However it has, as yet, been little exploited for the purposes of quantitative spectroscopy. It therefore seems worthwhile to give an account of the experimental procedure for setting up a S.F.P., for both continuous and single shot scanning of line profiles. Moreover we shall mention some points in connection with this instrument which have not previously been discussed in the literature.

Chabbal [ref.20] has given a very extensive theoretical treatment of a S.F.P. and Cooper and Grieg [ref.1] and Grieg [ref.21] have described in detail the piezoelectric driven S.F.P. which we consider. These form the main references for this instrument.

2.2 Instrument function of the S.F.P.

For optimum measurement of line profiles the broadening produced by the instrument must be minimised consistent with good light gathering power. The (whole) $\frac{1}{2}$-width of the instrument profile is defined by :-

$$\Delta\lambda_I = \frac{\Delta\lambda_1}{N_{EFF}} \qquad \ldots 2.1$$

Where $\Delta\lambda_1$ is the free spectral range of the Fabry-Pérot, and N_{EFF} is the 'effective finesse'.

Therefore N_{EFF} must be made as large as possible though, in practice, this requirement conflicts with the attainment of a good light gathering capability. We will consider in the next section the practical attainment of the best compromise.

Chabbal [ref.20] shows that N_{EFF} results from the convolution of three functions, each with an associated finesse, such that :-

$$\frac{1}{N_{EFF}^2} \backsim \frac{1}{N_D^2} + \frac{1}{N_R^2} + \frac{1}{N_S^2} \qquad \ldots 2.2$$

N_D is the surface defects finesse.

Four sources contribute to this:-

1) Spherical curvature of the plates: flatness to λ/n gives an associated finesse $N_D = n/2$.
2) Microdefects of the plate surface: defects of mean depth λ/n, with a Gaussian distribution, give $N_D = n/4.7$
3) Lack of Parallelism: plates parallel to λ/n have an associated finesse $N_D = n/1.73$
4) Bowing of the moving plate: this causes an additional plate curvature which can be treated in 1).

N_R is the reflection finesse

$$N_R = \frac{\pi\sqrt{R}}{1 - R} \qquad \ldots 2.3$$

Where $R = \sqrt{R_1 R_2}$ is the mean reflectivity of the plates.

N_S is the scanning finesse

$$N_S = \frac{2f^2}{r^2} \frac{\Delta\lambda_1}{\lambda} \quad , \qquad \ldots\ldots 2.4$$

for a circular scanning aperture of radius r and using a lens of focal length f to image the fringe pattern at this aperture.

2.3 Experimental treatment of finesse

We shall consider the analysis for a given set of plates, in this case a pair of fused silica flats. The final value of N_{EFF} is limited by N_D since this quantity is a function of the plates used. This finesse will therefore be considered first :-

(a) Surface defects finesse

Spherical curvature of the plates was measured using the Fizeau fringe test [ref.22]. Fig.2.1 shows such a test on λ4358Å, HgI. Fig.2.2 shows the flatness (converted to λ 5461Å, HgI) as a function of temperature for a one centimetre Fabry-Pérot aperture. The corresponding finesse at room temperature was 28 ± 4.

For fused silica plates, N_D due to microdefects should be $\gtrsim 45$ at λ5461Å [ref.70] and so can be neglected compared with the above.

Again careful adjustment of the fixed Fabry-Pérot plate can render the effect of lack of parallelism negligible.

The effect of variation of the moving plate speed can be seen from Fig.2.3 where a continuous scan of a HgI line,



Fig. 2·1 Fizeau fringe test of plate curvature. λ4358 Å, Hg I.

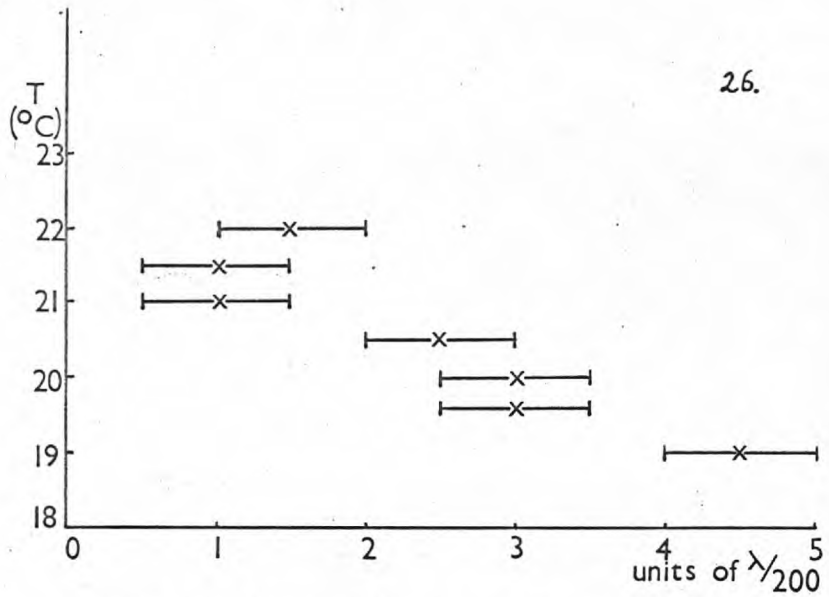


Fig. 2·2 Plate flatness. 1 cm. aperture. λ 5461 Å, Hg I. Fused silica F-P plates

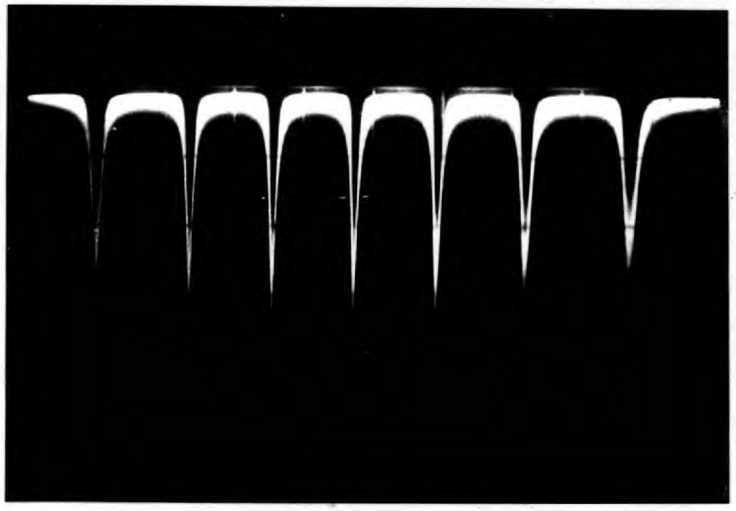


Fig. 2·3 Continuous F-P scan of λ4799 Å Cd I 2 μsec./division.

λ 5461Å, is shown. (Discussion of the continuous scanning procedure is more conveniently left to Section 2.6.) This scan shows the reduction of plate speed and therefore in time to scan $\Delta\lambda_I$, as the plate reaches its maximum amplitude. In addition, however, the finesse is reached due to bowing effects. The bowing finesse can be increased - at the expense of a reduction in light gathering power - by reducing the Fabry-Pérot aperture or by making the moving plate diameter larger than the piezoelectric tube diameter [ref.21]. However, we shall mainly be concerned with the central few fringes of a scan and will not consider this effect further.

We shall therefore consider the overall finesse N_D for the fused silica plates used as $N_D = 28 \pm 4$.

(b) Reflection finesse

Silver coatings were evaporated on the plates using an Edwards Model 12 EA coating plant. When ion bombardment cleaning had been performed a base pressure $\sim 2 \times 10^{-5}$ mm Hg could be attained with this equipment.

The fixed and scanning plates were coated simultaneously so that $R_1 \simeq R_2$. Initially the plant was calibrated by evaporating known lengths of Ag wire on the plates and subsequently measuring reflectivity, R_1, and transmission, τ photoelectrically using a spectrometer equipped with a tungsten lamp continuum source. The calibration is shown in Fig.2 - 4 together with the étalon transmission [ref.20],

$$\tau_E = \left(1 - \frac{A}{1-R}\right)^2$$

calculated from the measured values of R and τ.
(A = mean plate absorption = $1 - \sqrt{R_1 R_2} - \sqrt{\tau_1 \tau_2}$)

Also shown in Fig. 2.4 is the reflection finesse N_R, as a function of R, from 2.3. For later coatings the transmission was monitored during the evaporation. A D-C stabilised, high pressure, mercury lamp chopped at 50 c/s was used as a source and the plate transmission and a reference beam monitored simultaneously on a double beam C.R.O.

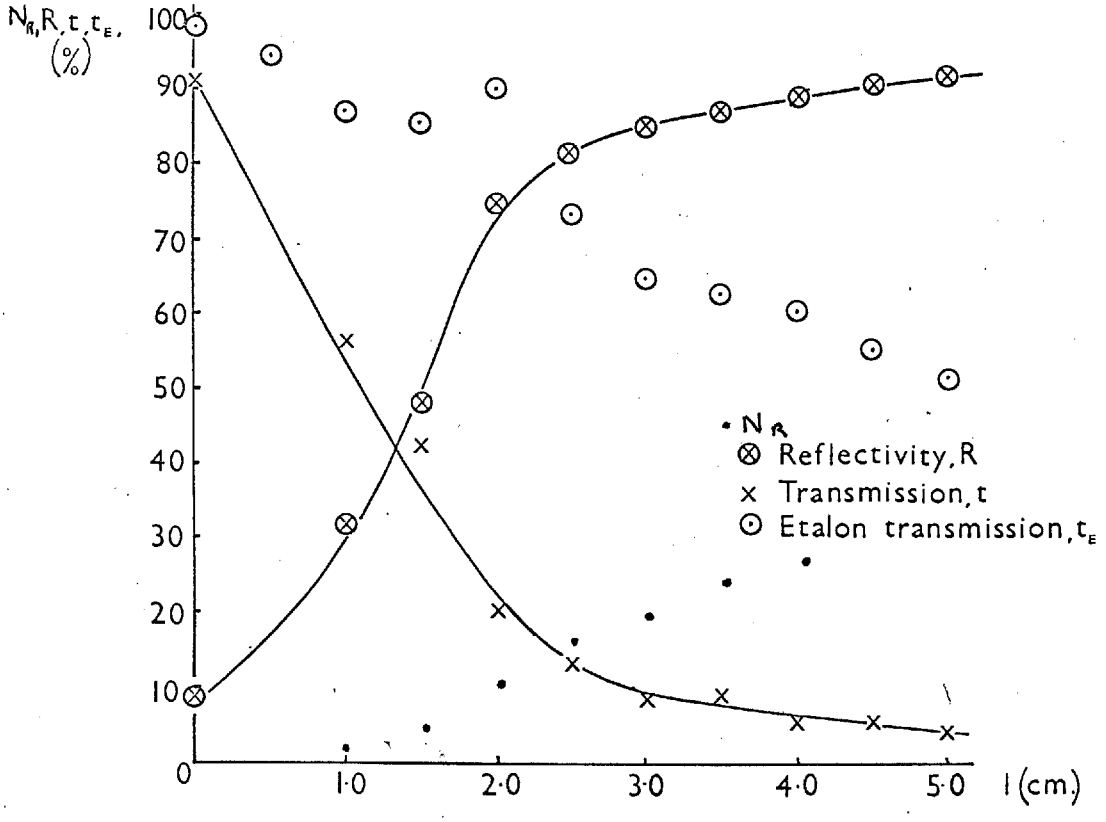


Fig 2·4 Calibration of coating plant. Freshly deposited Ag.
l = length of Ag wire deposited

(c) Scanning finesse

This could be calculated directly from 2.4. Usually, however, we require a monchromator after the S.F.P. in order to isolate a particular line. We shall therefore consider the scanning aperture as the rectangular entrance slit of the monochromator [see Fig.2.5].

Using the Fabry-Pérot relation :-

$n\lambda = 2d\cos i$, i.e. $i = \cos^{-1}(\frac{\lambda}{\lambda_o})$

Where $\lambda_o = \lambda - \Delta\lambda$ is the wavelength transmitted for $i = o$.

If $\frac{\Delta\lambda}{\lambda_o}$ is small,

$$i \sim \sqrt{\frac{2\Delta\lambda}{\lambda_o}}$$

The transmission of the aperture for an angle of incidence i is [see Fig. 2.5] for $y \geq x$:-

$$\tau = \frac{2}{\pi}\sin^{-1}(\frac{x}{y}) = \frac{2}{\pi}\sin^{-1}(\frac{x}{fi})$$

$$\text{i.e. } \tau \sim \frac{2}{\pi}\sin^{-1}(\frac{x}{f\sqrt{\frac{\lambda_o}{2\Delta\lambda}}})$$

Fig.2.6 shows a plot of the transmission of the aperture against $\Delta\lambda$. This is therefore the scanning function. Also shown in the figure is y as a function of x. Thus if $y = x$ we get the usual rectangular scanning function of width,

$$\Delta\lambda = \frac{\lambda x^2}{2f^2} ,$$

which we expect for a circular aperture of radius x.

In general, however, we get a non rectangular scanning function which is asymmetric towards the blue.

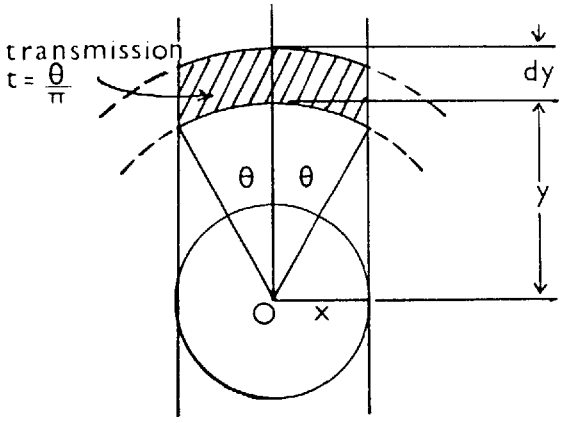


Fig 2·5 Rectangular scanning aperture.

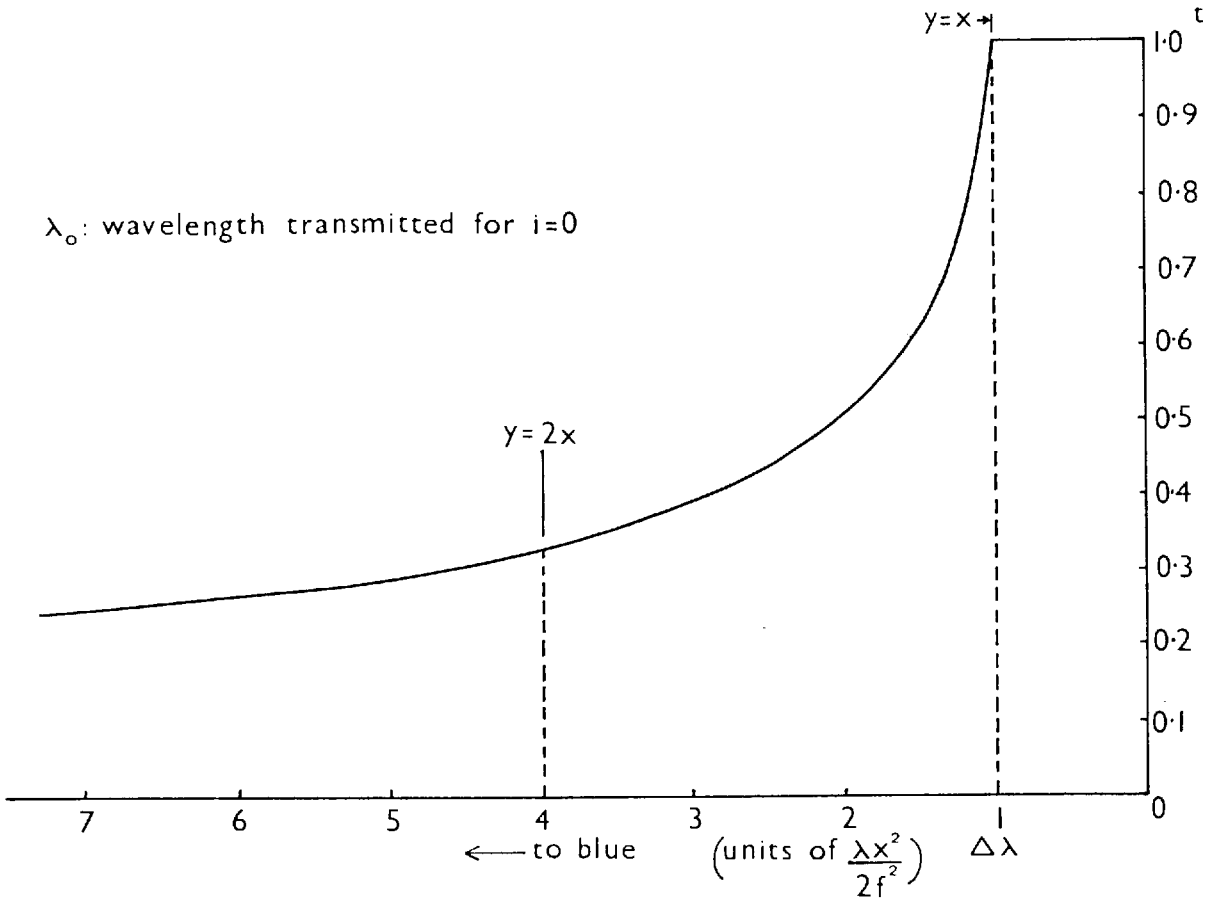


Fig 2·6 Transmission, t, of aperture versus $\Delta\lambda$.

Scanning finesse with a rectangular aperture.

2.4 Effective finesse: Variation with wavelength

Chabbal [ref.20] has shown that for optimum transmission of the Fabry-Perot system it is best to have :-

$$N_D \backsim N_R \backsim N_S \qquad \ldots 2.5$$

In which case, from 2.2, $N_{EFF} \sim 0.6 N_D$.

It is possible to make N_R and N_S arbitarily large. However, N_D is inherent in the plates (i.e. it is the limiting finesse) and though this can be increased by reducing the aperture this will be at the expense of signal to noise ratio. In the particular case considered in Section 2.3,

$N_D = 28 \pm 4$ at $\lambda 5461\text{Å}$

Thus if criterion 2.5 is satisfied we have,

$$N_{EFF} \sim 17.$$

Now in order to measure the width, B, of a broadened line it is usual to set $\Delta\lambda_1$ such that,

$$B \gtrsim \frac{\Delta\lambda_1}{2} \qquad \ldots 2.6$$

Thus we expect from 2.1 and 2.6

$$\frac{B}{\Delta\lambda_I} \backsim \frac{N_{EFF}}{2} \backsim 8$$

In this case measurements of B should be accurate to about $\pm$ B/16 even without detailed knowledge of the instrument function shape.

Thus optimum length gathering power together with a narrow instrument width is given by coating the plates to give :-

$N_R \backsim 28$ at $\lambda 5461\text{Å}$

and achieving $N_S \backsim 28$ at $\lambda 5461\text{Å}$

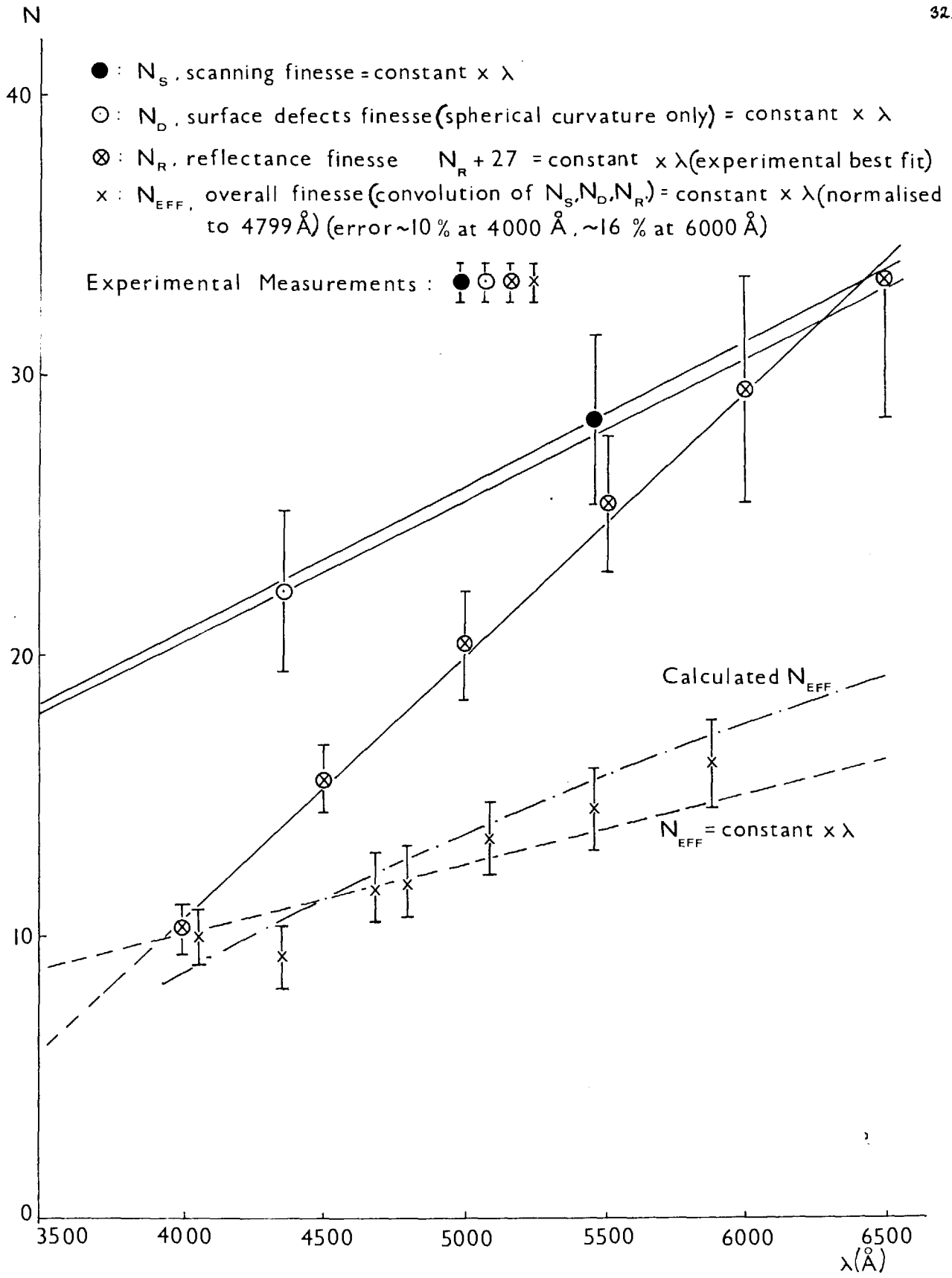


Fig 2·7 Finesse, N, versus wavelength, λ, (fused silica F-P plates.)

We shall now consider the variation of N_{EFF} with wavelength using the above values of N_D etc.

Both N_D and N_S vary linearly with wavelength. These linear relationships, normalised to the measured quantities, are plotted in Fig.2.7. The mean values of reflectivity and transmission of the plates were measured as a function of wavelength. These values are shown plotted in Fig.2.8. Corresponding to the measured values of R from Fig.2.8 the variation of N_R with wavelength is plotted in Fig.2.7. The relationship is closely linear but does not pass through the origin, the best fit straight line being,

$$N_R + 2\ell \alpha \lambda .$$

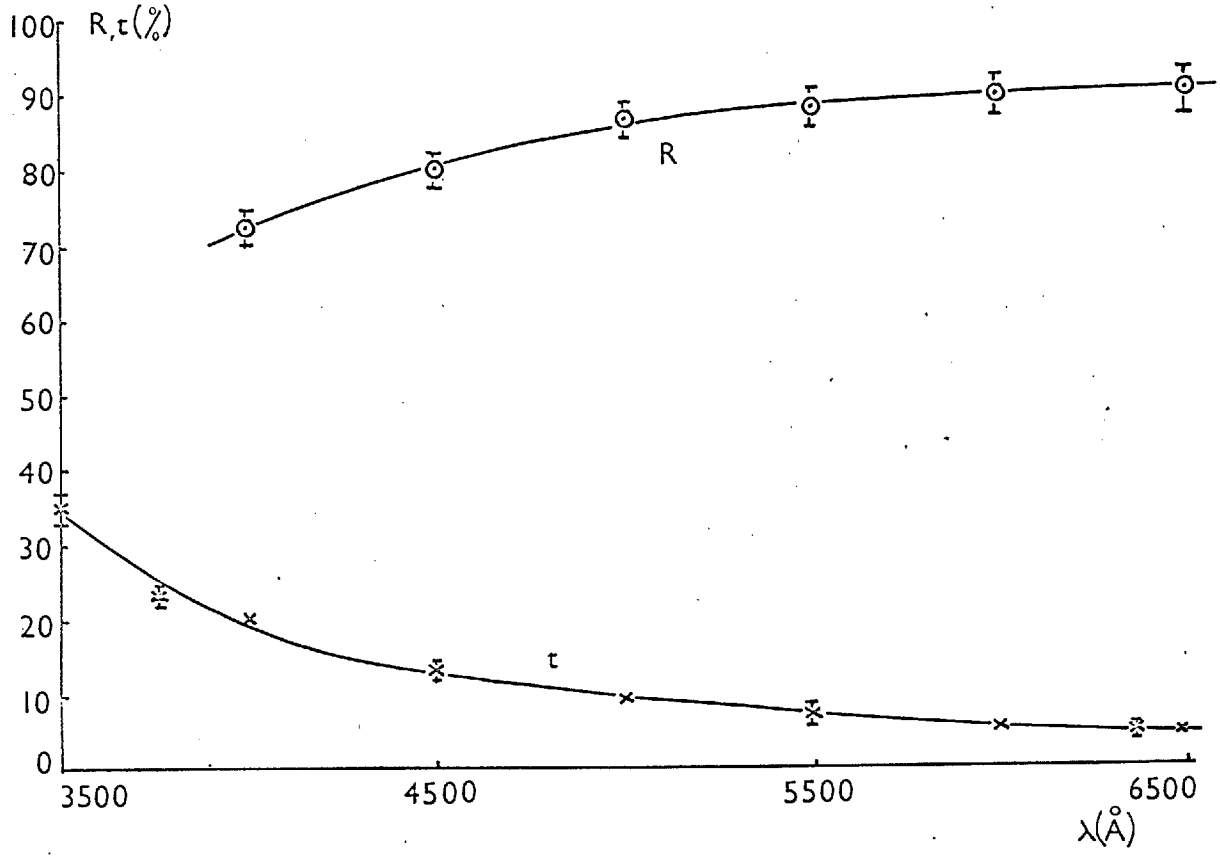


Fig 2·8 Reflectivity, R, and transmission, t, versus λ. Fused silica F–P plate, freshly coated with Ag.

The variation of N_{EFF} with wavelength using 2.2 and the measured values of N_D, N_R and N_S is also shown in Fig.2.7.

To check the calculated N_{EFF} several lines were scanned through at slow speed (i.e. $\sim 2\mu s/\Delta\lambda$, at $\lambda 5461\text{Å}$) using the procedure described in Section 2.6, which follows, and N_{EFF} in each case measured from the half-width of the central fringe of the scan. These values compare well with the calculated values of N_{EFF} as is seen from Fig.2.7.

In all measurements of instrument functions it is arranged that broadening of the line used for measurements is negligible. Low pressure lamps were used in this work, the line source widths being measured with widely spaced Fabry-Pérot plates. These are tabulated below :-

λ	Source	Line width (Å)
4046	HgI	0.02 ± 30%
4348	HgI	0.02 ± 30%
4678	CdI	0.03 ± 30%
4799	CdI	0.02 ± 30%
5085	CdI	0.03 ± 30%
5461	HgI	0.03 ± 30%
5895	NaI	0.06 ± 0.01

Correction for the source width only had to be made for $\lambda 5895\text{Å}$ in the previous results.

A useful result from this analysis is that N_{EFF} varies approximately linearly with wavelength. N_{EFF} = constant x λ (normalised to the experimental N_{EFF} for $\lambda 4799\text{Å}$) is plotted in Fig.2.7. Measurement of the instrument profile at one or

two wavelengths could therefore be used to give the instrument width at all wavelengths from λ 4000Å - λ6000Å with an error of < 10%. Correspondingly the instrument function shape will not alter appreciably through this range though dispersive wings will become more apparent at lower wavelengths.

Another result from the above analysis is that the instrument profile can probably be well estimated from the relevant formulae without resorting to scanning a 'narrow line'. This is useful in scanning a plasma line which is so narrow that an 'unbroadened' line cannot be found for measurement of the instrument width.

2.5 Light gathering power

As mentioned previously Chabbal [ref.20] shows that the optimum condition for the use of a Fabry-Pérot with regard to both resolution and light gathering capacity is that

$$N_D \sim N_R \sim N_S .$$

In fact from the light gathering point of view he shows that if,

$$\frac{N_D}{2} < N_R < 2N_D \qquad \ldots 2.7$$

the optimum transmission is not changed by more than 20%. Criterion 2.7 can be seen to be satisfied from λ 4000Å to λ 6000Å from Fig.2.7. Conveniently, the optimum value of R given by equation 2.5 also gives a good value for the étalon transmission ($\sim$ 65% from Fig.2.4) in our case.

Again it can be noted that since the Surface defects transmission coefficient is

$$\tau_f = \frac{N_F}{N_R}$$

(where $1/N_F^2 = 1/N_R^2 + 1/N_D^2$)

then increasing the aperture decreases N_D so that reducing N_R to satisfy

$$N_R = N_D$$

may cause the absorption of the silver coating to be increased [ref.30]. This means that τ_E may be reduced. This occurs because τ_E does not vary monotonically with R for silver coatings [see Fig.2.4]. Thus in such a case the overall transmission may not be increased in spite of the effective finesse being reduced.

In the system used for scanning lines another limitation on the light gathering power is often set by the monochromator. For all the work described in this thesis a small Hilger constant deviation spectrograph was used. To match this f/9 instrument with the Fabry-Pérot of 1 centimetre aperture a 9 centimetre focal length imaging lens should be used. To give the same scanning finesse corresponding to the previous considerations a slit width 2mm is desirable corresponding to accepting a bandwidth $\sim$120Å at λ5000Å. In practice rarely could a bandwidth of this magnitude be accepted without a considerable number of lines being viewed.

Therefore the slit width must be reduced giving an asymmetric (though albeit narrower) scanning function and reduced luminosity. The system was therefore often limited by the poor dispersion of the constant deviation (rather than the f-number of this instrument).

2.6 Continuous scanning of line profiles

The set-up used for the continuous scanning of line profiles from a stationary source is shown in Fig.2.9.

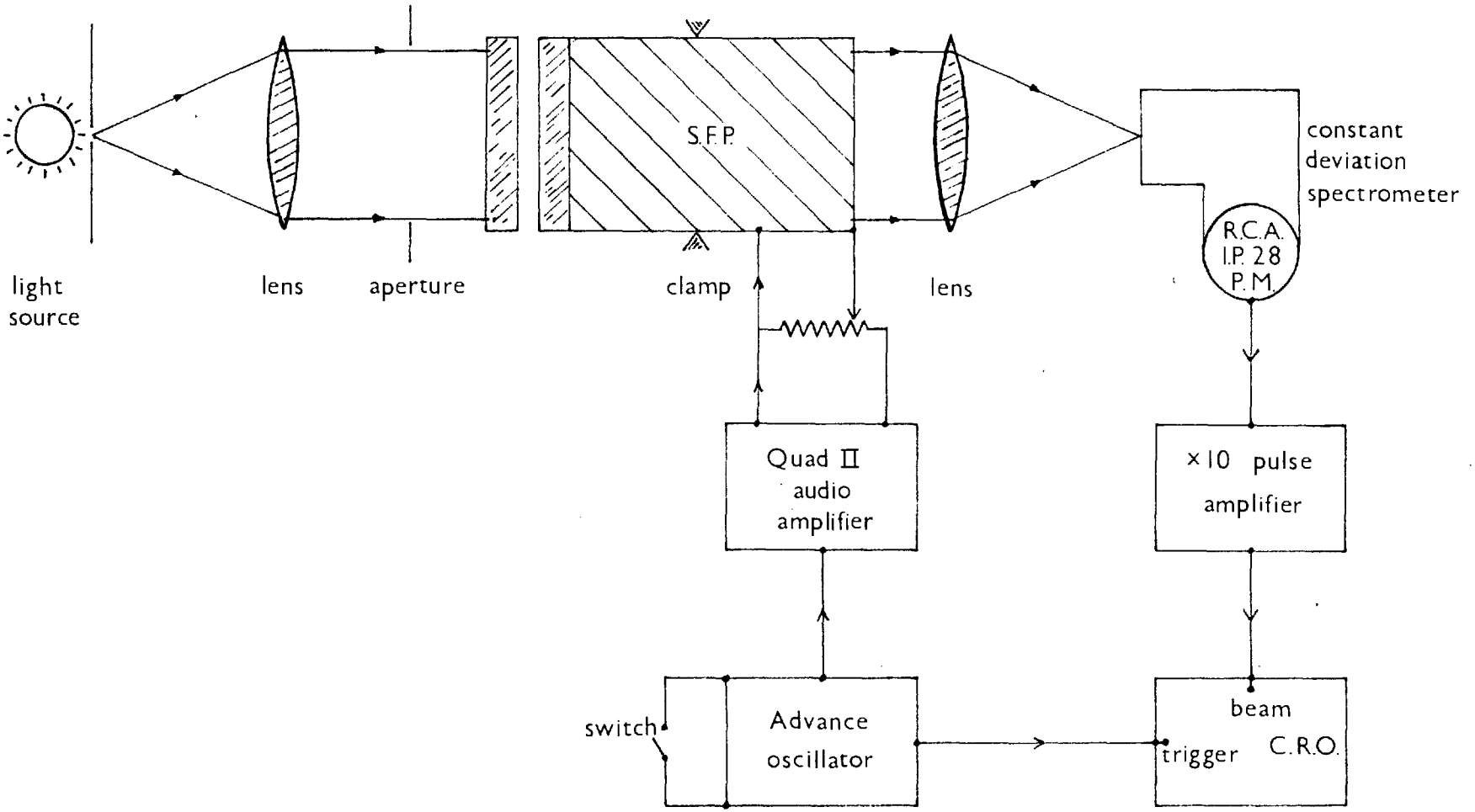


Fig. 2·9 Line profile recording system using the rapid-scanning Fabry-Pérot : (i) continuous scanning with time-independent light source.

This arrangement was used for obtaining instrument profiles on lines emitted by low pressure lamps and also for studying the radiation from an R.F. plasma torch and a conventional shock tube (see Chapter 10).

An 'Advance' oscillator was used to drive the piezoelectric element via a Quad II amplifier. A 6 inch long tube was used throughout this work. This resonanted in its longitudinal mode at an input frequency $\sim$15 K.C/s. An applied voltage $\sim$30v was capable of giving a scanning rate $\sim$0.3μ sec per free spectral range at λ5461Å. Increased power input was found to cause either the tube, or the bonding of the plate to the tube, to fracture and the theoretical limit of $0.1\mu s/\Delta\lambda_{,,}$ quoted by Grieg, was not achieved in practice.

For stable running the tube was first clamped lightly at its centre and then driven continuously for several minutes to allow it to achieve an equilibrium position. The clamp was then tightened. The output from the photomultiplier (usually an R.C.A. IP28) was amplified $\sim$10x using the transistor circuit described by Cherry and Hooper [ref.23] and matched into an Tektronix 555 C.R.O. equipped with a G-type plug in unit. The minimum response time of the detecting system was $\sim$15n.sec.

2.7 Single shot scanning of line profiles

The set-up which was used for scanning the line profiles emitted by transient discharges is shown in Fig.2.10. A Z-pinch source, as described in detail by Curzon [ref.24], is shown in this figure. The use of the units used for the S.F.P. can be understood with reference to Grieg's thesis [ref.21] or reference 1 .

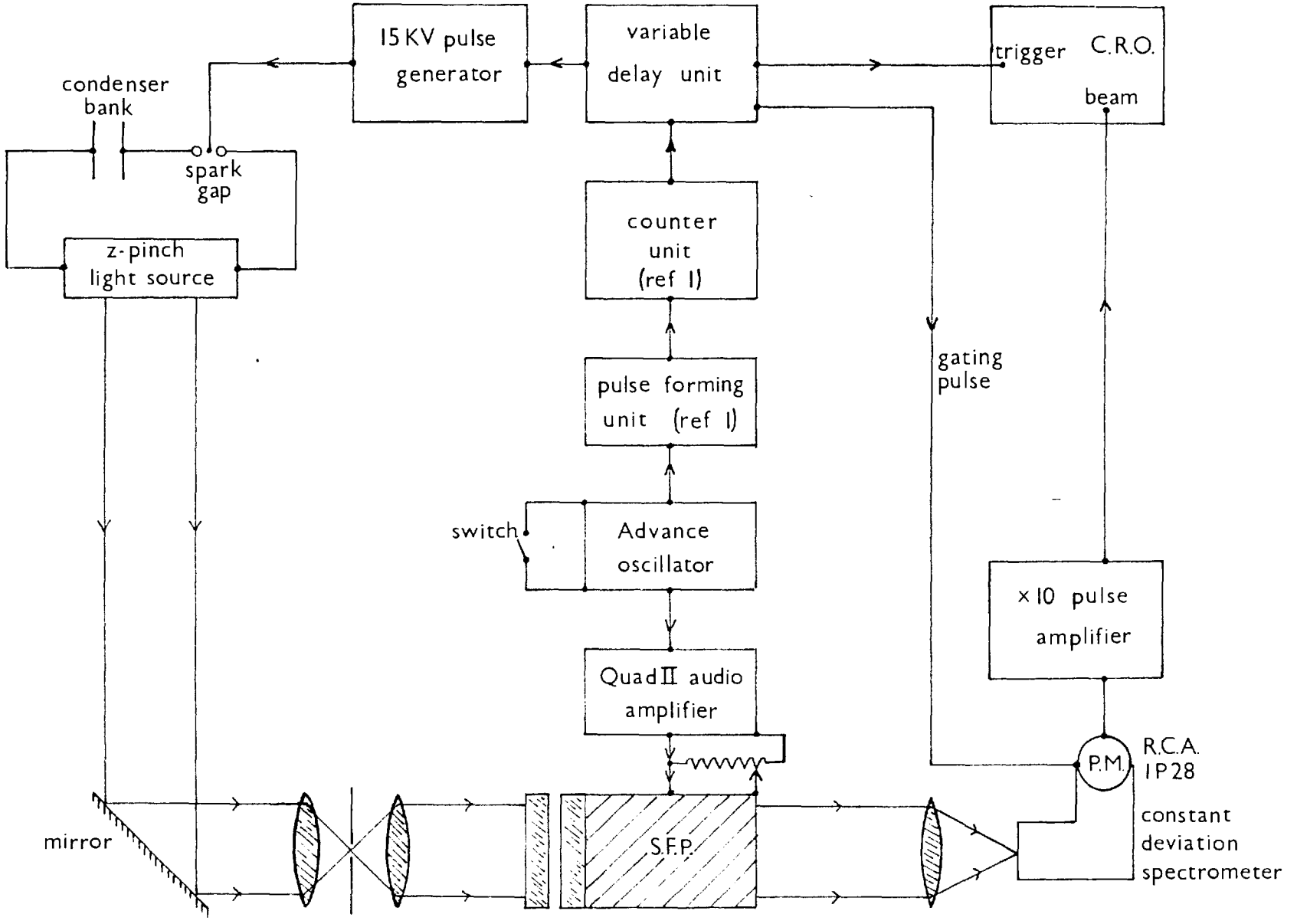


Fig 2.10 Line profile recording system using the rapid scanning Fabry-Pérot :(ii) single shot scanning with a z-pinch transient light source.

It was found necessary to make the loads on each side of the phase splitter in the pulse forming unit different (i.e. ratio 0.02:1). This meant that an output pulse was obtained every cycle of the oscillator rather than every half-cycle. Originally slight distortion of the oscillator voltage waveforms meant that the output pulses every half cycle were not equally spaced in time and consequently two different triggering times were possible.

With this apparatus it was found to be possible to scan through a line profile of maximum finesse in $\sim$ 0.3μ sec (at λ 5461Å) at any required time in the discharge history predictable to $\sim$0.1μ sec.

For convenience the instrument profile was usually obtained from a subsequent shot in the afterglow of the transient discharge rather than using a low pressure lamp and the system of Fig.2.9. In this case it was necessary, using widely spaced Fabry-Pérot plates, to check that the afterglow profile was effectively unbroadened compared with the profile under study. In addition, to avoid saturation of the photomultiplier by the 'pinch' intensity, the photomultiplier was gated during the peak light output. This was conveniently done by applying a positive pulse (amplitude 80v, duration 20μ sec) from the delay unit to the first dynode of the photomultiplier. The time of gating could then be varied at will.

The continuum background on a line profile shot could be obtained by taking a subsequent shot in a nearly, line free, region of the spectrum. Neglect of the continuum would give a larger line $\frac{1}{2}$ - $\frac{1}{2}$ width than the actual value

W by an amount,

$$\delta = x/I_m W$$

Where $x d\lambda$ and $I_m d\lambda$ are the continuum and line intensities, respectively, in a wavelength interval $d\lambda$ centred on the peak line intensity.

Often it is not easy to find a suitable line free region near the line under study and therefore working conditions are best chosen such that x/I_m is as small as possible. This is particularly true for a 'crowded' spectrum such as that emitted by AII.

2.8 Measurement of line shifts

No attempt was made to measure Stark shifts using the S.F.P. for the following reasons:-

Firstly slight jitter in triggering meant an uncertainty in time, and correspondingly wavelength, in correlating successive shots.

Secondly, even if an unshifted profile of the same line (from say a Geissler tube) were recorded on the same shot as a plasma shifted profile, the finite scanning aperture used causes a shift in wavelength of the transmission maximum,

$$\Delta\lambda \sim \Delta\lambda_1/2N_F \qquad \text{from Fig.2.6.}$$

This means that solid angle accepted must be the same for the shifted and 'unshifted' line sources for this systematic shift to be unimportant. Difficulty can thus be experienced in finding a bright enough 'unshifted' line source to show up against the bright plasma line. In any case the accuracy of the shift measurement would not be

good unless d were large compared with W. In fact, as we shall see in Chapter 5, the most difficult shifts to treat theoretically (and therefore those which are most interesting to study) are those which are small and to the blue.

In the advent a far more suitable instrument for measuring shifts has been designed and built by Burgess [ref.25]. We shall therefore only consider calculated values of shifts in this thesis.

CHAPTER 3

MEASUREMENT OF IMPACT BROADENED WIDTHS OF AII LINES EMITTED BY A LINEAR PINCH

3.1 Introduction

The following seven chapters describe one consistent course of work. The aim of this was to investigate, both experimentally and theoretically, the electron impact broadening of lines emitted by singly ionised argon ions in a plasma.

For an adequate investigation of the theory we can see from 1.8 that we require measurements of electron broadened line $\frac{1}{2}$ - $\frac{1}{2}$ widths, W, at known values of Ne and Te.

In this chapter some measurements of W for several AII lines, using a linear pinch discharge in pure argon as a source, will be described.

3.2 Source used and previous work

The source used for these initial measurements was a Z-pinch in pure argon built by Grieg [ref.21]. A condenser bank of 1944 μF. capacity capable of being charged to voltages up to 5 kv was connected across the discharge tube. This could be discharged by a single spark gap in argon triggered by a 15 kv. pulse applied to an auxiliary electrode set in the gap. This device, together with the associated charging and triggering equipment was fully described in reference 21. The discharge could be viewed side on through the fine copper gauze earth return which covered the tube.

Spectroscopic results on this device were obtained by two previous authors, [refs. 11 and 21]. Under typical conditions (which we used later on) of 2 kv bank voltage and 0.25 torr filling pressure, the following results are of relevance :-

(a) Time integrated spectra taken by Burgess [ref.11] and resolved spectra by Grieg showed the predominant line radiation was of AII.

(b) No impurity lines were found which were likely to cause trouble in this work by overlapping strongly with those lines of AII whose broadening parameters had been calculated by Griem, and which were therefore of interest to us.

(c) Line width measurements on $\lambda 4806\text{Å}$ AII were made for a range of conditions by Burgess who scanned the line on a shot to shot procedure using a photoelectric recording spectrometer. He obtained good fits of the observed profile to the dispersive profile expected for electron impact broadening. Assuming Griem's broadening parameter [ref.2] the width led to value of Ne at peak compression $\sim 2.2 \times 10^{18}$ cm^{-3} (at 2.0 kv, 0.25 torr). A similar peak Ne was calculated by Grieg [ref.21] under slightly different initial conditions (2.5 kv, 0.25 torr).

(d) From a Boltzmann plot of relative AII line intensities Burgess obtained a figure for Te $= 26{,}000^{\circ}$K $\pm$ 20% at the first pinch. A somewhat lower figure was obtained by Burgess using pressure measurements of Measures [ref.26], Ne from (c) and assuming $N_i = N_e$.

(e) Burgess deduced that the plasma was optically thin to λ 4806Å radiation from the equality of the width of this line and that of λ 4848Å. These lines should have the same widths when optically thin [ref.2] but different when optically thick, due to their different intensities.

However calculation of the optical depth of λ4806Å, using his values of Ne and Te, led Burgess to conclude that the plasma dimensions for optical thinness were less than those measured from Framing camera photographs.

This led to Burgess postulating the existence of a hot, highly ionised narrow core to the plasma. Such a narrow core seemed to be substantiated by the small plasma dimensions found by Measures [ref.26] using a pressure probe.

These points will be further discussed in the light of results described in Chapter 4.

3.3 Limits on the required line width

It was desirable in our measurements that electron impacts should be the major source of plasma broadening. In this case the line shape should be defined uniquely by Ω (Te) and consequently this parameter could be determined to the maximum accuracy. Therefore the following limits were arbitarily set :-

(a) At low Ne and high Ti Doppler broadening becomes important. If we set the (arbitary) criterion that the electron impact width, 2W, should by $\gtrsim$ 98% of the total line width, we have from 1.12 :-

$$W \gtrsim 5.9g$$

Taking Burgess' value of To (from 3.2d) and setting Ti = Te (i.e. assuming L.T.E.)

$$W \gtrsim 0.27\text{Å}$$

In fact this criterion is not very temperature dependent since g α $Ti^{\frac{1}{2}}$ and W (= Ω (te)Ne) also only increases rather slowly with temperature [see Chapter 5].

(b) At high (ion) densities the ions may contribute significantly to the line width as well as the electrons. The resultant $\frac{1}{2}$ - $\frac{1}{2}$ width of the profile is then given by 1.11,

Where $R \alpha N^{1/6} Te^{-\frac{1}{2}}$
and $\alpha \alpha N^{\frac{1}{4}}$
) reference 2

If we again make the criterion that 98% of the width is due to electron impacts and use Griem's values of and α for λ4806Å we obtain:-

$$W < 7\ \text{Å} \qquad \text{(for Ni} \sim \text{Ne)}$$

However at this limit many lines overlap completely. Even apart from this a far more stringent condition is imposed practically, i.e. by the minimum desirable separation of the Fabry-Pérot plates. To avoid dust being ground between the plates when these are oscillating this is best kept > 0.1mm. This means $\Delta\lambda$, < 12Å at λ 5000Å and correspondingly a maximum resolvable width $2W \sim 6$Å (from 2.6).

(c) If two lines are rather closely spaced then, assuming the upper states do not mutually perturb one another, the resultant profile can be computed simply knowing the widths and relative total intensities of the lines and

adding the separate profiles incoherently. However this introduces the complication of knowing the relevant line oscillator strengths. Therefore Ne is best kept as low as possible [consistent with (a)] for such lines so that they are effectively isolated.

(d) In addition to the above criterion it is desirable that the observed profiles are not appreciably distorted by radiative transfer.

For the case of dispersive profiles the equation of radiative transfer for L.T.E. is given by [ref.27] :-

$$I_\nu = S_\nu \left[1 - \exp\left(-\tau_o / 1+(\nu/w)^2\right)\right] \qquad \ldots 3.1$$

Where S_ν , the source function, is independent of ν for L.T.E.

τ_o is the optical depth at the line centre.

In the optically thin case, $\tau_o \ll 1$, the observed profile, I_ν , is dispersive with $\frac{1}{2}$ - $\frac{1}{2}$ width W.

For τ_o large the profile is not dispersive and has a $\frac{1}{2}$ - $\frac{1}{2}$ width W' which, by solving 3.1, is given by :-

$$W'/W = \sqrt{\left(\tau_o / \ln\left(2/(1+e^{-\tau_o})\right) - 1\right)} \qquad \ldots 3.2$$

Burgess [ref.11] has shown that the shape of the profile is rather insensitive to τ_o.

Thus, if we require less than 5% increase in width due to self absorption, we require from 3.2,

$$\tau_o < 0.25 \qquad \ldots 3.3$$

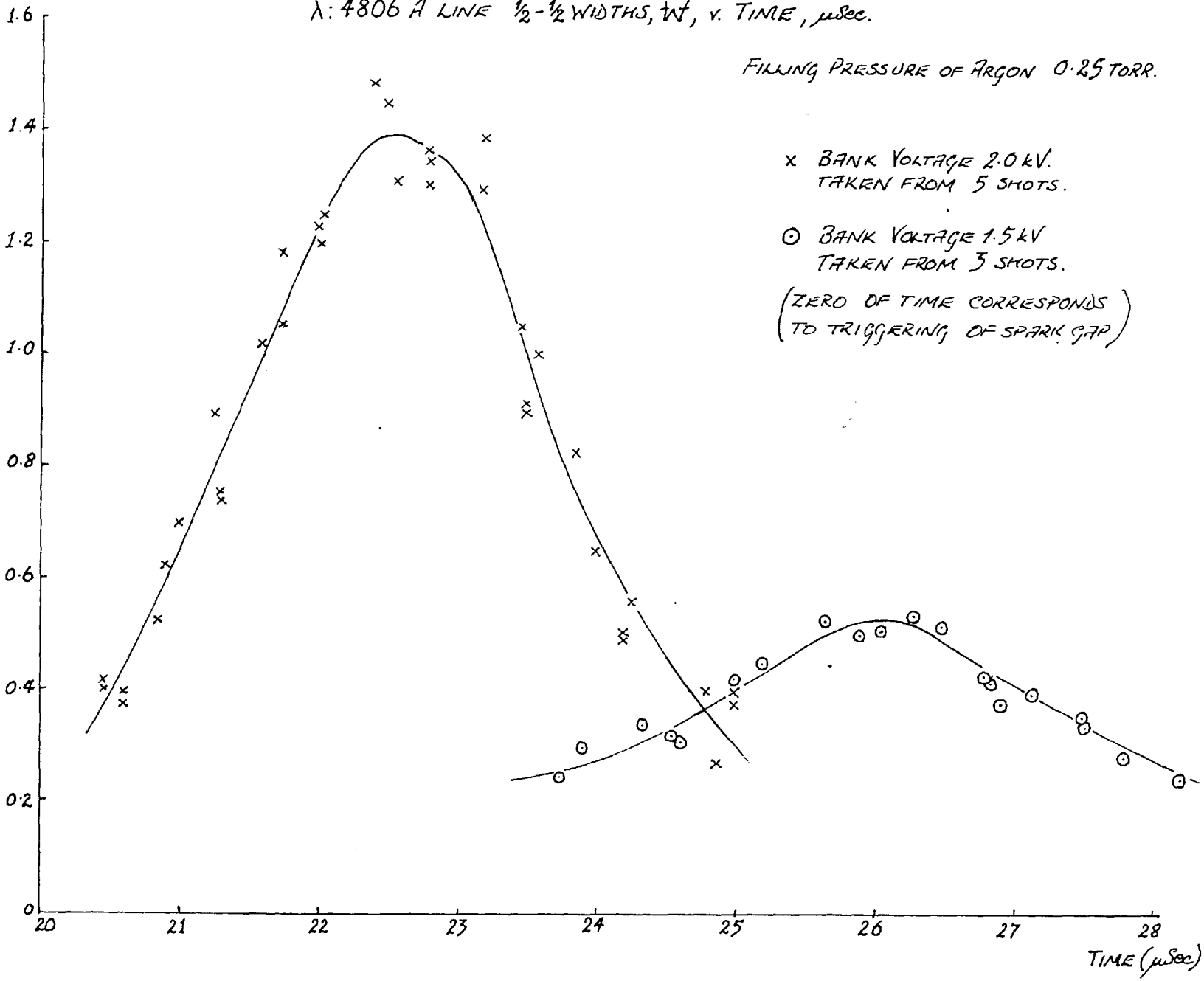
3.4 Choice of working conditions

Suitable working conditions, chosen to satisfy the above criteria, were found from a series of line profile and framing camera measurements.

Initially single shot scans of λ 4806Å AII were taken, using the procedure outlined in Section 2.7, for a variety of different bank voltages and pressures. Results of measurements of W at two bank voltages are shown in Fig. 3.1. The excellent reproducibility of the results of several shots is readily seen on this figure. Measurement of W for quantitative purposes was best done at peak compression where W was quasi-stationary.

Measurements at higher voltages proved unsuitable due to the large line widths obtained (violating the criterion in Section 3.3) or, at lower filling pressure, because the time variation of W was too rapid for convenient measurements to be made.

Framing camera photographs were taken of the discharge for bank voltages of 1.5kv and 2.0 kv using a Barr and Stroud type C.5 rotating mirror camera. The speed typically used was 0.63 μ sec per frame with an exposure time $\sim$ 0.3μ sec per frame. Framing camera photographs, current waveforms and total intensity of λ 4806Å were monitored simultaneously under each of the following conditions.


λ: 4806 Å LINE ½-½ WIDTHS, Wt, v. TIME, μSec.
FILLING PRESSURE OF ARGON 0·25 TORR.
× BANK VOLTAGE 2·0 kV. TAKEN FROM 5 SHOTS.
⊙ BANK VOLTAGE 1·5 kV TAKEN FROM 3 SHOTS.
(ZERO OF TIME CORRESPONDS TO TRIGGERING OF SPARK GAP)
1·6
1·4
1·2
1·0
0·8
0·6
0·4
0·2
0
20
21
22
23
24
25
26
27
28
TIME (μSec)

Filling pressure (Torr)	
1.5 kv	2.0 kv
Breakdown irrepro-ducible	0.11
0.25	0.25
0.50	0.50
1.0	1.0

The camera aperture was adjusted so that overexposure of the film was avoided in order to allow rough measurements of the 'pinch diameter' to be made.

Under all the above conditions the peak compression seen from the framing camera photographs was seen to coincide in time with the peak AII line emission and continuum emission and with maximum width of the line profiles. Thus the peak Ne and Te occurred at peak compression.

No conclusive difference was seen when photographing with a red filter to pick out AI (whose line emission is strongest in the red) or a blue filter for AII.

Breakdown of the discharge tube was not very reproducible at 0.11 torr, 1.5 kv. Also the pressures higher than 0.25 torr showed larger pinch diameters with consequently greater possibilities for self absorption [ref.27].

Therefore the most convenient conditions decided on were 1.5 kv and 2.0 kv at a filling pressure of argon of 0.25 torr.

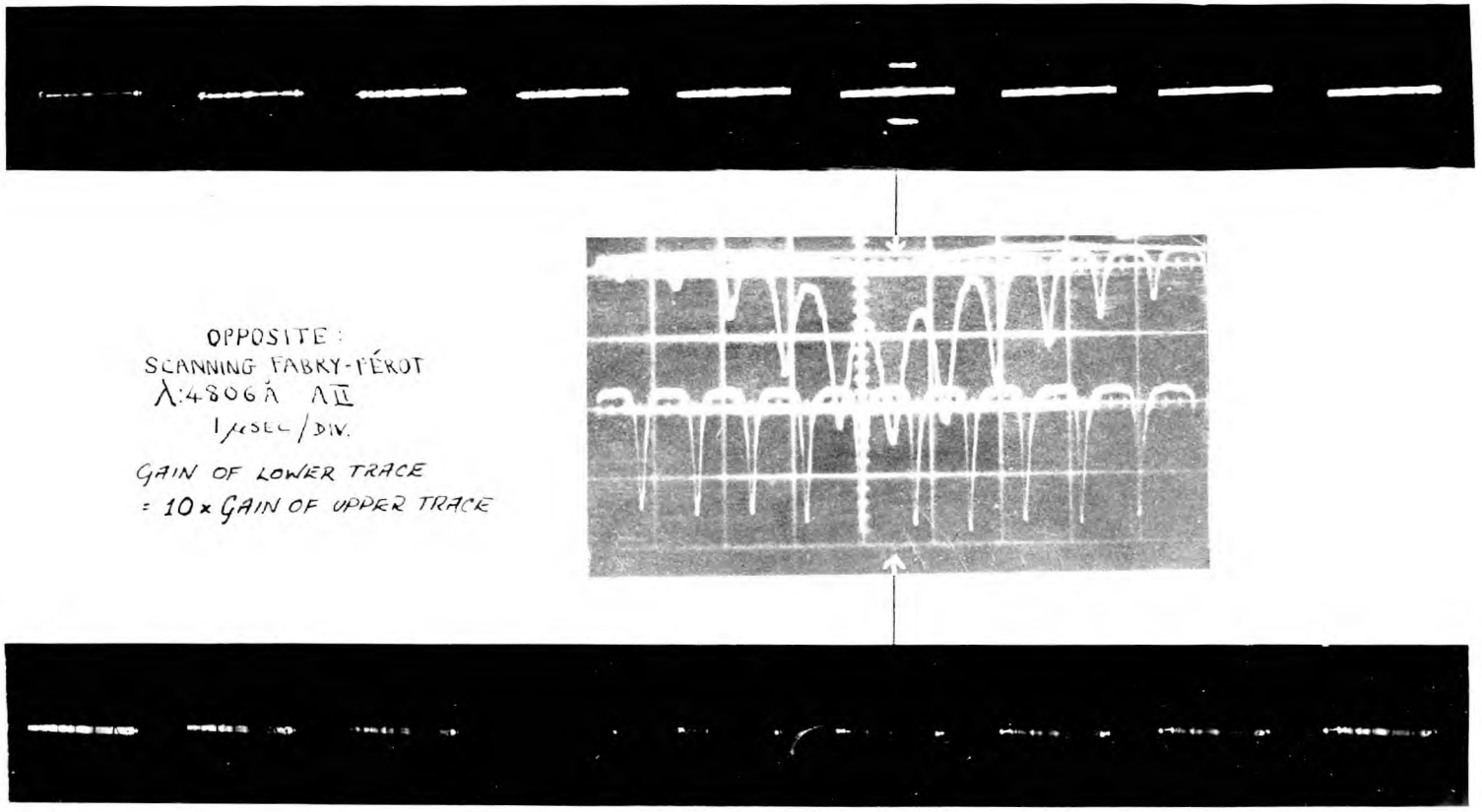
FIG 3.2. LINEAR PINCH IN ARGON

TIME CORRELATION OF λ : 4806 Å LINE PROFILES AND FRAMING CAMERA PHOTOGRAPHS

BANK VOLTAGE : 2·0 kV. FILLING PRESSURE : 0·25 TORR. FRAME INTERVAL 0·6μS.

DISCHARGE TUBE DIAMETER INDICATED ON FRAME 11.

FRAME 11



OPPOSITE :
SCANNING FABRY-PÉROT
λ:4806 Å AII
1 μSEC / DIV.

GAIN OF LOWER TRACE
= 10 × GAIN OF UPPER TRACE

FRAME 22

A typical Fabry-Pérot fringe sequence taken at 2.0 kv, 0.25 torr for λ 4806Å is shown in Fig.3.2. Also shown in this figure are the time correlations with the framing camera photographs. The total AII line intensity is correlated with the frame number in Fig. 3.3

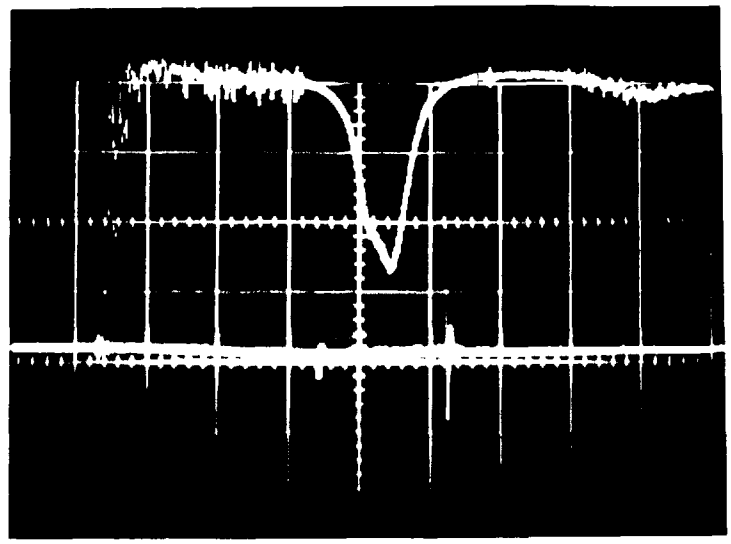


Fig 3·3 upper trace: AII line intensity.

lower trace: Framing camera pulses.

1st pulse (−ve) ≡ 3rd frame.

2nd pulse (+ve) ≡ 17·5th frame.

(5 μsec / div.)

3.5 Check of optical thinness of plasma

It is necessary to show that the plasma was optically thin under the two conditions chosen, for the strongest line studied (i.e. λ 4806Å). Since the purpose of this work was to measure line widths it was convenient to put these to additional use as a test of optical depth, using a method suggested by Burgess [ref. 11].

This test consists of the comparison of the observed widths of lines, 2W', which should have equal widths, 2W, in the limit $\tau_o \ll 1$. If these lines have different strengths then the values of τ_o and hence W' will be different irrespective of the value of W.

The best line to use with λ 4806Å for this test is λ 5062Å due to the widely differing strengths of these two lines. Also Griem [ref.2] quotes the optically thin widths as equal (in frequency units).

For these singly ionised lines τ_o can be expressed in the form [ref.27] :-

$$\tau_o = \left(\lambda^4/8\pi^2 U_1 c\right)\left(g_m A_{mn} N_1/\Omega(T_e) N_e\right) \exp\left(-W_n/kT_e\right) \times \left(1-\exp\left(-h\nu/kT_e\right)\right) S \qquad \ldots 3.4$$

Using equations 3.2 and 3.4 the ratio of the observed widths of λ 4806Å and λ 5062Å can be evaluated as a function of τ_o for λ 4806Å. This relation is plotted in Fig.3.4.

Thus if the minimum detectable difference in widths of these lines were 10% an upper limit to τ_o of about 0.4 could be set for λ 4806Å and correspondingly about 0.06 for λ 5062Å.

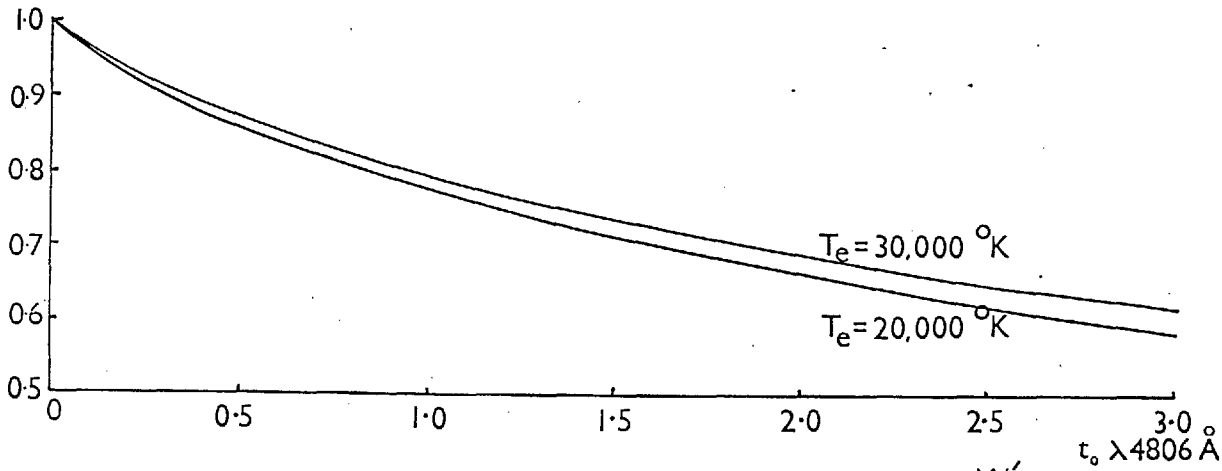


Fig. 3·4 Ratio of optically thick widths of $\lambda 5062$ Å to $\lambda 4806$ Å, $\frac{W'_{5062}}{W'_{4806}}$, versus t_o for $\lambda 4806$ Å

These figures would correspond to $\sim$ 10% increase in broadening of λ 4806Å and $\sim$3% for λ 5062Å.

The usefulness of this test lies in the fact that absolute values of Ω (Te) need not be known. Other cases of lines of equal W, for which this test could be used, could be expected as follows :-

(1) Assuming, as in Griem's theory, that the lower state broadening of lines can be neglected then all lines which arise from the same upper state should experience the same electron impact broadening and shift (in frequency units).

The justification of this assumption in the case of heavy element emitters will be discussed in Chapter 9.

(2) All lines within a particular multiplet will have approximately the same impact widths and shifts for the upper state (again in frequency units). This is because the perturbing level schemes will be much the same for all levels within a multiplet (assuming relatively small J-splitting compared with l-splitting). Thus if lower state

broadening is neglected these lines would be expected to have the same resultant widths and shifts. In fact, Griem has calculated the parameters Ω and k/Ω for the strongest line in each multiplet only. Again the justification of the above assumption will be discussed more fully in Chapter 5.

The experimental ratio of line $\frac{1}{2}$ - $\frac{1}{2}$ width, to that of λ4806Å for λ5062Å and two other lines of multiplet 6 is shown below:-

(The measurements were made at peak compression at 2.0 kv and a filling pressure of 0.25 torr.)

Line Å	Optically thin ratio (frequency units)	Optically thin ratio (wavelength units)	Measured ratio (wavelength units)
4833	1.00	1.06	1.05
5062	1.00	1.07	1.10
4848	1.00	0.93	1.01

The experimental error in these ratios was $\sim$10% so that to within this error all these lines were optically thin.

The same conclusions were obtained for the conditions 1.5 kv, 0.25 torr.

3.6 Measurement of other AII line widths

A total of nine AII lines were studied under both conditions chosen in 3.4. Since $\lambda 4806\text{Å}$ was the strongest of these all lines could be assumed optically thin from Section 3.5. Further an estimate of the Zeeman splitting of each line could be made knowing the current at the pinch and the relative intensities and splitting of the components from ref.28. Assuming every Zeeman split component had the same Stark width the increase in width for all lines was $< 1\%$.

A typical line profile is shown in Fig.3.5. This figure also shows the good fit of the experimental profile to the expected dispersive shape, which was found for all lines studied. The effects of plasma inhomogeneity - which would tend to give asymmetric non-dispersive profiles - would therefore appear to be small.

It seems most likely therefore that the dominant broadening mechanism for all the lines studied was electron impact giving a line $\frac{1}{2}$ - $\frac{1}{2}$ width W. The measure values of W are tabulated in Fig.3.6 for the nine lines studied.

3.7 Discussion of results

Using Griem's values of Ω (Te) and 1.8 together with the values of W tabulated in Fig.3.6 the corresponding values of Ne for each value of W are tabulated in Fig.3.7.

Burgess' value of Te = 26,000°K was used for the 2.0 kv, 0.25 torr measurements. The same value was used for 1.5 kv, 0.25 torr. This is not too unreasonable as the values of Ω are rather slowing varying functions of Te

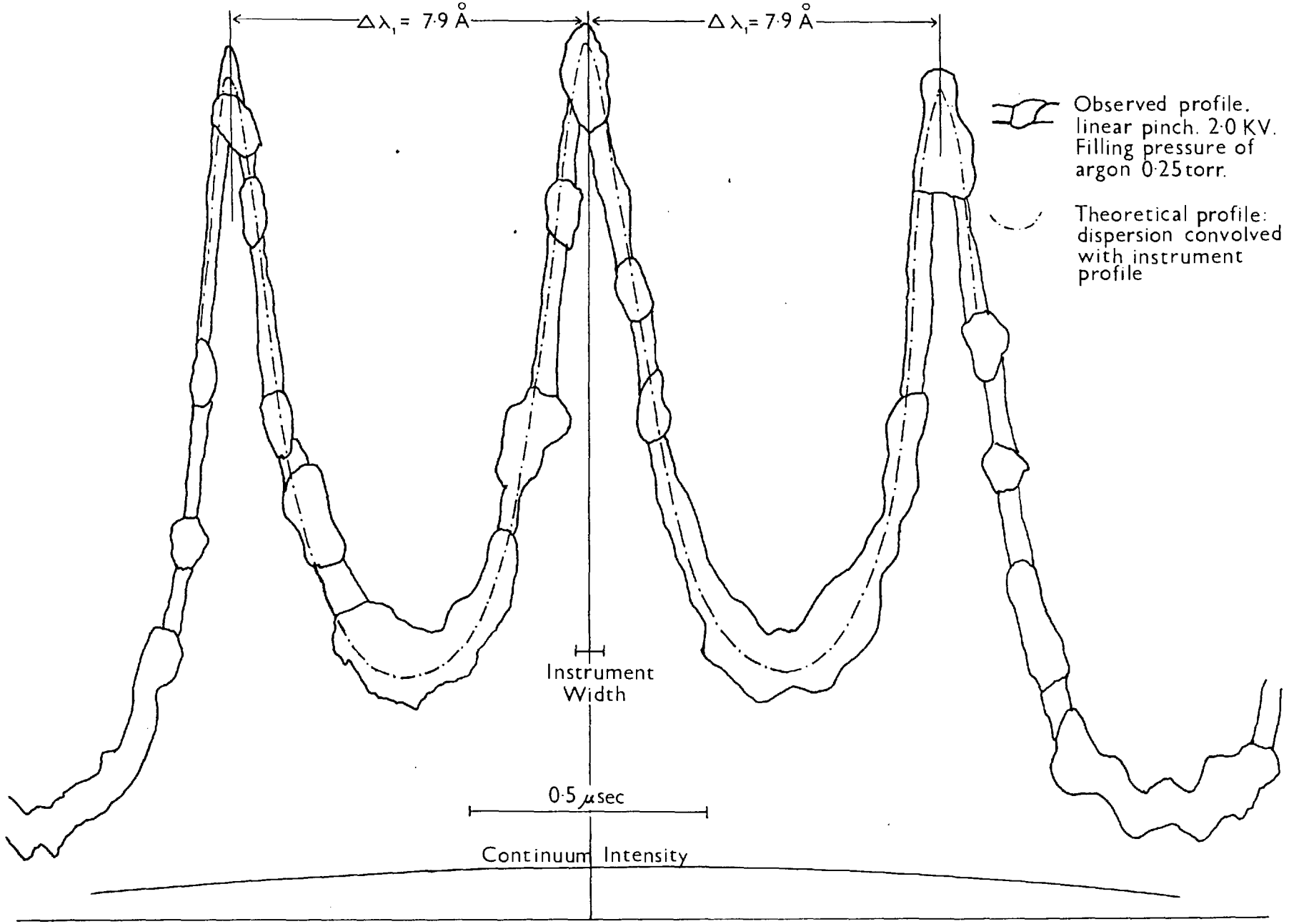


Fig 3·5 Comparison of theoretical with observed line profiles. (λ 4848 Å A II)

FIGURE 3.6

MEASURED $\frac{1}{2}$ - $\frac{1}{2}$ WIDTHS, W, OF SOME AII LINES

LINEAR PINCH : 0.25 TORR FILLING PRESSURE OF ARGON

Multiplet number	Line (Å)	Transition Lower - Upper	Tube volts (kv)	W (Å)
1	4460.6	$3d\,^4D_{2\frac{1}{2}} - 4p\,^4P^o_{2\frac{1}{2}}$	1.5 2.0	0.35 ± 0.03 0.75 ± 0.08
2	4013.9	$3d\,^4D_{3\frac{1}{2}} - 4p\,^4D^o_{3\frac{1}{2}}$	1.5 2.0	0.43 ± 0.08 /
6	4806.1	$4s\,^4P_{2\frac{1}{2}} - 4p\,^4P^o_{2\frac{1}{2}}$	1.5 2.0	0.53 ± 0.04 1.40 ± 0.10
	4933.2	$4s\,^4P_{1\frac{1}{2}} - 4p\,^4P^o_{1\frac{1}{2}}$	1.5 2.0	0.49 ± 0.04 1.48 ± 0.13
	4847.8	$4s\,^4P_{1\frac{1}{2}} - 4p\,^4P^o_{\frac{1}{2}}$	1.5 2.0	0.49 ± 0.04 1.30 ± 0.10
	5062.0	$4s\,^4P_{\frac{1}{2}} - 4p\,^4P^o_{1\frac{1}{2}}$	1.5 2.0	0.60 ± 0.04 1.52 ± 0.16
7	4348.1	$4s\,^4P_{2\frac{1}{2}} - 4p\,^4D^o_{3\frac{1}{2}}$	1.5 2.0	0.30 ± 0.05 0.80 ± 0.10
	4266.5	$4s\,^4P_{2\frac{1}{2}} - 4p\,^4D^o_{2\frac{1}{2}}$	1.5 2.0	0.34 ± 0.05 1.10 ± 0.07
10	3850.6	$4s\,^4P_{1\frac{1}{2}} - 4p\,^4S^o_{1\frac{1}{2}}$	1.5 2.0	0.71 ± 0.20 /

[ref. 2]. In any case Te cannot be appreciably different for the two conditions. This is because the differences in Ne given in Fig.3.7 can largely be accounted for by the relative compression ratios estimated from the framing camera photographs.

FIGURE 3.7

Line used (Å)	Ne(units of $10^{18}cm^{-3}$)	
	1.5 kv	2.0 kv
4460.6	0.99	2.6
4013.9	1.1	-
4806.1	0.72	1.9
4933.2	0.63	1.9
4847.8	0.64	1.7
5062.0	0.71	1.8
4348.1	0.71	1.9
4266.5	0.83	2.7
3850.6	-	1.7

The average value of Ne (at 2.0kv) is in good agreement with the results of Burgess and Grieg [refs. 11 and 6 respectively). However, some discrepancies - which are outside experimental error - occur in the table:-

(1) λ4460Å has a smaller width than λ4806Å though the two lines have the same upper state (Fig.3.6). This suggests that lower state broadening accounts for the difference in widths. The fact that the lines of multiplet 6 appeared internally consistent with the assumption

of no lower state broadening (Section 3.5) is not necessarily contradictory to this. The lower levels of the multiplet 6 lines, as the upper levels, are of the same term and do no differ much in energy so the resultant widths (with lower state broadening important) could quite easily be the same.

Also the value of Ne obtained from λ 4460Å was larger than that from λ 4806Å. This is because Griem quotes different values of Ω (Te) for these lines even accounting for the λ^2 factor in conversion to wavelength units. More definitely d/W (which is independent of λ) has quoted values which are completely different and in opposite directions. Since Griem has only considered the upper state of each line in his calculations [ref. 2] the quoted parameters for at least one of the lines must be incorrect.

(2) The widths of the lines of multiplet 7 differ. These lines have the same lower state so we cannot account for this by (1). Also the stronger line (λ 4348Å) is narrower so that reabsorption cannot account for this. It seems most likely, therefore, that the difference is caused by the different upper states. This conclusion is rather disturbing from the point of view of the optical depth test but the overall consistency of the four multiplet 6 lines suggest that reabsorption is, in fact, unimportant.

Again the widths of the λ 4348Å line differs from the multiplet 2 line λ 4014Å in spite of the common upper state. This is again indicative of the importance of lower

state ' · interactions. Similar to (1), Griems quoted values of d/W for the two multiplets are different.

To summarise, we have shown that the Z-pinch provides a useful tool for studying Stark broadening. It is easy to attain suitable values of W and thus Ne with this device and therefore enable measurements of W to be made without other sources of broadening being of any importance. The effect of reabsorption seems unimportant and the symmetry of the observed profiles suggest that effects of plasma inhomogeneity are also unimportant.

We have shown from the relative line width measurements that discrepancies occur from Griem's calculated widths in such a way as to indicate unwarranted simplifications have been in the theory.

However, it is obviously desirable to put the above results on a more quantitative basis, i.e. primarily by making an independent measurement of Ne. At the time this work was done it was not thought possible (unjustifiably as seen later in Chapter 6) to make an accurate independent measurement of Ne on this discharge.

Measurement of the width of a line with a checked broadening parameter was not favoured. There were many reasons for this.

Firstly, one would have to rely on neutral species on which values of Ω have been checked, (see Fig. 1.1). If the neutral element had a low ionisation potential the element would either be largely ionised under our conditions or the lines too broad to be observable (say $\sim$ 100Å for AI

lines). For an element with a high first ionisation potential demixing problems could occur and the lines could still be so broad that working conditions, not satisfying Section 2.5, would have to be tolerated.

In any case, though this method could (and has) been used under different conditions it is not strictly an independent measurement [see Chapter 5].

As any absolute line measurements are rather susceptible to experimental error,and in any case the internal consistency of measured AII line oscillator strengths at this time. was poor [ref.29], attention was turned to the possibility of measuring Ne from the plasma refractivity.

It was thought that large gradients of Ne in an unstabilised pinch would cause refraction of a laser beam probe out of the plasma. Therefore attention was turned to the possibility of measuring the refractivity, using a laser, on the more diffuse plasma produced by a stabilised discharge.

This forms the topic of the following Chapter.

CHAPTER 4

STUDY OF AII LINE BROADENING USING A B_z STABILISED, PINCHED PLASMA

4.1 Introduction

The main reason for transferring attention to the B_z stabilised pinch as a source was to allow measurements of Ne to be made, independent of any assumption in Stark Broadening Theory, to correlate with measured electron impact broadened line widths. This device was used since Dangor and Wheeler [ref.32] had already shown the feasibility of making laser interferometric measurements of Ne on the plasmas produced.

In particular attention was concentrated on $\lambda 4880\text{Å}$, AII. The Stark width of this line was required for use in estimating electron temperatures in the plasma by a method suggested by Burgess and Cooper [ref.27]. This method involved measurement of τ_o, for the $\lambda 4880\text{Å}$ line emitted by a L.T.E. argon plasma, by means of resonant absorption of the AII laser line $\lambda 4880\text{Å}$. These absorption measurements were performed by another member of this department (Troughton, to be published).

We shall also discuss some measurements of Te using the same basic suggestion of Burgess and Copper but employing measured optically thick line widths. This method had the advantage, in our case, that the absolute value of the optically thin Stark widths [or Ω(Te)] need not be known.

4.2 Source used

The source consisted of a Z-pinch discharge in a tube of 9.2cm internal diameter with an inter-electrode distance of

38cm. This was driven by a condenser bank of 1000μ.f.d. which could be charged up to 5 kv. and triggered by a single spark gap.

Provision was made for the application of a B_z stabilising field by discharging a 'bank' of capacity 2000μ.f.d., at voltages up to 5 kv, through a coil around the discharge tube. The current in this coil could be crowbarred at its first maximum to provide a magnetic field constant in space and time to within 5% throughout the duration of a discharge.

The device was designed and built by A.E.Dangor and C.B.Wheeler of the Plasma Physics Department and a comprehensive discription of the apparatus will appear in the former's Ph.D. thesis (to be published).

4.3 Initial diagnostics of the B_z pinch

An extensive investigation of the characteristics of various laser systems for the measurement of plasma refractivity has been performed by Dangor (to be published) and Dangor and Wheeler [ref.32].

For our measurements a Mach-Zehnder system was adopted, giving good time response and high luminosity. The integrated refractivity along the tube axis was determined with a Helium-Neon laser operated at λ6328Å [Fig.4.1].

The line profiles were viewed perpendicular to the plasma column using an AII laser to line up on λ4880Å [Fig.4.1].

The timing system shown in block form in Fig.4.2 was used to enable simultaneous measurements of both Ne and the line profiles. The crowbar was triggered at the first half cycle peak of the magnetic field and the discharge triggered

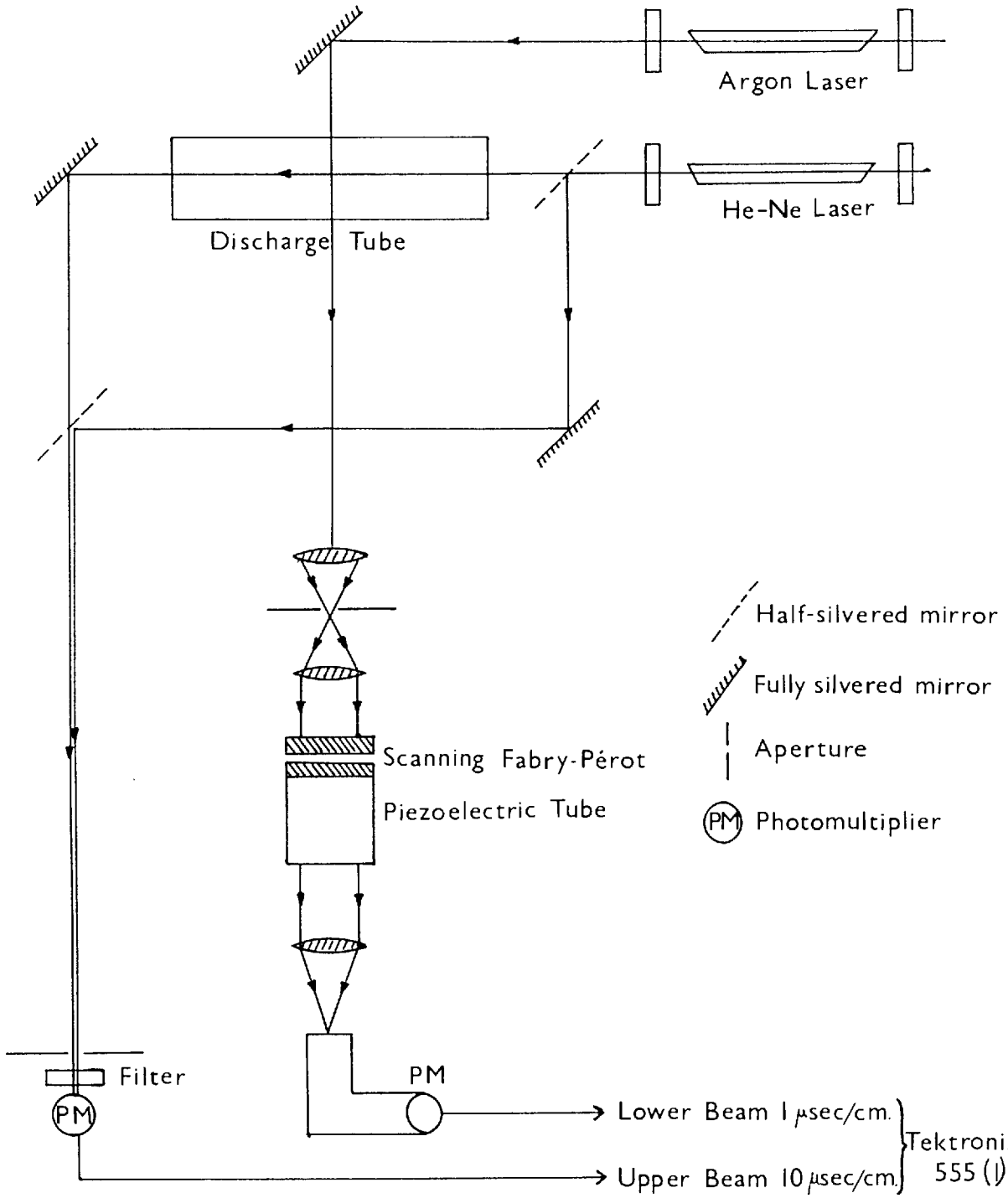


Fig. 4·1 B_z stabilised Z-pinch, optical system.

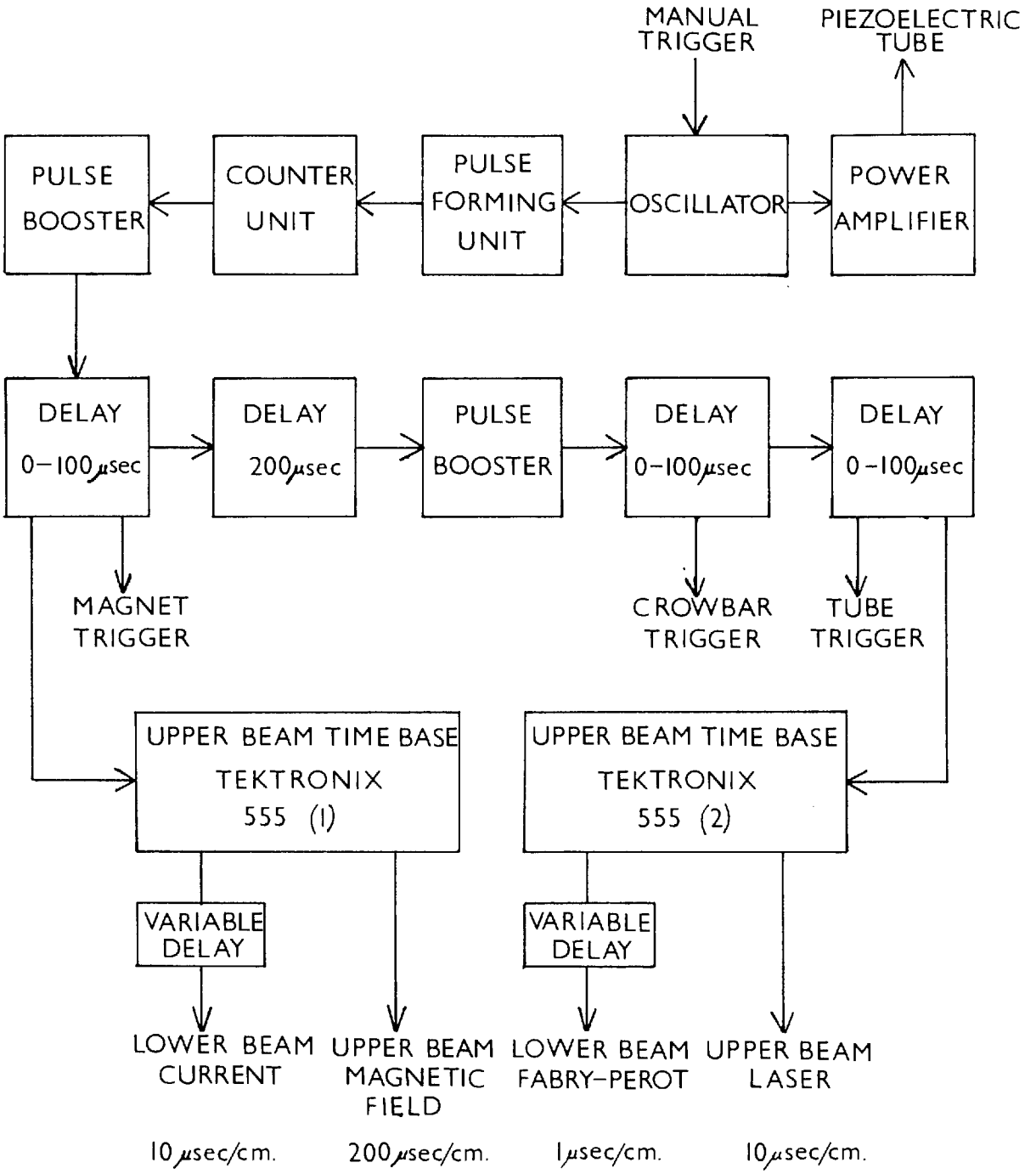


Fig. 4·2 B_z stabilised Z-pinch. Block diagram of control system.

$\sim$100μsec later so that a uniform B_z field existed during the plasma's lifetime. The sequence of laser fringes and the S.F.P. profiles were recorded and correlated in time on a Tektronix 555 C.R.O. with provision for delaying the time base of one beam. The B_z field and discharge current could be similarly recorded.

Preliminary spectra were taken with a Hilger medium quartz spectrograph. These spectra, taken at a filling pressure of argon of 0.20 torr and a variety of discharge conditions, showed predominantly the lines of singly and doubly ionised argon. Some of the lines which were investigated in this work are indicated on Fig.4.3.

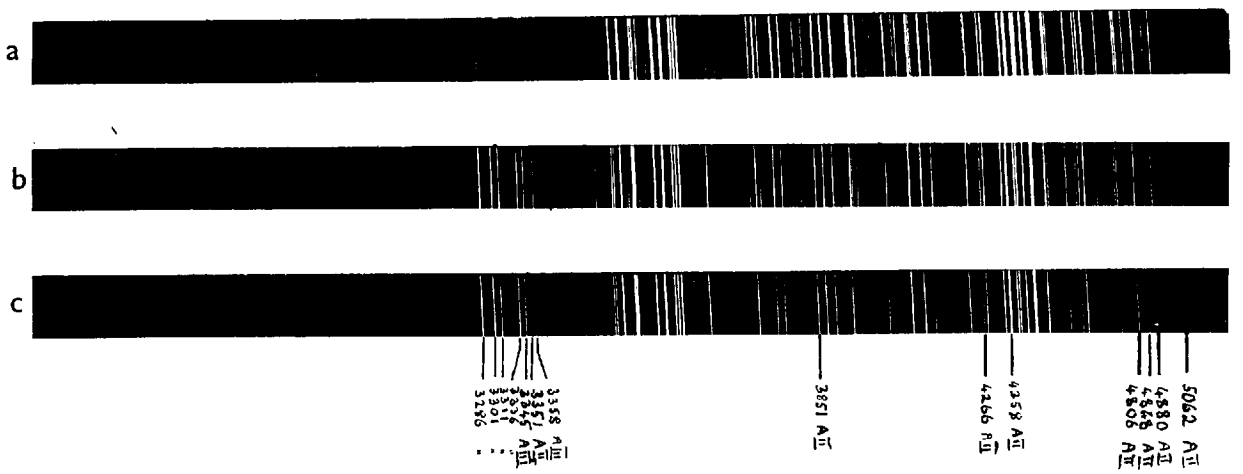


Fig 4-3 Medium Quartz Spectrograph.
Argon, 0·20 torr. B_z = 5 Kgauss.
Bank voltage. a) 1·0 k.v.
b) 1·5 k.v.
c) 2·0 k.v.

Initial simultaneous measurements of Ne and the line profiles were very reproducible from shot to shot for given initial conditions of filling pressure and bank voltages. Therefore, for simplicity, subsequent measurements of Ne and the line profiles were done separately. Further, the rates of growth and decay of Ne, at the conditions studied, were not fast enough for the time response of the detecting system to be critical. Therefore subsequent measurements of Ne were made with a Fabry-Pérot system since, for a given change in refractive index, this gave twice the number of fringe shifts given by the Mach-Zehnder system. Consequently Ne could be determined to twice the accuracy.

Assuming that the dominant contribution to the plasma refractive index, μ, is given by free electrons :-

$$\mu = [1-(W_p/W)^2]^{\frac{1}{2}} \backsim 1 - (Ne e^2 \lambda^2/2\pi mc^2) \qquad \ldots 4.1$$

[ref.33] where W is the probing frequency.

We shall justify in Chapter 6 that this is the main contribution to μ.

The optical path difference caused by introduction of plasma in the tube is :-

$$\left.\begin{aligned} \delta = \int_0^L \mu dl &= n\lambda \text{ (Mach-Zehnder)} \\ &= n\lambda/2 \text{ (Fabry-Pérot)} \end{aligned}\right\} \qquad \ldots 4.2$$

Where n is the number of fringe shifts

L is the tube length.

Therefore for a Fabry-Pérot system, from 4.1 and 4.2 :-

$$\overline{NeL} = 1.69 \times 10^{17} n \ \text{cm}^{-2} \qquad \ldots 4.3$$

The optical set up used is shown in Fig.4.4 and the variation of Ne with time for three bank voltages is shown in Fig.4.5. The extreme reproducibility through the first compression is shown by the two runs at 1.5 kv [Fig.4.5] Between these two runs the discharge tube was changed and pumped down to a backing pressure of 0.01 torr only.

The line profiles were obtained on a single shot basis similar to that described in Chapter 3. In the present case, however, the $\lambda 4806\text{Å}$ line was appreciably broader than $\lambda 5062\text{Å}$ showing that self absorption was important.

Results obtained at one initial condition are shown in Fig.4.6. On this figure the time scale of the line profile sequence is indicated on the time base of the laser fringe sequence. The maximum line width and peak AII, AIII and continuum intensities occur at the same time as a turning point on the laser fringe sequence. This could therefore be interpreted unambiguously as the time of peak Ne. Thus the rise and fall of Ne could be ascertained using 4.3.

Also from figures 4.5 and 4.6 it can be seen that Ne is constant to $\sim$5% over the time of the four fringes of maximum finesse shown in Fig.4.6. The continuum intensity was also nearly constant over this time. Therefore Te, and consequently Ω (Te), could be assumed reasonably constant.

The instrument profile of the S.F.P. was measured as before from an afterglow shot when Ne (from the laser measurements) had fallen to a known fraction of its peak value. The AII laser line could not be used since the high spatial coherance of the beam would give a smaller limiting solid angle, and consequently larger N_F, than for the plasma measurements.

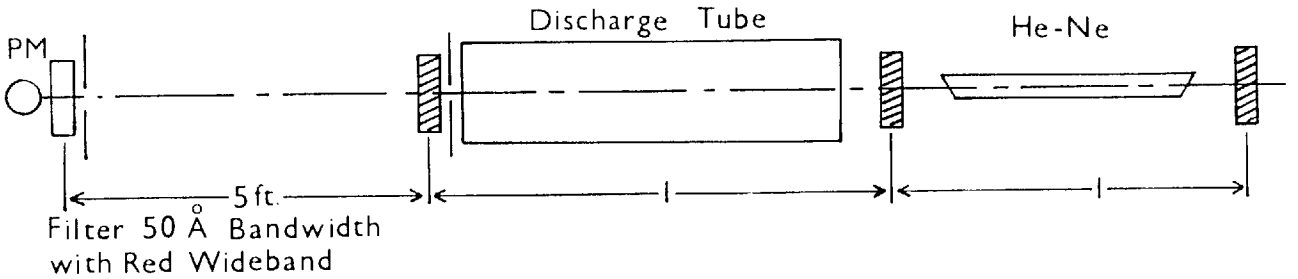


Fig 4·4 Laser Fabry–Pérot, General Arrangement.

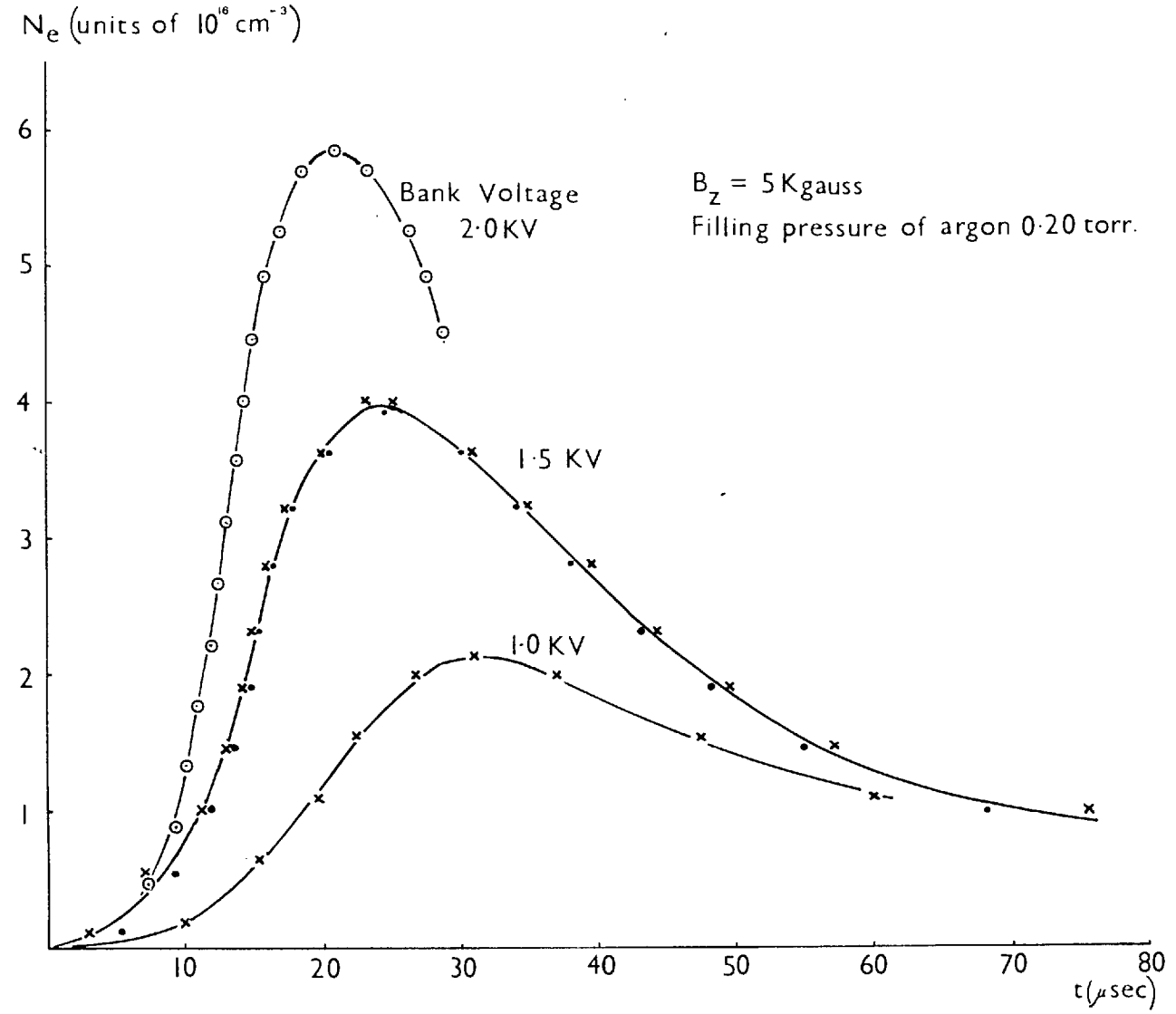
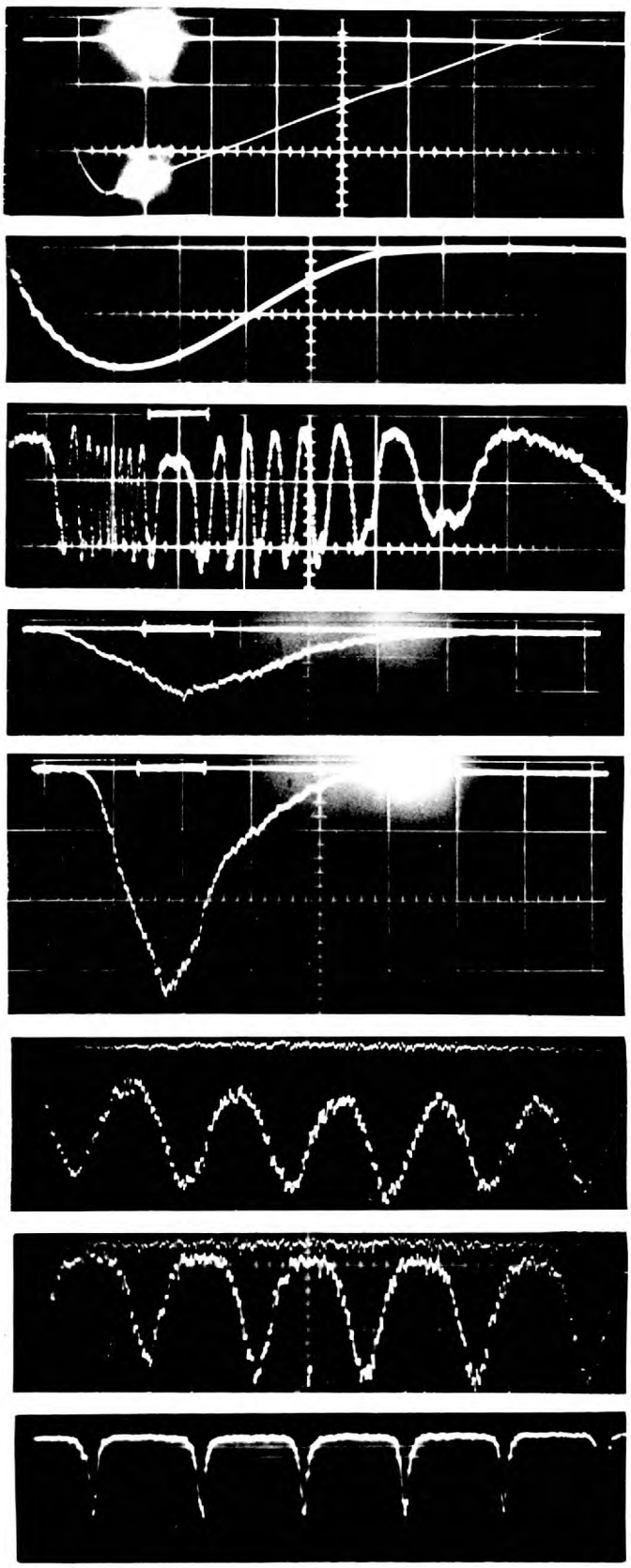


Fig 4·5 N_e integrated along axis versus t, time from zero current.

FIG 4.6.

B_z STABILISED Z-PINCH



1. MAGNETIC FIELD
   TIME BASE 200μs/cm.
   PEAK $B_z \simeq$ 5 K.GAUSS

2. CURRENT
   PEAK I $\simeq$ 75 K.AMPS

3. LASER FABRY-PÉROT
   FRINGES (6328 Å)

4. AII LINE EMISSION
   3350.9 Å

5. AIII LINE EMISSION
   3344.7 Å
   TIME BASE FOR 2-5,
   10μs/cm, CORRESPONDS
   TO BRIGHT-UP ON 1.

6. SCANNING FABRY-PÉROT
   AII, 4806 Å

7. AII, 5062 Å
   TIME BASE FOR 7 & 8,
   1μsec/cm, CORRESPONDS
   TO BRIGHT-UPS ON 2-5.

8. AII, 4806 Å
   TIME BASE, 1μs/cm,
   INITIATED 70μs.
   AFTER PEAK I.

Some results for peak Ne and corresponding line $\frac{1}{2}$ - $\frac{1}{2}$ widths, assuming dispersive profiles, are shown below :-

	Line (Å)	Measured W'	Theoretical W	W'/W
Ne	4880	0.18 ± 0.016	0.028	7.1 ± 0.6
4.0×10^{16} cm^{-3}	4806	0.16 ± 0.016	0.028	5.7 ± 0.6
± 2%	5062	0.10 ± .008	0.031	3.2 ± 0.3
Ne	4880	-	-	-
2.2×10^{16} cm^{-3}	4806	0.090 ± .008	0.015	6.0 ± 0.5
± 2%	5062	0.061 ± .006	0.0165	3.7 ± 0.4

Each measured W' quoted was the average of three shots. Also quoted are the theoretical widths assuming Griem's broadening parameters [ref.2] and arbitarily using Te = 20,000°K. The measurement of Te is discussed later in this Chapter.

4.4 Optically thin line widths

It is obvious from the previous results that the ratio of the measured width of λ4806Å to λ5062Å is much greater than one would expect if the lines were optically thin. This conclusion is independent of knowledge of Te or Ω(Te) but only makes the assumption (Chapter 3) that these lines have the same widths when optically thin.

To allow for the effects of self absorption we have to estimate the optical depth, τ_o, at the centre of each line using 3.4. $\tau_o/5$ as a function of Te and Ne is plotted in Fig.4.7 for λ4806Å and λ5062Å. At low

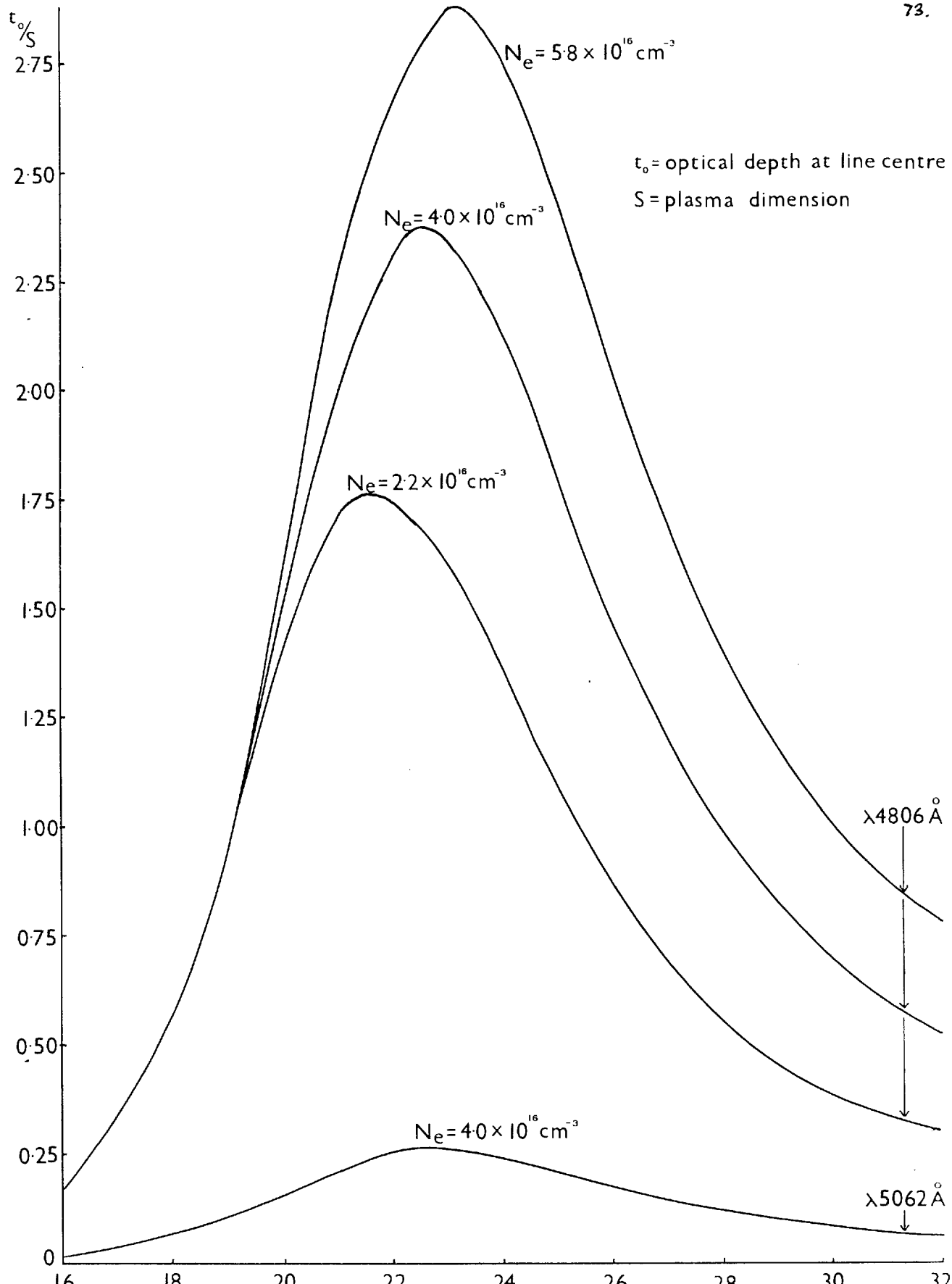


Fig. 4·7 t_o/S versus T_e for two AII lines.

temperatures this quantity is independent of Ne due to the substitution of N_1 = Ne in relation 3.4.

If the ratio of the optically thick (measured) width to the optically thin width is known, τ_o can be found from relation 3.2. This relation is plotted in Fig.4.8.

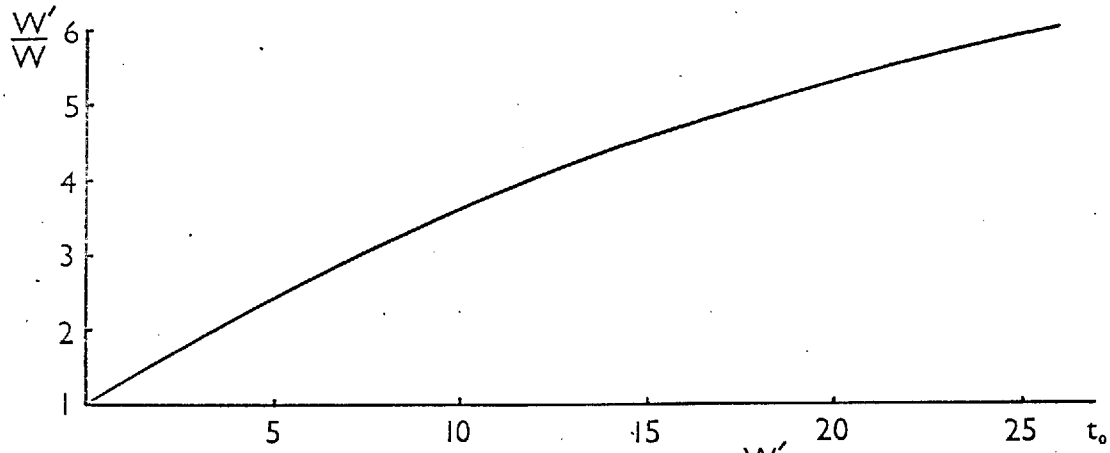


Fig. 4·8 Ratio of optically thick to thin line widths W'/W versus t_o for a dispersive profile.

Assuming the ratio W'/W for λ4806Å at Ne = 2.2 x 10^{16} cm^{-3} (above table) differs from unity on the basis of self absorption only, then from Fig. 4.8 :-

$$\tau_o = 26 \pm 4$$

However, under these conditions it can be seen from Fig.4.7 that the maximum possible value of τ_o/S is 1.72.

Thus even if we consider the plasma as filling the tube under these conditions (i.e. S = 9.2 cm) we have :-

$$\tau_{o\ max} = 15.8 \pm 0.8$$

(Estimating the error from the uncertainties in Amn, peak Ne and U_1.)

The only way the above values of τ_o can be resolved is by using a value of Ω (Te), in plotting Fig.4.7, different from the value quoted by Griem for Te = 20,000°K. If the electron temperature of the discharge were higher than W'/W would be decreased and consequently τ_o decreased. In such a case a value of τ_o inconsistent with $\tau_{o\ max}$ may not occur.

4.5 Measurement of the plasma diameter, S

To put the above discussion on a more quantitative basis it was desirable to have an estimate of S. Thus the radial distribution of continuum intensity, Ic(r), was determined.

$$Ic \alpha N_z N_e Z^2 T_e^{-\frac{1}{2}} \qquad \text{[ref.3]}$$

Therefore assuming one stage of ionisation was predominant and that radial gradients in Te were not too severe:-

$$Ic^{\frac{1}{2}} \alpha N_e ,$$

and due to macroscopic charge neutrality the $Ic^{\frac{1}{2}}(r)$ distribution should be representative of the singly ionised argon ion distribution.

Thus the distance between points where $Ic^{\frac{1}{2}}(r)$ had fallen by a factor of two from its peak value was taken as the plasma diameter, S.

The arrangement for scanning the continuum on a multi-shot basis is shown schematically in Figure 4.9. With carefully polished ends the light pipe was capable of giving a transmission ~70% in the visible. The response of the system was found by scanning a ground glass screen, illuminated with a strip lamp, by means of the moveable

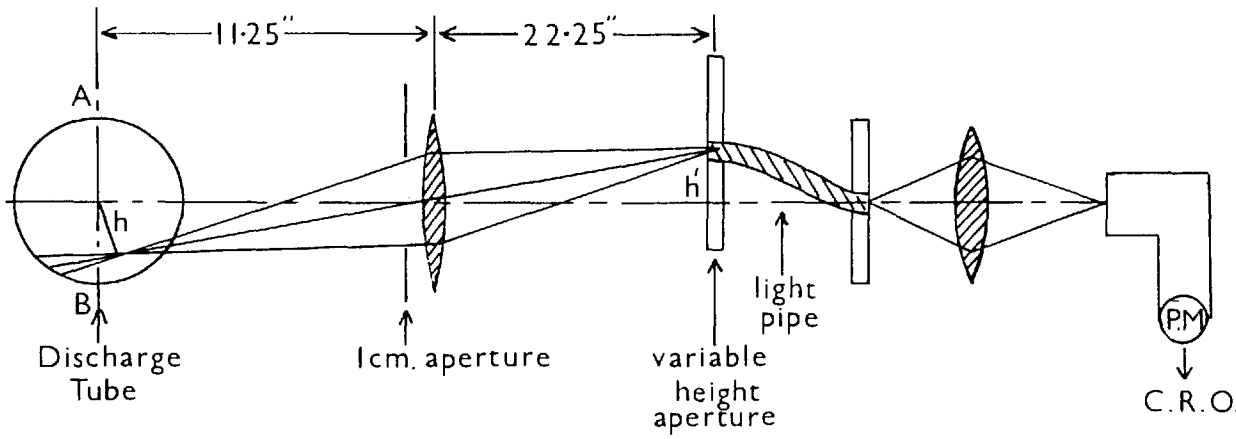
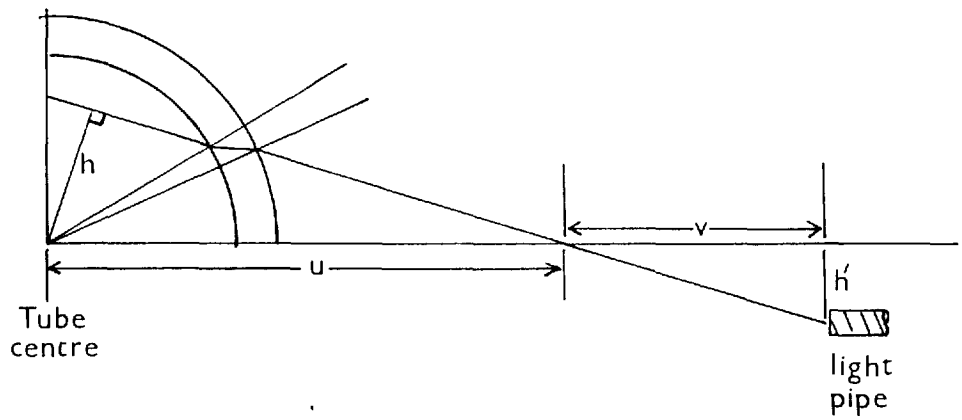


Fig. 4·9 Arrangement of apparatus for continuum intensity scanning.



Tube radius (external) = r
" thickness = dr
" refractive index = μ

Fig. 4·10 Lens effect of discharge tube.

aperture. The D.C. signal recorded was constant to ~5% over a 4cm length corresponding to the axis AB (Fig. 4.9).

The continuum band chosen was a 10Å region centred on λ5111Å, which can be seen to be line free from the spectra of Fig.4.3. The only interference to the continuum was likely to be the wings of the rather weak lines of λ5100Å and λ5121Å of AII (see references 34 and 35). This was completely negligible under our conditions. The continuum radiation across the discharge was thus recorded on a shot-shot basis using an overall response time $\simeq$0.15μ sec.

The measured heights h' were converted to distances of acceptance cone from the tube centre, h, [Fig.4.9] with a correction for the lens effect of the tube, by [referring to Fig.4.10] :-

$$h = r \sin i - dr \sin i \left[1 - \sqrt{(1-\sin^2 i)/(\mu^2-\sin^2 i)}\right] \quad \ldots 4.4$$

where $\sin i = u/(r\sqrt{1+v^2/h'^2})$ $\quad \ldots 4.5$

A smooth curve was drawn through the zonal distribution thus obtained and a 25 step Abel inversion performed using the method of Pearce [ref.36]. This was done using an Elliot 803A computor programme, similar to that described by Key [ref.37], but with provision for inputting the response of the detecting system and outputting $Ic^{\frac{1}{2}}(r)$ as a function of r.

Typical distributions of continuum intensity, before and after inversion, are shown in Fig.4.11. Values of S obtained at different conditions are tabulated below :-

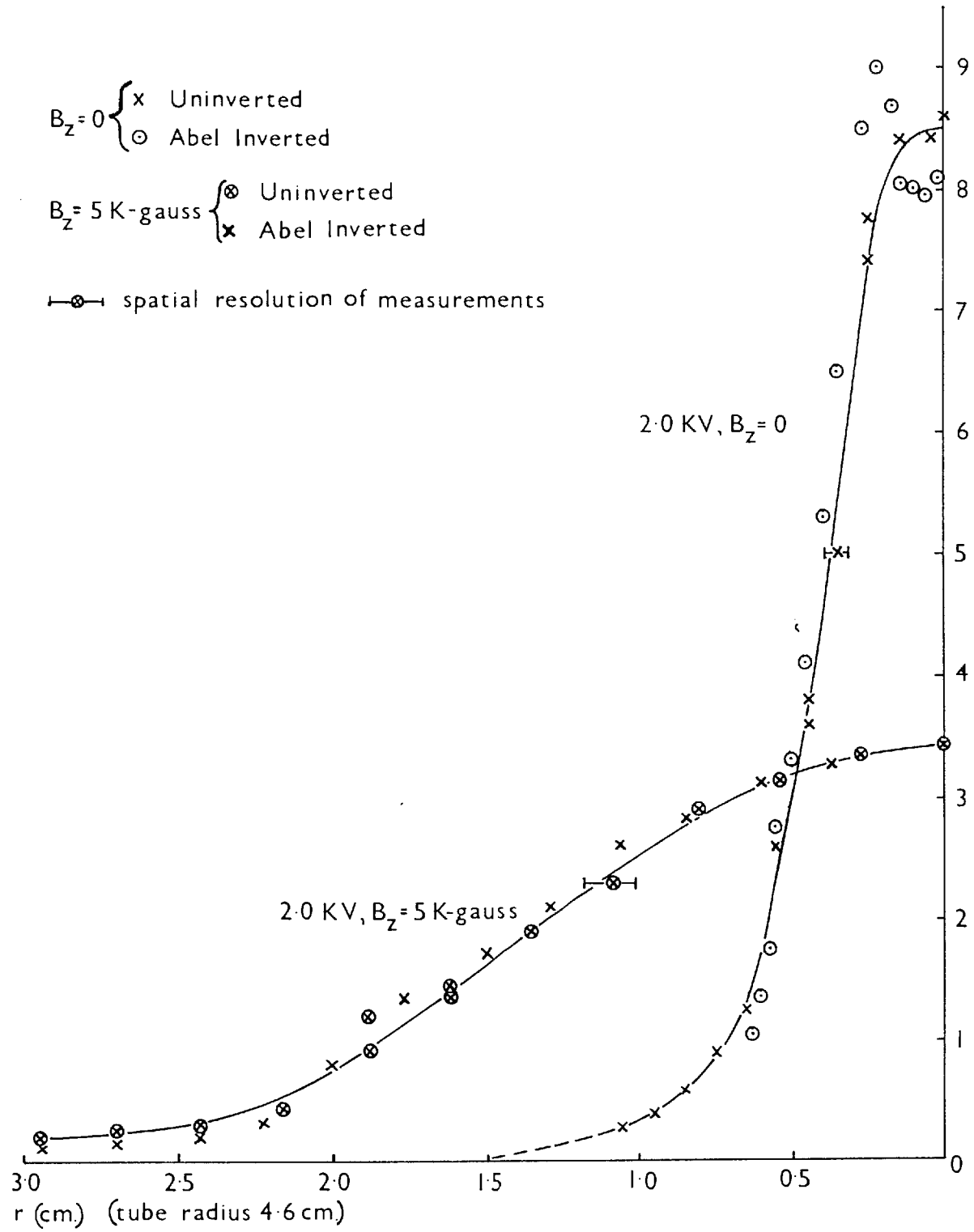


Fig 4·11 Radial distribution of continuum intensity. Arbitrary intensity scale. Filling pressure of argon, 0·20 torr.

Plasma diameter (5 cm) at peak compression

Discharge voltage (kv)	1.0	1.5	2.0
Bz = 0	2.6	1.4	1.15
B~5k Gauss	7.5	4.8	4.0

4.6 Correction for optical depth

On using these measured values of S the discrepancies in τ_o become larger. As discussed above, such a situation could only occur due to a discrepancy in Ω. We shall therefore assume the correct value is $k\Omega$ and attempt to estimate k.

Both W'/W and τ_o will be reduced by a factor k so 3.2 gives :-

$$W'/kW = \left(\left[\tau_o/k\sqrt{\ln\left(2/(1+e^{-\tau_o/k})\right)}\right]-1\right)^{\frac{1}{2}} \quad \ldots 4.6$$

For $\tau_o/k > 4$ this can be simplified to :-

$$k^2 - (\tau_o/0.69)\,k + (W'/W)^2 = 0 \quad \ldots 4.7$$

Neglecting the positive root, since this would correspond to the physically impossible situation in L.T.E. of $W'/kW < 1$, we have :-

$$k = \tau_o/1.38 - \left((\tau_o/1.38)^2-(W'/W)^2\right)^{\frac{1}{2}} \quad \ldots 4.8$$

The solution of 4.8 using the results for W'/W at Ne = 4×10^{16} cm^{-3} is shown graphically in Fig.4.12. τ_o for λ5062Å as a function of that for λ4806Å was found from Fig.4.7. The error limits on the plotted curves are from

the estimated errors in W'/W.

A unique value of k is obtained as a solution:-

$$k = 2.72 \pm 0.4$$

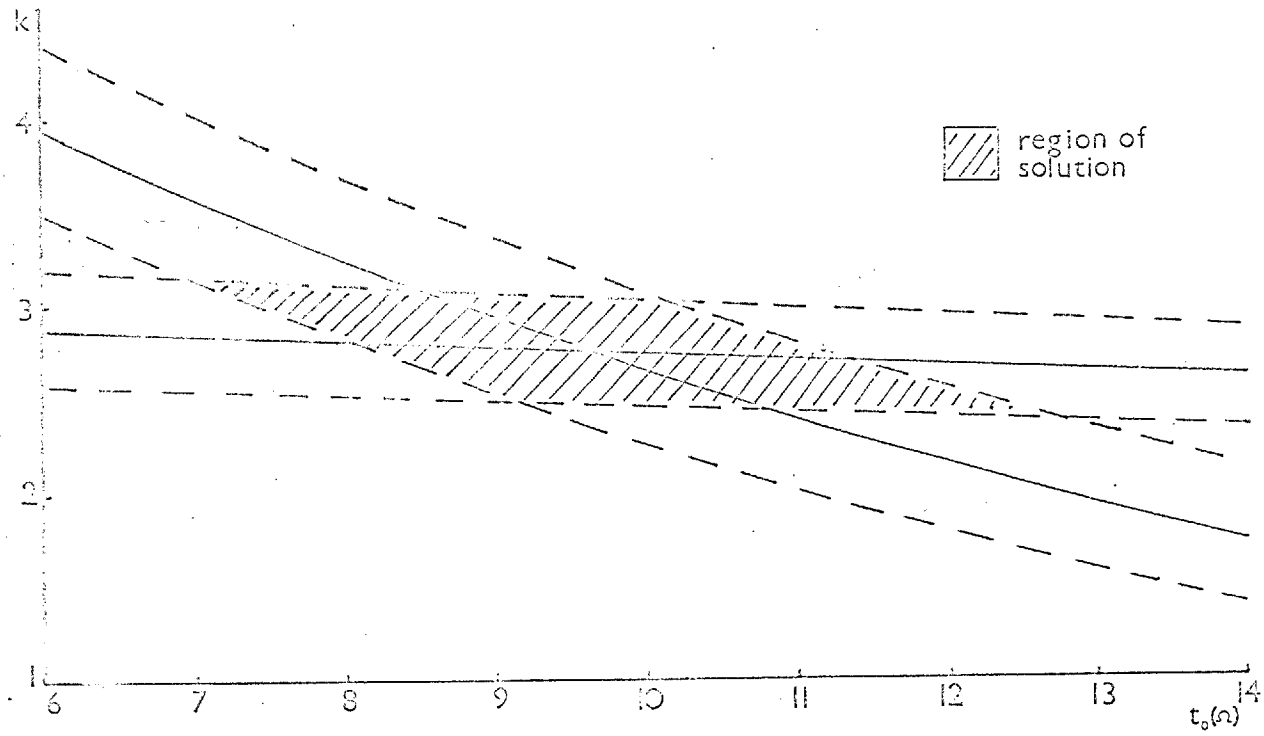


Fig 4.12 Correction factor, k, to line width, ΩN_e, versus $t_o(\Omega)$ (λ 4806 Å)

Thus Griem's value of $\Omega(Te)$ at 20,000°K must be multiplied by 2.72 ± 0.4 to give internally consistent values of W'/W for λ4806Å and λ5062Å. If the theory is assumed to be correct then to give $\Omega(Te) = 2.72\Omega(Te=20,000^{\circ}K)$ we require the plasma temperature, $Te > 100,000^{\circ}K$. At such temperatures AII would be completely burnt out contrary to

the experimental observations. Thus the calculated values of Ω must be incorrect.

4.7 Estimation of Te from AII line widths

To estimate the magnitude of the discrepancy between experimental and calculated widths it is necessary to know Te. An estimate of this can be made, from the results already described in Section 4.6, as follows :-

The upper limit to τ_o for λ4806Å from Fig.4.7 and using the value for S tabulated above is :-

$$\tau_{o_{max}} = 11.2 \pm 1.1$$

This was effectively calculated by considering a slab of plasma of thickness S and infinite extent. Burgess [ref.11] has shown that for a cylindrical plasma the effective τ_o can be reduced by ~20% from this figure. In either case $\tau_{o_{max}}$ is within the limits given in Fig.4.12

Also from Fig.4.12 the lowest value of τ_o consistent with the other results is :-

$$\tau_{o_{min}} \simeq 7$$

Thus from Fig.4.7 and using the measured value of S we should expect Te to line between 20,000°K and 26,000°K.

i.e. $Te = 23{,}000^{\circ}K \pm 3{,}000^{\circ}K$

For this Te the calculated Ω is 7.3×10^{-3}Å.

We obtain Ω (Te = 23,000°K) = 2.72 Ω (Te = 20,000°K)

$= (19 \pm 2) \times 10^{-3}$Å.

We therefore conclude that the calculated broadening parameter is more than a factor of two too low. A similar

conclusion is reached for $\lambda 4880\text{Å}$ since the measured width and calculated width and reabsorption is nearly the same as for $\lambda 4806\text{Å}$.

4.8 AIII line widths

In the work described above the optically thin widths of three AII lines were inferred from measurements of optically thick profiles without assuming the calculated Ω's. Nevertheless additional errors arose in making corrections for self absorption as compared with a study of optically thin lines.

The possibility of studying AIII lines was therefore investigated. This did not interfere with the original object of this work since, in general, the effects produced by hyperbolic orbits of the electron perturbers would be more pronounced than for AII lines. Further, if measured line widths much greater than the calculated values were found then Stark broadening as a method of determining Ne could be extended to much higher temperatures than hitherto thought possible. In addition continuous laser action has been reported for several AIII lines [ref.38] so that AIII Stark widths would be of importance for plasma diagnostics by means of resonant interaction with an argon plasma [ref.39]

τ_o was estimated for the AIII lines of multiplets one to three using 3.4 with N_1 and U_1 replaced, respectively, by N_2 and U_2. No information existed on AIII transition probabilities so these were calculated on the Coulomb approximation [ref.31] :-

AIII TRANSITION PROBABILITIES (COULOMB APPROXIMATION)

Multiplet	Line (Å)	gm	Amn (units of $10^7 sec^{-1}$)
1	3285.9	7	21.1
	3301.9	5	20.9
	3311.3	3	21.3
2	3480.6	7	20.4
	3503.6	5	15.6
	3499.7	3	16.9
3	3336.1	9	25.4
	3344.7	7	22.2
	3358.5	5	21.0

In addition no AIII impact broadening parameters had been calculated. Estimations of these, for the lines tabulated above, were therefore made using the same basic prescription which Griem had used for singly ionised emitters [ref.2]. These calculations are described in the following chapter.

The calculated values of τ_o led to the conclusion that at least the lines of multiplets 2 and 3 should be uneffected by self absorption even when viewed end on to the plasma column. The value of Te given in Section 4.7 was used for these estimates.

Therefore measurements of AIII line profiles were made viewing end on to the plasma. Thus acceptance of light was along the same axis as used in the laser measurements of Ne.

4.9 Measurement of AIII line widths

The same experimental arrangement as for AII lines was employed except that quartz optics were used. Unfortunately the only piezoelectric tube available had a glass plate with a transmission of only ~30% at λ3500Å. Use of this with a fixed (unmatched) quartz flat with aluminium coatings (R = 87%, T = 9%) enabled an overall finesse of 7 to be achieved on λ3341.5Å Hg I.

In addition only a small Hilger quartz spectrograph, with an inverse dispersion of 100Å/mm at λ3500Å, was available. Thus with slits narrow enough to isolate AIII lines the system was monochromator limited (Chapter 2). Even then the lines of multiplet 2 could not be effectively isolated from nearly AII lines.

Nevertheless, sufficient light was available to give a good signal to noise ratio on the lines of multiplets 1 and 3. The viewing solid angle was restricted by the tube end window such that with the large plasma diameters in the stabilised discharges the plasma could be considered homogeneous. Little error would then occur by using the end on laser measurements of Ne.

Measured widths, B, of some AIII lines are tabulated below. Also included in this table are the calculated widths obtained by convoluting the calculated Stark and Doppler profiles for an arbitarily chosen temperature of 30,000°K.

Again the line widths are considerably larger than the calculated widths. In fact, the observed widths are larger than the AII widths under the same conditions. Since the electrons are more tightly bound in AIII this cannot in general happen. It seems likely, therefore, that the AIII lines are optically thick.

Results for the measured widths B of some AIII lines.

	Multi-plet	Line	B'	W cal	B cal	B'/B
Ne = $4x10^{16}cm^{-3}$	1	3285.9	0.16 ± .02	.0058	.072	2.2
		3301.9	0.16 ± .02	.0058	.072	2.2
		3311.3	014 ± .02	.0058	.072	2.0
	3	3336.1	0.14 ± .02	.016	.083	1.7
		3344.7	0.13 ± .03	.015	.082	1.6
		3358.5	0.13 ± .03	.012	.079	1.6
Ne = $6x10^{16}cm^{-3}$	1	3285.9	0.36 ± .06	.0088	.075	4.8
		3301.9	0.34 ± .04	.0088	.075	4.5
		3311.3	0.28 ± .04	.0088	.075	3.7
	3	3336.1	0.34 ± .04	.023	.092	3.7
		3344.7	0.28 ± .04	.022	.091	3.1
		3358.5	0.20 ± .04	.018	.088	2.3

The fact that τ_o for each line is large is substantiated by the ratios of the observed line widths within a multiplet. For large τ_o we expect, from 3.2, the ratio of a line width, B', to that of the strongest line in the multiplet, Bs', to be:-

$$B'/Bs' \simeq \sqrt{\tau_o/\tau_{os}} \simeq \sqrt{gnAmn/gnsAmns}$$

The quantities on the right and left hand sides of the above relation are tabulated below using the results from the previous two tables.

Multi-plet	Line (Å)	B'/Bs' (Ne=6x10^{16})	$\sqrt{\frac{gnAmn}{gnsAmns}}$
1	3285.9	1.00	1.00
	3301.9	0.89	0.84
	3311.3	0.74	0.66
3	3336.1	1.00	1.00
	3344.7	0.82	0.82
	3358.5	0.59	0.68

4.10 Estimation of Te from AIII line widths

Since the lower states, Wn, of AIII lines within a multiplet have practically the same energy the optically thin widths could not be inferred as in Section 4.7. The fact that τ_o was considerable for the AIII lines suggested that Te was higher than measured from the AII line widths. Therefore Te was re-estimated from the AIII line widths.

τ_o is plotted as a function of Te for two AIII lines in Fig.4.13. In this case Doppler broadening is important so that τ_o is a function of Ne as well as Te. The values of Te corresponding to the values of B'/B given in the above table. are :-

Ne = 4x10^{16} cm^{-3}	3285.9	26,800°K
	3336.1	26,300°K
Ne = 6x10^{16} cm^{-3}	3285.9	32,800°K
	3336.1	30,400°K

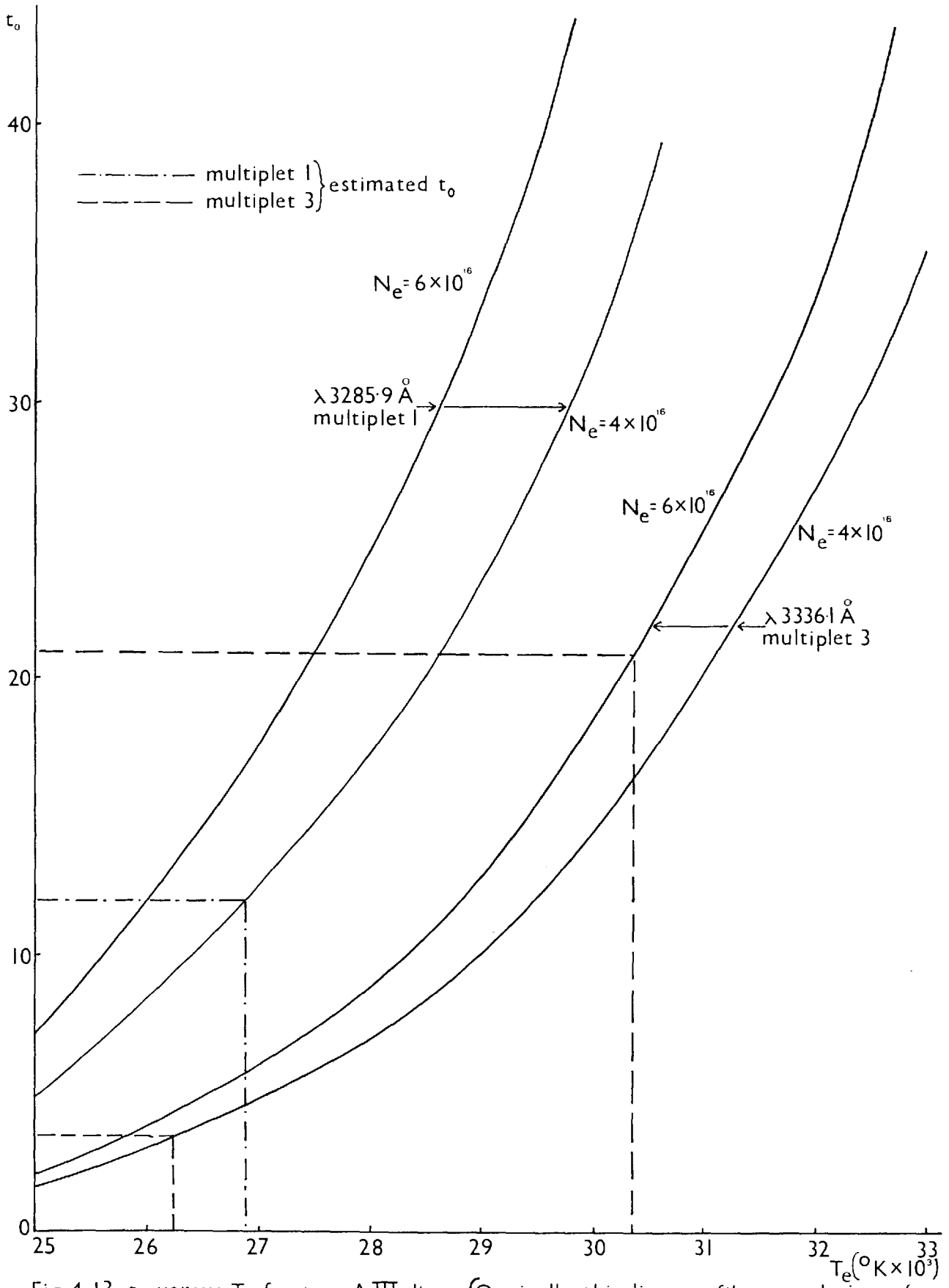


Fig. 4·13 t_o versus T_e for two A III lines. (Optically thin line profile convolution of Doppler and Stark profiles.)

Errors $\sim$15% in B'/B lead to errors $\sim$ 30% in τ_o and correspondingly $\sim$3% in Te. The calculated Stark width for multiplet 3 lines was checked later and found to be in agreement within experimental error. The small systematic differences in the temperatures given by the multiplet 3 and 1 lines could be accounted for if the Stark width of the latter line was underestimated by a factor $\sim$2.

In all the above calculations involving optical depth L.T.E. has been assumed. This is justified for AII in Chapter 7. However, for the AIII lines L.T.E. only extends down to the upper states for Ne $\geq$ 1 x $10^{17}cm^{-3}$, i.e. for Ne $\geq$ 1 x $10^{17}cm^{-3}$ the collisional depopulation rate of the upper state is $\sim$10 x larger than the radiative decay rate. At lower values of Ne (as in the previous results) the collisional depopulation rate is reduced. However, since the AIII lines are very optically thick the radiative decay rates of their upper states is substantially balanced by reabsorption. Thus collisional rates still dominate over radiative rates and the population ratio Nm/Nn will not differ appreciably from its L.T.E. value. Consequently the source function, S_ν , is not lowered near the line centre as in a case considered by Hearn [ref.40].

However, in spite of the resonance line of AIII being appreciably reabsorbed the ratio N_n/N_2, which occurs in the expression for τ_o, is likely to be overestimated by a factor of up to two (for Ne = 4 x $10^{16}cm^{-3}$ - see Chapter 7). Therefore consideration of divergences from L.T.E. would mean that the estimated values of Te are $\sim$7% higher than given in the above table. The corrected values are :-

Ne	Te
$4 \times 10^{16} cm^{-3}$	$28,500 \pm 2,000^{\circ}K$
$6 \times 10^{16} cm^{-3}$	$33,500 \pm 2,500^{\circ}K$

4.11 Discussion of results

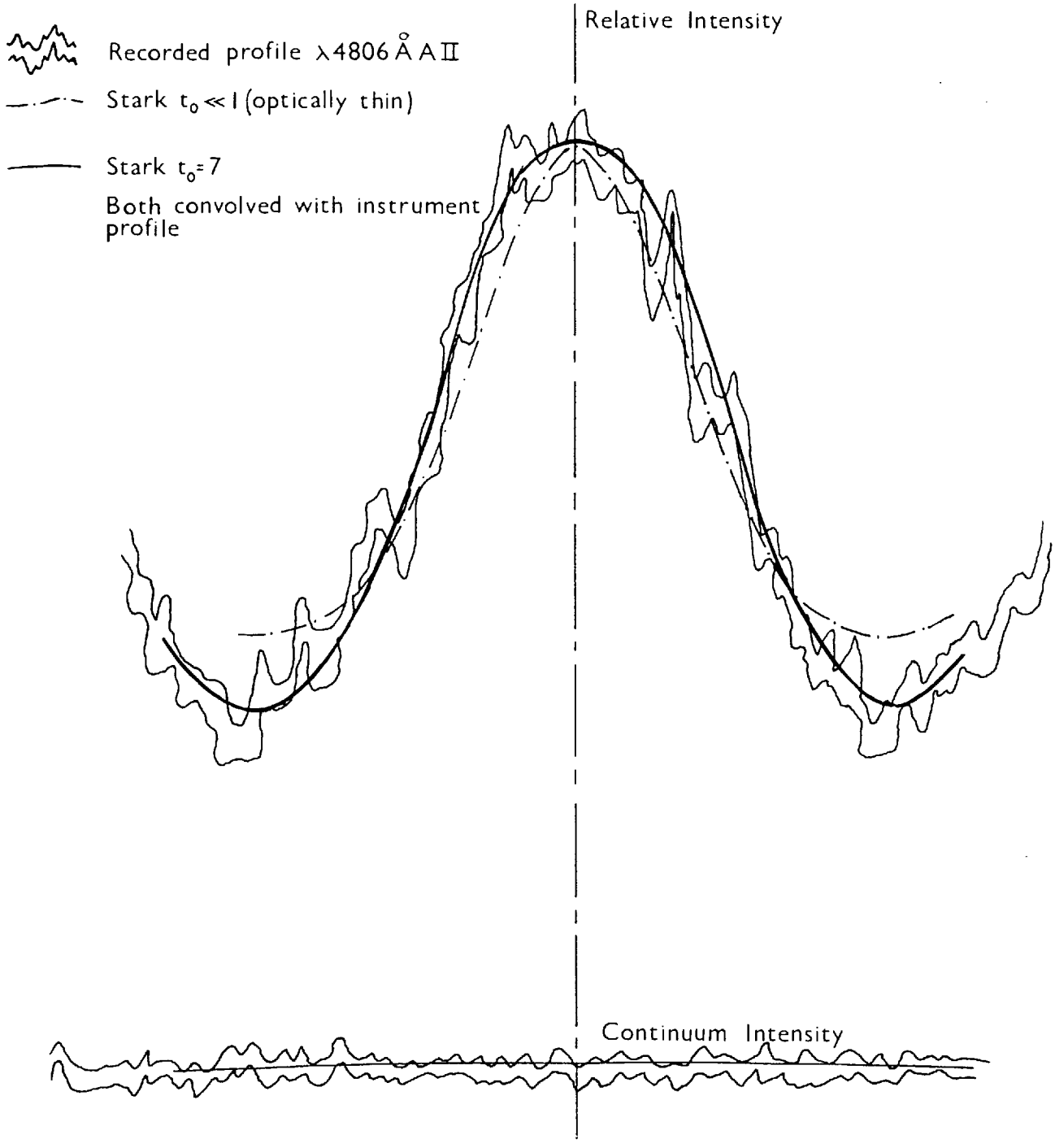
It is necessary, initially, to account for the differences in the estimations of Te given in sections 4.7 and 4.10 (for $Ne = 4 \times 10^{16} cm^{-3}$).

The reason for these discrepancies is almost certainly caused mainly by plasma inhomogeneity in the radial direction. Thus if we consider the axial value of Te as given by the AIII result,

i.e. $Te = 28,500 \pm 2,000^{\circ}K$

we should expect for $\lambda 4806\text{Å}$ $\tau_o = 4.3$

However, cooler outer regions of the plasma could increase the reabsorption since for $Te < 28,500^{\circ}K$, τ_o passes through a maximum as seen in Fig.4.7. Therefore the value of τ_o estimated from the AII line widths is not likely to be very meaningful in terms of the plasma core temperature and does not contradict the AIII results. In fact the larger value of $\tau_o = 7$ gives a theoretical curve which fits the observed $\lambda 4806\text{Å}$ profile well, as seen in Fig.4.14. For this fit the theoretical profile for $\tau_o = 7$ estimated from 3.1 was convolved with the instrument profile using a computor programme (for an Elliot 803A) supplied by Dr. R.C.M.Learner of the Spectroscopy Department.



B_z stabilised pinch Bank voltage, 1·5 KV Magnet voltage, 1·0 KV
Filling pressure of argon 0·20 torr.

Fig. 4·14 Fit of optically thick Stark profile to observed profile.

The above considerations do not appreciably affect the value for k obtained in Section 4.6. This is because λ5062Å is comparatively little affected by reabsorption, i.e. τ_o for λ5062Å, corresponding to $\tau_o = 7$ for λ4806Å is ~ 0.9, i.e. the line is broadened $\sim$25% by reabsorption and the corresponding value of k is 2.4. If the plasma is uniformly at the core temperature for λ5062Å, $\tau_o \sim 0.58$. In this case the line is broadened $\sim$15% by reabsorption and k = 2.7. Both these values are within the estimated value of $k = 2.7 \pm 0.4$ from Section 4.6.

If we therefore take,

measured $\Omega = (2.7 \pm 0.4)\,\Omega$ (Te = 20,000°K) and calculated $\Omega = \Omega$ (Te = 28,500°K) the ratio of measured to calculated broadening parameters for multiplet 6 lines is 2.4 ± 0.3. For λ4880Å the ratio is 2.5 ± 0.3.

In the above discussion the effect of Bz field trapping was ignored, i.e. the value of Ne characterising the emitted profiles was assumed to be equal to the axial measured value of Ne. This assumption was justified by the lack of an axial dip in the radial continuum distribution and the fact that the values of Te estimated from the AII and AIII line widths were not appreciably different.

Further Pert [ref.41] shows that considerable field trapping will occur if :-

$$\sigma \gg rc^2/8\pi vx^2$$

where σ is the conductivity of a cylindrical collapsing plasma shell of thickness x moving with a velocity v. σ refers to the shell at a radius r.

From the radial continuum distribution at 1.5 kv 0.20 torr (Ne = 4 x 10^{16}cm^{-3} at peak compression) we obtain :-

$$x = 0.5 \text{ cm} \pm 30\%$$
$$\text{Mean } v = 10^5 \text{cm sec}^{-1} \pm 20\%$$

If we consider conditions at peak compression, $r = 2.4$ cm $\pm$ 10%.

Thus $rc^2/8 \quad vx^2 = 4 \times 10^3 \pm 30\%$ mho cm^{-1}

From reference 42 assuming L.T.E., Te = 28,500°K and Ne = 4 x 10^{16}cm^{-3} so the plasma pressure is $\sim 3 \times 10^5$ dyne cm^{-2}. Corresponding to these conditions Wheeler [ref.43] gives,

$\sigma \sim 100$ mho cm^{-1}.

Thus very little field trapping is likely to occur at peak compression.

We shall now consider the effect of Zeeman splitting. Due to the more diffuse plasma and smaller current, at the pinch, compared with the discharges in Chapter 3 the self magnetic field Bθ of the plasma is small compared with the applied Bz field. Since no field trapping occurs Bz is likely to be the same over the whole time scale of the discharge due to the long period of the crowbarred magnetic field bank. Therefore the narrow line widths recorded in the afterglow of the discharge indicated that the effect of Zeeman splitting could also be neglected at peak compression.

On the basis of the above considerations, therefore, the figures quoted for k are reasonable. This means that the values of Ne quoted by Burgess [ref.11] and Burgess and Cooper [ref.44] together with the result in Section 3.7 are a factor of 2.3 $\pm$ 0.3 too high due to the use of Griem's calculated broadening parameter for λ4806Å.

Two other points are of interest in connection with the previous linear pinch work described in Section 3.2.

Firstly, at one initial condition Grieg calculated Ne at peak compression to be [ref.21]

$$Ne = (2.5 \pm 0.5) \times 10^{18} cm^{-3}$$

At the same condition we obtained, during the work described in Section 3.4

$$W = 3.5\text{Å} \pm 20\% \text{ for } \lambda 4806\text{Å}.$$

With the use of the measured value of Ω this corresponds to:-

$$Ne = (1.9 \pm 0.4) \times 10^{18} cm^{-3}$$

This value is in far better agreement with Grieg's result than if the calculated value of Ω were used.

Secondly, the discrepancy over observed plasma dimensions noted in Section 3.2 can now be readily accounted for. Use of Burgess' value of Te [ref.11] gives the plasma dimensions,

$$S \leq 3 \text{ mm}$$

for $\leq 10\%$ reabsorption, as was observed experimentally. In fact τ_o, with the measured value of Ω inserted, will be reduced by a factor of 2.4 ± 0.3 from its originally estimated value. Thus a plasma diameter as large as one centimetre could well be consistent with optical thinness of $\lambda 4806$Å.

Finally, it is desirable to account for the large discrepancies with calculations which have been recorded in this Chapter. The work performed to attain this end is described in the following chapter.

CHAPTER 5

CALCULATIONS ON STARK BROADENING FOR ISOLATED SPECTRAL LINES

5.1 Introduction

In this Chapter the results of calculations performed to re-estimate impact broadening parameters for isolated lines are described. In particular AII $\lambda 4806\text{Å}$ and $\lambda 4880\text{Å}$, are considered. These calculations followed the same basic prescription given by Griem [ref.2]. The reason why this approach was adopted when several discrepancies with Griem's calculations had already been found (Chapter 3 and 4) are tabulated in the following section.

A brief outline of the theory used by Griem will then be presented. Emphasis will be made on noting the physical assumptions made at each step in the calculations. For simplication electron impact broadening only is considered.

Finally the validity of the various assumptions will be commented on in the light of the results of the calculations.

5.2 Reasons for calculations

(1) It was required to calculate AIII widths and shifts to compare with experimental measurements (Chapter 4).

(2) While Griem used the tables of C.E. Moore [ref.91] to obtain the perturbing energy levels for AII lines a more recent publication by Minnhagen [ref.34] gives 200 more levels. Inclusion of levels missing from reference 91 would always have the effect of increasing the calculated width.

In the case of λ4880Å inclusion, in the calculations, of the two nearest perturbing levels not given in Moore's tables would be expected to increase the calculated width appreciably.

(3) The width of the upper state, Eα, of a given line perturbed by bound and continuum 'perturbing levels', Eα', is governed by two factors. Firstly the larger $|E\alpha-E\alpha'|$ the smaller the effect Eα' has on the width of Eα. Secondly the smaller the wave function overlap between Eα and Eα' the smaller the effect of Eα'.

Griem used, arbitarily, only the nearest five Eα' in most of his calculations (private communication). However distant Eα' might be expected to have a large effect on the width of Eα, in spite of the large $|E\alpha-E\alpha'|$, due to the high density of states near the ionisation limit. It was therefore desirable to study the convergence properties of the width on using increasing numbers of Eα' in the calculations.

(4) Previous width calculations were only for the strongest line in each multiplet [ref.2]. The multiplet splitting in AII is generally small so the quantities $|E\alpha-E\alpha'|$ and radial wave function overlap of Eα and Eα' are generally similar for all upper states of a multiplet. Thus the broadening of all multiplet lines should be similar. However the relevance of this point to previous assumptions made indicated the desirability of separate width calculations for each line.

(5) Several cases of differences in the quoted parameters for lines with the same upper state can be found in ref.2 (cf. Chapter 3, Section 7). Such inconsistencies occur for some lines in AI, AII, CII, SII and NII.

(6) There is the possibility, from the discussion in Section 3.7, that lower state broadening of some AII lines may not be negligible. This can also be seen by inspecting the AII term scheme. For example, in the case of λ 4848Å there are only two levels which can be found from the term scheme that perturb the upper state more strongly than levels which perturb the lower state.

Broadening of the lower states could be investigated, initially, by independent calculations of parameters for these states.

5.3 Electron impact broadening of isolated lines

In this Section a brief outline of the theory used by Griem will be given. The main references for this outline are Chapter 4 of Griem's book [ref.2] and Barangers article in reference 92.

The starting point for calculations is the expression for the power radiated by an atom by spontaneous transitions from an initial state m to a final state n.

i.e. $P_{mn} = (4w^2/3c^3)\, g_n \, |\langle n | \underline{d} | m \rangle|^2$ ...5.1

where $\underline{d} = e\underline{r}$ is the dipole moment operator of the atom.

If we consider a set of initial states, m, and final states, n, such that w_{mn} is reasonably constant then the power radiated per unit frequency interval is :-

$$dP/dw = (4w^4/3c^3) \sum_{m,n} \delta(w-w_{mn}) \, |\langle n | \underline{d} | m \rangle|^2 \rho_m \quad \ldots 5.2$$

where ρ_m is the statistical weight of an initial state m.

The sum in 5.2 is called the shape, L(W), of the spectrum of lines from states m to n. For one line this is called the line shape. More convenient to use is the Fourier transform of L(W), the Autocorrelation function, C(t).

$$C(t) = \int_{-\infty}^{\infty} e^{+iWt} L(W)dW = \sum_{n,m} e^{+iW_{mn}t} |\langle n | \underline{d} | m \rangle|^2 \rho_m \quad \ldots 5.3$$

Introducing the time development operator,

$$\underline{T}(t) = e^{-iHt/\hbar},$$

such that $\underline{T} | a \rangle = e^{-iWat} | a \rangle$,

where $| a \rangle$ is an eigen state of H, 5.3 can be written in matrix notation :-

$$C(t) = \text{Trace} (\underline{d}\ \underline{T}\ \underline{d}\ \underline{T}^{\dagger} \underline{\rho}) \quad \ldots 5.4$$

where $\underline{\rho}$ is defined by :-

$$\underline{\rho} = \langle m | \underline{\rho} | m \rangle$$

i.e. $\underline{\rho}$ is a diagonal matrix.

In the particular case of broadening by perturbations the general expression for C(t) given in 5.4 becomes :-

$$C(t) = \text{Trace} \left\{ \underline{d}\ \underline{T}\ \underline{d}\ \underline{T}^{\dagger} \underline{\rho} \right\}_{A_V} \quad \ldots 5.5$$

where the trace is over states of the emitting system only, the trace over the perturbing states resulting in the statistical average denoted A_V.

This simplification arises from two assumptions:-

A1. The perturbers are considered as classical particles giving rise to a time dependent field which disturbs the emitting atom. For this to be valid the size of the perturber

wave packet must be small compared with its impact parameter.

A2. It is assumed that a perturbation of the emitting atom does not appreciably affect the orbit of the particle causing the perturbation. For this to be so the energy exchange between perturber and emitter must be $\ll$ the perturber energy (i.e. $\sim kT_e$ for electrons). Then ρ in equation 5.4 remains diagonal.

These two assumptions do not hold for all perturbers but, for 5.5 to be used, they must hold for those perturbers that cause most of the broadening.

A further assumption is now made :-

A3. Far more collisions cause transitions to nearly substates α,α' ... from the upper level m and β,β' ... from the lower state n than between m and n (or $\alpha'\beta'$ etc.).

Then 5.5 can be expressed in matrix notation as :-

$$C(s) = \left\{ \sum_{\alpha\alpha'\beta\beta'} \langle \alpha | \underline{d} | \beta \rangle \langle \beta | \underline{T}_n^{\dagger} | \beta' \rangle \times \langle \beta' | \underline{d} | \alpha' \rangle \langle \alpha' | \underline{T}_m | \alpha \rangle \right\}_{Av} \quad \ldots 5.6$$

It is assumed above that the density matrix is constant and does not affect the line shape (cf. A1 and A2).

A4. It is now assumed that lower state broadening can be neglected since the ion is more tightly bound in state n than in m. Thus :-

$$\langle \beta | \underline{T}_n^{\dagger} | \beta' \rangle = \langle n | \underline{T}_n^{\dagger} | n \rangle = e^{iWnt} = \text{a constant}$$

$$\therefore C(t) = \left\{ \sum_{\alpha\alpha'} \langle \alpha | \underline{d} | n \rangle \langle n | \underline{d} | \alpha' \rangle \langle \alpha' | \underline{T}_m | \alpha \rangle \right\}_{Av} \quad \ldots 5.7$$

In this expression only the T_m term is affected by the average. The Hamiltonian in T(t) is the sum of the unperturbed Hamiltonian of the atom, H_o, and the total interaction, $V_T(t)$.

$$\text{i.e.} \quad T(t) = \eta\, e^{-(i/\hbar)\int_o^t [H_o + V_T(t)]dt} \qquad \ldots 5.8$$

Here η makes the operators act in the correct time order.

It is more convenient to consider the interaction only, by defining another operator, U(t), such that ,

$$T(t) = e^{-(i/\hbar) H_o t}\, U(t) \qquad \ldots 5.9$$

Then one may write :-

$$U(t) = e^{-(i/\hbar)\int_o^t V_T'(t)dt} \qquad \ldots 5.10$$

$$\text{where } V'(t) = e^{+(i/\hbar) H_o t}\, V_T(t)\, e^{-(i/\hbar) H_o t} \qquad \ldots 5.11$$

To calculate the average in 5.7 it is necessary to consider the time development of U(t) which can be related to T(t) via 5.9.

The time development of U(t) can be expressed in the form

$$\Delta U(t,0)_{Av} = \left\{U(t+\Delta t,0) - U(t,0)\right\}_{Av}$$

$$= \left\{[U(t+\Delta t,t) - 1]\, U(t,0)\right\}_{Av} \qquad \ldots 5.12$$

Substitution of 5.10 into 5.12 with $V'_T(t)$ as the sum of all the perturber interactions $V'_1(t)$, $V_2'(t)$ etc. could, in principle, allow 5.12 to be solved for U(t,0). With the use of 5.9 equation 5.7 could then be evaluated.

However in general the interactions of the different perturbers overlap in time and application of the time ordering operator η would be extremely difficult.

A.5 It is at this stage that a considerable simplification can be made if the so called 'Impact Approximation' is valid.

Thus suppose a value of Δt can be found such that :-

(i) Many collisions occur in Δt. Then the two terms on the R.H.S. of 5.12 can be arranged separately.

(ii) The first term on the R.H.S. of 5.12 is small. Then 5.12 can be expressed as a differential equation and readily solved to give $U(t,0)_{Av}$. This can be done as follows :-

The fact that many collisions occur in Δt and yet $[U(t+\Delta t,t)-1]$ remains small means that the average collisions must be weak, i.e.

$$\int_t^{t+\Delta t} V'i(t)dt \quad \text{is small.}$$

Therefore using 5.10 we can write :-

$$[U(t+\Delta t,t)-1]_{Av} = [\cap e^{-i/\hbar}\int_t^{t+\Delta t} V'_1(t)dt\ e^{-i/\hbar}\int_t^{t+\Delta t} V'_2(t)dt \ldots\ldots -1]_{Av}$$

This expression can be expanded in the form :-

$$[U(t+\Delta t,t)-1]_{Av} \sim [\ (1+C_1+\ldots)(1+C_2+\ldots)\ldots -1]_{Av}$$

Since terms such as C_1 are small, cross products can be neglected and the difficulty with the time ordering is resolved, i.e. :-

$$[U(t+\Delta t,t)-1]_{Av} \sim [C_1+C_2+\ldots]_{Av} \sim NC_{Av} \qquad \ldots 5.13$$

Where N is the total number of perturbers.

We now use the fact that the standard perturbation expansion of 5.10 is :-

$$U(t+\Delta t,t) = 1-(i/\hbar)\int_{t}^{t+\Delta t} V'(t)dt + (i/\hbar)^2\int_{t}^{t+\Delta t} ds \int_{t}^{s} V'(s)V'(r)dr$$

$$+ \ldots \qquad \ldots 5.14$$

The effect of collisions outside the interval Δt can be neglected and for those in Δt the limits can be extended from $t = -\infty$ to $+\infty$ i.e. collisions are assumed to be completed in time Δt. Then from 5.13 and 5.14 one can express 'C' in terms of the scattering S matrix :-

$$C = S - 1 \qquad \ldots 5.15$$

since :-

$$S = 1 - (i/\hbar)\int_{-\infty}^{\infty} V'(t)dt + (i/\hbar)^2 \int_{-\infty}^{\infty} ds \int_{-\infty}^{s} V'(s)V'(r)dr$$

$$+ \ldots$$

Thus 5.13 can be evaluated using the scattering matrix of a single electron. Consequently the solution of 5.12 in differential form can be expressed, using 5.9, as $T_{Av}(t) = e^{-(i/\hbar)H_o t}\, e^{NC_{Av}t}$

i.e. $$T_{Av}(t) = e^{-(i/\hbar)[H_o + \phi]t} \qquad \ldots 5.16$$

Where $$\phi = i\hbar N \int (S - 1) \qquad \ldots 5.17$$

The integral implying averaging over all possible angles, velocities and impact parameters for a collision, i.e. from 5.15 :-

$$C_{Av} \equiv \int (S - 1)$$

The average is made over a volume V so that multiplication by N gives a $\emptyset$ matrix proportional to N_e. Thus the effect of the impact approximation is to consider a time independent operator $\emptyset$ (α N_e) as added to the unperturbed Hamiltonian, H_o.

The validity criteria for the impact approximation may be derived from (i) and (ii) above,

i.e. $T \gg \Delta t \gg t_c$

Where T is the time for U to become appreciably different from unity, i.e. $T \sim 1/W$, and t_c is the <u>duration</u> of a collision.

The first inequality arises from the fact that the average collision must be so weak that even many collisions in Δt do not appreciably effect the autocorrelation function.

The second inequality arises because all the weak collisions must be completed in Δt so that the effect of each electron outside the time Δt can be disregarded.

The above criterion may thus be wrtten :-

$$1/W \gg \Delta t \gg \rho/V$$

The maximum impact parameter for electrons which contribute to the broadening is ρ_D, in which case the impact approximation holds for frequencies from the line centre given by :-

$$W \ll V/\rho_D$$

i.e. $W \ll W_p$ (where $\frac{1}{2}\, mv^2 \sim kT_e$)

Finally the effect of strong collisions in the interval Δt must be considered. If there are strong collisions in Δt then U(t) and the autocorrelation function are changed by a large amount so that, from above, the Impact approximation is invalidated. However if there is only one strong collision

in Δt there is no difficulty with applying the time ordering operator and the Lorentz-Weisskopf theory can be used to calculate the contribution to the width.

Direct addition of the impact and strong collision widths is not strictly correct. A strong collision in Δt completely interupts the emitted wavetrain so that all weak collision effects in Δt should be emitted from the calculation. However since, from the impact approximation, the effect of weak collisions must be small not much error is incurred by including them.

If two or more strong collisions occur in Δt then difficulty is experienced in applying the time development operator so the combined effects of strong and weak collisions cannot be calculated.

Assuming the impact approximation is valid we have from 5.7 and 5.16 :-

$$C(s) = \sum_{\alpha\alpha'} \langle \alpha \mid \underline{d} \mid n \rangle \langle n \mid \underline{d} \mid \alpha' \rangle \langle \alpha' \mid e^{-i(H_m+\phi)t/\hbar} \mid \alpha \rangle \quad \ldots 5.18$$

The inverse Fourier transform is then taken to give the line shape :-

$$L(W) = -\hbar/\pi \; \mathcal{I}_m \sum_{\alpha\alpha'} \langle \alpha \mid \underline{d} \mid n \rangle \langle n \mid \underline{d} \mid \alpha \rangle / (\hbar W - H_m - \phi) \quad \ldots 5.19$$

A.6 The above expression is considerably simplified in the isolated line case when the separate components in 5.19 refer to lines of quite different wavelengths. In addition, if we assume quasi-static Stark splitting is negligible we can omit H_m as this will simply define a sharp origin of frequency. Thus we have :-

$$L(W) = (1/\pi) W_m \langle m \mid \underline{d} \mid n \rangle \langle n \mid \underline{d} \mid m \rangle / \left[(W-d_m)^2 + W_m^2 \right] \quad \ldots 5.20$$

This is a Lorentzian profile of width w_m and shift d_m where :-

$$w_m = -(i/\hbar)\, \mathcal{G}_m \langle m \mid \emptyset \mid m \rangle$$

and $$d_m = (i/\hbar)\, \mathcal{R}_e \langle m \mid \emptyset \mid m \rangle \qquad \ldots 5.21$$

Therefore in our case we only need to evaluate the matrix $\langle m \mid \emptyset \mid m \rangle$.

This quantity can be calculated from 5.17. One further assumption is made in this calculation:-

A.7 It is assumed that the dominant interaction is long range. The dipole interaction in 1.4 is then the most important term so that the perturber orbits are straight lines,

$$\underline{r}(t) = \underline{\rho} + \underline{V}t$$

The final result is expressed in the form:-

$$(1/i\hbar)\langle m \mid \emptyset \mid m \rangle = -(4\pi/3) N_e (\hbar/m)^2 \iint (dv d\rho / v\rho)\, f(v)$$
$$\times \sum_{\alpha'} |\langle m \mid \underline{R} \mid \alpha' \rangle|^2 [A(z_{\alpha\alpha'}) + iB(z_{\alpha\alpha'})] \qquad \ldots 5.22$$

This relation, and the quantities involved, will be considered in more detail in the following section.

The integral over ρ in 5.22 diverges for small impact parameters due to the breakdown of perturbation theory for strong collisions. The integration is therefore cut off at some (velocity dependant) ρ , ρ_{min}, defined by the perturbation theory breakdown.

A.8 It is now assumed that strong collisions account for a relatively small part of the widths [$\lesssim$ 20%]. In this case

no difficulty is encountered in making the impact approximation, A5. Further little error is made by assuming that a strong collision, defined as above, interupts the light train completely.. Thus the effect of strong collisions is estimated by a Lorentz-Weisskopf expression (1.7) with $\rho_W = \rho_{min}$ and this term is added to equation 5.22.

Therefore even though the Lorentz-Weisskopf term is only a rough approximation, the final result for widths should be accurate to $\sim$ 20%. This is the main reason for quoting the theoretical errors in calculating W as $\lesssim$ 20%. Calculated shifts can be expected, in general, to have larger theoretical errors [ref.2].

It should also be noted that in the evaluation of ϕ (equation 5.17) only the 2nd term in the calculation of $\int$S-1 is retained. (The first term vanishes due to the averaging.) This 2nd term takes account of inelastic collisions only so that elastic contributions are estimated by adjusting ρ to reproduce the Lindholm result in the adiabatic, low V, limit. (This point will be further discussed laterin the Chapter.)

5.4 Calculations on the Stark broadening of AII λ4806Å and λ4880Å

5.4(i) General results

The impact broadened width and shift of a level α was calculated from 5.21 and 5.22 giving :-

$$-(W_\alpha - id_\alpha) \simeq -4\pi/3 \, N_e \, (\hbar/m)^2 \iint (dv d\rho / v\rho) f(v) \times \sum_{\alpha'} |\langle \alpha | \underline{R} | \alpha' \rangle|^2 [A(Z_{\alpha\alpha'}) + iB(Z_{\alpha\alpha'})] \quad \ldots 5.23$$

(This is equation 4.71 of reference 2)

The ion broadening parameter, α, of level α was calculated from equation 4.89 of the same reference:

$$\alpha = (4\pi N/3)[(1/3W_\alpha)(\hbar/m)^2 \sum_{\alpha'} \langle \alpha \; \underline{R} \; \alpha' \rangle^2 / a_{\alpha\alpha'}]^{\frac{3}{4}} \quad \ldots 5.24$$

The reduction of the above relations to a convenient form for computation, and the definitions of the quantities involved, is given in Appendix I. (Note that the expression for the radial matrix elements, $|\langle \alpha | \underline{R} | \alpha' \rangle|^2$ given in Appendix I differs from that in reference 31. There were three misprints in this reference, as confirmed by Professor Bates, (Private communication.)

The input data for these calculations consisted of all the odd and even levels of the species considered (tabulated in ref.34 or ref.91) together with the relevant series limits and up to seven temperatures.

Output for a required level, α, consisted of the impact width, shift and ion broadening parameter at each temperature. In addition the 'strong' and 'weak' collision contributions to the width and 'weak' contribution to the shift were obtained as a function of velocity squared of the perturbing electron. Provision was made in the computations for handling up to 50 perturbing levels.

General results for $\lambda 4806\text{Å}$ are shown in figures 5.1 and 5.2. These results were obtained with 30 perturbing levels which were selected from all the levels governed by L-S coupling tabulated in Minnhagen [ref.34].

At low T_e the electrons are only energetic enough to cause transitions to levels α' near to α. As T_e is increased in-

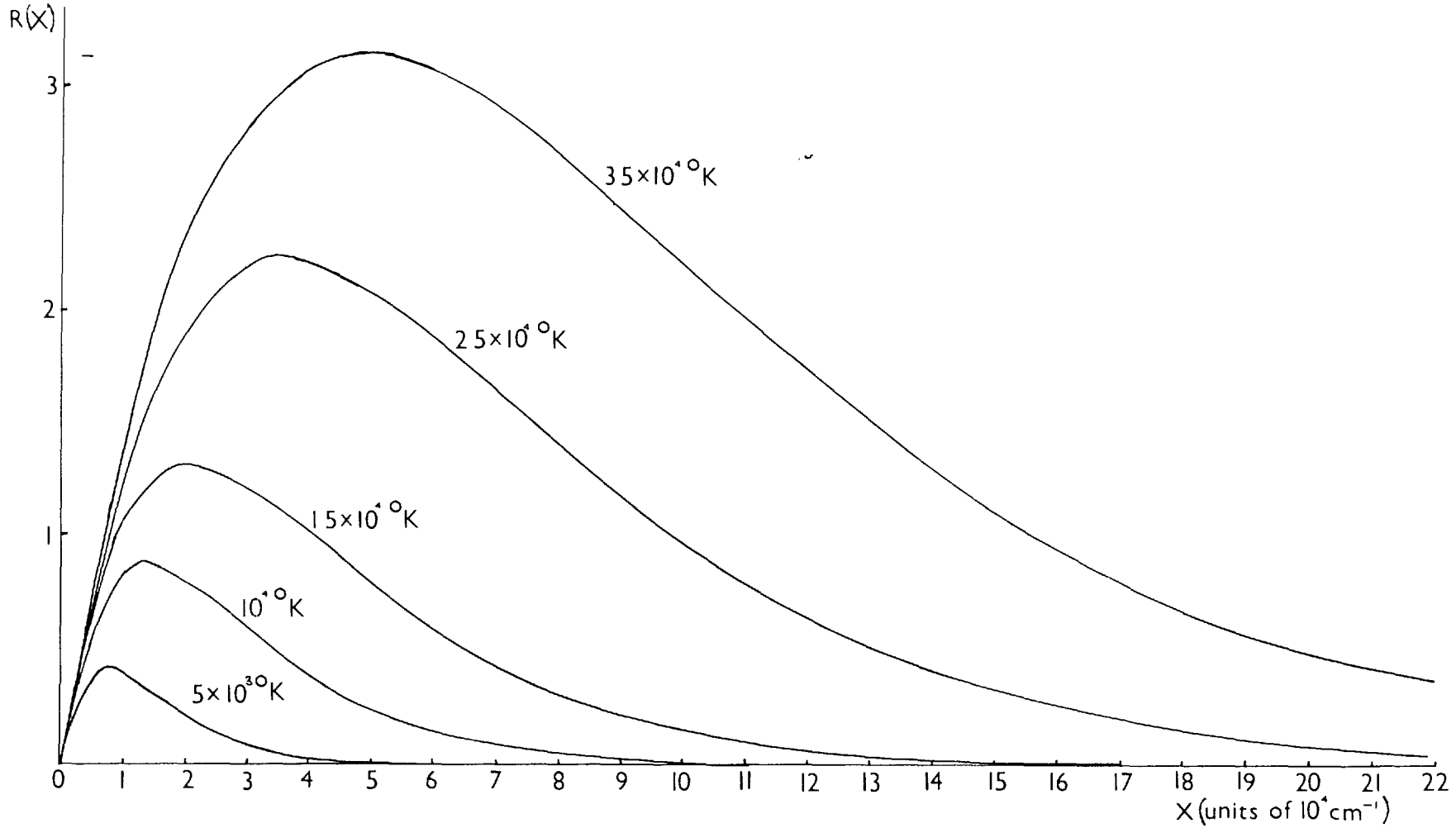


Fig. 5·1 Real part of integrand R(X) versus X. λ4806 Å, A II, multiplet 6. X ∝ perturber energy.
Line $\frac{1}{2}$-$\frac{1}{2}$ width, $W_\alpha = 1{\cdot}318\ T_e^{-\frac{3}{2}} \int_0^\infty R(X)dX$ at $N_e = 10^{16}\ cm^{-3}$.

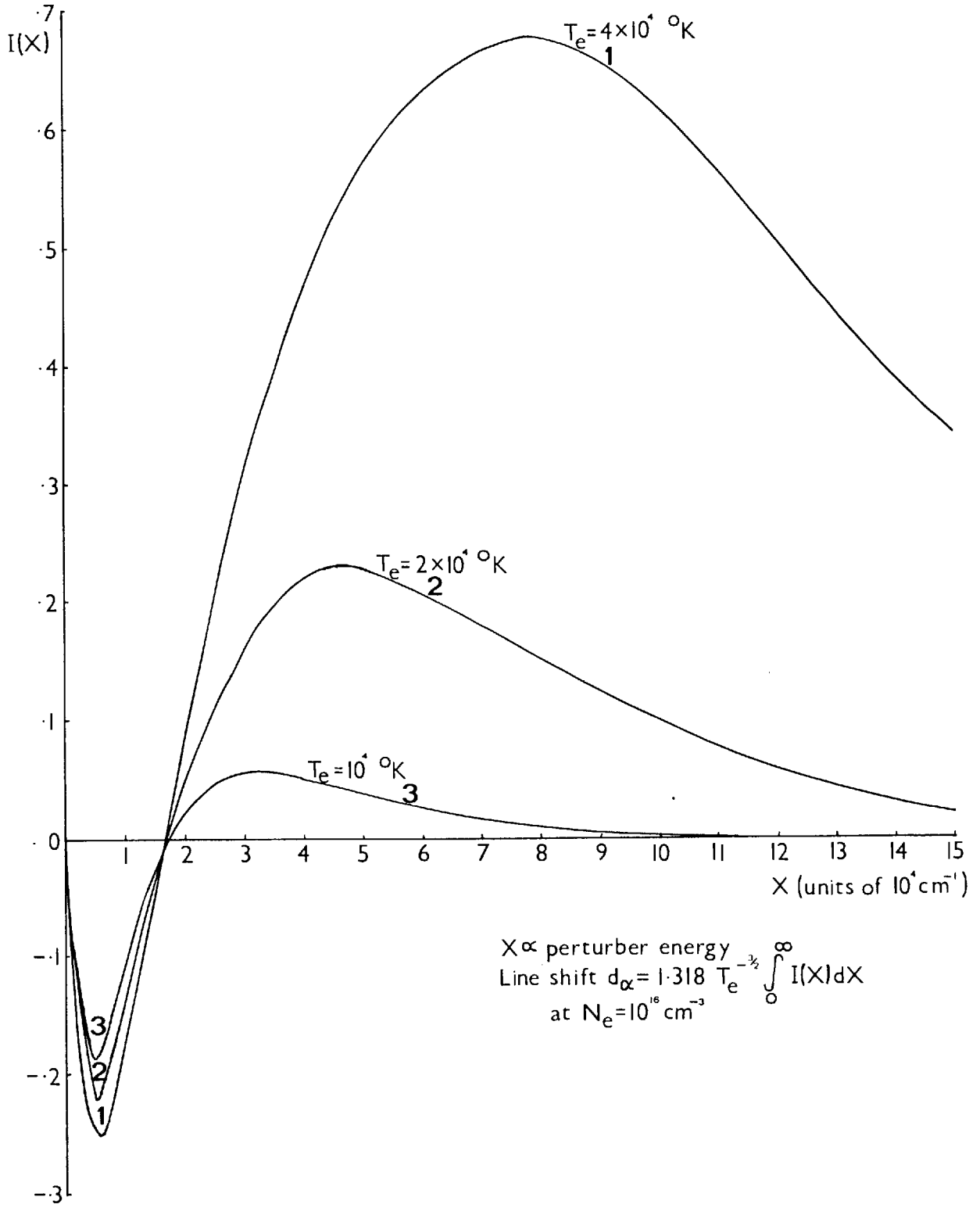


Fig. 5·2 Imaginary part of integrand, I(X), versus X. λ4806Å

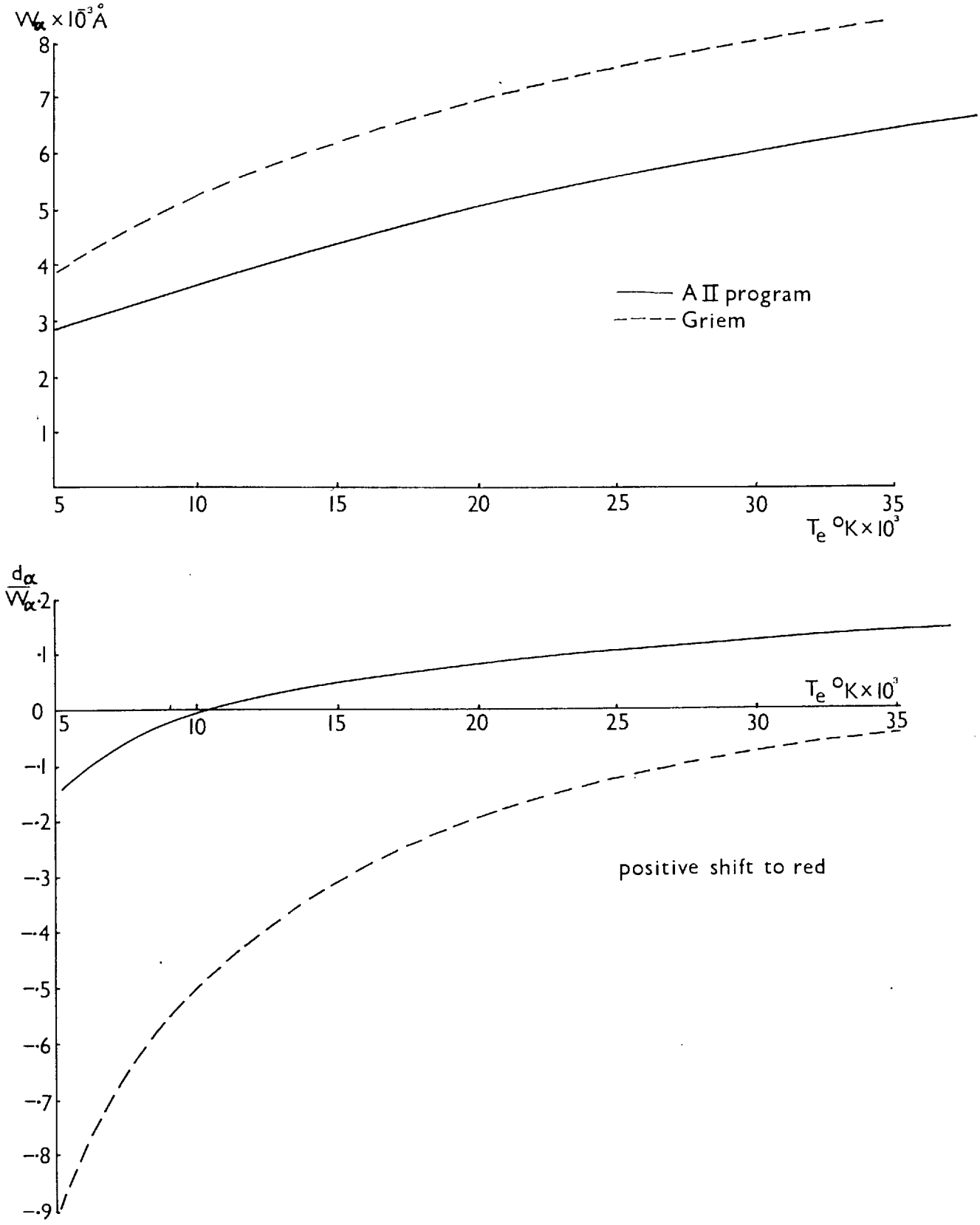


Fig. 5·3 W_α versus temperature; $\frac{d\alpha}{W_\alpha}$ versus temperature. λ4806 Å multiplet 6, $N_e = 10^{16}$ cm^{-3}

elastic transitions to further α' became important so W_α increases monotonically with T_e (figures 5.1 and 53).

As on the simpler theories (Chapter 1) shifts are caused only by elastic collisions. The magnitude of the shift is defined by the quadratic Stark coefficient,

$$C_\alpha \propto \sum_{\alpha'} f_{\alpha\alpha'}/(E_\alpha - E_{\alpha'}) \quad \text{(Section 5.4(ii))}$$

At the low T_e limit both W_α and d_α are given by the Lindholm theory [ref.3]. The dominant contributions to the above sum for λ4806Å are from levels α' below α. Therefore the shift is to the blue and the magnitude of $d\alpha/W\alpha$ is $\sqrt{3}$ [ref.3]

As T_e is increased in-elastic collisions occur to levels α' near to α. For these levels the corresponding terms in the above sum must be omitted since they no longer contribute to the shift.

At high T_e only distant $E\alpha'$ contribute to the sum. Since the density of states is generally greater for $E\alpha' > E\alpha$ (as for example in the case of λ4806Å) then $C\alpha$ is negative so the shift (in wavelength units) is to the red.

For λ4806Å the quantities $f\alpha\alpha'/(E\alpha - E\alpha')$ are such that d/W is a rapidly varying function of T_e. [Fig.5.2 and 5.3]

Whereas the results for λ4806Å show the expected general trends the magnitudes of $W\alpha$ and $d\alpha$ differ from Griem's values [ref.2] by a considerably greater amount than expected from computational deviations. However at low T_e, where the collisions are mainly elastic, the agreement is quite good.

5.4(ii) Treatment of the relevant matrix elements

One reason for the discrepancies noted above is the incorrect treatment of the relevant matrix elements in ref.2. It is therefore worth considering these in some detail.

The matrix elements which should be used in the line broadening calculations can be obtained from evaluation of the quadratic Stark coefficient which is used in the calculation of the ion broadening parameter, α [ref.2].

Condon and Shortley [ref.93] give the quadratic Stark shift of a level (α, J, M) due to $(\beta, J+1, J, J-1)$ as

$$\Delta(\alpha,J,M) = \mathcal{E}^2/hc\ [J^2a_- + (J+1)^2a_+ - (a_+ + a_- - a_o)M^2] = C_\alpha \mathcal{E}^2$$

Where $\mathcal{E}$ is the field strength,

$$a_- = |\langle \alpha,J | \underline{P} | \beta,J-1 \rangle|^2 / (E_{\alpha J} - E_{\beta J-1})$$

and a_+ and a_o refer to similar expressions for $J \rightarrow J+1$ and $J \rightarrow J$. The total shift is obtained by summing over all β.

The relevant matrix elements are therefore :-

$$J^2a_- + (J+1)^2a_+ - (a_+ + a_- - a_o)M^2$$

Averaging over M values with $M^2_{AV} = \sum_{-J}^{J} M^2/(2J+1) = 1/(3J(J+1))$

The above relation $= (1/3)[J(2J-1)a_- + J(J+1)a_o + (J+1)(2J+3)a_+]$

From p.99 ref.93, $|\langle \alpha,J | \underline{P} | \beta,J-1 \rangle|^2 = \underline{S}(\alpha J, \beta J-1)/((2J+1)J(J-1))$

Where $\underline{S}$ is the line strength.

Similar expressions exist for $J \rightarrow J$ and $J \rightarrow J+1$

$\therefore$ For each level $J \rightarrow J'$ the matrix elements are :-

$$R^2 = \underline{S}(\alpha J, \beta J')/(2J+1) = f(\alpha J, \beta J') \quad * \qquad \ldots 5.25$$

If multiplet (J) splitting is negligible,

$E_{\alpha J} - E_{\alpha J-1} \propto E_{\alpha J} - E_{\beta J} \simeq E_{\alpha J} - E_{\beta, J+1}$, then in the calculation of Δ we can use ref.94 giving :-

$$\sum_{\substack{\text{multiplet} \\ \text{to } 1,S,L,J}} R^2 = (1/2J+1) \sum_{J \rightarrow J, J\pm1} \underline{S}$$

$$= R^2_{\text{mult}} \, l_> (4l_>^2 - 1)\sigma^2/(2L+1) \qquad \ldots 5.26$$

If term (L) splitting is also negligible we can use the relation from ref.94 :-

$$\sum \underline{S} = [(2S+1)(2L+1)/(2l+1)] \, l_> (4l_>^2 - 1)\sigma^2$$

Where the sum includes all lines from an array $l\pm1$, $L, L\pm1$, S to a term l,S,L. The relative strength for lines ending on level l,S,L,J of this term is, $2J+1/(2S+1)(2L+1)$.

Thus the total matrix element is now :-

$$\sum_{\substack{\text{array} \\ \text{to } 1,S,L,J}} R^2 = \sum \underline{S}/2J+1 = l_> (4l_>^2 - 1)\sigma^2/(2l+1)$$

$$= l_> (2l_> + 1)\sigma^2 \text{ for } l \rightarrow l+1$$

$$\text{or} \quad l_> (2l_> - 1)\sigma^2 \text{ for } l \rightarrow l-1 \qquad \ldots 5.27$$

This is the relation quoted by Baranger [ref.92], and Griem [ref.15] but incorrectly given in ref.2 as,

$$l_> (2l_> - 1)\sigma^2 \text{ for } l \rightarrow l\pm1.$$

*Note that $f(\alpha J, \beta j') \neq f(\beta J', \alpha J)$ in general, so the term matrix element is misleading. We will, however, conform with ref.2 and continue to use this expression.

The good agreement with Griem's results for HeI, λ3889Å where fine structure is negligible, and therefore 5.27 was used, is shown below :-

T_e= 20,000°K	Griem [ref.10]	Appendix I programme
W	0.123	0.122
α	0.20	0.208

For heavy ions, in particular AII, J splitting is usually negligible but L splitting is not. Thus 5.26 was used to obtain the results given in Section 5.4(i). (The multiplet strengths, R^2_{mult}, were obtained from ref.94.)

The values of α for λ4806Å and λ4880Å using the prescription recorded in 5.4(i) are compared with Griem's values below:-

T_e= 20,000°K	Griem [ref.2]	Appendix I programme	
α, λ4806Å	.009	.0012x	.0013*
α, λ4880Å	.014	.0069x	.0094*

x Using all perturbing levels from ref.34

* Using the nearest 5 perturbing levels as done in ref.10.

The large differences in α for these two lines are due to one or both of the following reasons:-

(1) The matrix element $l_>(2l_> - 1)a^2$ has been used for both $l \rightarrow l \pm 1$ [ref.2] rather than that given in 5.27.

(2) This matrix element has been applied to <u>each</u> transition from a state l, S, L, J to l ± 1 rather than that given in 5.25.

Both these incorrect procedures were given in ref.95. That at least one of them was used in ref.2 can be seen by comparing W for three NII lines obtained using the programme described in Appendix I and matrix elements $l_>\,(2L_>-1)\sigma^2$ for transitions from α to each of the nearest 5 perturbing <u>levels</u> α'.

Line (NII)	T_e (°K)	Griem ref.2	Appendix I Programme
3006Å	10,000	9.8×10^{-3}	9.8×10^{-3}
	20,000	12.6×10^{-3}	12.6×10^{-3}
3838Å	10,000	19.0×10^{-3}	19.1×10^{-3}
	20,000	25.0×10^{-3}	27.0×10^{-3}
5495Å	10,000	6.0×10^{-3}	6.5×10^{-3}
	20,000	8.6×10^{-3}	9.7×10^{-3}

5.4(iii) <u>Convergence of width and shift</u>

The basic programme given in Appendix I was modified to investigate the convergence of the width and the shift on using increasing numbers of perturbing levels in the calculation. Results at different temperatures for λ4806Å are shown in figures 5.4 and 5.5. With only one perturbing level in the calculation the width is largest at the lowest temperature. This is because the width is dominated by elastic collisions. At

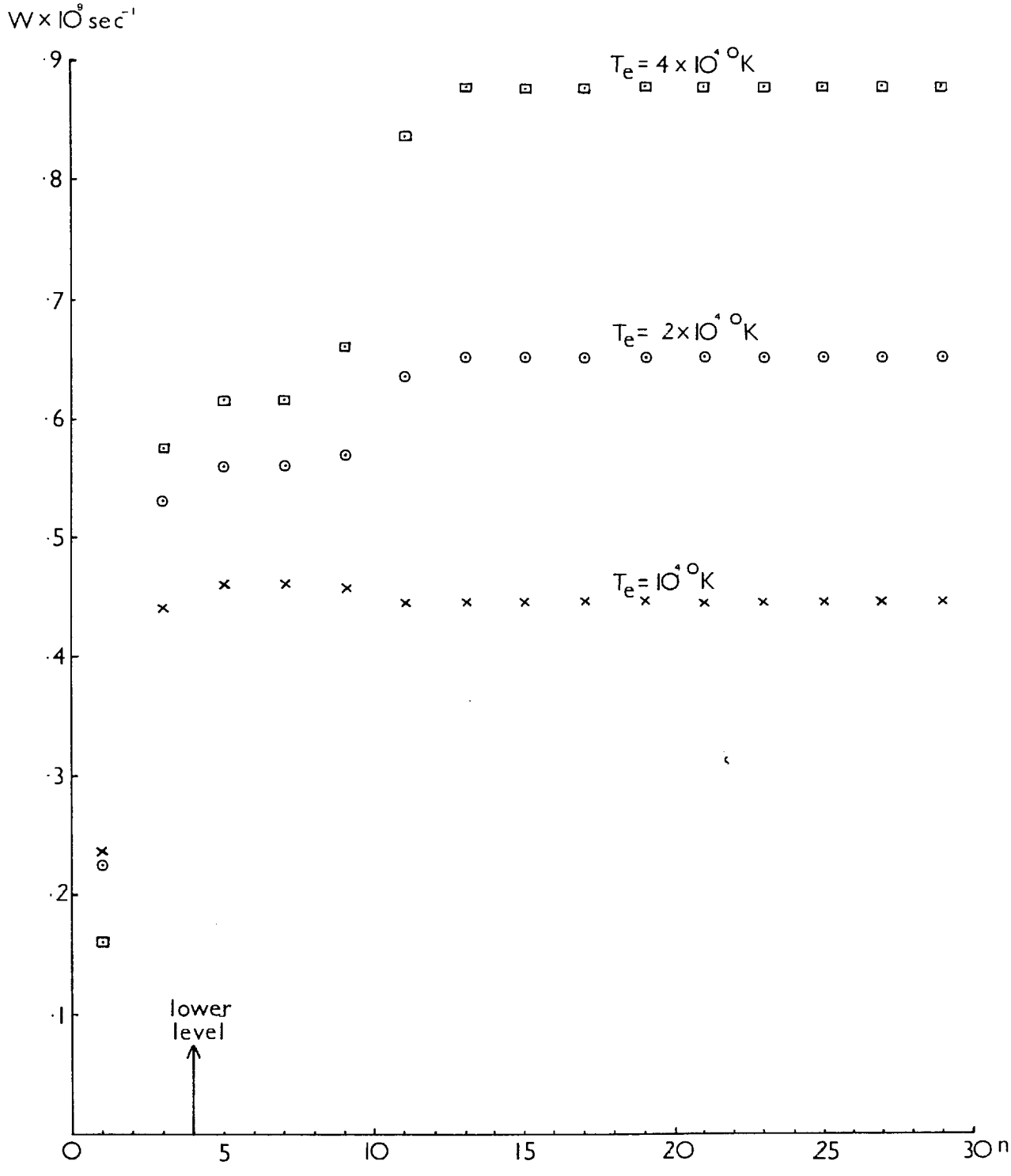


Fig. 5·4 W_α versus n, number of perturbing levels used in the calculations. (λ 4806 Å)

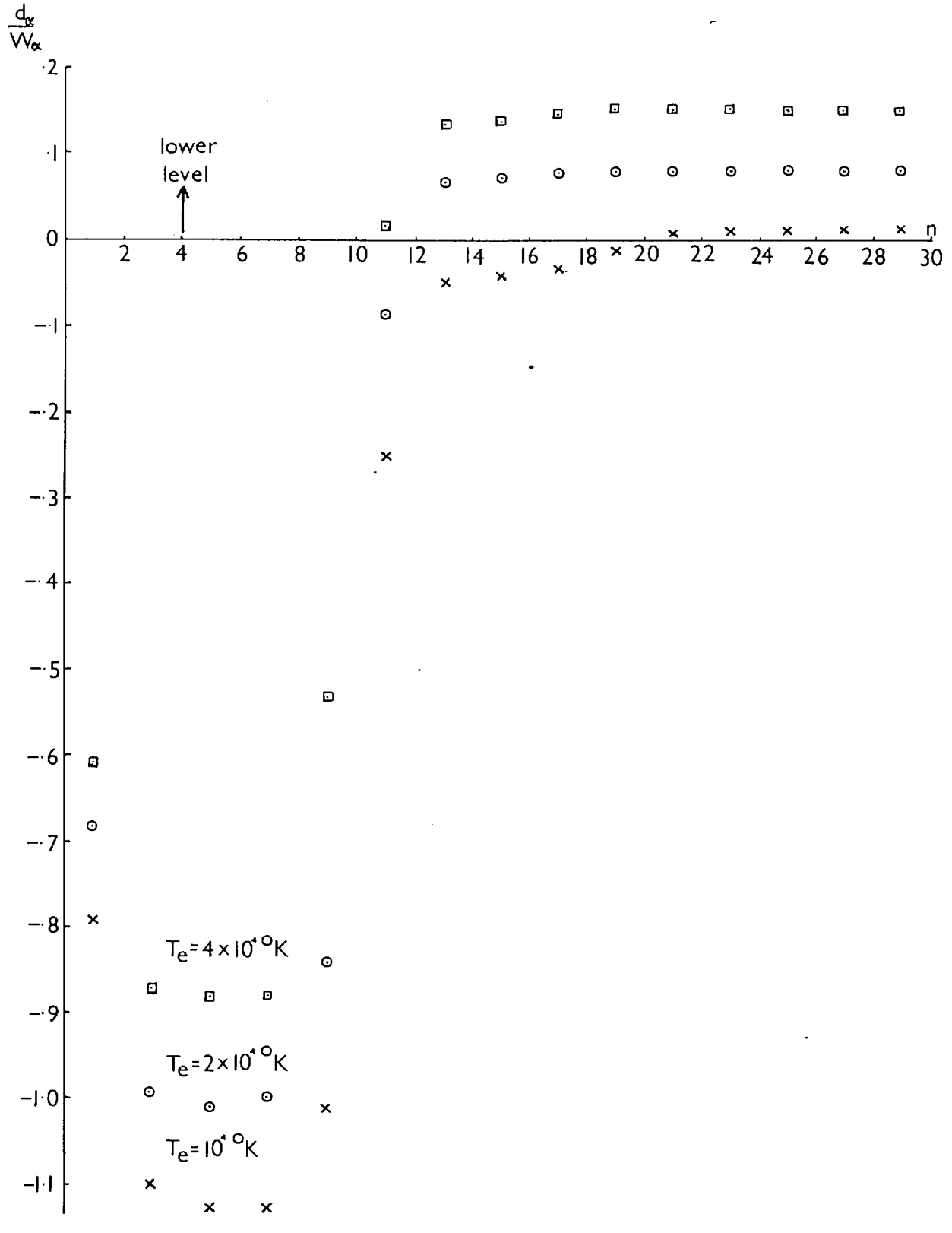


Fig. 5·5 $\frac{d_\alpha}{W_\alpha}$ versus number, n, of perturbing levels used in calculation. λ 4806 Å

higher T_e more electrons are 'allowed' to cause weak in-elastic collisions until the width becomes dominated by the weak collision term. As more levels are included the weak collision width increases monotonically with T_e as expected.

In comparison with the calculations in reference 2 the following points are of interest:-

(a) At the temperatures at which the experimental results of Chapter 4 were obtained ($T_e \simeq 30,000^{\circ}K$) 13 perturbing levels are required to give adequate convergence of the width, (fig.5.4). The same width is obtained for 30 as for 13 levels suggesting that inclusion of further perturbing states in the calculation is not necessary in this case. However the arbitary use of 5 levels by Griem will obviously not give a result near the 'limit' except at lower temperatures when the width is mainly due to elastic collisions.

For $\lambda 4880\text{Å}$ 9 levels out of a total of 23 were found necessary to give good convergence of the calculated width at $T_e = 30,000^{\circ}K$.

(b) The effect on the shift of including an increasing number of levels in the calculations is even more drastic (fig.5.5). With a small number of levels the calculated shift is large and to the blue as the dominant $E\alpha'$ are near and below $E\alpha$ [cf. Section 5.4(i)]. As distant $E\alpha'$ are above $E\alpha$ inclusion of more levels increases the calculated shift to give a small positive (red) value in the limit, (fig.5.5).

Again 13 levels are required to give adequate convergence of $d\alpha/W\alpha$ at $T_e = 30,000^{\circ}K$.

(c) While (a) and (b) show that calculations involving the arbitary use of a small number of levels cannot be justified they also indicate a serious breakdown of assumption A2, the 'no back reaction' condition.

Since this assumption is only necessary for the in-elastic collisions the relative contribution of these to the total width must be considered. Then the extent of the breakdown of A2 can be examined.

The way elastic and in-elastic collisions are treated on the Griem theory can best be seen with reference to fig.5.6.

The larger the impact parameter ρ and the larger the velocity the weaker the collision. The differentiation between weak and strong collisions is therefore defined by a curve of the form $\rho = \rho_W$ in fig.5.6.

The differentiation between elastic and in-elastic collisions is defined by a curve of the form E = I in fig.5.6. In the low velocity limit the collisions are all completely elastic. At high velocities the collisions are all completely in-elastic.

Relative numbers of the different types of collision are obtained by folding in the distribution of impact parameters, cut off at some shielding distance $\sim \rho_D$, and the Maxwellian speed distribution.

The expression for $W\alpha$ derived by Griem (equation 5.22) is from the 2nd order term in the perturbation expansion of 5.1. This involves matrix elements for $1 \rightarrow 1 \pm 1$ and therefore accounts for in-elastic contributions to the width only. However as was indicated physically by the discussion in

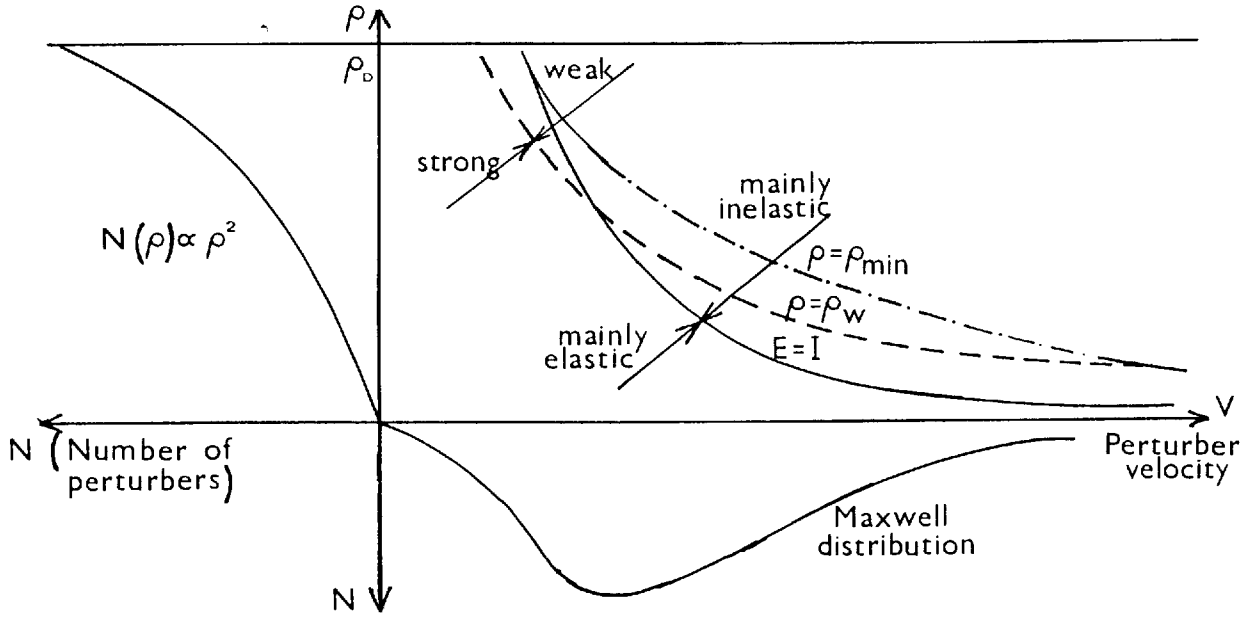


Fig. 5·6 Different types of broadening collision.

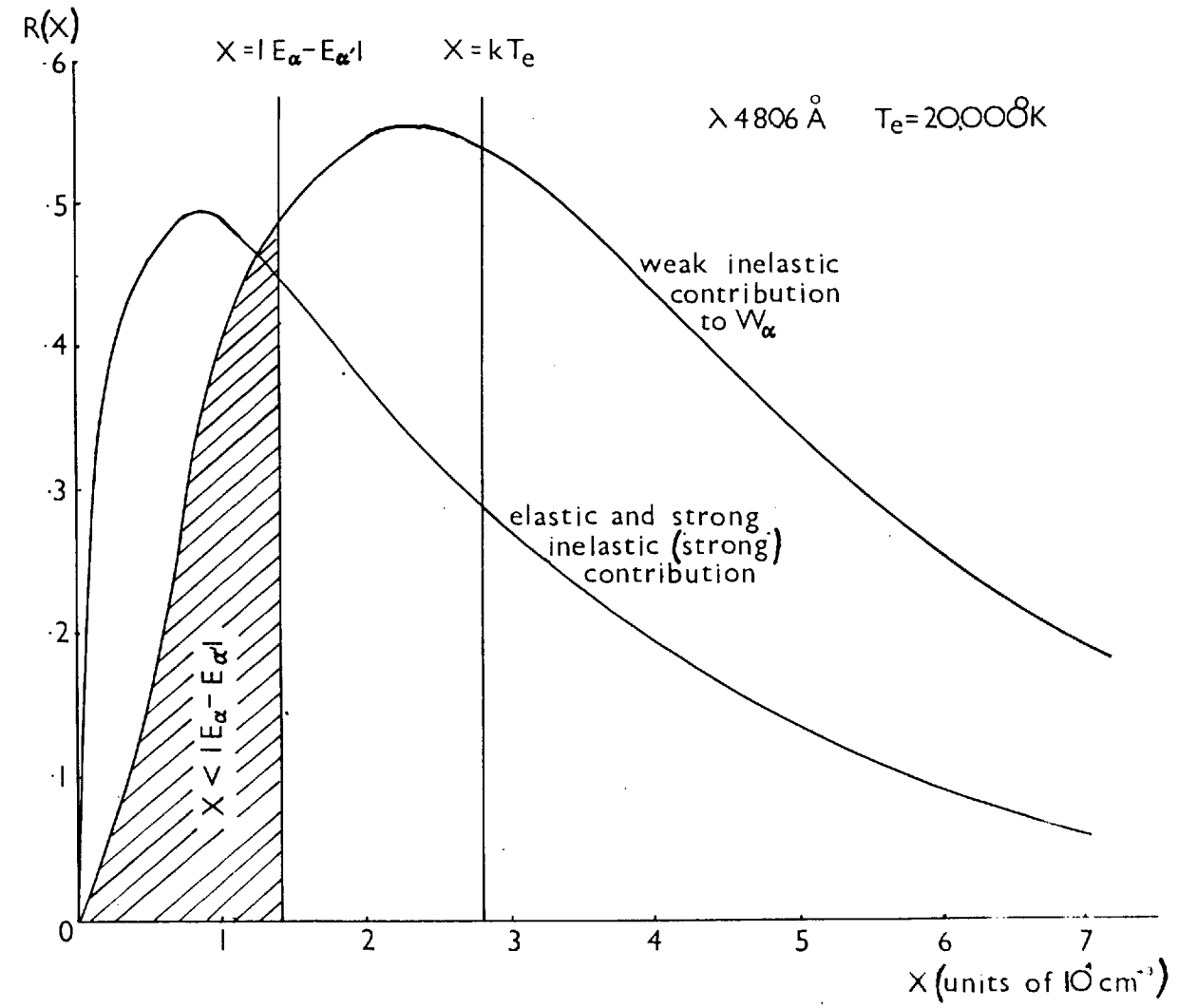


Fig. 5·7 R(X) versus X using one perturbing level in the calculations.

5.4(i) elastic contributions to the shift are also included. But elastic contributions to the width are in higher orders of the perturbation expansion.

Therefore equation 5.22 is exact in the high velocity limit except that strong collisions must be included in a Lorentz-Weisskopf term. To obtain elastic contributions to the width Griem matches the $\rho = \rho_w$ curve to the E = I curve at low velocities to give the $\rho = \rho_{min}$ curve. Thus the Lindholm width is obtained in the strong collision term at low velocities. In the intermediate energy regime weak in-elastic collisions are accounted for, and elastic and strong in-elastic contributions in the 'strong' collision term. The exact form of $\rho = \rho_{min}$ curve is only good at each end of the energy scale. Thus the treatment of elastic collisions may not be too good in the intermediate range. In particular weak elastic collisions are not being included in the calculation.

The ρ_{min} cut-off for the breakdown of the perturbation theory should strictly be chosen such that the width and shift satisfy a dispersion relation (Griem and Shen ref.96). This is satisfied by the expression given by Vainshtein and Sobel'man [ref.97]:-

$$W\alpha + id\alpha \rightleftharpoons N_e \int 1-e^{-(\eta+i\phi)}$$

Where $\eta + i\phi \sim \sum_{\alpha'} R_{\alpha,\alpha'}(A+iB)$ and $R_{\alpha,\alpha'} = |\langle \alpha | \underline{R} | \alpha' \rangle|^2$

The integration is over all impact parameters and velocities. η is a damping constant and ϕ a real phase shift. The exact forms of the above expressions are such that for $\phi \sim 0$ the only contribution to $W\alpha$ is from inelastic collisions and the relation for $W\alpha$ reduces to 5.22.

i.e. Inelastic contribution to $W\alpha$ for a given ρ and V,

$$W\alpha \sim \sum_{\alpha'} R_{\alpha',A}$$

For $\eta \gg 1$, i.e. strong inelastic collisions, $e^{-(\eta+i\phi)} \sim 0$

Then $$W\alpha \sim N_e \int = N_e \int f(V) V dV \int_0^{\rho_{min}} 2\pi\rho \, d\rho$$

which is the Lorentz-Weisskopf expression .

For $\eta \sim 0$ all collisions are elastic and reduction of the above relations gives this contribution as,

$$W\alpha \sim 1 - \cos \sum_{\alpha'} R_{\alpha',B}$$

In general, when both elastic and inelastic terms are important,

$$W\alpha \sim N_e \int (1 - e^{-\eta} \cos \phi)$$

Thus, due to the averaging procedure, the two types of collision cannot be 'separated out'. Because of this computational difficulties are increased on using this prescription.

However an estimate of the ratio of weak inelastic to weak elastic contributions to $W\alpha$ for a given ρ and V is given by :-

$$R' \sim \sum_{\alpha'} R_{\alpha',A} / \{1 - \cos \sum_{\alpha'} R_{\alpha',B}\}$$

If we consider only one perturbing level and take $\frac{1}{2} mv^2 = kT_e$ ($T_e = 20{,}000^{\circ}K$),

$$\rho \sim \rho_{min},$$

then from the computor results the corresponding value of $Z^{min}_{\alpha\alpha'} \simeq 0.3$. Thus $A(Z_{\alpha\alpha'})$ and $B(Z_{\alpha\alpha'})$ can be obtained from ref.2 giving :-

$$R' \simeq 20.$$

Consequently most of the elastic collisions must be strong and their inclusion in a Lorentz-Weisskopf term is reasonable.

The ratio, R, on Griem's prescription, of weak inelastic to elastic and strong inelastic contributions to the width is obtained directly from the output of the computor programme (see fig.5.7).

Thus for all perturbers with energy $\frac{1}{2}mv^2 = kT_e$ (with $T_e = 20{,}000^{\circ}K$),

$$R \lesssim 1.7$$

i.e. 60% of $W\alpha$ is due to weak inelastic collisions of electrons with energy,

$$\epsilon = 2.8 \times 10^{-12} \text{ ergs.}$$

However the separation of the first perturbing level from $E\alpha$ is,

$$|E\alpha - E\alpha'| = 1.4 \times 10^{-12} \text{ ergs}$$

Consequently there is a serious breakdown of the 'no back reaction' condition, A2.

In fact it can be seen from fig.5.7 that an appreciable part of the 'weak inelastic' term is contributed by electrons with insufficient energy to cause an inelastic collision. This must be due to breakdown of A2 rather than accidental inclusion of elastic effects.

When more distant perturbing levels are included in the calculation inelastic collisions to these are more easily caused by fast electrons with small ρ, i.e. strong collisions. Thus the strong collision contribution to the width is increased. However for those electrons that cause weak inelastic collisions the breakdown of A2 is more serious than with only the nearest $E\alpha'$ in the calculation.

(d) The lower level of $\lambda 4806\text{Å}$ is the fourth nearest perturbing level to the upper state. Inclusion of this level in the calculation appreciably increases $W\alpha$ and $d\alpha$ (fig.5.4 and fig.5.5). Thus assumption A3 is invalid.

5.4 (iv) Strong collision contribution to width

The 'strong' and 'weak' collision contributions to $W\alpha$ for $\lambda 4806\text{Å}$ at $T_e = 20{,}000^{\circ}K$ are shown in fig.5.8. Thirty perturbing levels were used in the calculation which gave these results.

The total contribution to $W\alpha$ in each case is proportional to the area under the $R(x)$ — X curve in fig.5.8. Thus $\simeq 58\%$ of $W\alpha$ is due to strong collisions. For $\lambda 4880\text{Å}$ this figure was $\simeq 54\%$.

This means that one of the validity criteria of the Impact approximation is invalidated [Section 5.4(i)]. Both elastic and inelastic parts of the 'strong' term must be considered in estimating the effect of strong collisions on this validity criterion. Physically the only difference is that the elastic collisions are considered as giving large phase shifts and the inelastic collisions as completely interrupting the emitted radiation.

For the weak collisions it is also necessary to satisfy the criterion, $W \ll W_p$ for the impact approximation to be valid.

$$W_p = 9 \times 10^{3} N_e^{\frac{1}{2}} \text{sec}^{-1}$$

Previous measurements gave;

$$W = 0.07\text{Å} \quad \text{for } N_e = 4 \times 10^{16} \text{cm}^{-3}$$

So the approximation should be valid for distances $\Delta\lambda$ from the line centre given by:-

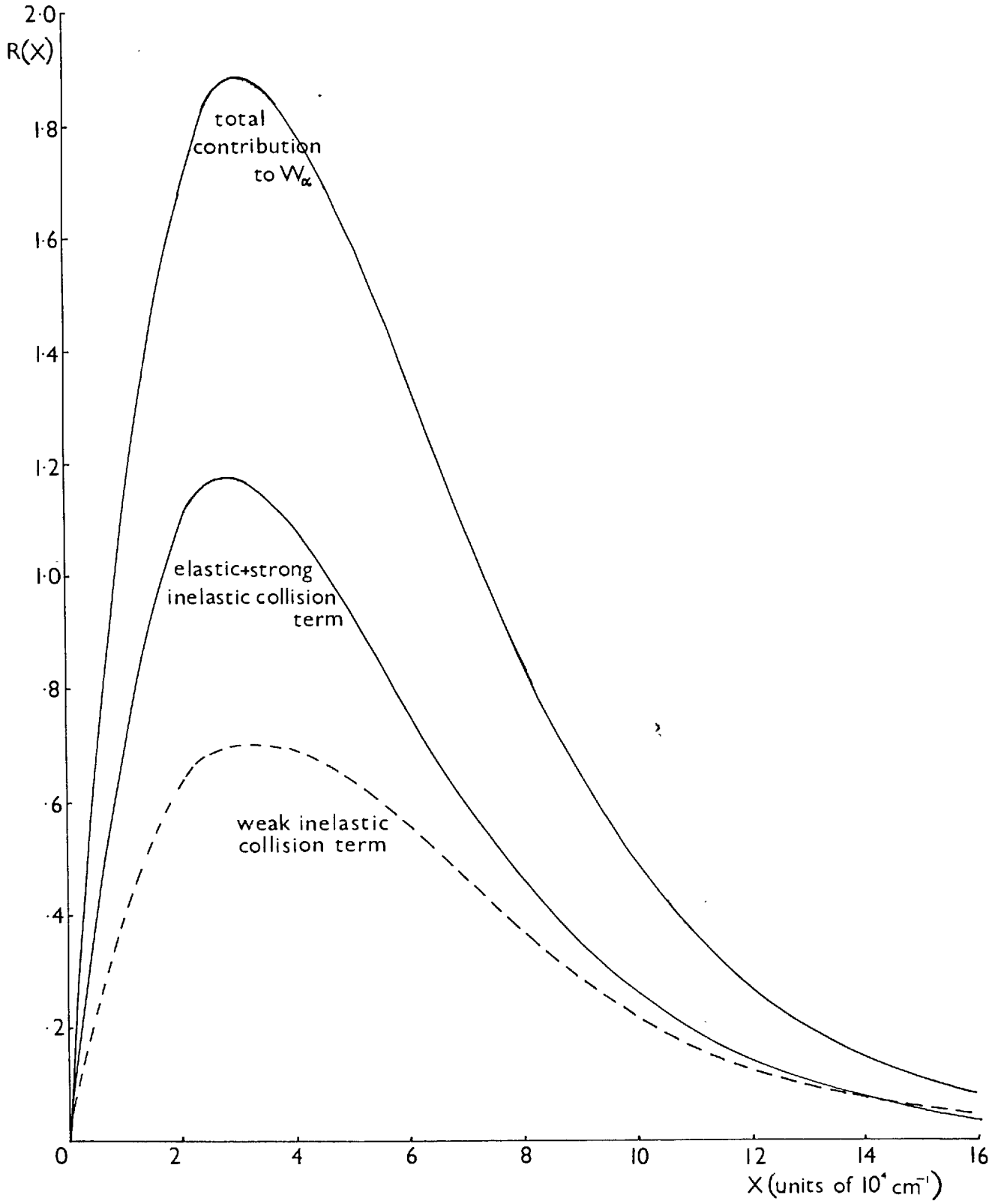


Fig. 5·8 Strong and weak collision contributions to W_α. λ4806 Å

$$\Delta\lambda \ll 14\text{Å}$$

This condition is well satisfied except in the far line wings.

The large size of the strong collision term will have two effects on the line profile:

(1) For the strong elastic collisions t_c is large so that [from Section 5.4(i)] the impact approximation is only valid nearer the line centre than if weak collisions alone were important. Thus divergences from a Lorentzian line shape could be expected nearer the line centre.

(2) Inclusion of weak collision effects on the emitter, when strong collisions are occurring, is likely to lead to an over-estimation of the total width (cf. Section 5.4(i)].

(3) A considerable uncertainty is incurred in the calculated width since the Lorentz-Weisskopf expression will only give a rough approximation to the actual physical conditions. Firstly there is some uncertainty in the value of ρ_{min} defined by the breakdown of perturbation theory. Secondly there should be a smooth transition between 'weak' and 'strong' collisions. The accuracy in the calculated shift is likely to be particularly poor since a large proportion of the collisions which contribute to the width (i.e. those collisions in the 'strong' term) are assumed to give no shift.

To further investigate the importance of strong collisions the ρ_{min} cut off used by Griem for HeI [ref.10] was inserted in the calculations. This ρ_{min} was simply the original value multiplied by a factor $\sqrt{1.55}$.

For both $\lambda 4806\text{Å}$ and $\lambda 4880\text{Å}$ the strong collision contribution to $W\alpha$ ($\alpha\rho^2_{min}$) was increased by a factor 1.55 as expected. However the weak collision term was reduced to such an extent as to keep the total width nearly the same as before.

This confirmed the possibility that much of the weak collision broadening was in fact caused by electrons for which $\rho \approx \rho_{min}$ rather than $\rho \gg \rho_{min}$. The importance of strong collisions is thus further emphasized.

5.4 (v) Validity of straight line classical path approximations

(a) Since most of the broadening has been shown to be caused by electrons with $\rho \approx \rho_{min}$ the validity of A1 is suspect.

The extent of a perturber wavepacket, $L \sim \hbar/\Delta P$
where ΔP is the spread in momentum of the wavepacket

$$\therefore \quad L \gtrsim \hbar/mV$$

From Appendix I we can express

$$\rho_{min} = (\hbar/mV) X \, (Z^{min}_{\alpha\alpha}/|E\alpha' - E\alpha|)$$

i.e. $$\rho_{min}/L \lesssim X(Z^{min}_{\alpha\alpha}/|E\alpha' - E\alpha|)$$

Evaluating the R.H.S., in the case of $\lambda 4806\text{Å}$, for electrons with $\frac{1}{2}mV^2 \sim kT_e$:-

$$X = 2.8 \times 10^4 cm^{-1}$$

$$Z\alpha\alpha' = 0.54 \text{ (with 30 perturbing levels in the calculation)}$$

$$|E\alpha' - E\alpha| = 7.2 \times 10^3 cm^{-1}$$

i.e. $$\rho_{min}/L \lesssim 2.1$$

For $\lambda 4880\text{Å}$ $\rho_{min}/L \lesssim 2.5$

Thus those electrons which cause most of the broadening cannot be adequately described as classical particles.

(b) We will now consider the effect on the calculated width of using hyperbolic orbits for the perturbers.

The scattering angle, θ, for a (classical) electron with impact parameter ρ is given by:-

$$\cot(\theta/2) = \rho m V^2/e^2 \quad \text{(for singly charged ions)}$$

Evaluating θ, $\rho \sim \rho_{min}$ and $\frac{1}{2}mV^2 \sim kT_e$:-

$$\therefore \theta \sim 96^\circ$$

Thus the electron orbits are strongly curved and assumption A7 is invalid.

For electrons which cause weak inelastic collisions, $\rho > \rho_{min}$ and $\frac{1}{2}mV^2 > |E\alpha - E\alpha'|$, the scattering angle will generally be less than the above value.

The inclusion, in the calculation, of hyperbolic paths (which should strictly include quantum mechanical corrections) means that the perturbers will come in closer to the emitter than if Coulomb effects were neglected. Thus the strong collision term would be altered. For those collisions still considered to be 'weak', $t_c \ll 1/w$ so the emitter can be assumed to be effectively unperturbed during the duration of a collision. Thus, due to the partial cancellation of the radial component of the electric field on the emitter during a collision, the broadening is decreased.

For slow electrons $t_c \not\ll 1/w$ so the radial components of the field reinforce and the broadening is increased. This effect is most pronounced for electrons with $\rho < \rho_{min}$ since the orbits are most strongly curved in this case. This is somewhat compensated by the increase of perturber velocity at the apex of the hyperbola making inelastic collisions more probable. However, overall, the strong collision width should be increased.

The decrease in width for weak collisions should be small, ($\rho > \rho_{min}$ so θ small). Thus the total width should be increased.

5.4(vi) Lower level broadening

To test assumption A4 the widths and shifts of the lower states of $\lambda 4806\text{Å}$ and $\lambda 4880\text{Å}$ were calculated independently of the upper states. The ratio of lower to upper state widths were:-

Line	W_L/W_U
4806	0.78
4880	0.47

Direct addition of W_u and W_L is liable to give an overestimation of the total width, $W\alpha$, since the addition should be done coherently using 5.6. In particular the 'strong' collision term would be overestimated. ρ min should be defined by:-

$$[U_u(t+\Delta t,t)U^*_L(t+\Delta t,t)-1] \longrightarrow 1$$

when upper and lower states are included in the calculation compared with,

$$[U_u(t+\Delta t,t)-1] \longrightarrow 1$$

for the upper state only.

Nevertheless the comparable sizes of W_u and W_L indicate that assumption A4 is invalid.

Thus conclusion is supported by the shift of $\lambda 4806\text{Å}$ measured by Burgess [ref.44]. This was small and to the blue at $T_e \sim 20{,}000^{\circ}K$ - a result confirmed later by Oertel (private communication). The calculated shift of the upper state of $\lambda 4806\text{Å}$ was small and to the red (fig.5.3). However the calculated shift of the lower state was larger and also to the red so inclusion of lower state interaction in the calculations would give a net blue shift.

Neglect of lower state interaction is therefore liable to give an appreciable underestimation of $W\alpha$ and cause considerable error in $d\alpha$, especially if the calculated shift of the upper state is small.

5.4 (vii) Ion broadening

Values of α, the ion broadening parameter, were tabulated in Section 5.4(ii) for $\lambda 4806\text{Å}$ and $\lambda 4880\text{Å}$. Use of 1.12 shows that ion broadening is completely negligible. This is still true for our measurements where doubly ionised species are important and therefore an increase in broadening by a factor $\sim Z^{2/3}$ can be expected [ref.2].

Also both lines were well isolated at the conditions studied i.e. for $\lambda 4806\text{Å}$,

$$W = .07\text{Å}$$

whereas the nearest strong line ($\lambda 4848\text{Å}$) is $\sim 42\text{Å}$ away. Thus assumption A6 is valid.

5.5 L-S coupling approximation

For all calculations the relevant matrix elements have been evaluated by assuming L-S couplimg. As these are not very 'good' quantum numbers for some AII states it is worth while re-estimating W_α employing more appropriate wavefunctions.

Using the results of Statz et al [ref.12] we can express the upper state of $\lambda 4806\text{Å}$ as a linear sum of pure L-S-coupled wavefunctions($3p^4 4p$ configuration):-

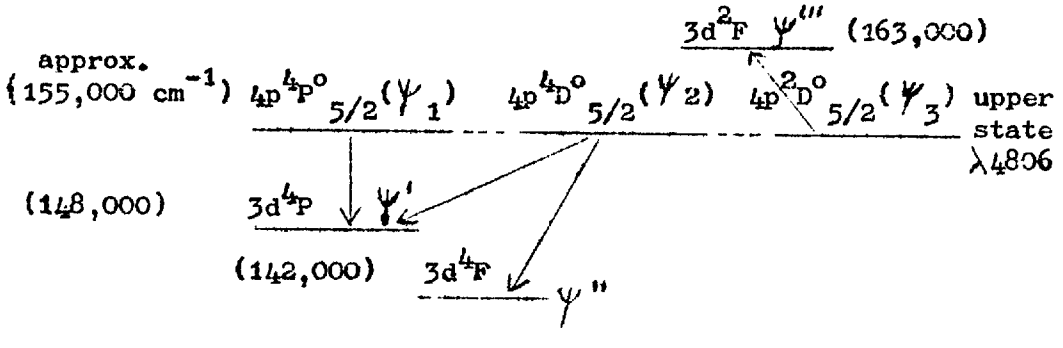
$$\psi_{J=5/2}\left[(3p)^4P^o\right] = 0.983\,\psi\left[(3p)^4P^o_{5/2}\right] - 0.178\,\psi\left[(3p)^4D^o_{5/2}\right] + 0.036\,\psi\left[(^1D)^2D^o_{5/2}\right] + \text{terms with smaller coefficients} = \sum_n a_n \psi_n$$

The matrix element coupling a level defined by E, ψ , is then :-

$$\left|\left\langle \sum_n a_n \psi_n \,|\, \underline{R} \,|\, \psi \right\rangle\right|^2,$$

neglecting second order terms arising from a similar splitting of level E, ψ.

The (nearest) perturbing level scheme for $\lambda 4806\text{Å}$ is now:-



The relevant matrix elements and corresponding energy differences are :-

$$|\langle a_1\psi_1 + a_2\psi_2 | \underline{R} | \psi' \rangle|^2 \quad , \qquad E\alpha - E(\psi')$$

$$|\langle a_2\psi_2 | \underline{R} | \psi'' \rangle|^2 \quad , \qquad E\alpha - E(\psi'')$$

$$|\langle a_3\psi_3 | \underline{R} | \psi''' \rangle|^2 \quad , \qquad E\alpha - E(\psi''')$$

Omitting terms such as $\langle \psi_3 | R | \psi' \rangle$ which vanish as we now have pure L.S wavefunctions.

The quadratic Stark coefficient for the nearest perturbing levels only is :-

$$C\alpha(\Sigma L.S) \propto a_1^2 |\langle \psi_1 | \underline{R} | \psi' \rangle|^2 / (E\alpha - E(\psi'))$$

$$+ a_2^2 |\langle \psi_2 | \underline{R} | \psi'' \rangle|^2 / (E\alpha - E(\psi'))$$

$$+ 2a_1a_2 \langle \psi_1 | \underline{R} | \psi' \rangle \langle \psi_2 | \underline{R} | \psi' \rangle / (E\alpha - E(\psi'))$$

$$+ a_2^2 |\langle \psi_2 | \underline{R} | \psi'' \rangle|^2 / (E\alpha - E(\psi''))$$

$$+ a_3^2 |\langle \psi_3 | \underline{R} | \psi''' \rangle|^2 / (E\alpha - E(\psi'''))$$

Compared with the expression used before :-

$$C\alpha(L.S) \propto |\langle \psi_1 | \underline{R} | \psi' \rangle|^2 / (E\alpha - E(\psi'))$$

Evaluation of these expressions gives:-

$$C\alpha(\Sigma L.S) = 0.98\, C\alpha(L.S)$$

Inclusion of more distant perturbing levels reduces the difference.

A similar calculation for $\lambda 4880\text{Å}$ shows that the difference in this case should be $< 3\%$.

Thus divergences from L.S coupling will not cause serious errors in the calculated values of $\omega\alpha$ and $d\alpha$.

5.6 Line widths within a multiplet

To justify the assumption made in Chapter 3 that all lines within a multuplet were equally broadened, each multiplet 6 line width was calculated separately. The results are tabulated below :-

Line	J_u	W_u*	J_L	W_L	$W_u/4806$	W_T/W_{4806}	λ^2 Factor
4806	$2\frac{1}{2}$	5.0	$2\frac{1}{2}$	3.9	1.00	1.00	1.00
4933	$1\frac{1}{2}$	5.2	$1\frac{1}{2}$	4.1	1.04	1.04	1.05
5062	$1\frac{1}{2}$	5.5	$\frac{1}{2}$	4.3	1.10	1.10	1.10
4848	$\frac{1}{2}$	4.9	$1\frac{1}{2}$	4.0	0.98	1.00	1.01

(*W in units of 10^{-3}Å for $N_e = 10^{16}\,cm^{-3}$)

The values of W_u and $W_T = W_u + W_L$ (normalised to the values for $\lambda 4806\text{Å}$) agree well with the assumption of equal line widths (in frequency units). This result arises because the perturber level configurations are so similar for the upper and lower states of each line.

Correspondingly, even though many breakdowns of the theory occur, we should always expect equal line widths.

5.7 Summary of results

For convenience it was necessary to discuss the validity of various assumptions made in the theory in a different order from which they naturally arose. The results of the calculations are therefore summarised, in order, in the following Table. For clarity $\lambda 4806\text{Å}$ only is considered.

Assumption		Mathematical representation	Comments
A1	'Classical Paths'	$L \ll \rho$	Invalid $L \simeq 0.5\rho$
A2	'No back Reaction'	$\|E\alpha - E\alpha'\| \ll kT_e$	Invalid $\|E\alpha - E\alpha'\| \simeq kT_e$
A3	'Nearby sub-states, $E\alpha'$'	$\|E\alpha - E\alpha'\| \ll \|E\alpha - E\beta\|$	Invalid. Lower state, $E\beta$, is an important perturbing state.
A4	'No lower state interaction'	$W_L \ll W_u$	Invalid. $W_L = 0.8\, W_u$
A5	'Impact Approximation'	$W \ll W_p$ One strong collision at a time	Validity restricted due to large number of strong collisions. Also width may be overestimated.
A6	'Isolated Lines'	$\|\lambda' - \lambda\| \gg W$	Valid.
	'No ion broadening'	$W_T \simeq W$	Valid. $W_T = 1.01\, W$
A7	'Straight Line Paths'	Scattering angle, θ, small	Invalid. $\theta \simeq 96^\circ$ for $\rho \sim \rho_{min}$ and $\frac{1}{2}mV^2 \sim kT_e$
A8	'Small strong collision width'	$W_s \ll W$	Invalid. $W_s \sim 0.6W$

The comments hold good for $\lambda 4880\text{Å}$ also, though the approximations are generally slightly better in this case.

To summarise, the validity of many of the assumptions made in the theory has been shown to be limited. Accounting for some of the theoretical difficulties could be expected to increase the calculated width and therefore reduce the divergences with experiment.

In the following three Chapters further experimental measurements of $\Omega(T_e)$ are described. The accuracy of these values was increased, compared with the results in Chapter 4, by improving the independent diagnostic techniques for determining N_e and T_e.

The measurements were performed on an instabilised Z-pinch thereby avoiding several sources of inaccuracy incurred in obtaining the results in Chapter 4 — In particular large optical depth and the measurement of only the axial N_e.

CHAPTER 6

INTERFEROMETRIC MEASUREMENTS OF Ne ON AN UNSTABILISED Z-PINCH DISCHARGE

6.1 Introduction

The suitability of an unstabilised Z-pinch as a source for studying line profiles has already been briefly discussed in Chapter 3. To avoid self absorption of the emitted profiles it was necessary to observe the plasma column side on. Thus it was desirable that measurements of Ne should also be made by viewing along the plasma diameter [cf. Chapter 4].

That such a measurement is inherently possible by means of laser interferometry can be seen from the results given in Chapter 3; i.e. at the condition 2.0 kv, 0.25 torr :-

$$\overline{NeL} \sim 8 \times 10^{17} cm^{-2}$$

(Using the measured Ω (Te) from Chapter 4 and L from framing camera photographs.)

Thus one might expect $\sim 4\frac{1}{2}$ fringe shifts up to peak compression using a Fabry-Pérot laser interferometer (at λ6328Å) to measure Ne. However there are several additional difficulties as compared with the Ne measurements described in Chapter 4 :-

(1) The 'lifetime' of the unstabilised discharge is much shorter than the Bz stabilised discharge so that a faster time response system, than in Chapter 4, is necessary. This rules out use of the Ashby-Jephcott system [ref. 49].

(2) Much more optical pick up could be expected due to the much higher values of Ne attained.

(3) The laser beam would have to be transmitted side on through a Pyrex tube rather than through the plasma via Brewster windows. The beam would therefore be reduced in intensity by refraction and because of the crazing of the tube walls after several discharges.

(4) There is a greater possibility of absorption of the laser beam by the plasma. Also severe Ne gradients might be expected so that refraction of the beam out of the plasma could be important.

In the rest of this Chapter it is shown that these difficulties can be overcome. Moreover, an attempt is made to show that the value of Ne determined is the same as that which characterises electron impact broadening.

6.2 Comparison of luminosities of interferometer systems

There are two interferometer systems which are inherently capable of detecting the rapid changes of Ne expected [i.e. from Fig.3.1]. Because of a large expected reduction in intensity of the laser beam [point (3) above] it is worth comparing the luminosities of these systems :-

(a) Fabry-Pérot

This system is shown in Fig. 6.1.

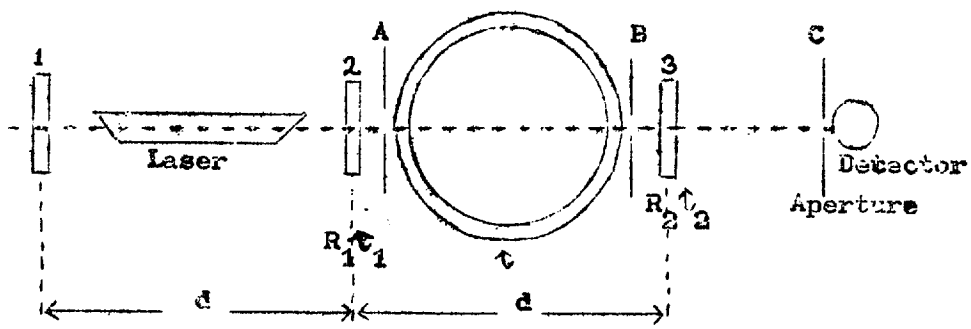


Fig. 6.1

If the laser intensity is Io and the overall transmission of the tube walls is τ the transmitted intensity received by the detector is :-

$$I = IoT'^2/(1-R')^2 \times 1/[1+(4R'/(1-R')^2)\sin^2\phi]$$

This is the well known Airy formula [ref.20] except that:-

$$R' = R\tau^2 \quad ; \quad R = \sqrt{R_1R_2}$$

and $$T' = T\tau \quad ; \quad T = \sqrt{\tau_1\tau_2}$$

Taking typical values of R and T (Chapter 2)

$$R = 0.90 \quad ; \quad T = 0.07$$

Thus, $\tau_E = 0.50Io$ and $N_R \sim 30$

While for $\tau = 0.80$:-

$$R' = 0.58 \quad ; \quad T' = 0.056$$

Thus, $\tau'_E = 0.02Io$ and $N'_R \sim 6$

Consequently a considerable reduction in performance of the system is obtained when the tube is inserted in the cavity.

(b) Mach-Zehnder

The best system, which would make use of beams from each end of the laser, is shown in Fig.6.2.

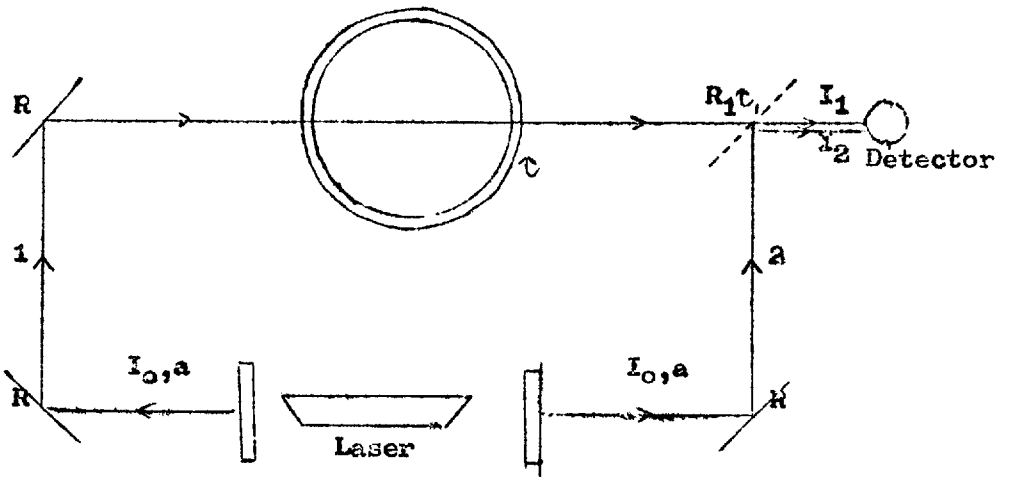


Fig. 6.2

Referring to Fig. 6.2,

$$I_1 = I_o R \tau \tau_1 \quad ; \quad I_2 = I_o R R_1$$

therefore Saddle to peak ratio at detector,

$$(\sqrt{I_1} - \sqrt{I_2})/(\sqrt{I_1} + \sqrt{I_2}) = 0 \quad \text{if } R\tau\tau \; , = R_1$$

For $\tau = 0.80$ and $R = 0.95$ this condition is satisfied for $R_1 = 0.4$ and $\tau_1 = 0.5$ (Chapter 2).

In this case the peak transmitted intensity is,

$$(a_1 + a_2)^2 = Io\,(R\sqrt{\tau\tau_1} + \sqrt{RR_1})^2$$
$$= 1.4Io$$

The peak intensity recorded by the detector should therefore be $\sim$ 70x that for the Fabry-Pérot system.

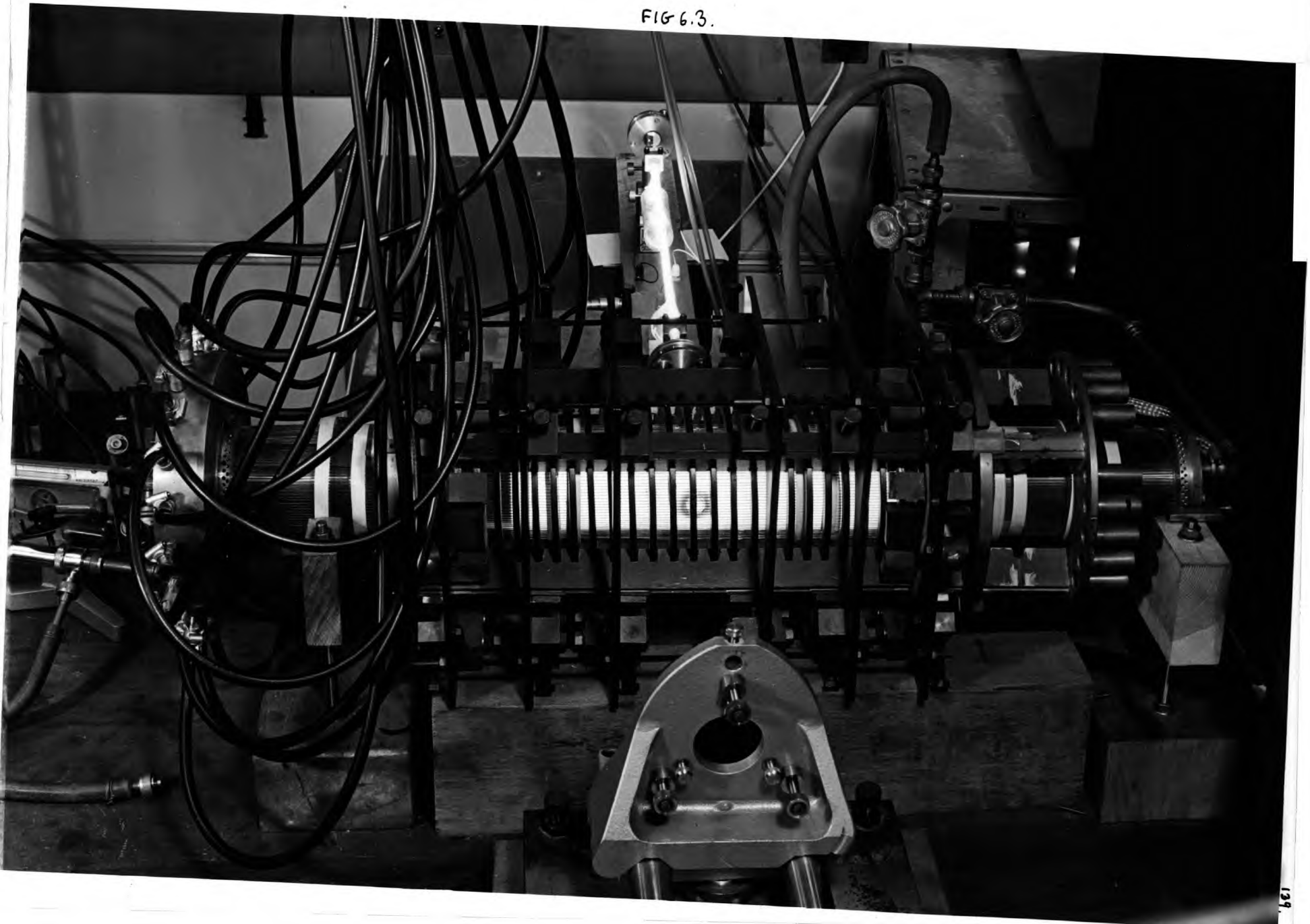
6.3 Initial measurements of Ne

Since only a few fringe shifts could be expected with the Fabry-Pérot [Section 6.1] this system was initially preferred to the Mach-Zehnder. If shortage of light proved to be a problem the later system could be employed.

For convenience, measurements were made side on to the Bz discharge tube but no stabilising field was applied. A photograph of the apparatus is shown in Fig.6.3.

The apertures A, B, C [Fig.6.1] were of 1mm diameter. A lens in front of A was sometimes found to be desirable to avoid excessive divergence of the laser beam by the discharge tube. An R.C.A.7625 photomultiplier with a response time $\sim$ 3n sec was used as a detector. The overall response time of the photomultiplier - C.R.O. was $\sim$ 15 n sec.

FIG 6.3.



A thin film products filter of peak transmission 70% and bandwidth 5Å was found to render optical pick up negligible under all conditions to be described [cf Section 6.1 (2)].

Setting up was initially performed by varying the optical path difference in the cavity 2 to 3 by using the vibrating mirror of the S.F.P. in place of mirror 3. It was found that with a detector signal $\sim$ 50m volts a fringe modulation $\sim$ 70% could be achieved. In later measurements setting up was more conveniently done by using a fixed mirror 3 and connecting its mount mechanically with a rotary pump. This gave sufficient vibration of the mirror to allow setting up of a fringe pattern on a slow time base ($\sim$2m sec/cm).

Initially fringe sequencies were recorded with a filling pressure of 0.20 torr and bank voltages of 1.5 kv and 2.0 kv. Turning points in these could be identified as corresponding to peak AII emission and therefore the number of fringes to peak compression found. The values of Ne calculated from 4.3 are tabulated below. The plasma diameters for Bz=0, recorded in Chapter 4, were used for L.

The measured values of Ne are compared with those measured on the stabilised pinch at the same initial conditions, [Chapter 4] and taking into account the different compression ratios from the plasma diameters with and without Bz stabilisation, i.e.

$$Ne = Ne'(d'/d)^2$$ (where ' refers to measurements with Bz stabilisation.)

Although the agreement between measured and estimated values of Ne were quite good it was preferable to have a better defined value of d than that from the continuum measurements.

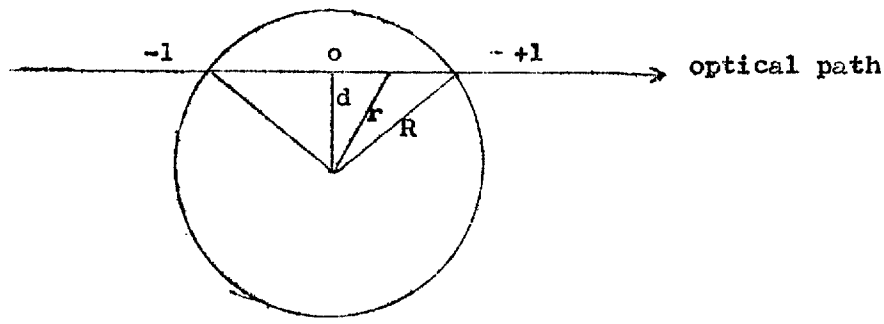
For this reason an attempt was made to obtain radial distributions of N_e.

Filling pressure 0.20 torr	Measured Ne cm^{-3}	Calculated $Ne'(d'/d)^2 cm^{-3}$
1.5 kv	4.4×10^{17}	4.7×10^{17}
2.0 kv	9.2×10^{17}	7.1×10^{17}

6.4 Abel inversion of laser measurements

Previously an effectively rectangular distribution of electron density Ne(r) was considered with the width of this distribution obtained from the continuum measurements.

For a non-rectangular but cylindrically symmetric distribution of Ne, the optical path difference for n Fabry-Pérot fringe shifts [for measurements at a height d above the tube centre] is given by:-



$$\delta(d) = \int_{-l}^{l} (\mu(\lambda)-1)dl = e^2\lambda^2/2\pi c^2 m \int_{-l}^{l} Ne(r)dl$$

$$= n(d)\,\lambda/2$$

therefore $$n(d) = e^2\lambda^2/\pi c^2 m \int_{d}^{R} Ne(r)rdr/(r^2-d^2)^{\frac{1}{2}}$$

This is completely analogous with the relation for the observed intensity, at a height d, in terms of the radial emission coefficient [ref.36]. The only difference is that we require absolute values of Ne(r).

The above relation can therefore be solved by the well known Abel inversion technique [ref.36] giving :-

$$Ne(r) = Const \int_{r}^{R} n'(x)dx/(x^2-r^2)^{\frac{1}{2}}$$

Therefore to obtain the radial distribution of Ne, Ne(r), measurements of the fringe shifts, N(d), to peak compression were performed at different heights, d, across the plasma column. These values were then Abel inverted using the basic computor programme of Key [ref.37]. This necessitated slight modification of Key's programme :-

For n(o) fringes up to peak compression at d = 0 and (arbitary) radial values of Ne,

$n_o, n_1, \ldots\ldots n_i$ for intervals dr

$$\sum_{i=o}^{m} [n_o Ne(o)/n_o + n_1 Ne(o)/n_o + \ldots.]dr = 1.69 \times 10^{17} n(o)$$

$$\text{i.e. } Ne(o) = \left(n_o / \sum_{i=o}^{m} n_i\right) \times 1.69 \times 10^{17} n(o)/dr$$

The programme was therefore modified to output absolute values of Ne(r) by use of the above expression,

i.e. $Ne(r) = n_i k$

where $k = 1.69 \times 10^{17} n(o) / \sum_{i=0}^{m} n_i dr$

and $r = idr$

Distributions of n(d) versus d for discharges at 1.5 kv and 2.0 kv (0.20 torr) are shown in Fig.6.4.

The results obtained from Abel inversion for 1.5 kv bank voltage are shown in Fig.6.5. To obtain some idea of the accuracy of the results three cut-offs were used, as indicated on Fig.6.4. These were actually extended out to d = 2.5 cm.

The best fit n(d) versus d curve gave on inversion, Ne(o) = $4.3 \times 10^{17} cm^{-3}$. For $r < 0.4$ cm the inverted distributions exhibited an axial dip in Ne $\sim$ 5% of thepeak Ne. Since this occurred with all three cut-offs it seems most likely that this was a real effect rather than an effect caused by inaccuracy of the Abel inversion technique. Therefore if pressure balance is assumed the core temperature must be rather higher than for $r > 0.4$ cm. The possibility of a hot core to a plasma with rather similar Gross conditions was first suggested by Burgess [ref.11,also see Chapter 4]. The results recorded here would therefore support this hypothesis. However, a discrepancy over plasma dimensions of the size noted by Burgess could not be accounted for by the values given here.

The three inverted curves gave a weighted mean for Ne(o) = $4.4 \times 10^{17} cm^{-3} \pm 9\%$.

For 2.0 kv bank voltage and 0.20 torr filling pressure the result was :-

$$Ne(o) = 8.4 \times 10^{17} cm^{-3} \pm 9\%$$

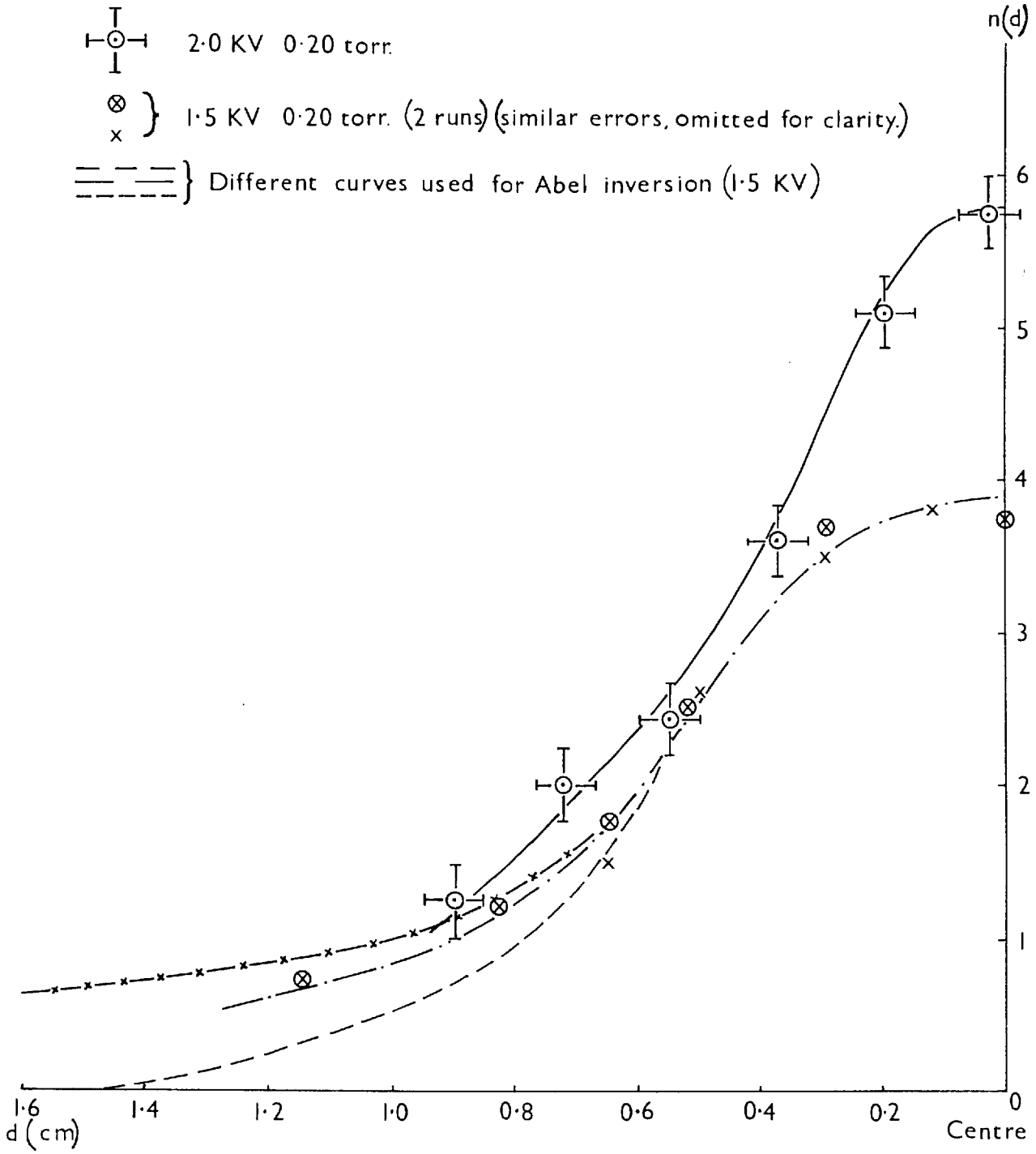


Fig. 6·4 Number of Fabry-Pérot fringe shifts to peak compression, n(d), versus d, distance across plasma.

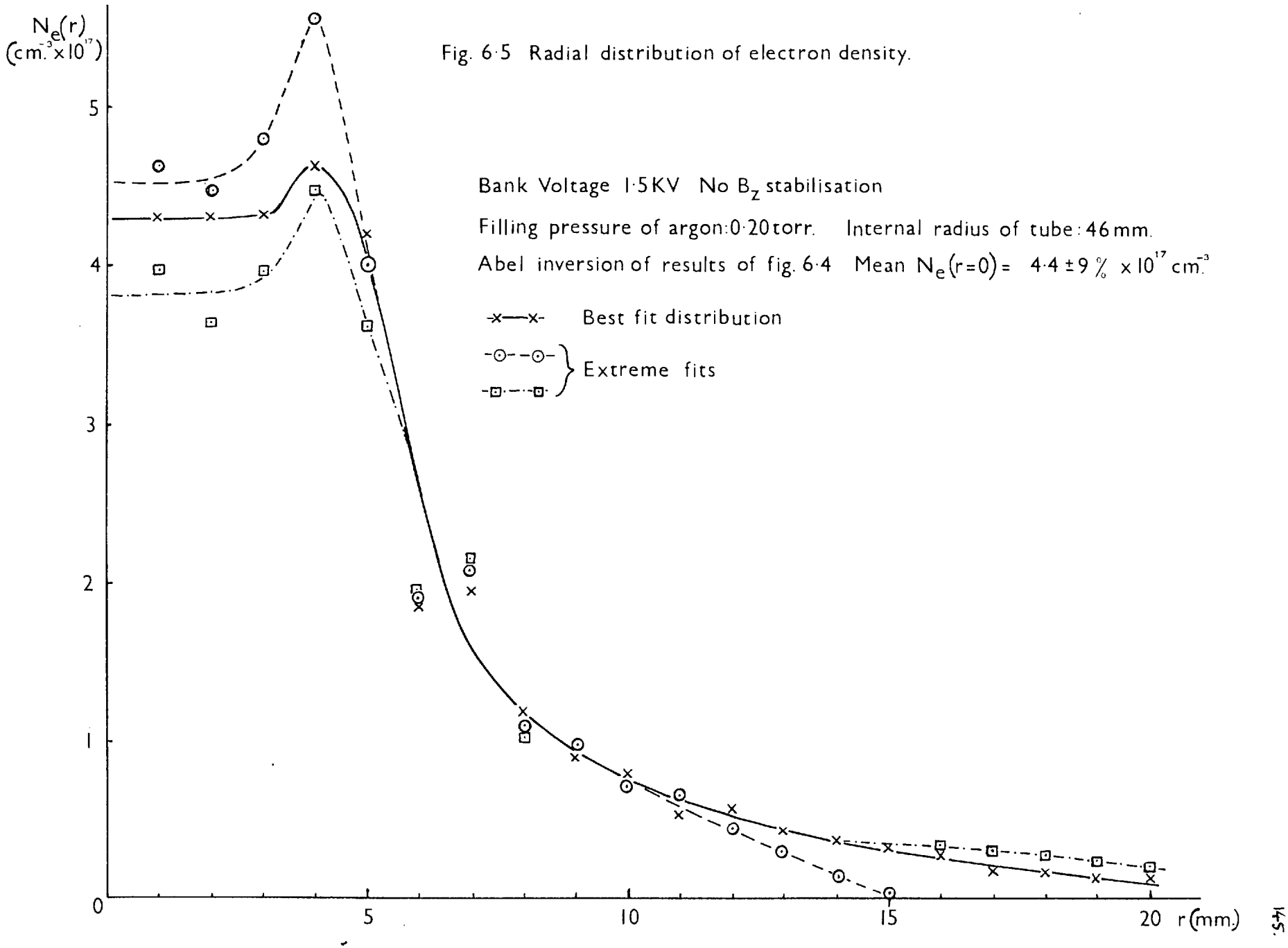


Fig. 6·5 Radial distribution of electron density.

These results agree very well with the initial estimates given in Section 6.3 though the widths of the Ne distributions are narrower than those of the continuum distributions. This is consistent with Te falling off at the edge of the plasma.

The largest error in Ne(r) obtained by this method was set by the inability to achieve a measurable number of fringe shifts, n(d), for large d. This could be overcome by using a quartz tube and monitoring the laser at $\lambda 3.39\mu$. In addition the accuracy of the Abel inversion technique could be improved (see for example ref.45).

For large d incoming shock fronts can cause turning points in n(d) versus time before the time of peak compression. However comparison with continuum measurements enabled interpretations of results for large d to be made without ambiguity. If necessary turning points could also be detected unambiguously by fast modulation of one of the plates of the Fabry-Pérot cavity (as in the initial setting up procedure).

Thus, inherently, there is no reason why radial distributions of Ne could not be measured much more accurately than 10% (say to $\sim 2\%$).

6.5 Contributions to plasma refractive index

It has previously been assumed that contributions from free electrons dominate the refractive index of the plasma. An attempt will now be made to justify this. Bound electrons, in fact, also contribute to μ so we can write :-

$$(\mu-1)_{TOTAL} = (\mu-1)_{F.E.} + (\mu-1)_{B.E.}$$

Where F.E. = free electrons

B.E. = bound electrons.

The free electron contribution can be expressed by the classical formula [ref.46] :-

$$(\mu-1)_{F.E.} = -(r_o/2\pi)\lambda^2 Ne \qquad \ldots \quad 6.1$$

It is necessary to show that :-

$$(\mu-1)_{F.E.}/(\mu-1)_{B.E.} = R \ll 1 \qquad \ldots \quad 6.2$$

R will be evaluated for the conditions, bank voltage 1.5 kv and filling pressure 0.20 torr. The conclusions obtained will, in fact, be generally applicable under all the plasma conditions studied here.

The analysis is somewhat simpler for a probing wavelength λ 3.39 μ which will therefore be considered first.

(1) $\lambda = 3.39\ \mu$

For a bound transition between an upper state m and a lower state n [ref.46] :-

$$\mu(W)-1 = -(e^2/2\epsilon_o)(1/(W_o^2-W^2_{mn})) \; Nn\, f_{mn} \qquad \ldots \quad 6.3$$

where W is the probing frequency.

This formula holds for [ref.46] :-

$$|W_{mn}-W_o| \gg \gamma$$

where γ is the classical dipole damping constant.

In our case the line shape is dominated by electron impacts. It is, however, still dispersive but the half width is 2W so the above inequality becomes

$$|W_{mn} - W_o| \gg 2W \qquad \ldots \quad 6.4$$

Converting 6.3 to wavelength units and summing over all upper states m and then all lower states n :-

$$(\mu(\lambda)-1)_{B.E.} = \sum_{n} \sum_{m \neq n} (r_o/2\pi) \lambda^2 \, Nn \, fmn / (1-(\lambda/\lambda mn)^2) \qquad \ldots 6.5$$

When m is lower than n, fmn is replaced by -fnm where fnm is the emission oscillator strength.

From 6.1, 6.2 and 6.5 :-

$$R = \sum_{n} \sum_{m \neq n} (Nn/Ne) \, fmn / (1-(\lambda/\lambda mn)^2)$$

Assuming L.T.E. :-

$$R = (Nz/BzNe) \sum_{n} \sum_{m \neq n} fmn \, g_n e^{-Wn/kTe} / (1-(\lambda/\lambda mn)^2) \qquad \ldots 6.6$$

For $\lambda mn \sim \lambda$ this relation breaks down. In this case the relation for classical radiation damping can be used, [ref.46], but with the damping constant $\gamma = 2W$. Then

$$(\mu(\lambda)-1)_{\lambda \sim \lambda mn} = (r_o \lambda^3/4\pi) (\Delta\lambda/(\Delta\lambda^2+W^2)) f_{mn} N_n (1-e^{-hv/kTe}) \qquad \ldots 6.7$$

where $\Delta\lambda_{mn} = \lambda - \lambda_{mn}$

The relation 6.6 for R together with 6.7 for the cases $\lambda_{mn} \sim \lambda$, must be summed over all species.

In the case under consideration

$$Ne = 4.4 \times 10^{17} cm^{-3}$$

and $$Te = 31,000^{o}K \qquad \text{[see Chapter 7].}$$

Corresponding to the above values, from reference 42 (and assuming L.T.E.) :-

$$\left.\begin{aligned} N_o &= 1.5 \times 10^{14} \\ N_1 &= 4 \times 10^{16} \\ N_2 &= 2 \times 10^{17} \end{aligned}\right\} \qquad \ldots 6.8$$

Some simplification of 6.6 can be made as the sum is dominated by the resonance transition in spite of the small λ_{mn} involved. Even when n is such that $e^{-Wn/kT}$ falls to $\sim 10^{-6}$, the maximum wavelength λ_{mn} that can occur [in the case of AlII for example] is $\sim 3{,}000\text{Å}$. Thus the maximum possible value of $\sum_{m>n} e^{-Wn/kTe} / (1-(\lambda/\lambda_{mn})^2)$ in this case is only 10^{-4} to 10^{-5} that value for the resonance transition.

R can therefore be roughly estimated by taking λ_{mn} as constant, equal to the resonance wavelength. In this case

$$(\lambda/\lambda_{mn})^2 \gg 1$$

Therefore $$R \sim (-Nz\ \lambda_{mn}^2 / BzNe\ \lambda^2) \sum_n g_n\ e^{-Wn/kTe} \sum_{m \neq n} f_{mn}$$

Using the Thomas-Kuhn-Reiche rule [ref.28]

$$\sum f_{mn} = Z = 1$$

and $$R \sim -Nz\ \lambda_{mn}^2 / Ne\ \lambda^2 \qquad \ldots 6.9$$

Summing over all species and using the data from 6.8 and reference 47 for the values of λ_{mn}, $R \sim -4 \times 10^{-4}$

Therefore the plasma refractivity at λ 3.39μ is dominated by the free electron contribution.

Thus Ne can be determined by a relation of the form

$$Ne\ \lambda_1^2 = k\ n_1 \lambda_1 \quad (\lambda_1 \equiv 3.39\mu)$$

as has previously been assumed.

(2) $\lambda = 6328\text{Å}$

Except for $\lambda_{mn} \sim 6328\text{Å}$ relation 6.9 can be used to evaluate R. In this case

$$R \sim 10^{-2}$$

However for wavelengths at which resonance effects are important, $\lambda \sim 6328\text{Å}$, the populations N_R are generally much higher than for $\lambda\, 3.39\mu$. It is therefore worth considering the case $\lambda \sim 6328\text{Å}$ separately by use of 6.7. The most important lines for which $\lambda \sim 6328\text{Å}$ are emitted by AII. Thus on substitution of the relevant quantities for AII into 6.7 we obtain

$$(\mu(\lambda)-1)_{\lambda \sim 6328\text{Å}} / (\mu(\lambda)-1)_{F.E.}$$

$$\approx -58 \sum_n \sum_m \Delta\lambda f_{mn} g_n e^{-W_n/kT_e} / (\Delta\lambda^2 + W^2)$$

$$\times (1 - e^{-h\nu_{mn}/kT_e})$$

where $\Delta\lambda$ is in Å

The nearest line to the probing wavelength $\lambda 6328\text{Å}$, is only $\Delta\lambda = 0.31\text{Å}$ away and might be expected to dominate in the above relation.

f_{mn} was calculated for this AII line ($4f\,{}^4F^o_{2\frac{1}{2}} - 6g\,{}^4F_{1\frac{1}{2}}$) using the Coulomb approximation [ref.31] giving :-

$$f_{mn} = 7.8 \times 10^{-3}$$

$\Delta\lambda$ will be altered by shifts of the plasma line but on upper limit to the above expression is given by :-

$$(n(\lambda)-1)_{\text{AII line}} / (n(\lambda)-1)_{F.E.} \lesssim (-58/\Delta\lambda)\, f_{mn} g_n e^{-W_n/kT}$$

$$\times (1-e^{-h\nu/kT})$$

(where $\Delta\lambda$ = 0.31Å the unperturbed separation)

$$\lesssim \quad -7 \times 10^{-4}$$

Contributions from other lines near the laser wavelength depend on their relative $f_{mn}/\Delta\lambda$ values but are usually far less than this. The total contribution from nearby plasma lines is therefore most probably much less than 1%.

In conclusion the contributions to the plasma refractive index at λ 6328Å from sources other than the free electrons should not amount to more than one percent, i.e. much less than experimental errors. However we expect the contribution at λ3.39μ to be even smaller.

6.6 Experimental investigation of free electron contribution to plasma refractive index (6328Å)

From the above discussion μ can be expected to be completely dominated by free electrons at λ3.39μ.

i.e. $Ne\,\lambda_1^2 = k\,n_1\lambda_1$

where n_1 = number of fringe shifts at λ3.39μ.

For the same Ne at λ6328Å we have

$$Ne\,\lambda_2^2 + A = k\,n_2\lambda_2$$

where A is the contribution from bound electrons

i.e. $A/Ne\,\lambda_2^2 = (n_2\lambda_1/n_1\lambda_2) - 1$

This ratio, from Section 6.5 is probably small and negative.

To verify this experimentally measurements were made at one plasma condition at both λ_1 and λ_2. To allow measurements to be made at λ3.39μ two quartz windows of aperture 1.2 cm were araldited on to the centre of the tube, diametrically

opposite each other. Measurements at λ 6328Å subsequently showed that these had no detectable effect on the radial distribution of Ne.

For measurements at 3.39μ a liquid N_2 cooled detector was used. The time response of this detector plus amplifier was only $\sim$ 1μ sec so that measurements could not be made at voltages above 1.25 kv (at 0.20 torr).

At this condition fringe shifts up to peak compression were :-

λ6328Å $\qquad n_2 = 2.75 \pm 0.25$

λ3.39μ $\qquad n_1 = 15.5 \pm 0.25$

giving $\qquad A/Ne\,\lambda_2^2 = 0.05 \pm 0.10$

Which confirms the conclusions of 6.5 to within experimental error.

Having confirmed the dominance of the free electron refractivity the absolute magnitude of μ can be estimated from 6.1, i.e. at 1.5 kv (0.20 torr)

$$(\mu - 1) = 7.9 \times 10^{-5} \quad (\lambda 6328Å)$$

so the approximation used in the calculations,

$$(\mu^2 - 1) \sim 2(\mu - 1) \qquad \text{(see ref. 46)}$$

was well justified.

6.7 Discussion

In the analysis of 6.5 a sharp differentiation was made between 'free' and 'bound' electrons by using the Debye expression for depression of ionisation potential in Saha's

equation to cut off $\sum_n g_n e^{-Wn/kTe}$.

The question now arises as to how the 'free' density achieved from laser measurements compares with that which gives rise to Stark broadening.

Griem [ref.48] considers the electron density Ne' obtained by the laser measurements (using 6.1) as being larger than that from Saha's equation due to the inclusion of very weakly bound electrons. The extra electrons he considers are those between the (Debye) reduced ionisation limit and a level approximately the photon energy, hc/λ, lower than this. However since it has been shown that all bound electrons contribute only $\sim$ 1% to the refractive index this term must be much less than 1% of Ne.

Further, Griem considers that those bound electrons whose Bohr radius exceeds the mean distance between free electrons or ions should be counted as 'broadening' electrons. Again this term is much less than 1% Ne.

Therefore it seems unlikely that uncertainties in the 'definition' of Ne could cause errors of more than $\sim$1% in applying the laser determined Ne to characterise Stark broadening. These errors are very small compared with those from experimental sources (i.e. $\sim$ 10% in Ne and $\sim$ 10% in W).

To summarise, the feasibility of making accurate independent measurements of Ne in an unstabilised Z-Pinch plasma has been demonstrated. The fact that refraction of the laser beam out of the plasma does not occur under the conditions we have studied means that gradients of μ and therefore Ne are small along a length of plasma $\sim$ 1 mm. (i.e. the 'width' of the laser beam). Correspondingly the plasma can be considered

uniform along the length viewed in the line profile measurements.

In addition the radial distribution of Ne can readily be obtained by straight forward Abel inversion.

CHAPTER 7

ELECTRON TEMPERATURE MEASUREMENTS

7.1 Choice of Diagnostic

The method of measuring the electron temperature of a plasma from the widths of optically thick line profiles, as described in Chapter 4, is only sensitive in certain temperature regimes. Moreover misinterpretation of results can be caused since the absorption at the centre of a line is a two valued function of temperature. It was therefore desirable to use a different diagnostic technique which was not subject to these limitations.

The method chosen was the measurement of the relative intensities of two lines emitted by different ionisation stages of an element. This ratio is a very sensitive function of Te [Ref. 50] but the regimes of Te in which a reliable theoretical relation can be given for the function are rather limited [Ref.50]

If the plasma is in complete L.T.E. the intensity ratio of lines of frequency ν and ν' from successive ionisation states is given by [Ref.50]

$$\frac{I'}{I} = \frac{2\,\nu' A'_{mn} g_m}{\nu A_{mn} g_m} \quad \frac{(2\pi m_e kT_e)^{3/2}}{N_e h^3} \quad e^{-\left(\frac{W'_m + E_z - \Delta E_z - W_m}{kTe}\right)}$$

Whether or not a model of complete L.T.E. can be applied to the plasma conditions studied previously will be disscussed later. It can be seen that the ratio, for L.T.E., also depends on Ne. Since this parameter was in any case measured accurately on the B_z stabilised pinch (Chapter 4) and unstabilised pinch (Chapter 5), no further restrictions was involved.

The observations of lines from AII and AIII was favoured since the intensity of AI lines would be very small at values of Te$\sim$30,000°K (Chapter 4) and they would in any case be too broad to be well isolated.

The AIII line λ3344.7Å and AII line λ3350.9Å were selected for the intensity measurements. These lines were bright and well isolated under all conditions studied, as seen from the spectra taken (Chapter 4). Also the lines are separated by only $\sim$5Å and the mean wavelength is at the peak response of an R.C.A. I.P.28 photomultiplier. It was therefore not necessary to make even a relative calibration of the detecting system at the two wavelengths.

7.2 Preliminary measurements of line width and shift

The instrument used for recording the line intensities was a Hilger medium quartz spectroscope fitted with an E.720 photomultiplier unit housing an R.C.A. IP.28 photomultiplier. This unit was fitted with a manual drive which enabled it to be used as a scanning spectrometer. One revolution of the scale (calibrated in degrees) attached to the drive corresponded to a 1mm translational movement of the exit slit.

Since the far line wings of a dispersive profile contribute a significant proportion of the total line intensity it was desirable to have the spectrometer exit slit as wide as possible to accept most of the total intensity of each line.

However, since the exit slit width in this case was limited to a relatively small value ($\sim$5Å corresponding to the separation of the two lines), it was necessary to obtain information about the width and shift of each line at each

condition at which Te was to be measured. Estimates could then be made of the proportion of the total intensity of each line accepted in each measurement.

The line profile measurements were carried out as follows :-

The instrument was focussed photoelectrically on λ3341.5Å HgI emitted by a low pressure mercury lamp with entrance and exit slits set at 5 microns. A calibration was made using a Hg lamp and a check made that the instrument was also in focus at λ4358Å. The widths of the Hg lines could be neglected compared with the instrument width obtained.

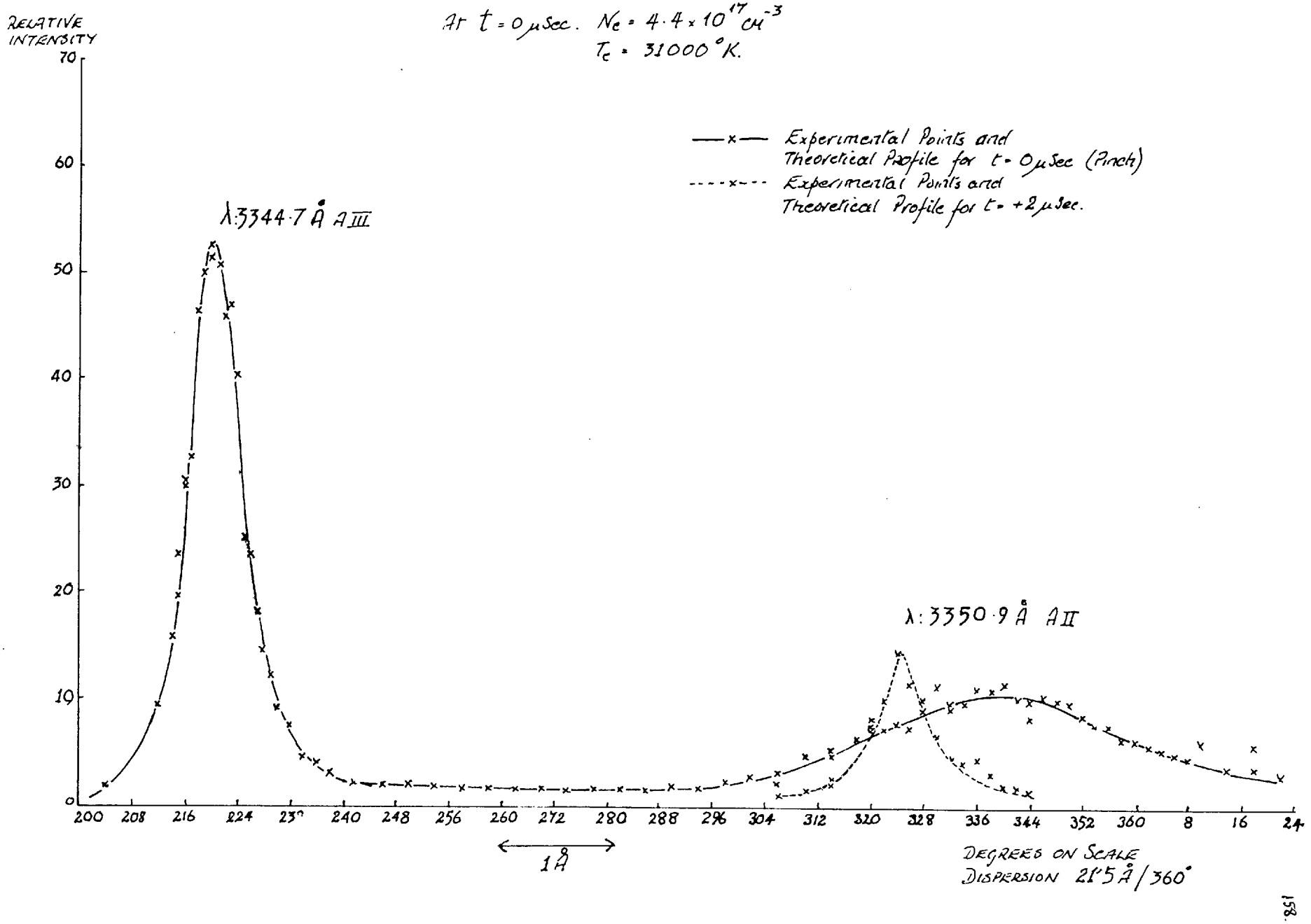
The AII and AIII lines were scanned across on a multishot basis at a condition previously studied (1.5 kv 0.20 torr) with a time response of the detecting system $\sim$ 0.15 μ sec. Care was taken to accept the same solid angle as in the instrument profile determination.

The intensities at different points across the line profiles were estimate from the C.R.O. traces at the pinch time (known from Chapter 6) and 2 μ sec later when N_e had fallen to a known value. The results are shown in Fig.7.1.

The profiles well in the afterglo agreed well with the λ3341.5Å HgI instrument profiles and their separation gave a dispersion of 21.5 $\pm$ 0.5 A/mm. This figure agreed with the Hg line calibration.

The measured line widths and shifts at the pinch (assuming unshifted afterglo profiles) are given in the table below. Also quoted are Ne (from Chapter 6), Te (anticipated from Section 7.3) and the theoretical upper state widths and shifts (calculated using the programme described in Appendix I).

Fig 7·1 MULTISHOT SCAN OF A II AND A III LINES FOR T_e MEASUREMENT.



	$Ne = 4.4 \times 10^{17} cm^{-3} \pm 9\%$ $Te = 31,000^{\circ}K \pm 1,000^{\circ}K$			
Line (Å)	Experimental W (Å)	Theoretical Wu	Experimental d	Theoretical du
3350.9 AII	1.30 ± 0.09	1.41 ± 0.14	1.01 ± 0.13	$+ 0.85 \pm 0.09$
3344.7 AIII	0.10 ± 0.05	0.14 ± 0.02	0.04 ± 0.01	0.19 ± 0.01

If the good agreement between experimental and calculated values of W and d/W for the AII line is assumed to extend to other conditions then (from the calculations) W and d/W should be fairly in sensitive functions of Te. Thus, at every condition at which Ne is known, W is given by $1.30\ Ne/4.4 \times 10^{17}$ and d/W is the same as in the above Table. Compared with the AII line the width and shift of the AIII line is negligible. Thus good estimates could be made for the best position of the exit slit, and consequently the proportion of the total intensity of each line accepted, in each measurement.

7.3 Intensity ratio measurements

In the measurement of the line intensities the entrance slit was set as narrow as possible consistent with a reasonable signal to noise ratio, (the width was 5μ except at conditions 4 and 5 below when a 10μ slit was used). The exit slit was set at 200μ (corresponding to $\backsim 4$Å) and placed symmetrically with respect to each line for all measurements. Backlash errors were avoided by first centring on λ3341.5Å HgI. An

estimate of the continuum intensity at each condition was made using a 50μ slit centred on λ3343Å.

The results obtained and the corresponding values of Te, assuming L.T.E. and using 7.1 are tabulated below. Ne was obtained from Chapters 4 and 6 and appendix 3. Values of A_{mn} were calculated on the Coulomb approximation [ref.31]. The depression of ionisation potential of AII, ΔEoo, was calculated using the Debye expression [ref.51].

Condition	Tube voltage kv	Magnet voltage kv	AIII/AII line ratio	Ne cm^{-3}	Te (^{o}K) assuming L.T.E.
1	1.0	1.0	0.8	3.2×10^{16}	24,000
2	1.5	1.0	5.2	4.0×10^{16}	28,900
3	2.0	1.0	7.1	5.8×10^{16}	30,900
4	0.5	0	0.1	7×10^{15}	< 20,000
5	0.75	0	2.5	3.6×10^{16}	27,000
6	1.0	0	3.5	1.1×10^{17}	29,600
7	1.5	0	1.6	4.4×10^{17}	31,050
8	2.0	0	1.1	9.2×10^{17}	31,900

Before discussing the errors in the measurements the extent to which a model of complete L.T.E. can be applied to the conditions studied will be examined.

7.4 Validity of L.T.E.

In a homogeneous time independant plasma complete L.T.E. corresponds to :-

(1) The free electrons being describable by a Maxwell-Boltzmann distribution characterised by Te.

(2) Ne being so high that electron collisional population and depopulation rates of all levels completely outweigh their radiative counterparts.

Considering free electron states first, the satisfaction of (1), following Wilson [ref.52], corresponds to :-

$$t_{ee} \ll t_{en} , t_{part} \qquad \ldots 7.2$$

The electron-electron relaxation time, t_{ee}, is given by Spitzer [ref.53]. For conditions in the above table it lies between 5×10^{-12} and 2×10^{-13} secs.

The energy heating time of the plasma, t_{en}, and the particle containment time t_{part}, can be roughly estimated from the Ne versus time curves, (e.g. Chapter 4). Under all conditions 7.2 is easily satisfied.

The satisfaction of (2) for free electrons corresponds to

$$t_{ee} \ll t_{rad} \qquad \ldots 7.3$$

The radiative decay time for Bremstrahlung, t_{rad}, can be estimated using [ref.52].

$$t_{RAD} \sim 1.4 \times 10^{11} Te^{\frac{1}{2}} Ne^{-1}$$

This lies between 1×10^{-3} and 3×10^{-5} at the conditions studied so 7.3 is also readily satisfied.

Thus under all conditions the free electrons have a thermal (L.T.E.) distribution.

For bound states it is necessary to estimate the critical Ne below which condition (2) is not satisfied.

There are, to date, three expressions for this critical Ne :-

(1) $Ne = 9.2 \times 10^{11} Te^{\frac{1}{2}} W^3(p,q)$ [Griem ref.51]

(2) $Ne = 1.6 \times 10^{12} Te^{\frac{1}{2}} W^3(p,q)$ [McWhirter ref.54]

(3) $Ne = 5.6 \times 10^{11} Te^{\frac{1}{2}} W^3(\infty)$ [Wilson ref.52]

... 7.4

Where $W(p,q)$ is the resonance level energy and $W(\infty)$ ionisation energy of the particular ionic stage considered (in e.V). These relations were all derived for H_2-like species. Applying them directly to AII and AIII species we get (with $Te = 30{,}000^{\circ}K$) for the critical Ne :-

	Critical Ne	
Criterion	AII	AIII
1	3.9×10^{17}	4.5×10^{17}
2	6.8×10^{17}	7.8×10^{17}
3	2.0×10^{18}	6.5×10^{18}

L.T.E. is always more difficult to satisfy for AIII and therefore this case only will be considered. Since the critical Ne given above ranges over a factor of 10 it is worth deciding which to use.

Condition (3) was derived by considering the 'thermal limit' in an ion, down to which thermal equilibrium (which as

seen above usually holds for the free electrons) extends. The ionisation potential for this limit W_t was then set = W (∞) for the thermal limit to extend down to the G.S. of the ion, i.e. to give complete L.T.E. Since the approximations involved were based on $W_t \ll W_i$ this would seem a dubious procedure. It was justified in (3) since it gave essentially the same result as the criterion used in (1) and (2) that the radiative decay rate from the 1st excited states of a H_2 like ion to the ground state should be much less (arbitarilly taken as 10%) than the collisional decay rate. Much the same result is obtained in such a case since W (p,q) is not greatly different from W(∞). This is not the case for AIII where the 1st excited state is very non-hydrogenic (i.e. $n^* = 2.1$ whereas $n = 3$).

We can certainly say that if criterion (3) is satisfied L.T.E. holds. Nevertheless, this condition is probably too stringent. On the other hand since the 1st excited state in AIII is so low conditions (1) and (2) (derived for H_2like ions) could give an underestimate of the Ne required for complete L.T.E. since there could be a larger energy gap than W(p,q) for which the criteria would be more stringent.

Condition (3) will therefore be taken as the one to be satisfied.

In fact this criteria can be relaxed since radiative population of the ground state is conterbalanced to some extent by absorption of photons and re-excitation.

The radiative population rate of the G.S. is thus reduced by approximately :-

$$R = \frac{\int_{-\infty}^{\infty} B_\nu \left(1-e^{-t_o/(1+(\nu/W)^2)}\right) d\nu}{\int_{-\infty}^{\infty} B_\nu \, t_o/(1+(\nu/W)^2) \, d\nu} \quad \text{for a dispersive line shape} \qquad \ldots 7.5$$

(Assuming the plasma conditions are near L.T.E.)

For t_o large this reduces to :-

$$R \sim 4/\pi t_o \qquad \ldots 7.6$$

(Roughly evaluating 7.5 for $-2W < \nu < 2W$)

If we consider the 1st excited state as being the most effective at populating the G.S. then t_o must be evaluated for the resonance line. Now for the upper state of the 3344.7Å AIII line (from Section 7.2) :-

$$\left.\begin{aligned} W &= 1 \times 10^{-1}\text{Å} \\ g &= 3.9 \times 10^{-2}\text{Å} \end{aligned}\right\} \quad \text{at } Ne = 4 \times 10^{17}\,cm^{-3} \text{ and } Te \sim 30{,}000^{\circ}K$$

The convolution of these two profiles gives very nearly a dispersive profile of $\frac{1}{2}$ - $\frac{1}{2}$ width 1.1×10^{-1}Å.

For such a line, therefore, we would assume a Stark profile in the estimation of t_o. This assumption will also be made for the AIII resonance line. In addition the width of this line will be taken to be the same as the λ3344.7Å line.

Both assumptions may not be very good since the ion will be less polarisable in the upper state of the resonance line compared with the upper state of the 3344.7Å line and the Stark broadening consequently smaller. However, the assumptions will lead, if anything, to an underestimation of t_o. Taking f_{mn} for the resonance line arbitarily as 1 and using 3.4 we have

$t_o \sim 17$ For condition (7) above.

However, we cannot assume that the critical Ne, given above, can be relaxed directly by the factor $4/17\Pi \simeq 7.5 \times 10^{-2}$ because radiative population of the G.S. from the second excited state is now important. For this transition t_o, calculated as above is ~ 1 so this line is therefore probably not appreciably reabsorbed. We shall therefore follow Griem [10].and assume that criterion can be relaxed by about order of magnitude to give :-

$$\text{Critical Ne} \simeq 6.5 \times 10^{17}$$

Thus on the basis of complete L.T.E. the line intensity ratios for the conditions Ne = $4.4 \times 10^{17} cm^{-3}$ and Ne = 9.2×10^{17} cm^{-3} were calculated from 7.1 (Fig.7.2). It should be noted that although the former Ne lies slightly below the critical Ne an uncertainty in the population ratio AIII/AII of 50% leads only to an uncertainty in Te $\simeq$ 2%. Thus we expect negligible theoretical errors at the above values of Ne. The line intensity ratios were calculated using two expressions for ΔE_{oo} :-

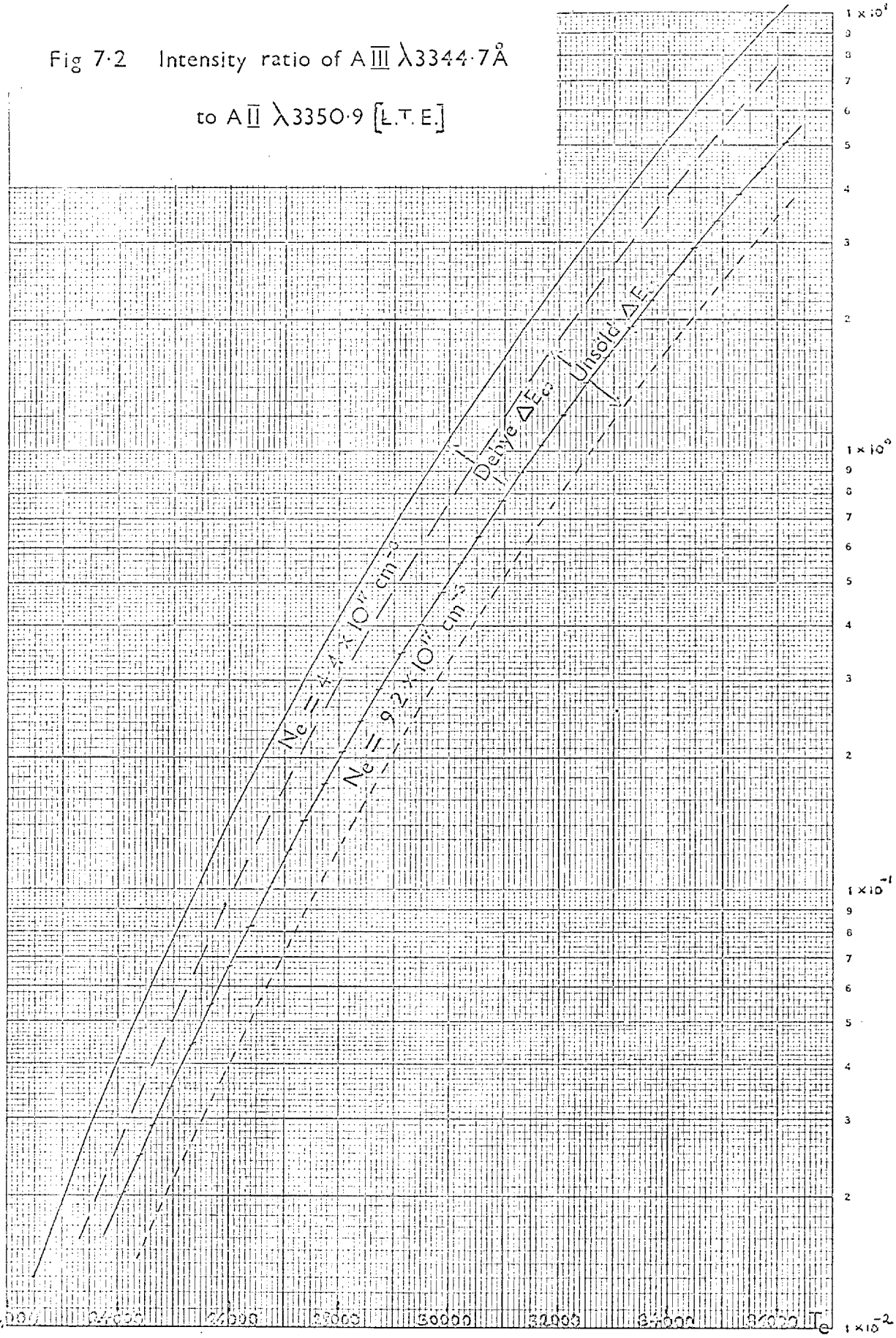
(1) Debye Expression $\Delta W_2 = 2.32/\rho_D \ cm^{-1}$ [ref.56]

(2) Unsöld Expression $\Delta W_2 = 7.05 \times 10^{-3} \ Ne^{1/3} cm^{-1}$ [ref.56]

While there is, as yet, no conclusive evidence as to which expression should be used [ref.55] the differences in Te obtained for a given intensity ratio are only $\sim$2% so the Debye expression will be employed in subsequent calculations.

Two further criteria must be satisfied for L.T.E. when the plasmas are time dependent and inhomogeneous:-

Fig 7·2 Intensity ratio of A III λ3344·7Å to A II λ3350·9 [L.T.E.]



(1) Changes of Te are small during the times over which ionisational and exitational equilibrium are established. The latter time is given by Griem [ref.51] as :-

$$\tau \sim \left[(1.15 \times 10^{7}(Z+1)^{3}N_{z+1}) / (f_{mn}Ne(N_{z}+N_{z+1}))\right]$$

$$\times((W_m - W_n)/W_h^z)(kTe/W_H^z)^{\frac{1}{2}} e^{(W_m-W_n)/kTe} \text{ secs.}$$

Where f_{mn} refers to the resonance transition of charge state Z.

For the case of AIII and AII ionisational equilibrium (z=1) and conditions 7 and 8

$$\tau \sim 10^{-8} \text{ secs}$$

This is obviously small compared with times $\sim 1\mu$ sec (from the AIII and AII intensity versus time traces) during which Te is nearly constant.

(2) Ions must not move into regions of very different Te in the times for equilibration as given above. The distance moved by an ion in such a time is given by Griem [ref.51] as :-

$$d \sim (7 \times 10^{14}/A^{\frac{1}{4}})(kTe/W_H^z)^{\frac{1}{2}}((W_m - W_n)/f_{mn}W_H^z)^{\frac{1}{2}} e^{(W_m-W_n)/2kTe}$$

$$\div 10^{\frac{1}{3}}N^{z+1} \text{ cms}$$

Here $d \sim 4 \times 10^{-3}$ cms so this condition is again easily satisfied as can be seen by inspection of the radial Te distribution (see Chapter 8).

In conclusion the plasmas studied at conditions (7) and (8) above are describable by the L.T.E. model. Uncertainties in Te from theoretical difficulties should be only $\sim 3\%$ at these conditions.

7.5 Estimate of Te for plasmas not in L.T.E.

The majority of the plasma conditions studied (above table) cannot be adequately described by a model of L.T.E.

In addition Ne is too high for coronal or semicoronal equilibrium to hold. Wilson [ref.52] gives a criterion for the latter case which becomes :-

$$Ne \lesssim 2 \times 10^{14} \text{ for AIII at } T_e = 30{,}000^{\circ}K$$

Therefore a detailed analysis of the rate equations populating the upper state of each line should strictly be performed. Since this is impossible in general the following procedure will be adopted :-

The neglect of radiative processes (especially radiative decays to the ground state) when N_e is less than the critical value at which L.T.E. ceases to hold, N_e^c, should lead to an overestimation of $N(Z+1,P)/N(Z+1,g)$ on using the L.T.E. relations.

However, $N(z,p)$ can be related accurately to $N(z+1,g)$ since L.T.E. is much easier to satisfy for AII. Therefore, for the conditions $N_e < N_e^c$, $N(z+1,p)/N(z,p)$ and hence I'/I should be overestimated. Consequently T_e should be underestimated.

Therefore for $N_e < N_e^c$ a model is required which, if anything, will lead to an underestimate of $N(z+1,p)/N(z+1,g)$. Then T_e can be estimated from the extreme values from this model and L.T.E. .

If the population processes for this model are assumed to occur via intermediate states i then, in the steady state and assuming optical thinness:-

$$n_e \sum_i n(z+1,i)\, X\,(i,p) = n(z+1,p) \sum_i [A(p,i)+n_e X(P,i)] \quad \ldots \quad 7.6$$

For state p, summing over all possible i.

If the populations of the levels i are assumed to be governed by a Coronal type relation :-

$$n_e n(z+1,g)\, X\,(g,i) = n(z+1,i)\, A\,(i,g) \quad \ldots 7.7$$

Then, from 7.6 and 7.7 :-

$$n(z+1,p)/n(z+1,g) = n_e \frac{\sum_i X\,(g,i)X(i,p)/A(i,g)}{\sum_i [A(p,i)+n_e\, X\,(p,i)]} \quad \ldots 7.8$$

Use of 7.7 should result in an underestimate of the ratio in 7.8 since self absorption and radiative and collisional population of state i has been neglected.

Inspection of the AIII term scheme shows that in 7.6 the most important i are below p.

For these i a comparison can be made of the terms A(p,i) and n_e X (p,i).

The de-excitation coefficient X(p,i) can be related to the excitation coefficient X(i,p) by [ref.54] :-

$$X(p,i)/X(i,p) = g(p)/g(i)\, e^{W(i,k)/kTe} \quad \ldots 7.9$$

The excitation coefficient is [ref.57] :-

$$X(i,p) = \left[8.5 \times 10^{-4} \bar{g}\, f(i,p)/T_e^{\frac{1}{2}} W(i,p)\right] e^{-W(i,p)/kT}$$

(Where W is in e.V, T_e in ^oK) $\quad \ldots 7.10$

The Gaunt factor $\bar{g}$ can be taken = 0.2 from Allen [ref.5].

f(i,p) can be related to A(p,i) by [ref.5] :-

$$f(i,p)/A(p,i) = (g(p)/g(i))\ \lambda^2_{ip}/6.7 \times 10^{15} \quad \ldots 7.11$$

(where λ is in Å)

Thus from 7.9, 7.10 and 7.11 :-

$$n_e X(p,i)/A(p,i) = 2.54 \times 10^{-20}\ \lambda^2_{ip}\ n_e/W(i,p)T_e^{\frac{1}{2}}) = R \quad \ldots 7.12$$

For λ_{ip} = 3344.7Å, AIII this ratio is :-

$$R = 4.4 \times 10^{-16}\ n_e$$

Generally, for the strongest transitions p → i, R > 1 at $N_e \gtrsim 10^{16} cm^{-3}$ (as in the conditions studied). Thus 7.8 can be simplified to :-

$$n(z+1,p)/n(z+1,g) = n_e \frac{\sum_i X(g,i)X(i,p)/A(i,g)}{\sum_i X(p,i)} \quad \ldots 7.13$$

Using relations above this can be reduced to :-

$$n(z+1,p)/n(z+1,g) = 2.6 \times 10^{-20} \frac{g(p)\ e^{W(p,g)/kTe}}{g(g)\ Te^{\frac{1}{2}}} \times \frac{\sum_i A(p,i)\ \lambda^2_{ip}\ \lambda^2_{ig}/W(p,i)W(i,g)}{\sum_i A(p.i)\ \lambda^2_{ip}/W(p,i)} \quad \ldots 7.14$$

Examination of the sums in 7.14 using values of A(p,i) calculated on the coulomb approximation [ref.31] shows that the dominant term is that where i is the lower state of λ3344.7Å. The expression is then essentially independent of transition probabilities and reduces to :-

$$n(z+1,p)/n(z+1,g) = 2.2 \times 10^{-16} n_e\ e^{-W(p,g)/kTe}\ /T_e^{\frac{1}{2}} \quad \ldots 7.15$$

Seaton [ref.57] considers his relation for the cross section (equation 7.10) to be good to a factor ~ 2x so the above relation should involve a similar uncertainty.

It is now necessary to relate n(z,p) with n(z+1,g). This can be done using Saha's equation if the thermal limit [ref.52] extends down to level p under all conditions. Wilson [ref.52] shows the thermal limit is at a level of binding energy W_t when :-

$$W_t^7 = 3 \times 10^{-28} W_z (kT_e)^{-1} N_e^2$$

Substituting $W_t = W(z+1,g) - W(z,p)$ (e.V.) and $kT_e = 3$ e.V., the limit should extend down through level (z,p) for $N_e > 10^{15}$ cm^{-3} - a condition satisfied in all cases which were studied.

Thus the appropriate Saha equation can be used [ref.50] :-

$$N_e N(z+1,g)/N(z,p) = 2g_{z+1,g}/g_{z,p} \; (mkT_e/2\pi\hbar^2)^{3/2} \; e^{-(W_z - W_p)/kT_e} \qquad \ldots 7.16$$

Combining 7.15 and 7.16 and inserting the relevant A_{mn} and ν values (cf equation 10.1) we get

$$I'/I = \tfrac{1}{4} T_e \, e^{-(W'_m + W_z - \Delta W_z - W_m)/kT_e} \qquad \ldots 7.17$$

Where $W'_m = W(z+1,p)$

$W_m = W(z,p)$

Relation 7.17 holds best for low N_e. Therefore a smooth transition will be assumed between I'/I for $N_e = 2.2 \times 10^{16} cm^{-3}$ (the lowest N_e measured) given by equation 7.17 and I'/I for $N_e = 4.4 \times 10^{17} cm^{-3}$ corresponding to L.T.E. (see Fig.7.3)

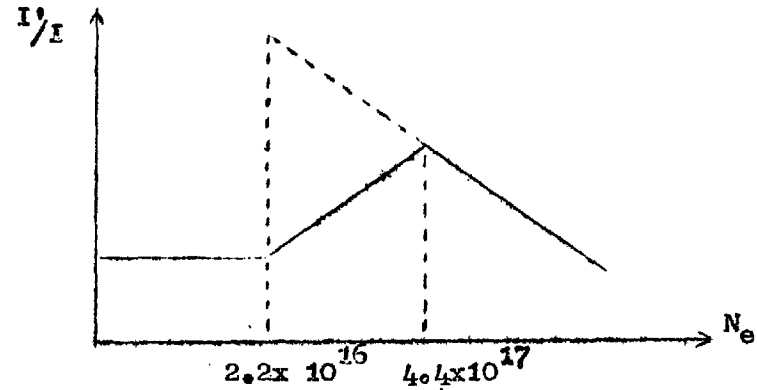


Fig. 7.3

The temperature at each N_e will be taken as that corresponding to matching the observed I'/I to that given midway between this smooth transition curve and the L.T.E. value. The theoretical error in T_e will be taken as the difference between this T_e and the L.T.E. value. Results obtained are:-

Condition	T_e (L.T.E.)°K	T_e (L.T.E.-'CORONAL')°K
1	24,000	27,000 ± 3,000
2	28,900	31,500 ± 2,500 *
3	30,900	32,500 ± 1,500 *
4	< 20,000	< 20,000
5	27,000	29,500 ± 2,500
6	29,600	30,800 ± 1,200
7	31,050	31,100 ± 1,000
8	31,900	31,900 ± 1,000

Errors from other sources comprised uncertainties in the line wing correction (~10%), in the continuum corrections (~10%) and in the calculated transition probabilities (probably not greater than 20%) - in all leading to uncertainties in T_e of only ~3% . In addition errors arose due to inhomogeneity of the plasma column. Uncertainties in the axial value of T_e were therefore ~ 5% (see Chapter 8). Therefore further errors ~ 6% must be added to the systematic errors from theoretical uncertainties given in the above table.

7.6 Plasma polarisation shift

One indirect result obtained from the above work was that the measured shift of λ3350.9Å provided further evidence against the existence of a plasma polarisation shift as

(* Note that these values agree well with those given at the end of Section 4.10)

predicted by Berg et al [ref.13] :-

Experimental shift d (Å)	Calculated electron impact shift dI	Calculated polarisation shift [ref.13] d_p
1.01 ± 0.13	0.85 ± 0.09	-0.62 ± 0.06

(account is taken of shifts of both upper and lower levels in the estimation of d_p).

Similar conclusions were reached from earlier results by Day and Griem [ref.71] and Burgess and Cooper [ref.44].

A revised model of the polarisation shift given by Griem [ref.72] would give for λ3350.9Å :-

$$d_p = -0.04Å$$

This could easily be accounted for within the results of the table above.

It would seem likely, however, that if instead of using a time averaged potential as in ref.72 a time dependant potential were used with the correct hyperbolic paths for the electrons then d_p would be included in the electron impact shift. Use of this model would then also include broadening effects.

CHAPTER 8

FURTHER MEASUREMENTS OF AII LINE BROADENING PARAMETERS

8.1 Width measurements

Line profiles of several AII lines were recorded at peak compression of the unstabilised plasma using the S.F.P. The initial conditions employed were 1.5 kV bank voltage and 0.20 torr filling pressure of argon since this discharge was examined in detail in the measurement of N_e (Chapter 6) and T_e (Chapter 7).

After each line profile shot a laser fringe sequence was recorded, integrating along an axis through the centre of the discharge tube. No detectable difference in the number of fringe shifts to peak compression was detected for any shot.

The measured line widths are tabulated below. Also included is the AII line used in the measurement of T_e (Chapter 7) :-

$N_e = (4.3 \pm 0.4) \times 10^{17} cm^{-3}$ $T_e = 31{,}500 \pm 1{,}000^{\circ}K$		
λ(Å)	Transition	W
4806	$4s\,^4P_{2\frac{1}{2}} \longrightarrow 4p\,^4P^{o}_{2\frac{1}{2}}$	0.89 ± 0.13
5062	$4s\,^4P_{1\frac{1}{2}} \longrightarrow 4p\,^4P^{o}_{1\frac{1}{2}}$	0.97 ± 0.10
4880	$4s\,^2P_{1\frac{1}{2}} \longrightarrow 4p\,^2D^{o}_{2\frac{1}{2}}$	1.08 ± 0.15
4266	$4s\,^4P_{2\frac{1}{2}} \longrightarrow 4p\,^4D_{2\frac{1}{2}}$	0.74 ± 0.10
3351	$4p\,^2F^{o}_{2\frac{1}{2}} \longrightarrow 4d\,^2F_{2\frac{1}{2}}$	1.30 ± 0.09

8.2 Distortion of profile due to plasma inhomogeneity

The recorded line profiles were obtained by integrating the radiation from an inhomogeneous plasma. The effect of this was estimated as follows. Consider the radiant distribution of N_e and T_e in fig.8.1 :-

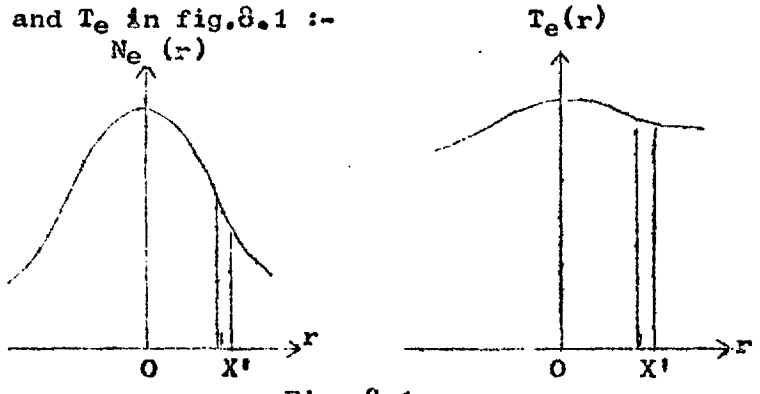


Fig. 8.1

The normalised Stark profile emitted by a plasma element at radius x' is, assuming optical thinness :-

$$L(\lambda, x') = (1/\pi W)(1/(1+((\lambda-d)/W)^2))$$

Where $W = \Omega[T_e(x')]N_e(x')$

$d/W = d/W\ [T_e(x')\ \text{only}]$

$= F[T_e(x')]$

i.e. $$L(\lambda,x') = \frac{(1/\pi\Omega[T_e(x')]N_e(x'))}{1+(\frac{\lambda}{[T_e(X')]N_e(X')} - F[T_e(X')])^2} \qquad \ldots 8.1$$

The total intensity emitted by the element (x', Δx') is

$$I(x') = k\, N_i(x')e^{-Wn/kT_e(x')} \qquad \ldots 8.2$$

where k is a constant.

Therefore the distribution of intensity from this element is given by :-

$$I(\lambda,x') = I(x')\, L(\lambda,x') \qquad \ldots 8.3$$

$N_1(x')$ can be related to $N_e(x')$ and $T_e(x')$ through the equations of charge neutrality and Saha :-

$$N_1(x') + 2N_2(x') \simeq N_e(x') \qquad \ldots 8.4$$

and $$N_2(x')N_e(x')/N_1(x') = G[T_e(x'),\ N_e(x')] \qquad \ldots 8.5$$

Thus from equations 8.1 to 8.5 we can obtain $I(\lambda,x')$ as a function of the variables $T_e(x')$, $N_e(x')$, $\Omega[T_e(x')]$ and $F[T_e(x')]$.

The observed distribution of intensity is obtained from:-

$$I_{OBS}(\lambda) = \sum_{x'} I(\lambda,x'),$$

assuming acceptance over a small solid angle.

The calculations of $I_{OBS}(\lambda)$ was programmed for an Elliot 803A computor. Input consisted of the values of N_e and T_e for 25 values of the radial distance x'.

The output consisted of both the observed profile, $I_{OBS}(\lambda)$, and the profile corresponding to x'=0, $I_{CENTRE}(\lambda)$. These were normalised to the same peak intensity. A brief description of the computor programme is given in appendix II.

The radial distribution of N_e was already known (Chapter 6). The radial distribution of T_e was inferred from the known continuum distribution (Chapter 4) and the relation,

$$I_c^{\frac{1}{2}}(r) \propto N_e(r)\, T_e^{-\frac{1}{4}}(r).$$

($T_e(r=0)$ was normalised to the value found in Chapter 7.) These distributions are shown in Fig.8.2.

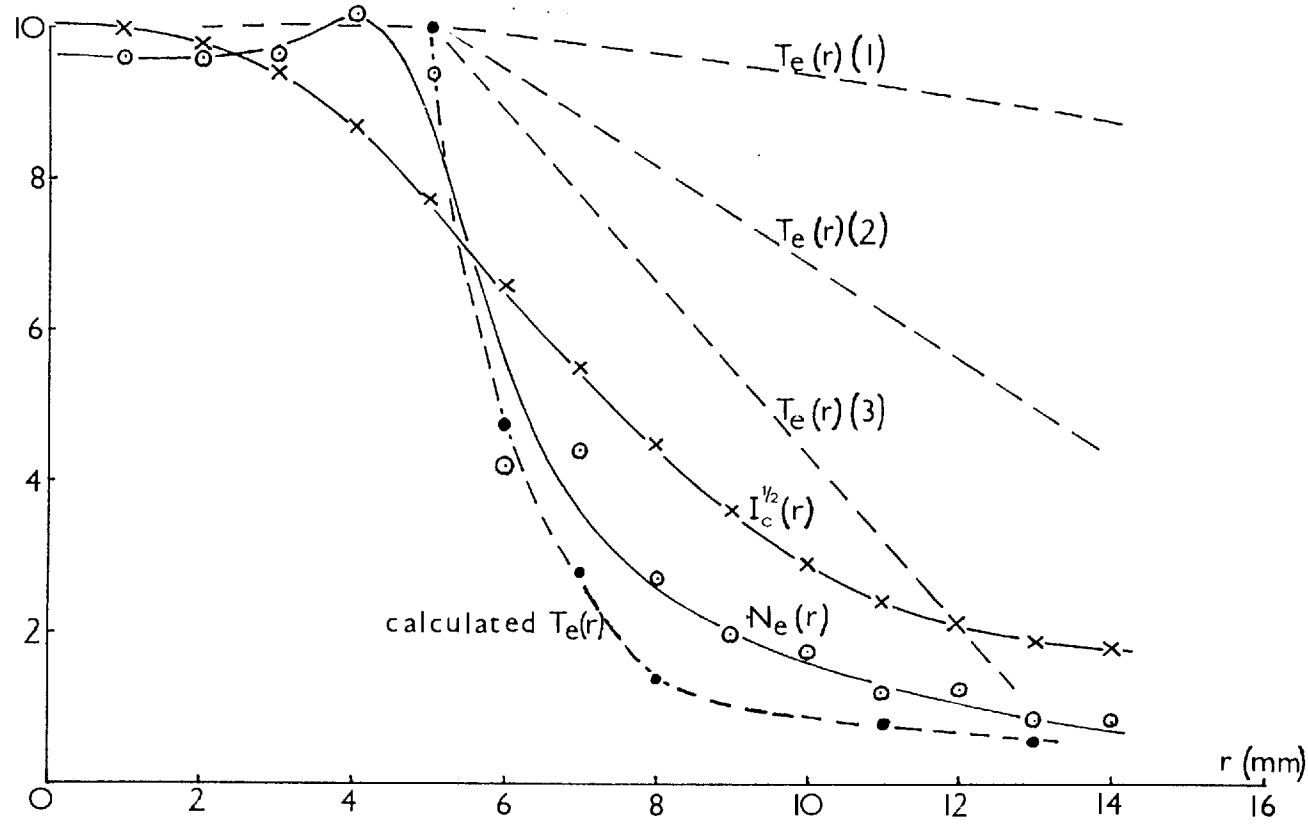


Fig. 8·2 Radial distribution of square root of continuum, N_e and T_e. (arbitrary scale.)

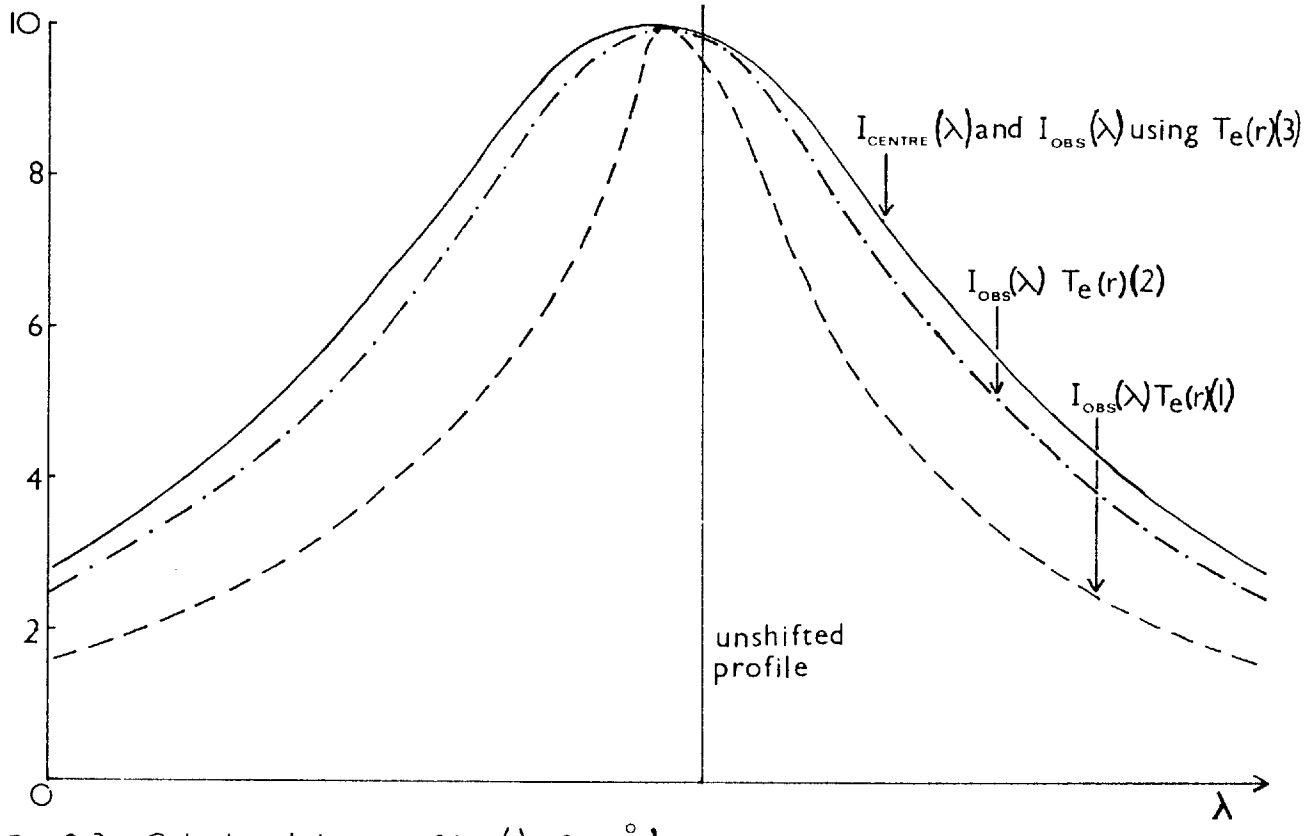


Fig. 8·3 Calculated line profiles (λ 4806 Å)

Since the error in $T_e(r)$ was $\sim$ 4x that in N_e (i.e. $\sim$ 40%) calculation of $I_{OBS}(\lambda)$ was also done for three distribution of $T_e(r)$ approaching $T_e(r)$ obtained from $I_c(r)$. (See fig.8.2.)

The profiles $I_{OBS}(\lambda)$ and $I_{CENTRE}(\lambda)$ for $\lambda 4806\text{Å}$ are shown in fig.8.3. To obtain, if anything, an overestimation of the distortion caused by plasma inhomogeneity Griem's values of d/W were used. These were more rapidly varying functions of T_e than the results in Chapter 5.

For both $T_e(r)$ distribution 3 (fig.8.2) and that from $I_c(r)$ the profiles $I_{OBS}(\lambda)$ and $I_{CENTRE}(\lambda)$ coincide to well out in the line wings. Thus the use of $N_e(r=0)$ and $T_e(r=0)$ to characterise the observed profile is well justified.

It should be noted that Doppler broadening is completely negligible for $N_e > 1.5 \times 10^{17}$ (from Section 3.3a and Chapter 4). Thus the line shape can be assumed to be dispersive (8.1). Also the AII line intensity is small for $r > 0.6$ cms so the value of T_e estimated in Chapter 7 was fairly representative of the axial T_e.

8.3 Measured values of $\Omega(T_e)$

Values of $\Omega(T_e)$ corresponding to the results tabulated in Section 8.1 are given below (Table 8.1). A comparison is made with Griem's values of $\Omega(T_e)$. Also included are the relative width measurements described in Chapter 3. Values of Ω for these lines were obtained by normalising W to that of $\lambda 5062\text{Å}$ and using the measured Ω for this line from Section 8.1. T_e was assumed to be the same for the two discharges. Systematic errors in Ω from this procedure amounted to $\sim$10%.

TABLE 8.1

Multi-plet	Line	Transition Lower ⟶ Upper	Experimental	Griem
1	4460.6	$3d\,^4D_{2\frac{1}{2}} - 4p\,^4P^o_{2\frac{1}{2}}$	14.0 ± 2.4	4.1
2	4013.9	$3d\,^4D_{3\frac{1}{2}} - 4p\,^4D^o_{3\frac{1}{2}}$	15.8 ± 2.7	4.3
6	4806.1	$4s\,^4P_{2\frac{1}{2}} - 4p\,^4P^o_{2\frac{1}{2}}$	20.2 ± 3.6	8.2
	4933.2	$4s\,^4P_{1\frac{1}{2}} - 4p\,^4P^o_{1\frac{1}{2}}$	21.4 ± 3.7	8.6
	4847.8	$4s\,^4P_{1\frac{1}{2}} - 4p\,^4P^o_{\frac{1}{2}}$	18.8 ± 3.3	8.3
	5062.0	$4s\,^4P_{\frac{1}{2}} - 4p\,^4P^o_{1\frac{1}{2}}$	22.0 ± 3.1	9.1
7	4348.1	$4s\,^4P_{2\frac{1}{2}} - 4p\,^4D^o_{3\frac{1}{2}}$	11.5 ± 2.0	4.7
	4266.5	$4s\,^4P_{2\frac{1}{2}} - 4p\,^4D^o_{2\frac{1}{2}}$	16.8 ± 2.8	4.5
10	3850.6	$4s\,^4P_{2\frac{1}{2}} - 4p\,^4S^o_{2\frac{1}{2}}$	26.0 ± 4.5	4.3
14	4879.9	$4s\,^2P_{1\frac{1}{2}} - 4p\,^2D^o_{2\frac{1}{2}}$	24.6 ± 3.4	7.7
109	3350.9	$4p\,^2F^o_{2\frac{1}{2}} - 4d\,^2F_{1\frac{1}{2}}$	29.6 ± 3.6	/

These results will be discussed in the following Chapter.

CHAPTER 9

DISCUSSION OF WORK ON IMPACT BROADENING

9.1 Discussion of AII Results

The improved agreement between theory and the experimental results of Chapter 8 (Table 8.1), on including more levels in the calculations and adding the lower state width directly, is indicated in Table 9.1 :-

TABLE 9.1

Average values of:-	$\frac{\Omega \text{ 5 levels}}{\Omega E}$	$\frac{\Omega u}{\Omega E}$	$\frac{\Omega u + \Omega L}{\Omega E}$
Total of 11 lines	0.35 ± 0.07	0.61 ± 0.12	0.95 ± 0.20

These calculations were performed using matrix elements $1, (21, -1)\sigma^2$ to couple each perturbing level. Due to the breakdown of many approximation made in the theory no further calculation of Ω using the correct coupling strengths, $f_{\alpha\alpha'}$, were made for most of the AII lines studied. Calculations for three AII lines using both coupling prescriptions indicated that the general conclusions that can be reached are identical but the absolute magnitude of $(\Omega u + \Omega L)/\Omega E$, given above, is likely to be in error by a factor of about 2x.

Thus the inclusion of more than 5 perturbing levels is essential in calculating Ω for most AII lines. In addition lower state broadening must be account for, i.e. Assumptions A3

and A_4 [Section 5.7] are generally invalid. To investigate the remaining source of error in the calculated values of Ω it is instructive to study the validity of other assumptions (given in Section 5.7) for all the AII lines which were measured.

That the 'no back reaction' and 'small strong collision term' assumptions are also invalid can be seen in Table 9.2 :-

TABLE 9.2

Multiplet	Line	$(E\alpha - E\alpha')/kT_e$ * $T_e = 20{,}000°K$	Strong collision term (%)
1	4460.6	0.51	48
2	4013.9	0.67	60
6	4806.1	0.51	48
	4933.2	0.53	48
	4847.8	0.58	46
	5062.0	0.53	48
7	4348.1	0.67	60
	4266.5	0.70	60
10	3850.6	0.92	62
14	4879.9	-0.54	41
109	3350.9	-0.21	36

(* α' refers to the nearest perturbing level to the upper state α)

The larger $|E\alpha - E\alpha'|/kT_e$ the worse the no back reaction assumption becomes. That the strong collision term is also larger when this quantity is large is not surprising. When $|E\alpha - E\alpha'|$ is large compared with kT_e only fast electrons on the tail of the Maxwellian distribution can cause inelastic

collisions. Consequently most of the broadening is caused by strong (elastic) collisions with $\rho < \rho_{min}$. It follows that the use of straight line classical paths becomes more unjustified in this case. To summarise, assumptions A1, A2, A7 and A8 all break down for the AII lines studied, the validity being worse the larger is $|E\alpha - E\alpha'|/kT_e$.

The importance of the size of $E\alpha - E\alpha'$ is also exhibited in the other theoretical assumptions. Thus if the perturber level separation is small for both upper and lower states a direct addition of Ω_u and Ω_L should give a good estimate of the total width since inelastic collisions would be dominant. The estimate would be particularly good if transitions between $E\alpha$ and $E\beta$ (and vice versa) were unimportant, e.g. if the line were 'forbidden'.

Neither situation is true in our cases. However some conclusions about the importance of lower state interaction can be reached even if $|E\alpha - E\alpha'|$ is large. Thus for a 'normal' emitter we expect the density of states to be larger above a given level α. This density would be higher the more weakly bound is the state α. Therefore if $E\alpha - E\alpha'$ is negative we expect $E\beta - E\beta'$ to be negative and $|E\beta - E\beta'| < |E\alpha - E\alpha'|$. In this case lower state broadening would be small compared with the upper state, especially for a tightly bound lower state.

This argument does not hold if $E\alpha'$ is below $E\alpha$ as is often the situation for AII lines. If the most important perturbing level to $E\alpha$ is $E\beta$ then for $E\beta$ the nearest perturbing level is at least as near as $E\alpha$. In this case upper and lower state broadening would be comparable.

Thus the sign of $(E\alpha - E\alpha')/kT_e$ should be of relevance in determining the importance of including the lower state in any

calculation of the line width. Consequently this sign should enable one to distinguish the relative effect of breakdown of assumptions A1, A2, A7 and A8 on one hand and A4 on the other.

To test this hypothesis the results of Stark broadening measurements on other singly ionised emitters will be considered.

9.2 Other singly ionised emitters

Two other sets of results on AII are available. Mazing [ref.98] studied many AII lines before the Griem theory was developed. N_e was not measured but the results are internally consistent with ours for $N_e = (1.3 \pm 0.2) \times 10^{17} cm^{-3}$. Oertel et al [ref.99] studied three AII lines. His value of Ω for the line studied in common [$\lambda 4806 \AA$] is in good quantitative agreement with that presented in this thesis. This is of interest because of the different experimental techniques used. Oertel et al used a T-tube source filled with argon seeded helium. N_e was measured from the width of a HeI line whose broadening parameter had already been checked [fig.1.1]. T_e was determined using the relative line to continuum intensity technique.

The first quantitative results on a singly ionised emitter were obtained by Davey and Griem [ref.71] who found good agreement between theory and experiment for NII.

Recently more results on singly ionised emitters have become available, i.e. on CaII, studied by J.R.Roberts [ref.100] and Yamamoto [ref.101], CII by J.R.Roberts [ref.100] and SII by Bridges and Wiese [ref.100].

Including all available results the ratio of experimental line width to calculated upper state width is plotted as a function of $(E\alpha - E\alpha')/kT_e$ (where T_e is the temperature at which each measurement was performed) in fig.9.1.

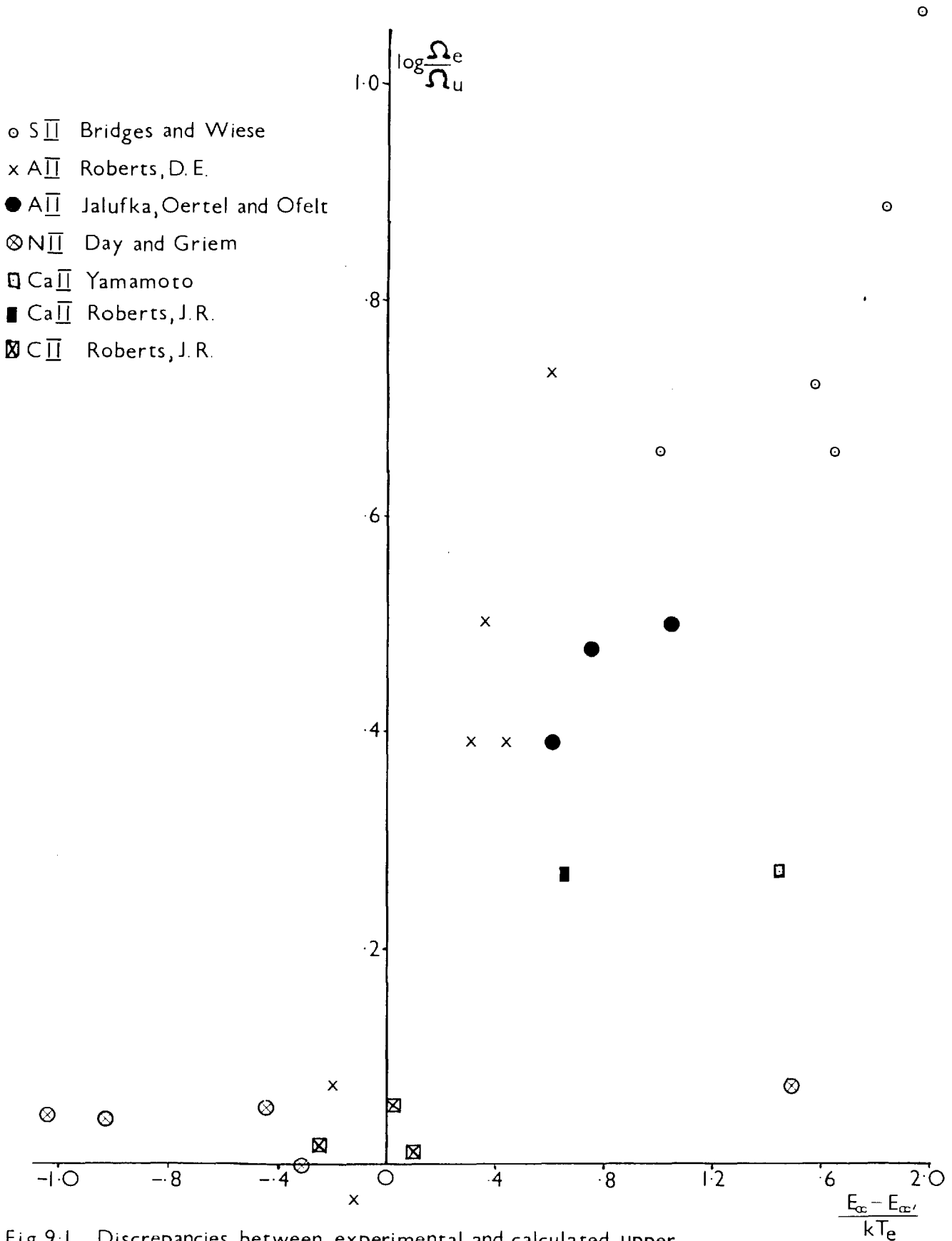


Fig 9·1. Discrepancies between experimental and calculated upper state widths for singly ionised emitters.

As suggested in §.2 the agreement with theory tends to become progressively worse as $(E\alpha-E\alpha')/kT_e$ becomes larger. Some rather large discrepancies from this trend need considering, however.

Firstly Yamamoto's CaII line width appears to be too low. This could possibly be accounted for by the neglect of large temperature gradients in the arc source used by this author.

Secondly the NII line for which $E\alpha-E\alpha'$ is positive is in far better agreement with theory than expected. However the second perturbing term to the upper state of this line is slightly more strongly coupled than $E\alpha'$ and an equal distance above E_∞. Thus consideration of one $E\alpha'$ is unjustified.

Thirdly the NII lines for which $(E\alpha-E\alpha')/kT_e$ is large and negative are in unexpectedly good agreement with theory. Calculation of Ω_L for these lines shows that Ω_L/Ω_u is in fact much lower than obtained with the AII lines. Nevertheless even accounting for this we should still expect much larger experimental than calculated widths. It therefore seems possible that a systematic error exists in these results.

On the basis of the above discussion the general applicability of Griem's theory will now be considered. In particular it is worthwhile noting why good agreement with theory was obtained before AII was studied.

9.3 General applicability of Stark broadening theory

For clarity several simplifying assumptions will be made. Firstly lines in the visible and near u.v. region only will be considered. If the wavelength of a line is sufficiently small lower state broadening will always be negligible. Secondly

T_o will be assumed to be such that the line considered is reasonably strong and N_e to be of the order normally achieved in experimentation. Variation of these parameters can readily shift the regime of applicability of various assumptions. Thus if T_e is sufficiently high practically all collisions will be inelastic. If N_e is sufficiently high ρ_D can approach ρ_{min} and all collisions will be strong.

Four main regions of $(E\alpha - E\alpha')/kT_e$ can be distinguished :-

(1) $$\frac{|E\alpha - E\alpha'|}{kT_e} \lesssim \frac{\hbar(kT_e)^{-\frac{1}{2}}}{\rho_D} :$$

e.g. H_2, H_e^+, Li^{++} ..., some Cs lines.

Here inelastic collisions are dominant and the neglect of the back reaction is well justified. Also the strong collision term is small and straight line classical paths are a good approximation even for charged emitters. For most (visible) lines lower state broadening can be neglected.

However some additional complications arise. Electrons with very large ρ can readily cause inelastic collisions so a shielding cut off $\sim\rho_D$ must be inserted in the calculations. Also large ion broadening and the overlapping of lines must be considered. Nevertheless, as expected, the agreement between theory and experiment is generally very good for the line cores.

(2) $$\frac{\hbar(kT_e)^{-\frac{1}{2}}}{\rho_D} < \frac{|E\alpha - E\alpha'|}{kT_e} \lesssim 0.2 :$$

e.g. Some CII and NII lines, HeI, some AI, oI and NI lines.

In this region the lines are isolated, ion broadening is fairly small and there is no need to consider Debye shielding.

Most approximations are still quite good. The majority of the heavy element lines studied before AII fall in this region so the good agreement with theory is not surprising.

(3) $\frac{E\alpha - E\alpha'}{kT_e} \gtrsim 0.2$

e.g. most strong AII, AIII, SII lines.

The agreement with theory becomes progressively worse as this quantity becomes larger. Strictly $E\alpha-E\beta$ must also be compared with $E\alpha-E\alpha'$. For large $E\alpha-E\beta$ lower state interaction is negligible though other approximations still hold badly.

(4) $\frac{E\alpha - E\alpha'}{kT_e} \gtrsim -0.2$

e.g. Several NII lines.

For visible lines there should be slightly better agreement with theory than in case (3) due to smaller lower state interaction.

9.4 Further theoretical work

While most of the theoretical difficulties arise from large perturber level separation it is not possible, within the present computational prescription, to account for this in a gross manner, i.e. the breakdown of the straight line path, small strong collision term (etc) assumptions each have to be treated separately.

Griem [ref.100] has recently recalculated the widths of the measured singly ionised lines (fig.9.1) accounting for lower state interaction and hyperbolic perturber trajectories. Much better agreement with experiment was apparently obtained, the average ratios of Ω_C/Ω_E being 1.1 compared with 0.5 for the

previous calculations.

Griem also found the ratio Ω_C/Ω_E uniformly high for NII and CII. The inconsistency of the NII results was also apparent from fig.9.1 but here the CII results fitted the expected trend.

In spite of the improved agreement between calculated and experimental widths several objections can be raised to these new calculations. These will now be considered in some detail.

The new calculations of Griem are performed as follows. It is initially assumed that complete degeneracy exists between $E\alpha'$ and $E\alpha$ and $E\beta'$ and $E\beta$. This allows the 2nd order ('weak inelastic') term in the perturbation expansion of the S-1 matrix to be evaluated exactly for hyperbolic perturber orbits. (In the same way as the HeII calculations of ref.108 were performed.) Divergence of the ρ integral occurs for large ρ (c.f. section 9.3 (1)] so Griem reinstates the non degeneracy and cuts off the integral at

$$\rho_{max} = \frac{V}{|W_\alpha - W_\alpha'|} * \frac{(V')^2}{V}$$

The $(V'/V)^2$ term accounted for acceleration of an electron, with velocity V and impact parameter ρ, to V' at the apex of the hyperbola.

For close collisions, where higher orders of the S-1 series are appreciable, Griem defined a ρ_{min} by the breakdown of perturbation theory and obtained a strong collision width, as before,

$$W_\alpha^S = \int \pi N V f(V) \rho_{min}^2 \, dv$$

Throughout the calculations a mean velocity, $\bar{V}$, was used.

For more than a few nearest perturbing levels terms in the expression for the weak inelastic width were found to go negative and therefore rejected. Consequently most of the width was found to lie in the strong collision term.

In discussing these calculations we will first consider the weak inelastic width.

The assumption of degeneracy seems a rather dubious approximation since, as shown above, most of the theoretical difficulties arise from exactly the opposite situation being true. We will investigate this assumption initially using straight line paths for the perturbers. The modifications incurred for hyperbolic orbits will be considered later.

As in the calculations described in Chapter 5 we can define a minimum cut off by :-

$$\rho_{min} = \frac{Z_{\alpha\alpha'}^{min}\, v}{W_{\alpha\alpha'}}$$

Similarly a maximum cut off can be defined by

$$\rho_{max} = \frac{Z_{\alpha\alpha'}^{max}\, v}{W_{\alpha\alpha'}}$$

This is the Griem cut off for $Z_{\alpha\alpha'}^{max} = 1$.

Physically $Z_{\alpha\alpha'} \geq 1$ corresponds to mainly elastic collisons so this cut off is reasonable,

i.e. $\rho_{max} = \frac{v}{W_{\alpha\alpha'}}$ is equivalent to $\frac{mv\rho_{max}}{\hbar} \simeq \frac{kT_e}{\hbar W_{\alpha\alpha'}}$

or saying electrons with energy $\sim \hbar W_{\alpha\alpha'}$ cannot cause inelastic collisions unless their angular momentum $\lesssim \hbar$.

In the calculation of the electron impact broadening of hydrogen lines [ref.109], where degeneracy does exist, the weak inelastic contribution is of the form :-

$$W_\alpha \sim R \ln \frac{\rho_{max}}{\rho_{min}}$$ where R is a matrix element.

i.e. $$W_\alpha \sim R \ln \frac{1}{Z^{min}_{\alpha\alpha'}}$$ in our case.

This expression can be alternatively derived directly from the calculations in Chapter 5,

i.e. $$W_\alpha \sim \sum R_{\alpha'} \; a(Z^{min}_{\alpha\alpha'})$$

for weak inelastic collisions.

For complete degeneracy $W_{\alpha\alpha} \sim 0$ so $Z^{min}_{\alpha\alpha'} \sim 0$.

In this case the small z limit for $[a\ (Z^{min}_{\alpha\alpha'})]$ can be used, i.e. $a(Z) = \ln \frac{1}{Z}$ [ref.10]. This limit is equivalent to all perturbers causing inelastic collisions and is reached if V is large even when E_α and $E_{\alpha'}$ are not degenerate.

The 'hydrogenic' approximation will now be compared with the previous calculations (Chapter 5) for $\lambda 4806\text{Å}$. With one perturbing level in the calculations the 'hydrogenic' case gives W_α only $\sim 14\%$ lower than before. The reason for this can be seen by comparing the values of a(Z) :-

Z	$a^H(Z) = \ln \frac{1}{Z}$	a(Z) [ref.4]	$a(Z)/a^H(Z)$
0.8	0.22	0.48	2.15
0.6	0.51	0.71	1.39
0.4	0.92	1.08	1.20
0.2	1.61	1.81	1.12
0.1	2.42	2.52	1.04

In the previous calculations most of the broadening occurred for $Z^{min}_{\alpha\alpha'} \leq 0.5$ which corresponded to $(1/2)mv^2 \geqslant kT_e$. In this region a(Z) and ln(1/Z) do not differ appreciably. However if the next nearest perturbing level is inserted in the calculations,

$$Z^{min}_{\alpha\alpha''} = \frac{W_{\alpha\alpha''}}{W_{\alpha\alpha'}} Z^{min}_{\alpha\alpha'} \quad \text{[Appendix I]} = 2.78\, Z^{min}_{\alpha\alpha'}$$

and $\ln \frac{1}{Z^{min}_{\alpha\alpha''}}$ is negative for $2.78\, Z^{min}_{\alpha\alpha'} > 1$

If more distant levels are included $\ln 1/Z^{min}_{\alpha\alpha''}$ is only positive for very small $Z^{min}_{\alpha\alpha'}$ (corresponding to large V). The contributions of different perturbing levels to W_α can be seen in fig.9.2 :-

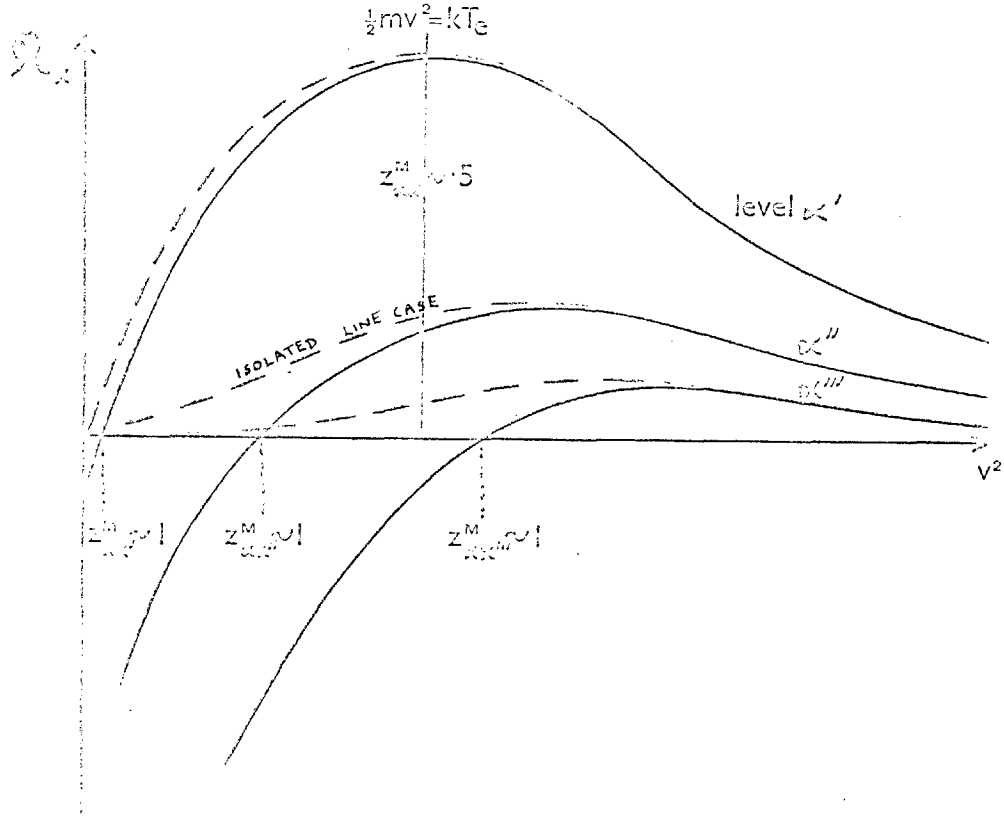


Fig 9.2 Inelastic contribution to W_α, $\mathcal{R}_{\alpha\alpha'}$ for different α' [Hydrogenic case.]

Effectively the only difference from the previous calculations (Chapter 5) is that the elastic cut off is more drastic. Thus only very fast (small z) electrons can cause weak inelastic collisions to distant $E_{\alpha'}$. Instead of slower electrons becoming gradually less effective at causing inelastic collisions, as in the previous calculations, there is a sharp cut-off for $Z_{\alpha\alpha'}$, $Z_{\alpha\alpha''}$ etc. = 1 corresponding to $\rho_{max} = \rho_{min}$.

The choice of a cut off for elastic collisions is rather arbitary so what appears to be a drastic approximation (i.e. $E_\alpha \simeq E_{\alpha'}$) is not completely unphysical. (For example two ρ_{min} cut-offs were employed in Chapter 5 though the 'transition' from fast to slow electrons was smooth in each case.)

The contribution of each perturbing level to W_α is normally taken as proportional to the area under each curve of the form given in fig.9.2 (cf Chapter 5).

We can therefore see why the 'weak inelastic' terms in Griem's calculations become negative for distant $E_{\alpha'}$. However his explanation, that this occurs because the degeneracy assumption is only valid marginally, is misleading since $|E_\alpha - E_{\alpha'}|/kT_e$ is ~ 1 for all singly ionised lines of interest (see fig.9.1).

While the calculation is physically quite reasonable the neglect by Griem of the 'negative' terms is incorrect. Firstly the parts of these terms which are positive, $Z_{\alpha\alpha'}$, $Z_{\alpha\alpha''}$ etc < 1, correspond to weak inelastic collisions and should be retained. Secondly the negative parts of these terms should be rejected but nevertheless some account taken of large $Z_{\alpha\alpha'}$. In fact Griem has completely neglected all elastic contributions to the width, as we shall show later.

It is now necessary to consider how the above discussion is modified if we use hyperbolic perturber orbits. As noted above Griem accounts for this by increasing ρ_{max} to $(V/W_{\alpha\alpha'})(V'/V)^2$ This can presumably be explained as follows. For a given ρ and V inclusion of a hyperbolic path increases V to V' at the apex of the hyperbola and, for constant angular momentum, ρ is reduced to $\rho V/V'$. Both effects make the perturber more capable of causing an inelastic collision and the cut off is now given by :-

$$\rho V/V' = (V/W_{\alpha\alpha'})(V'/V)$$

The ρ_{min} cut-off is reduced since partial cancellation of the electric fields for a close (strongly curved) trajectory tends to reduce the broadening effect of a fast electron compared with the straight line orbit case.

The ratio ρ_{max}/ρ_{min} is therefore increased. The effect of this for the nearest $E_{\alpha'}$ for λ 4806Å is to increase the broadening $\sim$15% over the straight line path case. For further $E_{\alpha''}$ the terms become negative at larger $Z_{\alpha\alpha''}$ (i.e. smaller velocities) than before. However the objections to the treatment of these terms still apply.

The strong collision width will now be considered. Again this can be derived from the previous calculations,

i.e. $W = \pi N v \rho_{min}^2$ (Appendix I)

(omitting integration over the Maxwell velocity distribution)

where $\rho_{min} = (2/3)^{\frac{1}{2}} (\hbar/mv) \left| \sum_{\alpha'} R_{\alpha'} [A(Z^{min}_{\alpha\alpha'}) + iB(Z^{min}_{\alpha\alpha'})] \right|^{\frac{1}{2}}$

For $W_{\alpha\alpha'} \sim 0$, $Z_{\alpha\alpha'} \sim 0$ and $A(Z_{\alpha\alpha'}) \sim 1$

$B(Z_{\alpha\alpha'}) \sim 0$

$\therefore \quad W = (2\pi/3v)(\hbar/m)^2 N \sum_{\alpha'} R_{\alpha'}$

The lower state strong collision width can be added directly since the expression is for inelastic collisions only,

$$\therefore \quad W = (2\pi/3v)(\hbar/m)^2 \; N\left\{\sum_{\alpha'} R_{\alpha'} + \sum_{\beta'} R_{\beta'}\right\}$$

This expression can be compared with that given by Griem

$$W = 2\pi/3v \; (\hbar/m)^2 \; N\left\{[\;] - (3/2)(e^2/\hbar v)^2\right\}$$

[ ] is equivalent to the sum of matrix elements, so the expressions are identical apart from the $-(3/2)(e^2/\hbar v)^2$ term which arises because ρ_{min}, as seen above, is smaller for hyperbolic orbits.

The strong collision term therefore takes no account of elastic collisions (large $Z_{\alpha\alpha'}$).

Finally it is worth considering the accuracy obtained by using a mean velocity, $\bar{V} = (8kT_e/\pi m)^2$, in the width calculations Employing this for the one level 'degenerate' case for $\lambda 4806\text{Å}$ gives a 30% lower width than when integration over a Maxwellian distribution is performed. Including distant levels would initially tend to decrease this discrepancy since progressively higher velocities are causing the main contribution to the elastic width. This will not, however, occur in Griem's calculations where distant levels have been rejected. In general we expect the use of $\bar{V}$ to be rather inaccurate in a calculation which is biassed in favour of high velocity perturbers and moreover accounts for acceleration along hyperbolic paths.

Since, in spite of the above objections, Griem obtained good agreement with experiment, it is worth considering the main source of his calculated width (i.e, the strong collision term) further.

Now on the previous calculations, if we simplify by considering only one perturbing level,

$$\rho_{min} \propto R_{\alpha'} \left| [A(Z^{min}_{\alpha\alpha'}) + iB(Z^{min}_{\alpha\alpha'})] \right|^{\frac{1}{2}}$$

$$\propto R_{\alpha'},$$

to within 2% for $Z^{min}_{\alpha\alpha'} \leq 0.5$, or over the range for which most broadening occurs, i.e. even though the relative contributions of elastic and inelastic collisions to this term is a function of velocity (or $Z_{\alpha\alpha'}$) the total contribution is practically independent of V and we get the same result for straight line path as assuming the strong collisions are all inelastic.

It should therefore be expected that incoherent addition of the upper and lower state strong collision widths given in Chapter 5 should give a total width comparable with Griem's. (or perhaps slightly higher since ρ_{min} is not lowered by hyperbolic path considerations.) This is not in fact the case, though previous calculations using incorrect matrix elements did (see Chapter 5 and ref.110). It is therefore instructive to compare the matrix elements $\left\{ \sum_{\alpha'} R_{\alpha'} + \sum_{\beta'} R_{\beta'} \right\}$ with those given by Griem.

Consider a transition from α, 1 to β, 1-1. All the relevant matrix elements are given by:-

$$R(\alpha, 1 \rightarrow \alpha', 1+1) = (1+1)(21+3)\sigma_1^2$$
$$R(\alpha, 1 \rightarrow \alpha', 1-1) = 1(21-1)\sigma_2^2$$
$$R(\beta, 1-1 \rightarrow \beta', 1) = 1(21+1)\sigma_2^2$$
$$R(\beta, 1-1 \rightarrow \beta', 1-2) = (1-1)(21-3)\sigma_3^2$$

$$\therefore \left\{ \sum_{\alpha'} R_{\alpha'} + \sum_{\beta'} R_{\beta'} \right\} = (1+1)(21+3)\sigma_1^2 + 41^2\sigma_2^2 + (1-1)(21-3)\sigma_3^2$$

- assuming array splitting is small, an approximation which is in fact never valid for the lines we consider.

Griem's expression can be reduced to:-

$$[4l^2_{\alpha\beta}\sigma^2_{\alpha\beta} + \sum_{\alpha' \neq \beta} 4l^2_{\alpha}\sigma^2_{\alpha'} + \sum_{\beta' \neq \alpha} 4l_{\beta}\sigma^2_{\beta'}]$$

This expression is incorrect as the sums here are over different levels. An expression of the form $4l^2\sigma^2$ should correspond to coupling between an array and a level.

Thus matrix elements of the form $l_\gamma(2l_\gamma-1)\sigma^2$ appear to have been incorrectly used to couple levels (cf. Chapter 5). The extent of the overestimation obtained can be seen by comparing the strong collision width using Griem's expression with that involving oscillator strengths, which are the correct coupling strengths between levels. For λ4806Å, using 3 perturbing levels α' and $3\beta'$ (as used in ref.100),

$$W_\alpha(\text{strong}) = .021 \text{ Å}$$

whereas Griem's expression gives $W_\alpha(\text{strong}) = .089$ Å .
(For $N_e = 10^{17}\text{cm}^{-3}$, $T_e = 30{,}000^\circ\text{K}$)

The use of only three perturbing levels for the upper and lower state seems rather arbitary. As seen above, due to the assumption of degeneracy, the contribution of each perturbing level to W_α(strong) depends only on its coupling strength and not on its separation from α or β. Inclusion of <u>all</u> perturbing levels in the strong collision term would increase W_α by a factor $\sim 4x$.

In conclusion, it does not seem likely that these new calculations can adequately explain the large experimentally

measured widths.

To ascertain what improvements can be made to the calculations we will consider the elastic contributions to W_α (strong) in the case of $\lambda 4806\text{Å}$. The proportion of elastic contributions to the strong collision width found in Chapter 5 can be obtained by using,

$$\rho_{min} = (2/3)^{\frac{1}{2}}(\hbar/mv)\left|\sum_{\alpha'} R_{\alpha'} B(z^{min}_{\alpha\alpha'})\right|^{\frac{1}{2}}$$

rather than $\rho_{min} = (2/3)^{\frac{1}{2}}(\hbar/mv)\left|\sum_{\alpha'}[A(z^{min}_{\alpha\alpha'}) + iB(z^{min}_{\alpha\alpha'})]\right|^{\frac{1}{2}}$

Thus we find $\sim 57\%$ of W_α is due to elastic collisions.

Inclusion of hyperbolic paths reduces the magnitude of W_α (strong) but also increases the number of inelastic collisions. In this case $\sim 43\%$ of W_α is due to elastic collisions.

Consequently elastic collisions should be considered in the strong collision term, even when hyperbolic paths are used. This is emphasized by the fact that we expect a large increase in width for the elastic term with hyperbolic perturber paths (see Chapter 5). Further, inclusion of these should enable a shift to be estimated. On the new Griem theory all collisions are inelastic so no shift is obtained.

The programme described in Appendix I could readily be used as a basis for calculations accounting for lower state interaction and hyperbolic paths. To include inelastic collisions involving the lower state energy differences $-(E_\beta - E_{\beta'})$, together with the relevant coupling strengths, would have to be included with the upper state terms. This would give the exact inelastic width for straight line orbits and ρ_{min} would be determined in a coherent manner. The negative

sign for the lower state energy differences would also ensure a shift in the correct direction. The strong collision term could then be modified to give, as the adiabatic limit, the Lindholm theory with hyperbolic orbits, i.e. as far as the width is concerned only the functions $B(Z_{\alpha\alpha}^{min}T)$ (Appendix I) would have to be modified. Unfortunately this calculation should strictly be done quantum mechanically.

The use of straight line paths for the weak inelastic collisions is probably not too bad since the orbits are not strongly curved for $\rho > \rho_{min}$. In any case this should give a better estimate than Griem's calculations, since no terms need be rejected. Further, since we expect most of the width to lie in the strong collision term, uncertainties in the weak inelastic term will not reflect strongly in total width. However it would probably be necessary to have a (velocity dependent) reduction of ρ_{min} for hyperbolic paths.

More refined calculations could be done with all the functions A(Z), B(Z), a(z) and b(z) modified for hyperbolic orbits. It would also be of interest to modify the inelastic collision cross section for threshold effects, ($\frac{1}{2} mv^2 \simeq W_{\alpha\alpha'}$) which are obviously of importance for the lines discussed here.

Finally it should be noted that other techniques are available for deriving the shift and width of an impact broadened line. In particular the Density Matrix formalism developed by Davis [ref.102] enables the expression for the shape of an isolated line to be obtained. This technique is considerably less laborious, mathematically, than the treatment using the autocorrelation function which was described in Chapter 5. Moreover it does appear to provide a basis for investigating the effect of neglecting the 'back reaction'. However it is not

at present apparent that any simplification in the actual calculation of widths and shifts would be obtained by using this, or other, techniques.

9.5 Further experimental work

The considerable difficulties in calculating Stark widths of isolated ion lines means a systematic experimental study of the validity of various approximations made in the theory would be of great value. The following experiments would certainly be of interest:-

(1) It is difficult to understand why some NII line widths agreed well with theory (see fig.9.1) and a check of these seems to be desirable. While the NII results are not wholly indicative of a systematic experimental error a check of the width of HeI λ 3889Å used as an N_e diagnostic would be useful, in particular comparing N_e obtained from this line width, a laser technique and absolute continuum intensities at different densities.

(2) Measurement of Ω for the AI red lines should provide information on the 'no back reaction' assumption since here $E\alpha - E\alpha'$ is large (and -ve) and there are no difficulties with hyperbolic orbits.

(3) To study the effect of lower state interaction lines with the same upper state and increasingly lower energy or 'forbidden' lower states could be observed. There are some neutral lines for which lower state broadening should be appreciable and therefore agreement with theory is surprising (e.g. AI blue lines).

(4) The importance of elastic collisions for ionised emitters could be deduced from AIII line widths. Here the perturbing

levels are rather distant and we expect inelastic collisions to be relatively unimportant.

(5) It would be of interest to compare the experimental and theoretical variations of Ω with T_e and N_e. On Griem's latest calculations [ref.100] one would expect Ω to decrease with T_e for ionised lines. This would not be the case if elastic collisions were important. The differences would be especially apparent at low T_e. The variation of Ω with N_e should show up any divergencies from a Lorentzian shape or overestimation of width due to the importance of strong collisions. High density studies (which are ideally suited to a Z-pinch, as seen in appendix III) where $\rho_D \sim \rho_{min}$ would enable the strong collision regime to be observed.

(6) Finally, it should be apparent from the previous chapters that all shift calculations are likely to be very inaccurate. Therefore any shift measurements, particularly as a function of T_e, would be of interest.

CHAPTER 10

MEASUREMENT OF N_e AND T_e IN AN R-F INDUCED PLASMA

10.1 Introduction

In this Chapter some preliminary diagnostics of an electrodeless R-F induced plasma in argon are described.

The purpose of this work was to obtain values of N_e and T_e pertaining to the plasma to determine whether the source was suitable for making more accurate T_e measurements which could be used in the determination of AI oscillator strengths. In particular the extent to which the plasma could be described by a model of L.T.E. was to be examined.

The plasma was excited in a quartz tube of internal diameter 5 cms by a five turn water cooled coil powered by a 'Raydyne' oscillator working at 4.5 Mc/s and 6 K.W A photograph of the plasma torch in operation is shown in Fig.10.1

The plasma torch used was developed by P.D.Johnson (Spectroscopy Dept.I.C.) and fuller details will appear in his thesis (to be published).

10.2 Measurement of T_e

Line profile scans using the S.F.P. fa iled to detect the presence of any of the strong lines of AII (e.g. λ 4806Å) but AI line radiation was very predominant. For these scans the optical set up of Fig.2.9 was used. The plasma torch was extensively shielded to keep 4.5 Mc/s pick up on the C.R.O. to a negligible value.



Fig. 10·1 Plasma torch in operation.

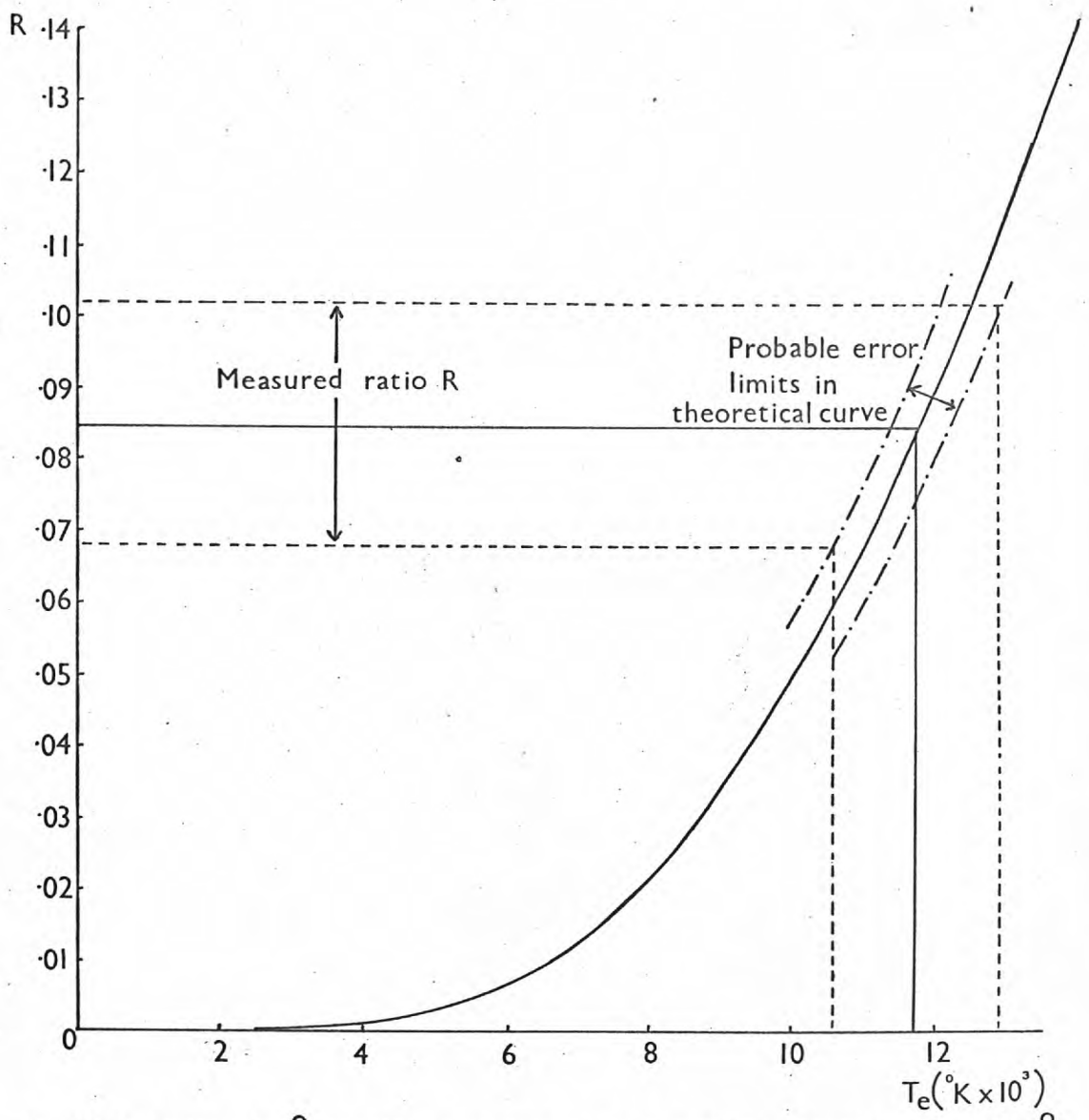


Fig. 10·2 Ratio of 1 Å continuum intensity to total line intensity of λ4259 Å AI, R, versus T_e (assuming L.T.E.).

Though the above result indicated that $T_e \leqslant 15{,}000^{\circ}K$ it it was necessary to obtain a better estimate to substitute into the criteria for L.T.E. (Chapter 7).

To obtain this estimate of T_e a measurement of the intensity of the AI line $\lambda 4259\text{Å}$ relative to the nearly continuum was performed. This ratio is a comparitively rapidly varying function of T_e (see below) so that uncertainties in A_{mn} for $\lambda 4259\text{Å}$ are not too serious a source of error. This was important as this work was preliminary to a more accurate measurement of AI oscillator strengths (P.D.Johnson, Ph.D. thesis - to be published). In addition the complication of making relative intensity calibrations - as is necessary in the Boltzmann plot method for obtaining T_e - was avoided.

The theoretical line to continuum intensity ratio can be derived as a function of T_e as follows :-

The line intensity, $m \to n$, neglecting stimulated emission is :-

$$I_{mn} = n_m A_{mn} h\nu_{mn}/4\pi \text{ energy time}^{-1}\text{vol}^{-1}\text{solid angle}^{-1}$$

Using Boltzmann's equations, Saha's equation (i.e. initially assuming L.T.E.)and the relation for quasi neutrality ($n_1 = n_e$ since n_2 must be negligible as AII lines were not seen in emission) then :-

$$I_{mn} = [g_m A_{mn} h\nu_{mn} h^3/8\pi U_1 (2\pi mek)^{3/2}]\, n_e^2 T_e^{-3/2}\, e^{+(W_o - \Delta W_o - W_m)/kT_e} \quad \ldots 10.1$$

To evaluate the bracket above U_1 was taken from ref.42. (U_1 is a comparitively slowly varying function of T_e.)

The value used for A_{mn} was the mean of Olsens value ($0.25 \times 10^7 \text{sec}^{-1} \pm 9\%$) [ref.58] and Drawins' value (0.40×10^7

sec^{-1} ± 15%) [ref.59], i.e. $A_{mn} = 0.32 \times 10^7 sec^{-1}$.

This value lies outside the quoted error limits of both authors but agrees well with the latest measurement (0.31×10^7 sec^{-1} ± 5%) by Coates and Gaydon [ref.68]

Substituting the values for A_{mn}, U_1 etc. into 10.1 we have :-

$$I_{mn} = 3.86 \times 10^{-30} n_e^2 T_e^{-3/2} \, e^{+(W_o - \Delta W_o - W_m)/kT_e}$$

$$\text{Watts. cm.}^{-3} \text{ sterad}^{-1} \qquad \ldots 10.2$$

(T_e in ^oK)

The error in the constant is probably 5-10%, mainly from A_{mn}.

The total continuum emission coefficient (free-free + free-bound) on the Unsold theory [ref.3] is given by :-

$$\epsilon_\nu = 5.41 \times 10^{-46} Z^2 n_i n_e T_e^{-\frac{1}{2}}$$

$$\text{Watts. cm}^{-3} \text{ sterad}^{-1} \text{sec.} \qquad \ldots 10.3$$

We can again use $n_1 = n_e$ and take $Z = 1$.

Also if we evaluate the continuum emission over a 1Å bandwidth near $\lambda = 4259\text{Å}$ we have a frequency interval,

$$\Delta\nu = (c/\lambda^2)\,\Delta\lambda \quad , \quad \Delta\lambda = 1\text{Å}$$

$$\therefore \quad \epsilon_\nu \Delta\nu = 8.9 \times 10^{-35} n_e^2 T_e^{-\frac{1}{2}}$$

$$\text{Watts. cm}^{-3} \text{ sterad}^{-1} \qquad \ldots 10.4$$

Olsen [ref.60] has measured the absolute continuum emission from a D-C thermal arc in argon over a wide frequency range. He found that the functional dependence, given in equation 10.4, on N_e and T_e appeared to hold well. In addition the theoretical frequency dependance held well in the visible spectrum. Nevertheless the absolute measured value differed

from the theoretical value by a factor ~ 5 x larger.

If we assume in our case that the frequency dependence holds well then we have a frequency independent continuum up to

$$\nu_c = 4.6 \times 10^{14} \text{sec}^{-1}$$

This corresponds to the interval between the ionisation limit of neutral argon and the $3d_6$ term between which the levels are reasonably well 'smeared'. Beyond this the levels become effectively discrete and 10.4 must be multiplied by a factor, [ref.60],

$$e^{-h[\nu-(\nu_c-\Delta\nu_o)]\,/\,kT_e} \qquad \ldots 10.5$$

(Taking into account the fact that ν_c is lowered by the depression of the ionisation limit by $\Delta\nu_o$, where $h\Delta\nu_o = \Delta W_o$.)

Therefore from 10.4 and 10.5

$$\epsilon_\nu \Delta\nu = 8.9 \times 10^{-35}\, n_e^2 T_e^{-\frac{1}{2}}\, e^{-h(\nu-\nu_c)/kT_e} \times e^{-\Delta W_o/kT_e}$$

$$\text{Watts. cm.}^{-3}\ \text{sterad.}^{-1} \qquad \ldots 10.6$$

Since reference 60 was published Olsen has re-estimated the absolute continuum intensity to be ~ 2.3 x; rather than 5 x, the theoretical value [ref.61]. This agrees well with the figure of ~ 2.5 x quoted by Coates and Gaydon (private communication). We shall therefore multiply 10.6 by 2.3 giving :-

$$\epsilon_\nu \Delta\nu = 2.05 \times 10^{-34}\, n_e^2 T_e^{-\frac{1}{2}}\, e^{-h(\nu-\nu_c)/kT_e} \times e^{-\Delta W_o/kT_e}$$

$$\text{Watts.cm.}^{-3}\ \text{sterad.}^{-1} \qquad \ldots 10.7$$

Thus we expect the 1Å bandwidth continuum to $\lambda 4259$Å AI line intensity ratio, from 10.2 and 10.7 :-

$$R = \epsilon_\nu \Delta\nu / I_{mn} = 0.53 \times 10^{-4} T_e \, e^{-(W_o - W_n - W_c)/kT_e} \quad \ldots 10.8$$

where $h\nu = W_m - W_n$; $h\nu_c = W_c$

This ratio, together with the probable error limits, is plotted in Fig.10.2.

Equation 10.8 is independent of ΔW_o (apart from the dependence of U_1 on this quantity). This result, arrived at by cancelling the terms $e^{-\Delta W_o/kT_e}$ in 10.2 in equations, and 10.7, is not strictly correct in the case of argon. ΔW_o for the continuum expression should be taken down to the Inglis Teller limit [ref.3] which is larger than the usual Debye expression for ΔW_o calculated from coulomb interactions in the plasma and substituted in Saha's equation. Nevertheless, the partial cancellation means that errors in the ratio from this source are extremely small ($< 1\%$) at values of T_e $\sim 10{,}000^\circ K$.

The experimental determination of R was performed with the optical set-up of Fig.2.9 with the S.F.P. removed. The radiation from the plasma torch was chopped and detected by an R.C.A. IP.28 photomultiplier. The output of this was matched to an A.C. coupled L-type plug in unit on a Tektronix type 555 C.R.O.

The slit widths of the monochromator were measured with a travelling microscope and together with the dispersion measured from the instrument calibration corresponded to an acceptance bandwidth of $\Delta\lambda = 1.1\text{Å} \pm 10\%$.

The entrance slit height was reduced to 2mm resulting in negligible curvature of the image .

With this system it was found that 300 c/s ripple of amplitude $\sim 20\%$ of the mean signal existed on both the line and

continuum radiation. This was undoubtedly due to harmonics from the R-F generator.

The mean value of the continuum (measured at $\lambda 4262\text{Å}$) to line ratio obtained was,

$$R = 0.085 \pm 20\%.$$

To arrive at this figure correction was made for the instrument function which meant that 80% of the total line intensity was accepted. (The line width and shape were obtained as described later.) Also the continuum measurement accepted some of the line wing.

This value of R, from Fig.10.2, corresponds to :-

$$T_e = 11{,}700\ ^{\circ}K \pm 700^{\circ}K\ .$$

10.3 Measurement of N_e

N_e was estimated from the widths of Stark broadened lines emitted by AI.

It was important from our point of view that this method did not rely on the assumption of L.T.E. but only that the electrons had a Maxwellian distribution - a condition easily satisfied (Chapter 7) at the temperature given above.

However, the results of the previous chapters showed that considerable discrepancies were likely to exist in the calculated values of $\Omega(T_e)$ for heavy element emitters. Fortunately, in the case of AI lines, these parameters had been checked by Griem [ref.15] using the experimental results of Gericke [ref.14]. In this comparison of experimental and theoretical values of $\Omega(T_e)$ Griem had to revise the plasma conditions quoted by Gericke on the basis of a more recent (calculated)

value of a line transition probability. The absolute intensity of this line ($\lambda 4348\text{Å}$, AII) was used to obtain the plasma conditions.

Gericke used $A_{mn} = 6.77 \times 10^7 sec^{-1}$

Griem used $A_{mn} = 12.8 \times 10^7 sec^{-1}$

A more recent lifetime measurement [ref.62] has yielded,

$$A_{mn} = 10.1 \times 10^7 sec^{-1}$$

The error in this quantity being only $\backsim 2\%$.

If we therefore re-estimate Gericke's plasmas conditions using this value we obtain:-

	$A = 12.8 \times 10^7 sec^{-1}$	$A = 10.1 \times 10^7 sec^{-1}$
T_e	$11,400^\circ K$	$11,520^\circ K$
n_e	$4.6 \times 10^{16} cm^{-3}$	$5.05 \times 10^{16} cm^{-3}$

The Debye theory for depression of ionisation potential and pressure correction [ref.51] was used in this re-estimation.

On this basis the measured widths and calculated widths (using $n_e = 5.05 \times 10^{16} cm^{-3}$) become (c.f. ref.15) :-

AI λ(Å)	2W measured	2W calculated
4345	1.1 ± 0.1	1.3
4335	1.5 ± 0.3	1.4
4333	1.1 ± 0.1	1.3
4300	1.0 ± 0.1	1.2
4272	1.0 ± 0.1	1.1
4266	1.1 ± 0.1	1.2
4259	1.2 ± 0.1	1.4
4251	0.7 ± 0.2	1.1
4201	1.0 ± 0.1	1.2
4198	1.0 ± 0.2	1.3
4182	1.2 ± 0.1	1.3
4164	1.0 ± 0.1	1.1
4159	1.1 ± 0.1	1.1

The mean ratio, R, of calculated to measured widths for these lines is :-

$$R = 1.16$$

Therefore to obtain N_e several line widths were measured to reduce random errors and an empirical correction made from the above table.

Two photomultipliers were used for the line width measurements. An R.C.A. IP.28 with an S-5 photocathode for the $3p^5 4s - 3p^5 4p$ series in the blue and $3p^5 4p - 3p^5 5d$ in the visible. For the $3p^5 4s - 3p^5 5p$ series in the red an R.C.A. 6217 with a S-10 photocathode was used.

Initially the strong red lines λ6965Å and λ7635Å were scanned. A typical scan of λ6965Å emitted by the plasma torch,

together with $\lambda 6438\text{Å}$ from a low pressure Cadmium lamp is shown in Fig.10.3.

The evaluation of this scan was carried out by means of a Voigt analysis (Section 1.4). Taking T_i = 10,000°K and a corresponding Doppler $\frac{1}{2}$ - 1/e width, g = 0.047Å the measured electron impact width was,

$$W = 0.017\text{Å} \pm 0.01$$

Taking Griems value of $\Omega(T_e)$ [ref.15] :-

$$N_e = 4 \times 10^{15}\text{cm}^{-3} \pm 50\%.$$

Since the measured line width is rather small it is worth estimating the extent of broadening from other sources.

Van Der Waals broadening can be calculated from equation 1.3. The neutral perturber density, No, can be estimated from (atomospheric) pressure balance and the assumption $T_i = T_e$. This gives:-

$$No = 7 \times 10^{17}\text{cm}^{-3}$$

and a corresponding Van Der Waals width of,

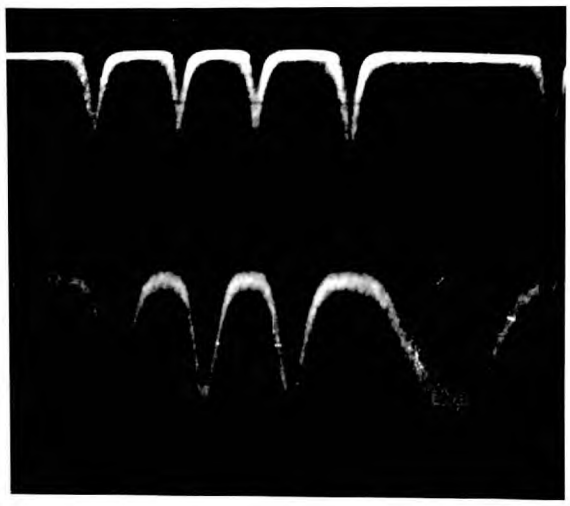
$$W_x \backsim 10^{-3}\text{Å}$$

Natural broadening gives a width,

$$W_x \backsim 10^{-3}\text{Å}$$

and in addition ion broadening would account for $\backsim 4\%$ of the total line width. These contributions can therefore be neglected.

The instrument width in the above scan was characterised by, $W_1 = 0.02\text{Å} \pm 15\%$ and $g_1 = 0.013\text{Å} \pm 15\%$.
Thus the expected line shape was, on using 1.14 and 1.15, a Voigt D/G = 0.72. The good fit of this to the observed profile



Time base 2 μsec/cm.

Fig. 10·3 Line profile scan: upper: λ6438·5 Å Cd I (low pressure lamp)
lower: λ6965 Å A I (plasma torch)

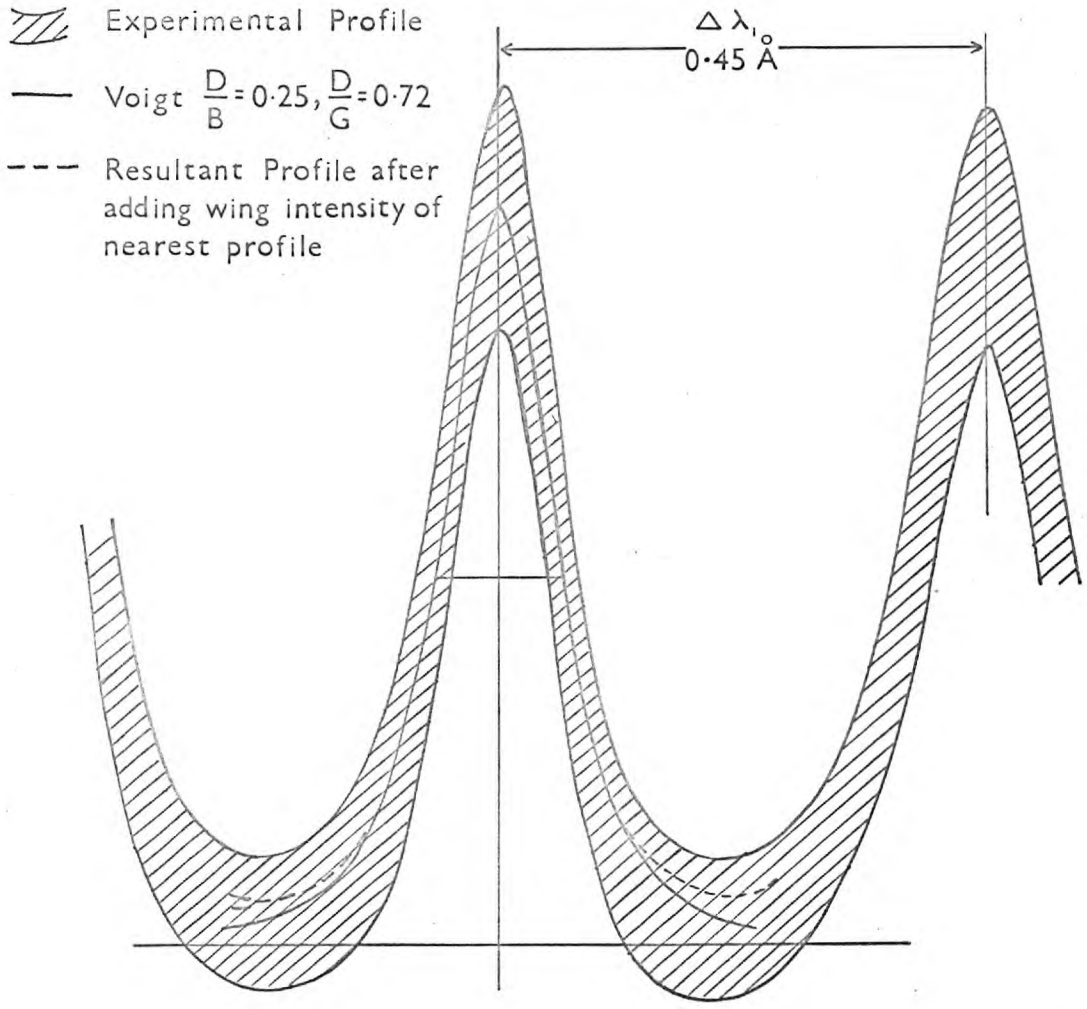


Fig. 10·4 Line profile scan: λ6965 Å A I (enlarged portion of Fig 10·3)

is shown in Fig. 10.4.

The rather tenuous nature of the plasma meant there were several disadvantages in studying the red lines in spite of their being strong and very well isolated.

Firstly the CdI line was not 'unbroadened' at the small $\Delta\lambda$, used. Secondly, the Doppler width was large. This meant that the assumption $T_i = T_e$ has to be made to estimate g. Even assuming g is known exactly the subtraction of this from the measured B considerably reduced the accuracy of W. Further $\Omega(T_e)$ had not been checked for the red lines.

For these reasons attention was concentrated on the blue lines for the measurement of N_e. The parameters $\Omega(T_e)$ for these are much larger than for the red lines.

e.g. For 4259Å, $N_e = 4 \times 10^{15} cm^{-3}$, $T_e = 10{,}000^{\circ}K$

$$\Omega(T_e) = 0.126 \times 10^{-3}\text{Å}$$

$$\therefore \quad W = 0.05\text{Å}$$

$$\text{and} \quad g = 0.03\text{Å}$$

So that competing broadening mechanisms are relatively less important.

The Stark $\frac{1}{2}$ - $\frac{1}{2}$ widths and corresponding values of N_e (from the previous table) obtained by scanning several blue lines are tabulated below :-

Line in Å	Upper level Moore's notation ref.35	W(Å)	units of $10^{15}cm^{-3}$
4158	$5p^5$	0.040	4.2 ± 20%
4198	$5p^6$	0.030	3.5 ± 20%
4200	$5p^2$	0.030	3.4 ± 20%
4259	$5p^{10}$	0.043	4.1 ± 20%
4266	$5p^5$	0.025	3.2 ± 20%
4272	$5p^4$	0.035	4.0 ± 20%
4300	$5p^3$	0.026	3.0 ± 20%
4335	$5p^8$	0.042	4.0 ± 20%

The values in the last column represent an average value of N_e obtained by integrating the line profiles through a possibly inhomogeneous plasma column.

In order to obtain some idea of the radial distribution of N_e a line profile (λ 5495Å) was scanned at different positions across the plasma column. This line was chosen because of its large broadening parameter so that Doppler broadening could be neglected. In addition a larger scanning aperture could be used (see equation 2.4) with a consequent increase in light gathering power over the previous measurements.

The measured values of W as a function of distance across the tube, d, are shown in Fig.10.5. Since the variation of W with d only was required the fact that the broadening parameter of λ5495Å had not been checked was unimportant.

The fall off in W versus d is seen from Fig.10.5 to be rather sharp. We should therefore expect imhomogeneity of

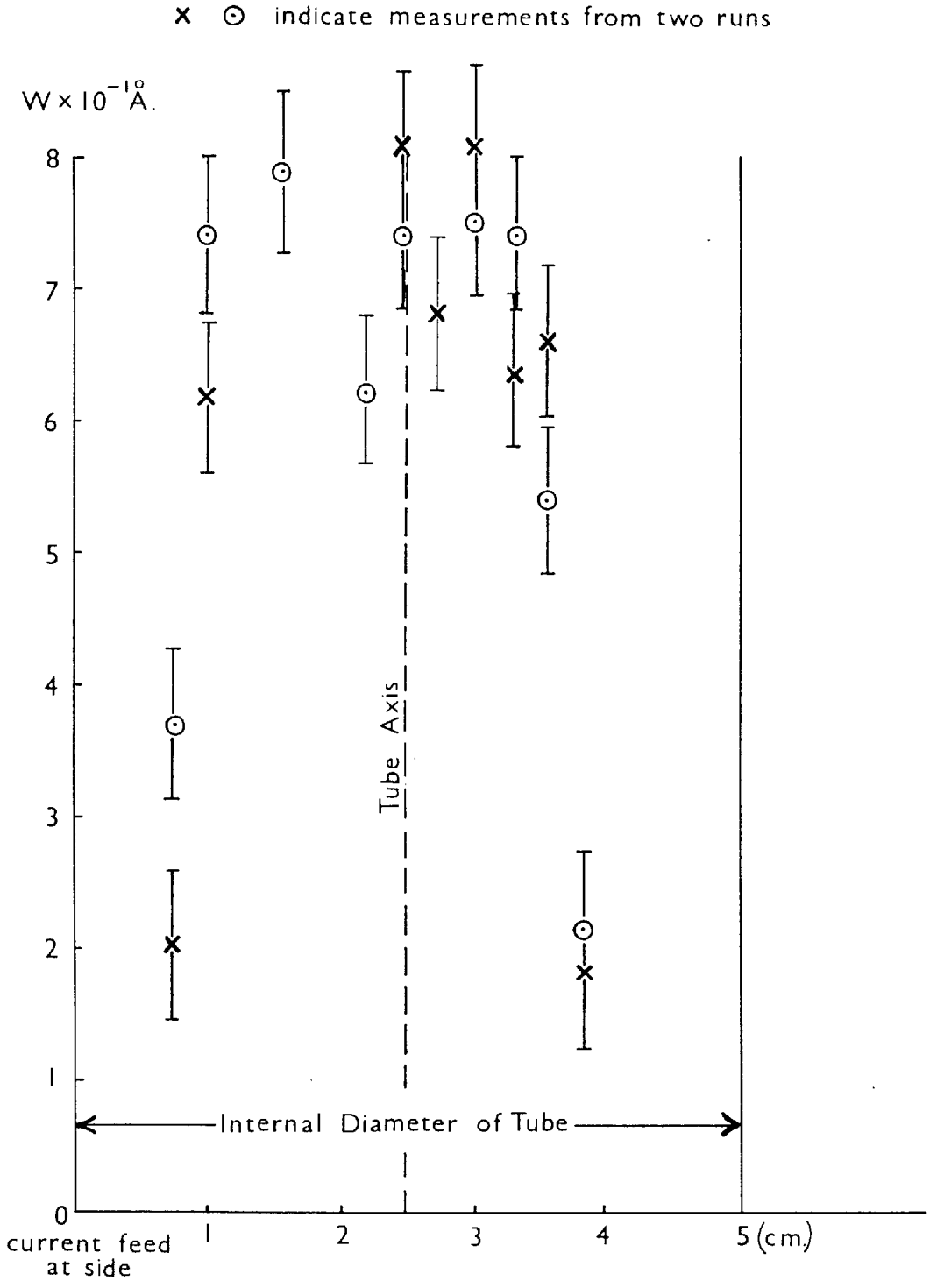


Fig. 10·5 λ 5495 Å A I Line Width, W, as a function of distance across tube, (plasma torch).

the plasma column to be relatively unimportant and the mean value of the plasma electron density to be, from the previous table :-

$$N_e = 3.8 \times 10^{15} \pm 20\% \text{ cm}^{-3}$$

(The λ 5495Å scan gave $N_e = 4.1 \times 10^{15} \pm 20\%$ suggesting that the calculated value of $\Omega(T_e)$ for this line is reasonably accurate.)

Attempts were made by single shot line profile scans to determine the effect on N_e of the 300 c/s ripple observed on the radiation (Section 10.2). Within the limits of experimental error [$\pm$ 20%] no variation in N_e could be detected.

10.4 Validity of L.T.E.

Using the criteria given in Chapter 7 we require :-

$$N_e > 2 \times 10^{16} \text{cm}^{-3}$$

for complete L.T.E. to hold. This estimate takes into account reabsorption of the AI resonance lines. The measured N_e shows that this criterion is not satisfied by a factor ~ 5 x.

However, the 'thermal limit' [ref.52] extends down through the first excited state of AI for $N_e \geq 2 \times 10^{15}$ so that all the excited states should be in thermal equilibrium with the continuum and only the G.S. population be different from its L.T.E. value.

Further, using the relations in Chapter 8 the effect of plasma inhomogeneity and time dependence (from the 300 c/s ripple) should be negligible.

10.5 Discussion

The above conclusions show that the assumption of L.T.E. in the determination of T_e (Section 10.2) was likely to give an overestimate of the ratio N_1/N_0 (c.f. Chapter 7). By a similar argument to that given in Chapter 7 this should not be more than a factor $\sim$ 50%. Consequently from Fig.10.2 a lower limit to $T_e \sim 10,000^{\circ}K$ is obtained. Use of this figure in the L.T.E. validity criteria does not alter the general conclusions of Section 10.4.

If atmospheric pressure balance and L.T.E. is assumed, then using the measured N_e we obtain :-

$$T_e = 8,800^{\circ}K \pm 200^{\circ}K$$

The differences in T_e from the two methods could be accounted for by plasma inhomogeneity.

Later results by Johnson [ref.63] for the excitation temperature of the plasma obtained using a Boltzmann plot confirmed the above results. The axial T_e in this case was $9,000 \pm 500^{\circ}K$.

Dymshits and Koretskii [ref.64] also obtained similar values of temperature for an R-F induced plasma in argon.

However Reed [ref.65], on a rather similar torch to the one we have described, obtained peak temperatures ($\sim 19,000^{\circ}K$) considerably higher than the values derived above. This was in spite of the lower power input used by Reed. The latter author obtained T_e from application of the Fowler-Milne method [ref.3] to the AI λ 7635Å line. However the use, by this author, of peak line intensities rather than total line intensities seems rather dubious. At the temperatures Reed

quotes the λ7635Å line would certainly be optically thin and Stark broadened. In this case the total intensity,

$$I \propto \text{peak intensity} \times \text{line width}$$

i.e. $$I \propto I_p N_e \propto N_1 f(T_e) \propto N_e f(T_e)$$

so $$I_p = f(T_e \text{ only})$$

Reed obtained a temperature drop of $\sim 19{,}000^{\circ}K$ to $\sim 10{,}000^{\circ}K$ over radial distances of about 1 centimetre. Such temperature variations would be accompanied by sharp variations in N_e and therefore we would expect the distribution of I to differ considerably from that of I_p. Nevertheless Reed found that values of I (as a function of distance across the tube) were at most 4% different from I_p.

The following explanation seems likely :-

An off-axis peak in the radial distribution of I_p was mis-identified as a Fowler-Milne type peaking. Such a peak would not be very pronounced with the temperature distribution obtained by Reed using the Fowler-Milne method. The temperature distribution (as a function of radius) could therefore have been fairly flat topped, (albeit possibly with an off axis peak) with a central temperature of the same order as we have obtained. In this case Stark broadening would not be the dominant broadening mechanism (c.f. the λ 6965Å line widths in Section 10.3) and the distribution of I not differ appreciably from that of I_p. Weight is added to this argument by the 'average gas temperatures' quoted by Reed. These were estimated on the basis of power-input and the heat capacity and ionisation energy of argon and were, in fact, of the same magnitude as our results (i.e. $\sim 9{,}000^{\circ}K$) .

Further, in the determination of the radial distribution of I_p, the Abel inversion technique of Nester and Clsen [ref.66] was used. Such an inversion is critically dependent on the quantity $I'(x)$. With relatively course steps in x for the numerical integration of Abel's integral it is not unusual to obtain 'overshooting' of the $I_p(r)$ versus r distribution to give the impression of an off axis peak.

Thus while there may have been an off axis peak in temperature in Reed's device it seems probable that his quoted temperatures are incorrect.

In the measurement of N_e, Section 10.3, it was assumed that the line profiles were optically thin. While application of equation 3.4 (with U_1, N_1 replaced by U_o, N_o) shows this to be true of the blue AI lines for $\lambda 6965\text{Å}$ we expect $\tau_o \sim 0.3$ corresponding to $\sim 10\%$ broadening by reabsorption. For $\lambda 7635\text{Å}$, $\tau_o \sim 1.3$.

These conclusions led to accurate temperature measurements on the plasma by estimating the self-absorption at the centre of $\lambda 7635\text{Å}$ (P.D. Johnson - Ph.D. thesis, to be published).

10.6 Check of $\Omega(T_e)$ for $\lambda 4159\text{Å}$, AI

It is worth recording here a check of the broadening parameter of $\lambda 4159\text{Å}$ which was made some time after the above results had been taken. This work was performed on a double diaphragm shock tube [ref.67] at the instigation of Dr. P. B. Coates and Professor A. G. Gaydon, of the Chemical Engineering Department, Imperial College. The experimental work was done with Dr. Coates.

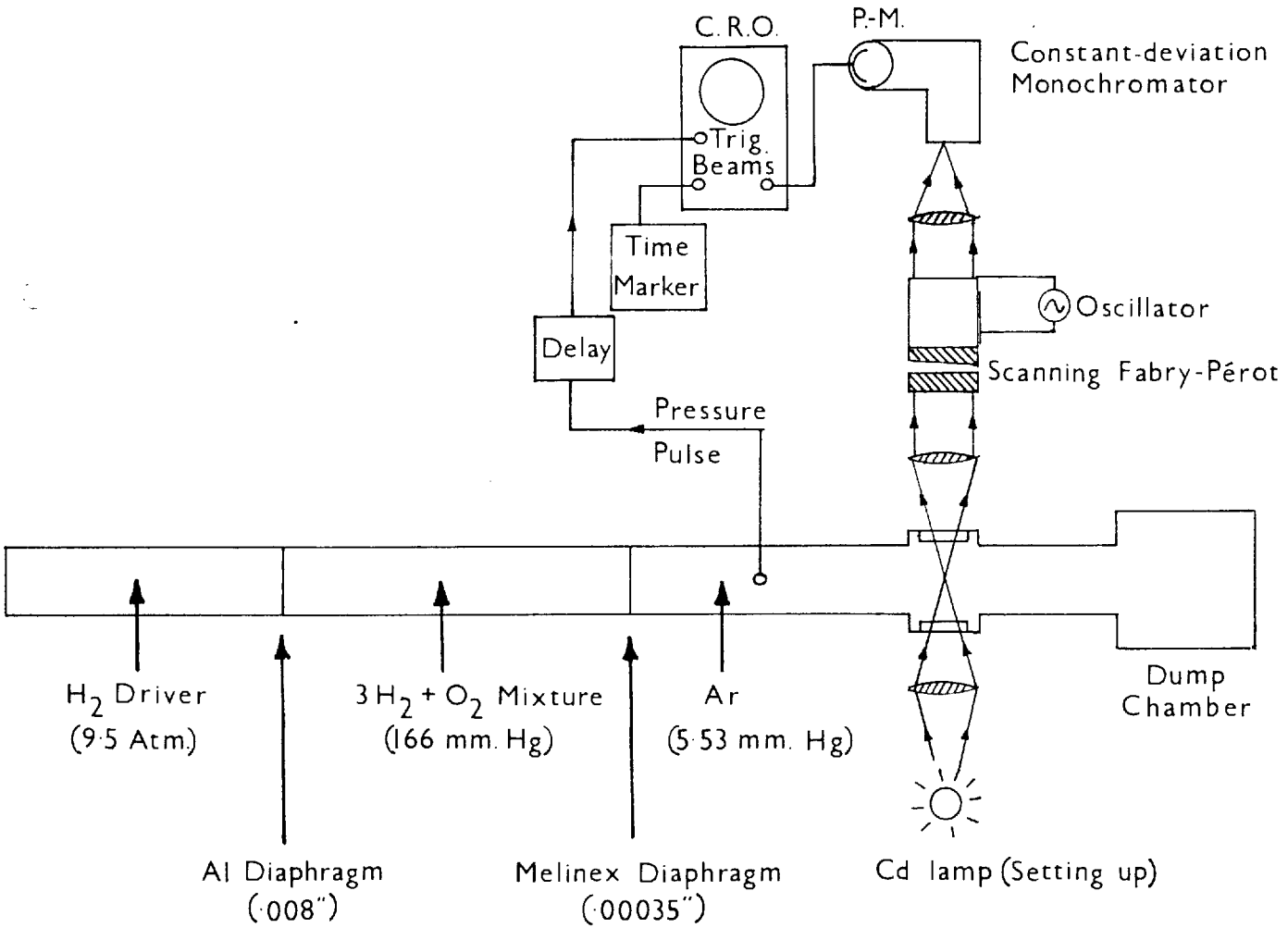


Fig 10·6 Arrangement for scanning lines emitted by a shock tube.

Since the occurrence of the shocked plasma opposite the viewing window could not be accurately predicted, after the sparking of the explosive mixture, the triggering system used for a linear pinch (Fig.2.9) could not be employed. However the shock velocity, for given initial conditions, was extremely reproducible. Therefore a pressure signal taken before the shock had reached the viewing window was used, via a delay unit, to trigger the C.R.O. The light output from the shocked plasma in pure argon could thus be recorded, via an IP.28 photomultiplier, reproducibly on the screen of the C.R.O. The S.F.P. was run continuously to modulate this light output. The set-up of apparatus, together with the initial filling pressures of the tube used in this experiment, are shown in Fig.10.6.

In this way the plasma broadened line profiles could be recorded though the position in time of the fringe of maximum finesse could not be predicted. Since the value of N_e, calculated from the shock velocity, was constant to $\sim$ 10% for at least 20μs this was not a very serious limitation. A scan obtained on λ6965Å is shown in Fig.10.7.

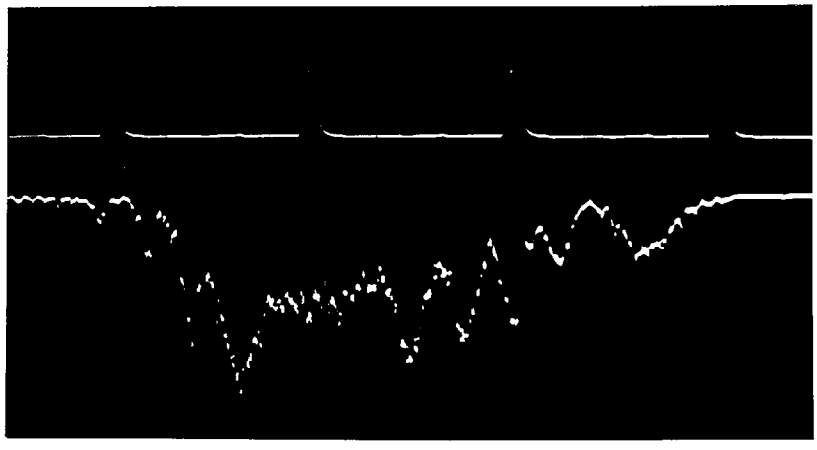


Fig.10.7 - Scan of λ6965Å, AI, emitted by Double Diaphragm Shock Tube

In this example a complete scan (c.f. Fig.2.1) consisted of four fringes with the outer ones of poorer finesse than the central two.

The plasma conditions in this experiment, calculated from the shock velocity of Mach 11.3 (c.f. Coates and Gaydon, ref.68) were :-

$$T_e = 10,200^{\circ}K \pm 50^{\circ}K$$

$$N_e = 2.05 \times 10^{16} cm^{-3}$$

$$N_o = 8.6 \times 10^{17} cm^{-3}$$

The width of the Stark broadened line λ 4159Å AI measured with the S.F.P. was,

$$W = 0.23 \pm 0.05Å$$

(Doppler width could be neglected)
This leads to:-

$N_e = 2.4 \times 10^{16} cm^{-3} \pm 20\%$ (using Griem's $\Omega(T_e)$ value from ref.17) and :-

$N_e = 2.1 \times 10^{16} cm^{-3} \pm 20\%$ (using the table on page 209) .

i.e. Excellent agreement between N_e calculated from the shock velocity and N_e from the line width using the corrected value of $\Omega(T_e)$ given in Section 10.3.

It therefore seems unlikely that any serious error arose, from theoretical considerations, in the N_e measurements on the plasma torch.

It was not possible to reach a similar conclusion for λ 6965Å. Calculation of the optical depth of this line, assuming wholly Stark broadened, led to an optical depth of

1.68 at the line centre (assuming Griem's $\Omega(T_e)$). This would lead to increase in line width due to reabsorption $\sim 50\%$ (see Chapter 2). However the Doppler width was not negligible so the procedure given by Renner [ref.61] should really be used. Unfortunately the F-P plates used for this work were rather poor, a finesse ~ 7-8 only being achieved. This was not good enough for the high resolution necessary for detailed analysis of the $\lambda 6965\text{Å}$ line.

Nevertheless this work showed that time resolved line profile measurements could readily be made on a shock tube source. It should also be possible to make accurate laser interferometric determinations of N_e on the shocked plasma (c.f. Chapter 6). Further, due to the high uniformity of the plasma (over a path length of 6.2 cms with a boundary layer of only $\sim$ 1mm) an Abel inversion, as in Chapter 6, would not be necessary. Compared with arcs, which suffer from large temperature gradients, the shock tube would appear to have several advantages for use in the study of the broadening of neutral atom lines.

CHAPTER 11

DOPPLER SHIFT MEASUREMENTS OF THETA PINCH ROTATION

11.1 Introduction

In this Chapter are described some experiments on the measurements of plasma rotation in the theta pinch. As in the work in the previous chapters the main diagnostic technique used was Fabry-Pérot interferometry.

The phenomenon of theta pinch rotation has been the subject of much attention both theoretically [ref.73] and experimentally [e.g. refs. 74, 75, 76].

Theoretical mechanisms for the origin of rotation in an electrodeless discharge have been summerised in a comprehensive review paper by Haines [ref.73]. The outcome of his work has been the retention of five theories which could in part or together account for rotation in the particular case of the theta pinch.

However, when this work was started experimental observation had almost entirely relied on high speed photographic observation of the instabilities associated with the rotation. On the other hand the experiment to be described was an attempt to measure the mass rotational velocity and angular momentum of the plasma.

This work was based on a suggestion by Dr. J. Cooper while a consultant at the Culham Laboratory. The experimentation was performed by the author in conjunction with Dr. M.Keilhaker and, together with work performed at Garching, was published in ref.85. Only the experimentation and analysis performed by the author, while at Culham, will be described here.

11.2 Doppler shift measurement of rotation

The determination of the azimuthal velocity of a plasma by means of observing the Doppler shift of radiation emitted by that plasma should provide a method of measuring rotational veolocties with far greater precision than by photographic techniques. Apart from this, however, it should be possible to study the rotation before the photographically detectable rotating instabilities ensue. Such a method would therefore seem desirable from the point of view of comparison with several theoretical models postulated to explain the origin of rotation.

The feasibility of measuring the mass rotational velocity of a plasma, assuming it rotates as a solid body, can be seen with reference to fig. 11.1.

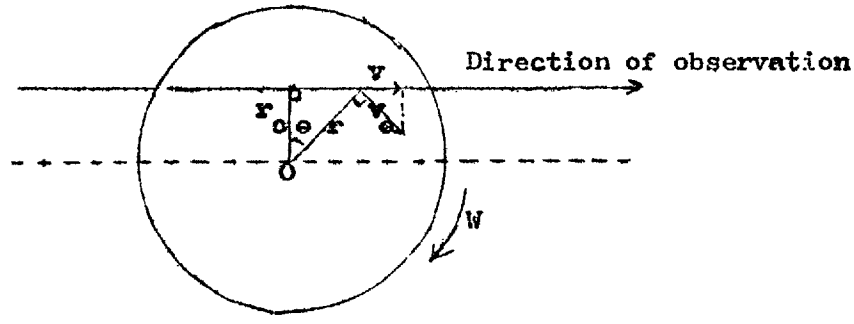


Fig. 11.1

$$V = V_\theta \cos\theta = rw \cos\phi = r_o w$$

i.e. At a given distance from the centre all the ions of a particular species will be travelling with the same velocity

along the direction of observation and the radiation therefore suffers a constant Doppler shift,

$$\Delta\lambda = \lambda v/c = \lambda r_o w/c \qquad \ldots 11.1$$

Thus on plotting $\Delta\lambda$ versus r_o we expect, for a rigidly rotating plasma, a straight line the slope of which gives w.

This is the principle on which the measurements to be described were based.

11.3 Measurement of line shifts using a Fabry-Pérot Etalon

By high speed photographic techniques plasma rotational velocities of up to 6×10^7 rad sec^{-1} have been detected [ref.76] For a plasma radius = 1 centimetre this would correspond to values of V up to 6×10^7 cms/sec., i.e. at λ 5000Å a Doppler shift $\sim$ 10Å. We would therefore require for Doppler shift measurements a detecting system of variable resolution capable of recording line shifts from 0 to 10Å. Further the high temperatures attained in θ pinches limit the measurement of shifts to those lines emitted by impurity ions. Since these are only present in low concentrations we also require a detecting system of high luminosity. These two requirements indicate the desirability of using a Fabry-Pérot interferometer [ref.86].

The method of measuring shifts used here was to cross one of the Haidinger fringes produced by the Fabry-Pérot with a 8 channel fibre bundle array, each bundle being connected to a photomultiplier. The signals recorded on each photomultiplier then enabled a histogram of the line profile to be built up. Since no moving parts were involved a very high time resolution could be attained.

The use of only 8 resolution elements meant that measurement of line profiles was rather in-accurate but, as will be shown, the limitations were less severe for the measurements of shifts.

The technique outlined above was generally similar to that of Breton et al [ref.77] for the measurement of line widths. However the use here of a tilted Fabry-Pérot, rather than a manochrometer, as the dispersive element gave a slight complication in the method. It is therefore worthwhile considering the optimum conditions for use of the interferometer

Firstly, as noted in Chapter 2, it is best to have

$$\Delta\lambda_1 \geqslant B/2$$

or $\geqslant d/2$ if the line shift is $>$ the width B.

The maximum dispersion will then be attained if $\Delta\lambda_1$ just covers the length of the fibre bundle array (see fig.11.2) . There are two ways of doing this :-

(1) By using an inner Haidinger ring and a suitable value f_1 for the focus length of the image lens.

(2) By using an outer ring and a lens of focal length $f_2 > f_1$.

The conflicting advantages of method (1) or (2) can be seen with reference to fig.11.2.

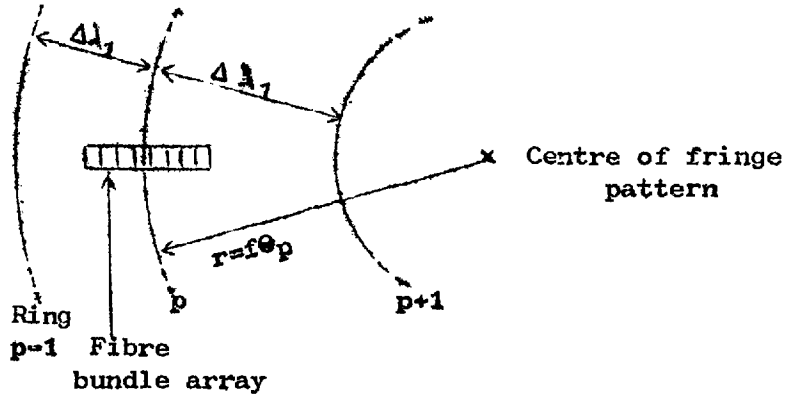


Fig. 11.2 - Haidinger fringe pattern crossed with fibre bundle array.

Any ring, P, of the Haidinger pattern can be focussed on the fibre bundle array by means of tilting the F-P through an angle θp.

Then if B is the luminance of the source the flux received by each photomultiplier is :-

$$\phi = B\Omega A \Delta s \cos \theta p / f^2 \qquad \ldots 11.2$$

Where A is the area of the F-P plates.

Δs is the area of one channel.

This is a maximum when θ and f are a minimum.

However, f determine the extent of the ring spacing (fig. 11.2) or $\Delta\lambda_1$, which must be matched to the width, s, of the fibre bundle array.

i.e. $S = f(\theta p_{+1} - \theta p)$ (where θ is small) ... 11.3

p is defined by :-

$$2d = n\lambda$$

$$2d \cos\theta p = (n-p)\lambda$$

or for θp small,

$$\theta p^2 = p\lambda/d$$

$$\therefore \quad \theta p_{+1}^2 - \theta p^2 \backsim 2\theta p\,(\theta p_{+1} - \theta p) \sim \lambda/d \qquad \ldots 11.4$$

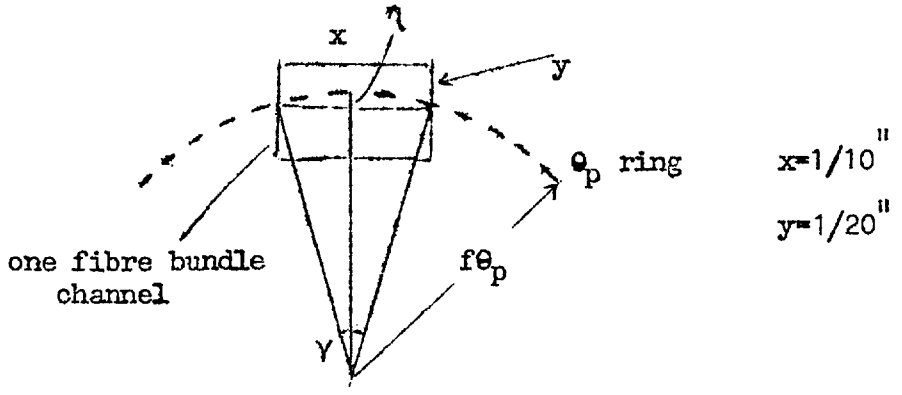
From 11.2, 11.3 and 11.4 :-

$$\phi \sim (B\Omega A \Delta s/4s^2)(\lambda/d)\ p^{-1} \qquad \ldots 11.5$$

The only variable in 11.5 for a given Δ_1 is p. For maximum ϕ we therefore require p to be a minimum. (Hence advantage of viewing the centre spot in a S.F.P.) Further, there is a loss of contrast obtained by using the F-P off axis (p large). However this is usually not important [ref.78].

Conflicting with the above requirement for p small we have two considerations :-

(1) Curvature of the ring on each rectangular channel causes the light flux corresponding to the wavelength interval ideally accepted by the channel to be different from the theoretical value. The effect of this can be seen with reference to the figure below :-



Curvature for fringe p, $\eta = f\theta p(1-\cos \gamma/2) \sim f\theta p\gamma^2/8$

$\gamma \sim x/f\theta p$

$\therefore \eta \sim x^2/8f\theta p$

The relative curvature, $\xi = \eta/y \sim x^2/8yf\theta p$

$\therefore$ Using 11.3 and 11.4, $\xi \sim x^2/6ysp$

For the particular array considered,

$y = \frac{1}{2}x = 6/10$

$\therefore \xi \sim 1/32p$

Thus for this quantity to be $\leq 1\%$ we require $p \geq 3$.

(2) Non-linear dispersion of the F-P should also be considered.

The inverse dispersion is given by :-

$$D^{-1} = d\lambda/d\theta p = \lambda \tan\theta p \qquad 11.6$$

$$\therefore \quad \delta(D^{-1})/D^{-1} = \sec^2\theta p\, \delta\theta p/\tan\theta p$$

$$\sim \delta\theta p/\theta p$$

Taking $\delta\theta p = \theta p+1 - \theta p$ we have, using previous relations :-

$$\delta(D^{-1})/D^{-1} \sim 1/2p$$

i.e. If p = 1 the dispersion across the length of the array (s) only stays constant to $\sim 50\%$. This effect can easily be accounted for though in practice excessive non-linear dispersion is inconvenient.

To summarise the above results, it is seen to be best to work on the 3rd or 4th ring. Thus if the 4th ring is used the dispersion over the light pipe array is constant to $\sim 10\%$ and the effect of ring curvature is $\sim 1\%$. To achieve these benefits the light flux received is reduced by a factor of 2x from its maximum value (11.2).

A great increase in light gathering power ($\sim$ 200x) could be achieved by using concentric circular fibre bundles. Such an array has in fact been made recently [ref.79] but one was not available for this experiment.

11.4 Experimental measurements

The experiment was performed on the 100μF bank 'OZWALD' at Culham Laboratory. Relevant technical data of this device is given below :-

Bank voltage	:	15 kV
Bank energy	:	22.5 K.J.
Pre-ionisation	:	1st and 2nd ½-cycles of bank
Working ½ cycle	:	3rd
Peak current	:	1.2 M.amp
Peak B_Z field	:	40 K.G.
½ period	:	7.2 μs
Coil length	:	21 cms
Internal coil diameter	:	5.5 cms
Mirror ratio	:	2:1
External tube diameter	:	5.0 cms
Filling gas	:	D_2
Filling pressure	:	normally 0.06 torr

(a) Choice of working conditions

In this experiment the étalon plates and fibre bundles (supplied by Dr. M. Keilhaker) were of glass, limiting measurements to the visible spectrum. However observed rotation had been in the later stages of the discharge (e.g. ref.76) when the temperature was high and consequently most of the line radiation was emitted in the U.V. by impurity ions.

Therefore an attempt was made to find conditions where the photographically observed rotation showed up earliest and a strong impurity line chosen such that shift measurements could be made as late as possible in the ½-cycle. The best possible comparison could then be made between Doppler shift and photographic observations.

Streak camera photographs were taken of the plasma by viewing through a slot at one end of the discharge tube. This was slightly off axis to render the asymmetric rotating

instability [ref.76] more easily observable. End on framing photographs were taken with the same camera. All photographs were monitored with a pulse corresponding to the streak (or framing) time displayed on the same C.R.O. as a di/dt trace of the discharge. Typical photogtaphs are shown in fig.11.3.

Rotation was observed to show up earliest at a filling pressure of 0.060 torr. Later (see Section 11.4d) this was shown to correspond to the plasma trapping a small amount of reverse trapped flux - a conclusion consistent with the findings of other workers [ref.80].

To decide on a suitable impurity line for the experiment the set up shown in fig. 11.4 was used to simulate the amount of light flux received in a shift measurement.

For $\Delta\lambda_1 = 1\text{Å}$ and $p = 4$, f was set according to 11.3 and 11.4. Equation 11.2 was then simulated with,

$$A' = A\tau\cos\theta p$$

where τ is the étalon transmission of the F-P.

Filters of 10Å bandwidth were available for several strong well isolated impurity lines identified on time-integrated spectra taken with a Hilger Medium Quartz spectrograph.

The line selected for study was CII λ 4267Å, multiplet 6. (Actually a doublet of separation 0.25Å.) The light flux received from this line was further increased by adding known proportions of CH_4 to the D_2 filling gas via a mixer. A 1% ratio of atomic C to H was found sufficient to give a suitably large signal to noise ratio on each P-M. over a time scale $\sim$ 1μsec. The signal on λ4267Å was also very reproducible from shot to shot.

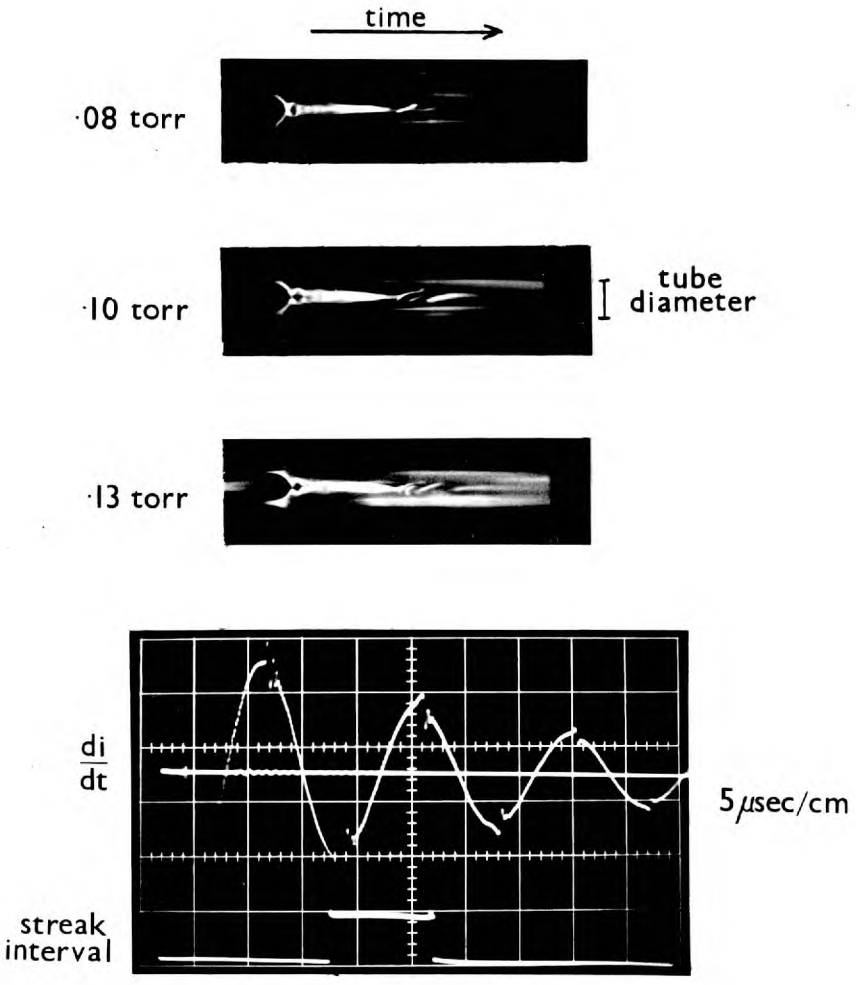


Fig 11·3. Streak photographs and $\frac{di}{dt}$ monitor.

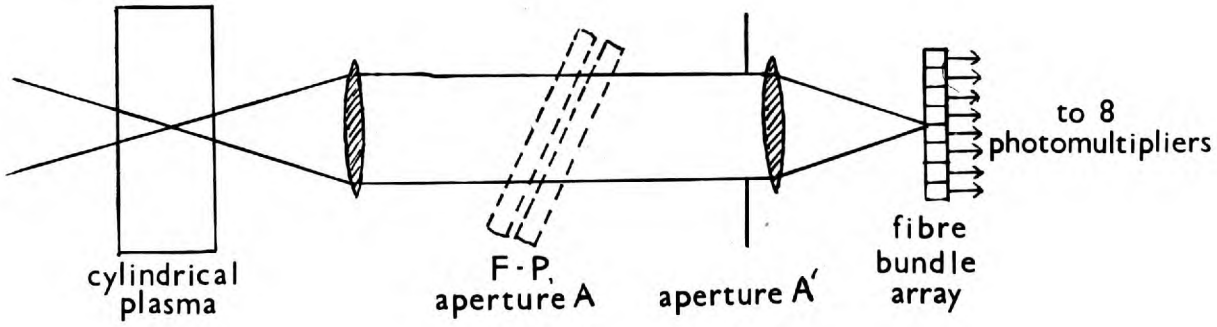


Fig 11·4. Plan view of Fabry-Pérot simulation arrangement.

(b) Calibration of the detecting system

Two methods were used for the relative calibration of each light pipe - P-M. system.

Firstly calibration was performed with a D.C. carbon arc pulsed by a rotating mirror as a light source. For convenience the E.H.T. voltages of the photomultipliers were adjusted so that each light pipe system gave approximately the same signal when the array was uniformly covered with light.

Secondly, to more accurately simulate the conditions under which shifts were to be measured, the set up shown in fig.11.4 was used to allow calibration using the plasma as a source. This was the same as for the shift measurements except that the F-P was removed. Since the length of the array, s, was illuminated by an effective plasma length sf'/f the uniformity of the radiation from this length could be checked. The apparatus in fig.11.4 was mounted on a table which could be raised vertically so that the check could be made at the different values of r_o used for the shift measurement.

The 8 photomultipliers were connected to 4 double beam C.R.O's via double screened cables such that the response time was $\sim$20n sec. The C.R.O's and P-M power packs were housed in a screened room.

Results obtained were as follows :-

With $f/f' = 4.0$ the relative sensitivity of a particular channel, measured over several shots at one height r_o, agreed to $\pm$ 4%. At different r_o the sensitivity of a channel was consistent to $\pm$ 5%. The mean values of the sensitivities of the channels averaged over all shots agreed with the carbon arc calibration to $\pm$ 3%.

Typical calibration shots on two channels are shown in fig.11.5.

(c) Measurement of Doppler shifts

The measurement of shifts was carried out using the set up of fig.11.4 with the F-P mounted between f and f'. The F-P mount was supplied by Dr. D. Bradley.

Since in this experiment we were limited to only 8 resolution elements per $\Delta\lambda_1$, it was not particularly important to have a finesse greater than 8. The F-P plates were measured to be flat to $\lambda/40$ over a 2" aperture at λ4358Å. Silver coatings with a MgF_2 protective overlayer gave the characteristics:-

Mean $\mathcal{T}$ = 0.16 ± 3%

" R = 0.78 ± 4%

giving N_R = 12.5 ± 12%

and $\mathcal{T}_E \sim$ 53% (this figure was used for the simulation experiment in (a)).

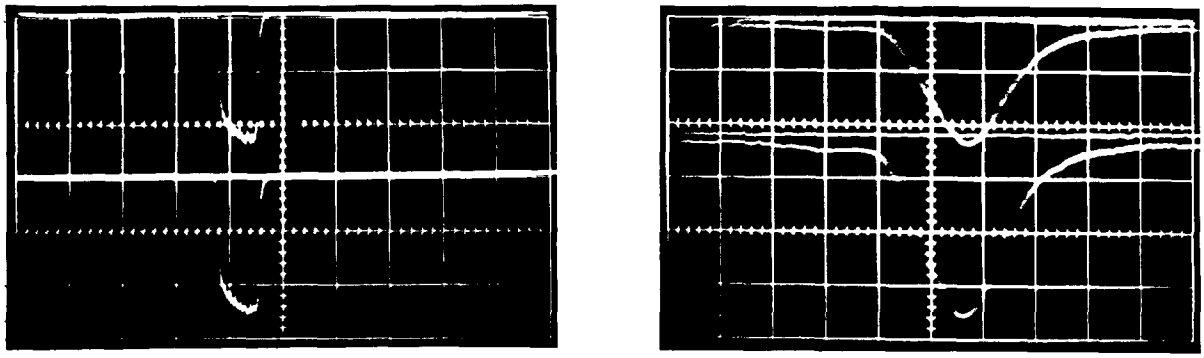
The overall finesse obtained by microphotometering a plate of the fringe pattern at λ4358Å gave :-

N = 11 ± 1

We could therefore expect N > 8 at λ4267Å.

$\Delta\lambda_1$ for the results to be described was 2.54Å ± 4% (at λ4267Å), measured from the diameters of successive Haidinger rings at λ4358Å (Hg I).

To obtain the 3rd or 4th ring of the λ4267Å pattern on the centre channel the λ4358Å line was first focussed in this position and a slight adjustment made to account for the variationof θ_p with λ.



Carbon arc
50 μsec/cm

Plasma
0·2 μsec/cm

Fig 11·5. Typical calibration shots (2 channels)

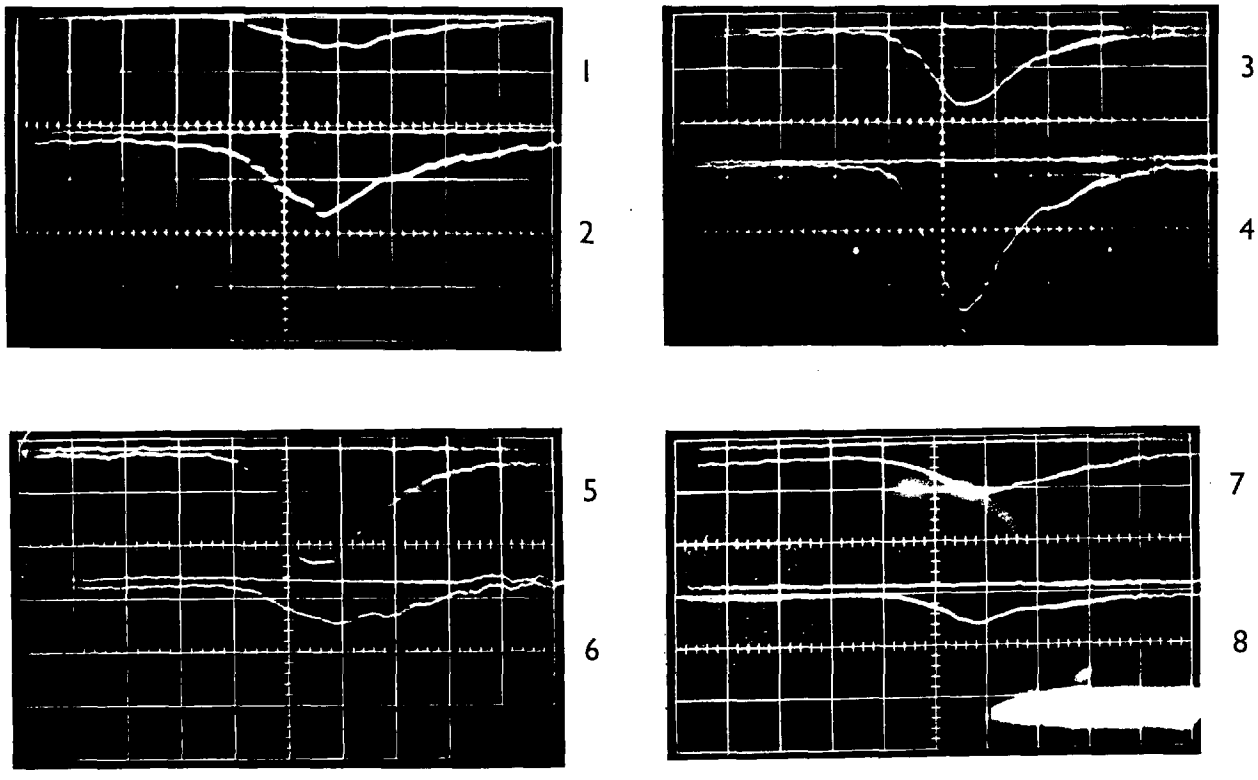


Fig 11·6. Recording of line profile on 8 channels (0·2 μsec/cm)

In the measurements taken the line width corresponded to $\sim \Delta\lambda_{1/3}$.

A typical series of traces recorded by the photomultipliers in one shot at a given r_o are shown in fig.11.6. To enable accurate time correlation between traces a bright up pulse was applied to the time base of each C.R.O.

The line profile at any given time was obtained as follows:-

Firstly, the relative intensities on each channel were obtained after correction for relative sensitivities. The wavelength interval, $\Delta\lambda_n$, accepted by each channel, n, was from 11.6 :-

$$\Delta\lambda_n = \lambda\int_{\theta_1}^{\theta_2} \tan\theta d\theta$$

$$\sim \lambda\theta\,\Delta\theta$$

$$\sim \lambda l_n x/f^2 \qquad \ldots 11.7$$

Where l_n = distance of centre of channel n from the centre of the circular fringe system (found with a mercury line, λ4358Å).

The line profiles obtained are of the form shown in fig.11.7 The area corresponding to each channel is proportional to the intensity recorded on that channel.

In practice a source could not be found which would give an origin of wavelength so only relative values were obtained, (taking the origin, arbitarily, as the start of channel 6). The median of each line profile was obtained such that equal wavelength intervals, $d\lambda$, either side of the median corresponded to equal intensities (fig.11.7). This is the definition for a profile which is not necessarily symmetric [ref.81] such as

expected in the case of $\lambda 4267\text{Å}$ (which is a doublet with components of different strengths).

Measurement of shifts in this manner were made at the three times indicated on fig.11.8 at different heights across the plasma.

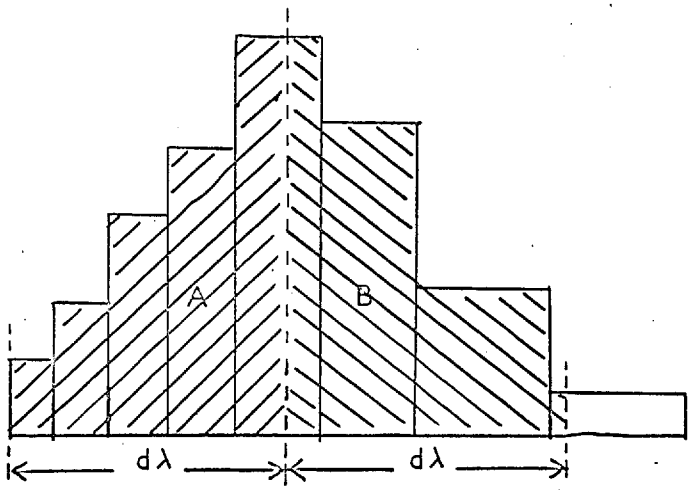


Fig 11·7. Median of assymetrical profile. (area A = area B)

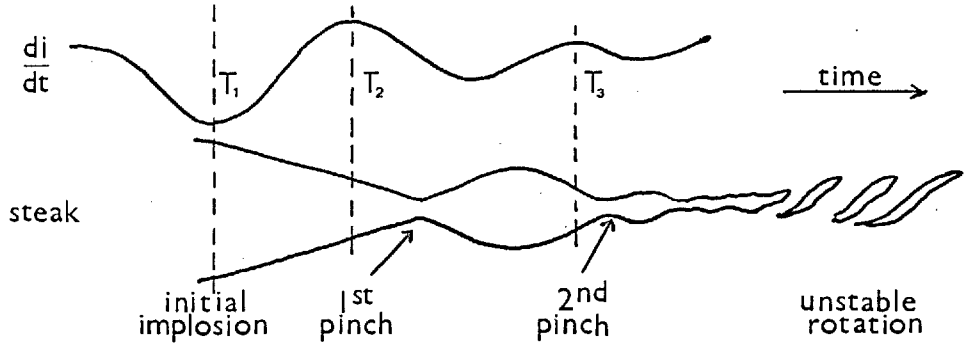


Fig 11·8. Time correlation of shift measurements and streak photographs.

The results are shown in fig.11.9 and typical line profiles in fig.11.10. Initially some trouble was experienced with small drifts of the line profile to smaller channel numbers (i.e. to longer wavelengths.) This was probably due to gradual relaxation

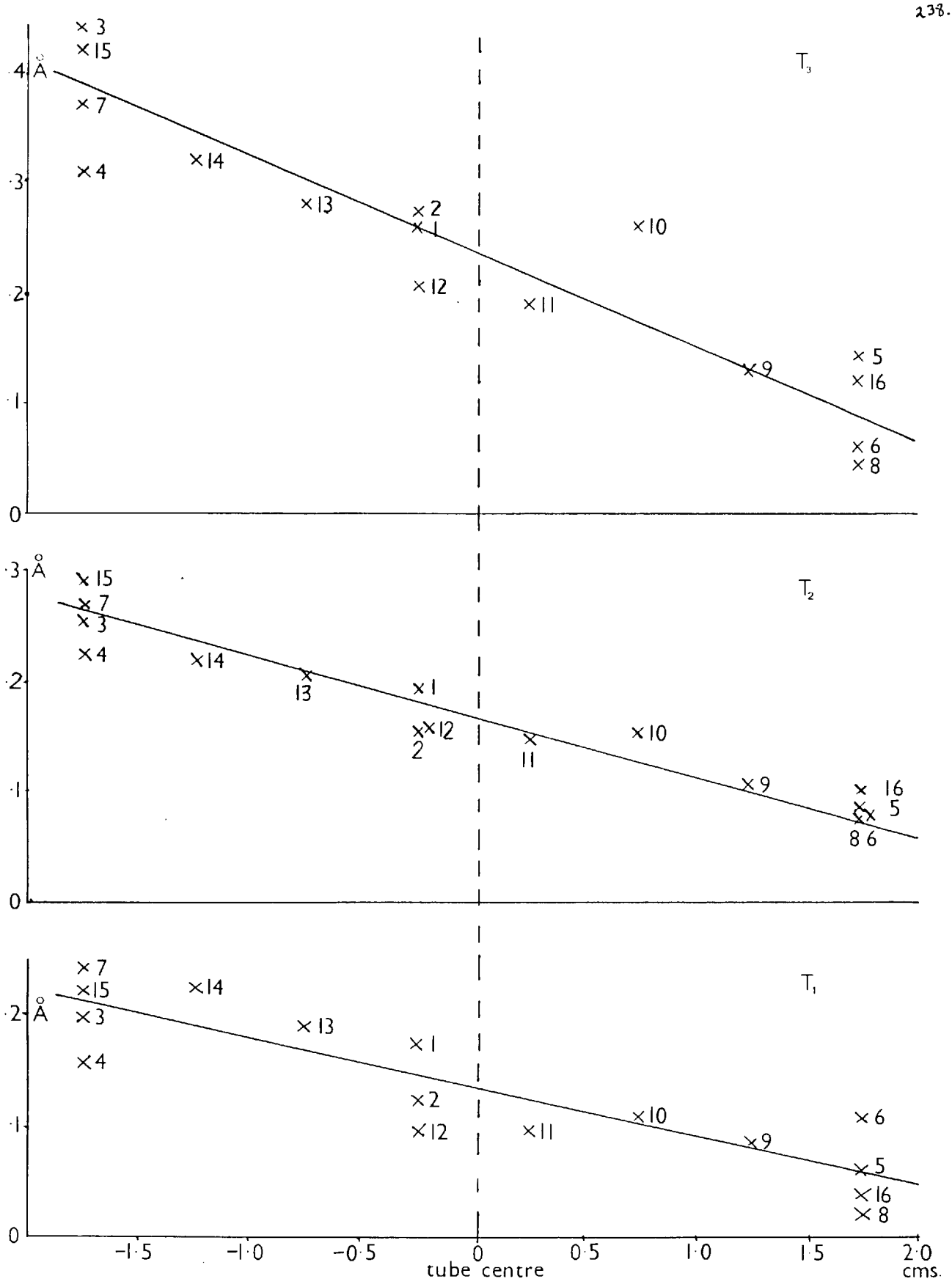


Fig 11·9. Measured shifts of λ4267Å C II versus distance across tube.

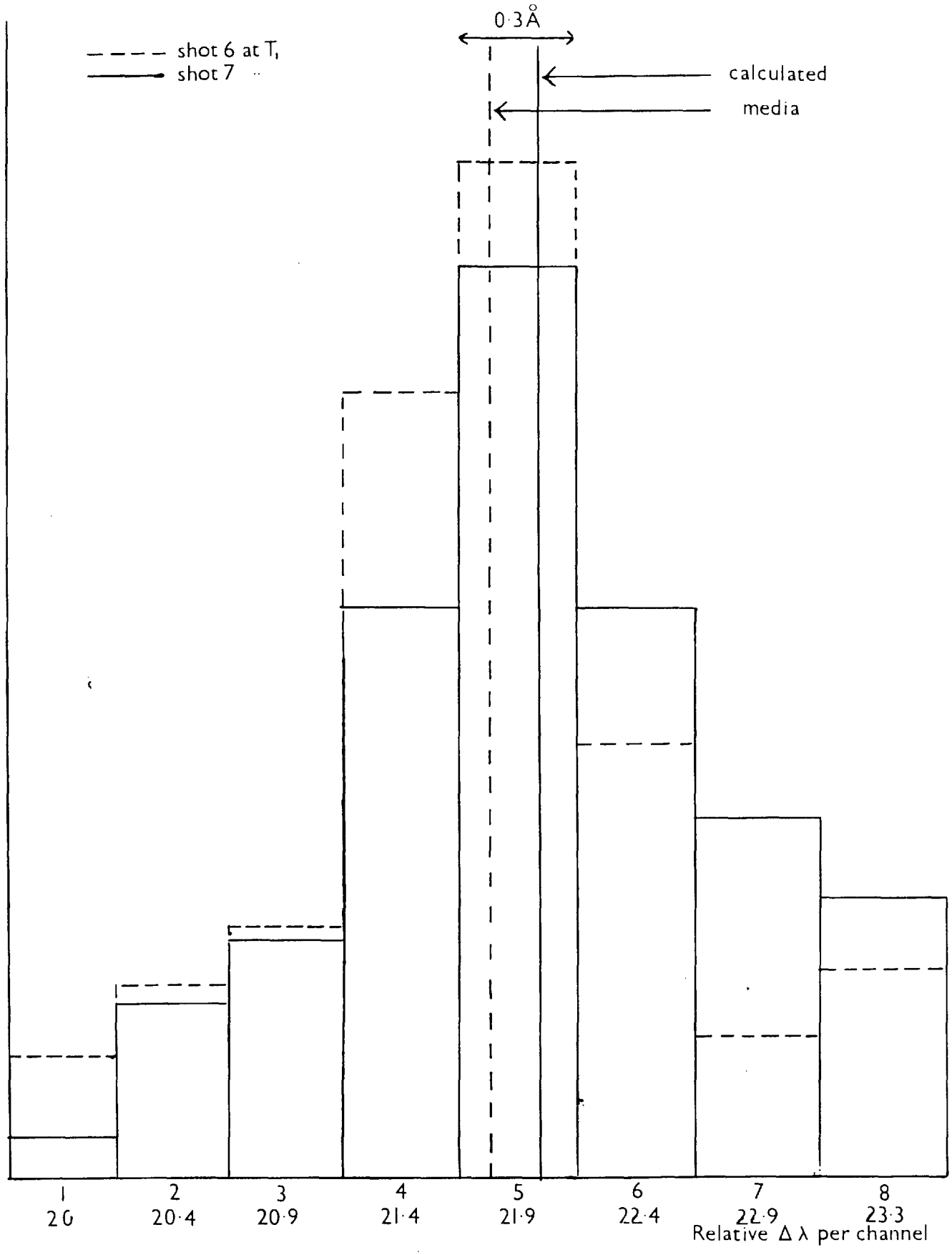


Fig 11·10. Typical line profiles across tube.

of pressure on the F-P plates. To randomise out possible errors from this source the tube was scanned in the order indicated by the numbers on the points in fig.11.9.

At each time a 'best fit' straight line was drawn through the measured shifts by means of linear regression analysis (see fig.11.9). The angular velocity at each time was calculated from the gradient of the line and equation 11.1 and the error in this quantity estimated from the statistically calculated standard deviation. Results are shown in Table 1 below.

TABLE 1

Measurement	Time from zero driving field (3rd $\frac{1}{2}$-cycle) μsec	W units of 10^4 rev sec^{-1}
Doppler shift	t_1 Initial implosion, 0.45	5.3 ± 0.7
	$t_2 \sim$ 1st pinch, 0.65	6.1 ± 0.5
	$t_3 \sim$ 2nd pinch, 0.95	9.5 ± 0.9
Streak	t_4 Start of Instability 2.25	190 ± 20

A streak photograph was taken with each line profile shot and the mean angular velocity calculated from these is also shown in Table 1. The streaks were interpreted on the basis of two rotating flutes, i.e.  so that each flute would appear in the streak viewing slot once every $\frac{1}{2}$ period of rotation.

(d) Measurement of moment of inertia of plasma

To obtain the angular momenta associated with the above values of W it was necessary to estimate the moment of inertia

of the plasma at each time from :-

$$I = Mk^2$$

The mass per unit length of the plasma, M, was estimated using the double magnetic loop technique of Green [ref.82]. An integrated loop signal correlated with a di/dt trace is shown in fig.11.11. Green shows that :-

$$M = B^2 \tau^2/4\pi^2 = B_o \sin^2 \omega t \; \tau^2/4\pi^2 \qquad \ldots 11.8$$

Where τ is the period of the radial plasma oscillations (found from fig.11.11), and B is the driving field (nearly sinusoidal).

Variations of M with time for two initial filling pressures are shown in fig.11.12. At P_o = 0.045 torr M gradually falls off due to end losses. The mean value of M at early times was normalised on this plot to the value of M corresponding to the initial filling pressure. (Taking into account 1% C impurity.) Thus from 11.8 :-

$$B_o \simeq 36 \text{ K Gauss}$$

The value of B_o calculated from thepeak current was,

$$B_o \simeq 50 \text{ K Gauss}$$

In fact collector-coil discontinuity effects could easily account for a drop $\sim$ 20% in the calculated B_o [ref.83]. Thus, in the calculation of M for P_o = 0.06 torr, the lower value of B_o was employed.

The variation of M with time for P_o = 0.06 torr shows the strong axial contraction typical of a reverse trapped flux configuration [ref.84]. Later M falls off due to end losses. At times t_1 and t_2 (fig.11.12) M has to be interpolated knowing $M(P_o)$.

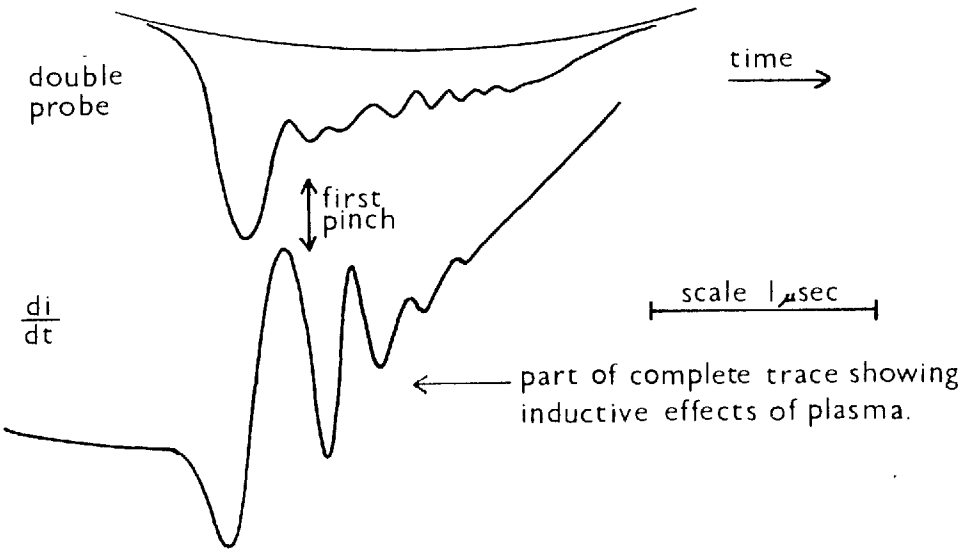


Fig. 11·11 Double probe signal and $\frac{di}{dt}$ monitor. P_o: 0·045 torr.

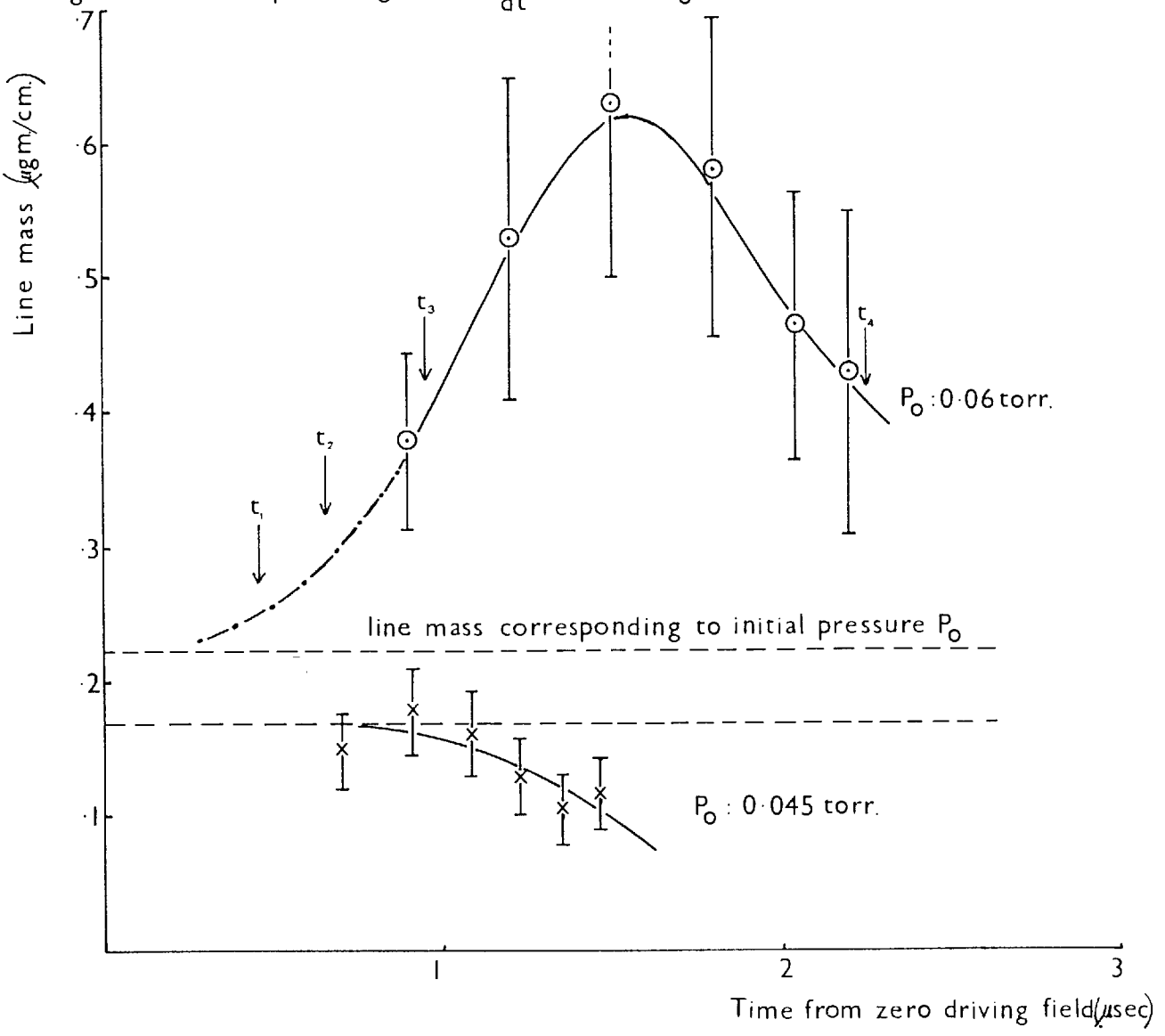


Fig. 11·12 Variation of plasma line mass with time.

The radial dimensions of the plasma were estimated from the Abel inverted continuum distributions using the method described in Chapter 4. These dimensions were checked with end on framing camera photographs (fig.11.3). The distribution at t_3 is shown in fig.11.13. At t_4 the separation of the rotating flutes was estimated from the streak photographs. The estimated radius of gyration at each time is tabulated below:-

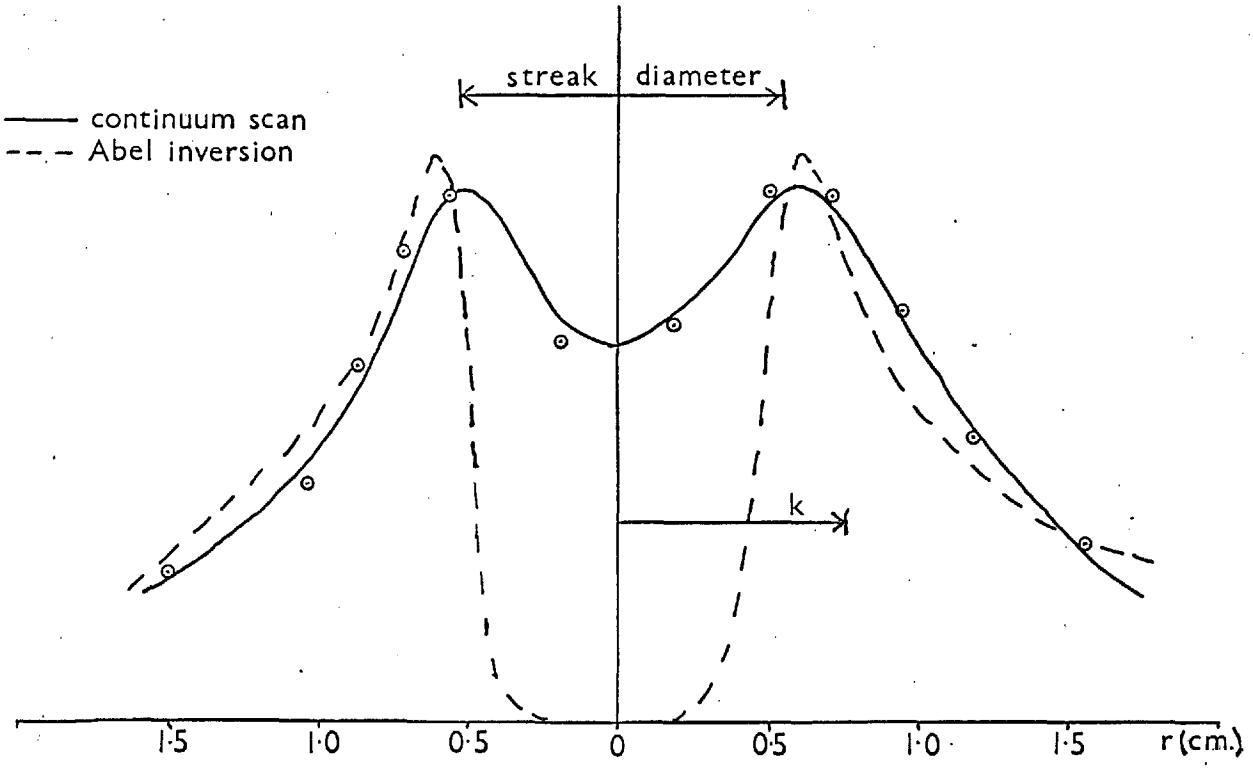


Fig 11·13. Radial distribution of continuum intensity at time T_1

TABLE 2

Time	Radius of gyration, kcms
t_1	1.75 ± 0.2
t_2	1.82 ± 0.1
t_3	0.75 ± 0.1
t_4	0.8 ± 0.1

The corresponding values of angular momentum at each time are given in Table 3 :-

TABLE 3

Measurement	Time	Angular momentum per unit length (e.g.s. units)
Doppler shift	t_1	0.25 ± .07
	t_2	0.25 ± .07
	t_3	0.27 ± .08
Streak photograph	t_4	2.9 ± 1.0

11.5 Discussion

The fact that a straight line could be drawn through the measured shifts meant that the plasma was indeed rotating as a solid body. Any spread of velocities due to different 'layers' of plasma rotating with different W would be reflected as a broadening of the line profile. The observed line width B (fig.11.10) was ~ 0.65Å. The instrument function was approximately Lorentzian with $\frac{1}{2}$-$\frac{1}{2}$ width ~ 0.13Å. Knowing the CII

doublet separation and relative intensities of the components the width of a Gaussion broadening mechanism could be roughly estimated, i.e. $g \sim 0.28$Å. This would correspond to an ion temperature $\sim$ 25 e.V. Such a value is not unreasonable for conditions at the 1st pinch so that any spread of rotational velocities must be small. In addition the observed direction of rotation at each time was the same as that predicted by all theories [ref.73], i.e. the direction in which an ion would move in the driving B_2 field.

Since the above conclusions rely implicitly on the assumption that the shifts detected were due plasma motion it is worth considering whether any other source of shift could give the observed results. Two other causes of line shift, i.e. Stark and Quadratic Zeeman shifts would give values of $\Delta\lambda$ symmetrical about the tube axis since N_e, T_e and the magnetic field are to a first approximation. (This was confirmed by the symmetry of the radial CII line intensity and continuum distributions.) Thus shifts from these effects would not vary linearly with r_o. Reasonable estimates show that in any case the shifts would be far smaller in magnitude than the observed values.

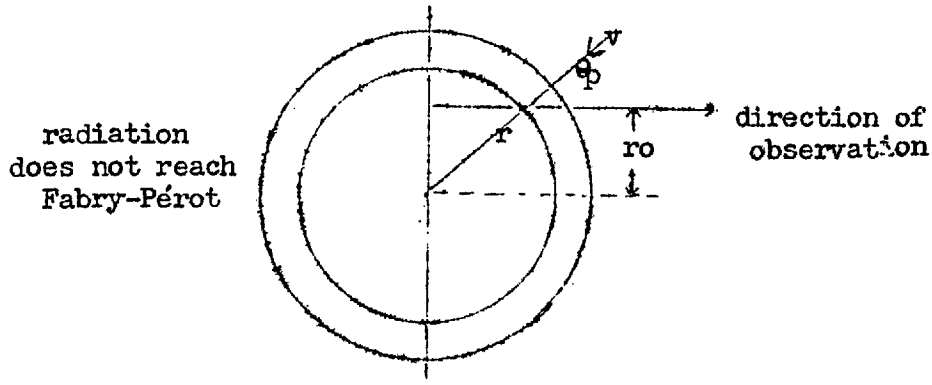
While the above reasoning shows that Stark and Zeeman effects are unimportant there is an appreciable shift in time of the line profile (fig.11.9), i.e. at the tube centre,

$$t_1 \text{ to } t_2, \quad \Delta\lambda = -0.04 \pm .01\text{Å} \text{ (to blue)}$$

$$t_2 \text{ to } t_3, \quad \Delta\lambda = -0.07 \pm .01\text{Å} \text{ (to blue)}$$

Three possible causes need to be analysed :-

(i) Radial implosion and oscillations of an optically thick plasma :



If the plasma were optically thick to the CII line a net inward velocity, V', would be obtained.

$$V' = V\sqrt{[1-(r_o/r)^2]}$$

i.e. $r_o = 0$, $\Delta\lambda = \lambda V/C$

∴ From t_1 to t_2 we expect $V \sim 3 \times 10^5$ cms/sec. The observed implosion velocity, from the streak photographs, is $\sim 4.5 \times 10^6$ cms/sec: i.e. while the observed shift is in the right direction the magnitude of the estimated velocity is far too low indicating that the plasma is not appreciably thick to the CII radiation. In fact evaluation of τ_o taking $N_e = 10^{17} cm^{-3}$ and knowing that the number density of CII ions should be only $\sim 1\%$ of this value gives, $\tau_o \ll 1$ at all reasonable values of T_e. It is therefore extremely unlikely that optical depth is important.

(ii) Plasma rotation and drift

Consider a plasma rotating with angular velocity W at t_1 and drifting with velocity V_D towards the collector plates (due to collector plate-coil discontinuities, ref.83). If at t_2 the angular velocity is W + dW and the plasma has drifted a distance x then the measured shifts at height r above the plasma centre, $\Delta\lambda$, are :-

t_1 : $\Delta\lambda_1 = \lambda Wr/C$

t_2 : $\Delta\lambda_2 = \lambda(W+dW)(r-x)/C$

$\therefore$ Shift in time, $\Delta\lambda_2 - \Delta\lambda_1 = \lambda dWr/C - \lambda V_D dt(W+dW)/C$

This relation does in fact give the observed variation of shift in time as a function of r.

Shift at $r = 0 = -\lambda V_D dt(W+dW)/C$

Substituting the measured values of dt, W+dW we get :-

t_1 to t_2 : $V_D = 3.5 \times 10^6$ cms/sec $\pm$ 1.0×10^6

t_2 to t_3 : $V_D = 2.8 \times 10^6$ cms/sec $\pm$ 0.6×10^6

However the maximum drift velocity measured from streak photographs, $\sim 0.6\mu s$ after t_3, gives :-

$$V_D = 6 \times 10^5 \text{ cms/sec} \pm 2 \times 10^5$$

so this mechanism cannot entirely account for the observations.

(iii) Radial plasma drift

If the discharge tube axis is not coincident with the magnetic B_z axis then plasma drift could occur which is not necessarily to the current feed in point. The measured shifts in time would correspond to a resolved drift velocities towards the direction of observation of :-

t_1 to t_2 : $V = 2.8 \times 10^5$ cms/sec $\pm$ 1.0×10^5

t_2 to t_3 : $V = 4.2 \times 10^5$ cms/sec $\pm$ 0.6×10^5

and corresponding drifts in this direction of 0.06 cms and 0.13 cms over each time interval respectively. Drifts as small as this are not contradicted by the streak measurements.

Thus the observed shift in time could be accounted for by

a drift of the plasma towards the direction of observation possibly with a small upwards drift (2) superimposed. Such a drift has been observed photographically by Bodin et al [ref.87].

It is now necessary to check that velocities measured on the CII ions are representative of the plasma as a whole,

i.e. $W_c = W_D$ (D ≡ deuterium ions)

To do this the change of momentum by elastic collisions must be considered,

i.e. $$n_c m_c \, dW_c/dt = \gamma (W_D - W_c) \qquad \ldots 11.9$$

Where W refers to gross translational velocities and γ is the effective momentum exchange cross section.

i.e. Taking $V = W + v$ where v is a thermal velocity

$$\gamma \sim \{M_D M_c/M_D+M_c\} (8/\pi (kT_D/M_D + kT_c/M_c) + |W_D-W_c|^2)^{\frac{1}{2}} \times n_D n_c \sigma V_{rel}),$$

assuming $\sigma(V_{rel})$, the effective ionic collision cross section, is roughly constant.

From 11.9 $W_c \sim W_D$ after a time,

$$t \sim n_c m_c/\gamma$$

Taking $n_D = 5 \times 10^{16} cm^{-3}$

$n_c = 5 \times 10^4 \ cm^{-3}$

$T_e \sim 10$ e.V.

and $\sigma \sim 30 \ (Z_e^2/mV_{rel}^2)^2$ from Allen ref.5

with $V_{rel} \sim (3kT_D/m_D)^{\frac{1}{2}}$

we get, $t \sim 1\mu$ sec.

Thus the measured rotational velocities should be roughly representative of the deuterium plasma.

To summarise the above discussion the plasma has been shown to rotate as a solid body in the early stages of the discharge, and in the direction predicted by theory. Nevertheless the measured velocities of rotation differed considerably from those estimated from streak photographs (Table 1). To see that this is, in fact, in accordance with expectation it is necessary to distinguish between the different angular frequencies which would exist in a rotating plasma. That is following Haines [ref.73] :-

Ω = Centre of mass angular frequency

W = Ion guiding centre angular frequency

W_i = Ion diamagnetic azimuthal current angular frequency.

These are related by,

$$\Omega = W + W_i \qquad \ldots 11.10$$

where Ω is the quantity measured from Doppler shifts.

It is now instructive to consider the stability of the rotating plasma by assuming a small perturbation of the form,

$$f(r)\, e^{i(Wt + m\theta)}$$

The following condition [ref.73] then arises for stability :-

$$1 - \sqrt{m} < 2\Omega/W_i < 1 + \sqrt{m}$$

The fastest growing instability mode is m = 2 so the most stringent condition is ,

$$-0.414 < 2\Omega/W_i < 2.414 \qquad \ldots 11.11$$

At time t_4 when fission has occurred the velocity measured is most probably that of the ion guiding centres, W. 11.11 is then more conveniently expressed in the form :-

$$-2.414 < 2W/W_i < 0.414 \qquad 11.12$$

Thus the stability criterion can be applied to times t_1 to t_3 by equation 11.11, and t_4 by 11.12, if W_i is known. This quantity can be estimated as follows :-

The angular momentum, per unit length of the plasma, associated with the ion diamagnetic current can be simplified to [ref.73] :-

$$L_i = \eta (m_i/\pi e)\phi \qquad \ldots 11.13$$

where ϕ is the reverse trapped flux

η is the proportion of the total current carried by the ions.

Both these quantities are referred to the time at which the plasma originally aquires its angular momentum.

We can express $\eta = T_i/(T_i+T_e)$

Before the CII radiation is burnt out we can approximate the conditions to L.T.E. and take $T_i \sim T_e$ or $\eta \sim 0.5$. This should be roughly true as indicated by Bodin et al [ref.76].

ϕ can be calculated on the assumption that at the start of the radial implosion the plasma conductivity is high and there is no field diffusion. Thus ϕ = trapped flux at 1st pinch.

Assuming magnetic pressure balance at the 1st pinch,

$$\text{Trapped } B_T = \text{Driving } B = B_o \sin 2\pi t_2/T$$

The area, A, of the plasma hole at the 1st pinch can be estimated from fig.11.13. Thus we obtain,

$\phi = B_T A \sim 44 \pm 20\%$ K.Maxwells .

11.4 then gives :-

$L_i \sim 0.74$ c.g.s. units.

W_i can therefore be calculated at all times from :-

$$L_i = MK^2 W_i ,$$

M and k being known from Section 11.4d. The results obtained are shown in Tabie 4 below.

TABLE 4

time	W_i rev/sec
t_1	1.6×10^5
t_2	1.8×10^5
t_3	2.6×10^5
t_4	3.8×10^5

Substitution of these figures into equations 11.11 and 11.12 gives the following results :-

Time	Condition for stability	$2\Omega/W_i$	$2W/W_i$	
t_1	$-0.414 < 2\Omega/W_i < 2.414$	0.66	✓	Stable
t_2		0.68	✓	Stable
t_3		0.73	✓	Stable
t_4	$-2.414 < 2W/W_i < 0.414$	✓	10	Unstable

Thus the small angular velocities measured from Doppler shifts satisfy the criterion for a stable mode of rotation while instability is predicted at time t_4.

While these preliminary experiments confirmed that the plasma, in its early stages, is rotating rigidly it is not easy from these measurements alone to distinguish between the different theoretical models proposed to explain the origin of the rotation [ref.73].

However, the models of Bostick and Wells [ref.88] and Velikhov [ref.89] can be excluded by the results recorded here. On these models the plasma separates radially or axially into two parts which rotate in opposite directions. However the CII line shift measurments show that the plasma rotates as a single rigid body, at least during its early stages. Further end on streak photographs show that the plasma is rotating uniformly along its length.

Which of the remaining models [ref.73] is important in our case cannot be decided on the basis of the Doppler measurements alone since similar values of angular velocities and acceleration times are predicted. Nevertheless these values are not inconsistent with the experimental results. For example Haines [ref.73] and Thonemann and Kolb [ref.90] show that the rotational velocity of the plasma at time $t = T_v$ should be,

$$\Omega_{T_v} \sim (V_o/r)(T_v/T_A)^2$$

where $V_o = I_{\theta o}/n_e$ = drift velocity of electrons at $t = 0$

T_v = drift time of electrons around the plasma column

T_A = Transit time of the Alfven wave

r = radius of plasma.

For our conditions $T_V \sim 0.05$ μs

and $\Omega_{TV} \sim 2 \times 10^4$ rev/sec, while the measured velocity at the nearest time to this, $t = 0.45$ μs, was $\Omega = 5 \times 10^4$ rev/sec.

ACKNOWLEDGEMENTS

The author would like to thank Dr. R. Latham who supervised this work throughout.

Dr. J. Cooper, while at Imperial College, supervised the initial stages of this programme.

I am indebted to Dr. D.D.Burgess for many stimulating discussions and for reading the preliminary draft of this thesis.

Considerable help and much constructive criticism has been forthcoming from several members of the Plasma Physics and Spectroscopy groups at Imperial College. In particular I should like to acknowledge Messrs. A.E.Dangor and C.B.Wheeler, Dr.A. Folkierski and Mr.J.Troughton (Plasma Physics) and Dr.G.J.Pert and Messrs. J.Davis, S.Budd and J.E.Jenkins (Spectroscopy).

Most of the apparatus used was built by Mr.P.J.Daly and the electronics by Mr.L.Nyman.

The author has worked with several members of other groups to whom many thanks are due:- Mr.P.D.Johnson (Spectroscopy, I.C.); Dr. M.Keilhacker, Mr.G.N.Harding, Dr.H.A.B.Bodin and Dr.G.B.F. Niblett (A.E.R.E.Culham Laboratory); Professor A.G.Gaydon and Dr. P.B.Coates (Chemical Engineering Dept., I.C.).

Any defects in the appearance of this thesis are not due to the typist who coped masterfully with my writing or to Mr.M.Jackson who spared no effort in preparing the diagrams.

Many thanks are due to Professor W.R.S. Garton for kindly allowing me to complete this thesis while a Research Assistant in his group.

During this work (1963-1966) the author was in receipt of a grant from the S.R.C.

Finally, I should also like to thank Miss Sylvia Holcombe for help and encouragement during the periods of stress incurred while writing this thesis and the Manager of Lloyd's Bank, South Kensington, without whose help this thesis would not be in existence.

APPENDIX I

Calculation of impact broadened AII line widths and shifts

(1) Reduction of formulae for computations

The widths and shifts are calculated from equation 4.71 (p.83, ref.2)

$$\langle \alpha \mid \Phi_a \mid \alpha \rangle = -(W_\alpha - id_\alpha) - (4\pi/3)N(\hbar/m)^2 \iint (dv d\rho/v\rho) f(v) \times \sum_{\alpha'} |\langle \alpha | Ra | \alpha' \rangle|^2 [A(Z_{\alpha\alpha'}) + iB(Z_{\alpha\alpha'})] \quad \ldots 1$$

Where $Z_{\alpha\alpha'} \equiv W_{\alpha\alpha'}\rho/v = \rho(E_{\alpha'} - E_\alpha)/\hbar v$ ... 2

Where W_α = width of level α

d_α = shift of level α

and $\langle \alpha \mid Ra \mid \alpha' \rangle$ are the radial matrix elements connecting α and the perturbing levels α'. The ρ integral :-

$$\sum_{\alpha'} \int (d\rho/\rho)\, R_{\alpha'} [A(Z_{\alpha\alpha'}) + i\, B(Z_{\alpha\alpha'})]$$

Where $R_{\alpha'} \equiv |\langle \alpha | Ra | \alpha' \rangle|^2$

Becomes $\sum_{\alpha'} R_{\alpha'} \int_{Z_{\alpha\alpha'}}^{\infty} [A(z)dz/z + iB(z)dz/z]$ ... 3

on use of equation 2.

The limits of ρ are 0 to ∞ but due to divergence at small ρ we cut off at ρ_{min} which Griem shows is given by

$$\rho_{min} \approx (2/3)^{\frac{1}{2}} (\hbar/mv) \left| \sum_{\alpha'} R_{\alpha'} [A(Z^{min}_{\alpha\alpha'}) + iB(Z^{min}_{\alpha\alpha'})] \right|^{\frac{1}{2}} \quad \ldots 4$$

This was chosen so that equation 1 tended to the correct expression in the low velocity (adiabatic) limit and also satisfied the high velocity limit where perturbation theory could be used throughout. Corresponding to this value of ρ_{min} :-

$$Z^{min}_{\alpha\alpha'} = W\alpha\alpha'\rho_{min}/v \qquad \ldots 5$$

Hence the ρ integral is :-

$$\sum_{\alpha'} R\alpha' \int_{Z^{min}_{\alpha\alpha'}}^{\infty} [A(z)dz/z + i\, B(z)dz/z]$$

$$\equiv \sum_{\alpha'} R\alpha' [a(Z^{min}_{\alpha\alpha'}) + i\, b(Z^{min}_{\alpha\alpha'})] \qquad \ldots 6$$

Substitution into equation 1 gives :-

$$W\alpha - id\alpha \approx (4\pi N/3)(\hbar/m)^2 \int (dv/v) f(v) \sum_{\alpha'} R\alpha' [a(Z^{min}_{\alpha\alpha'}) + i\, b(Z^{min}_{\alpha\alpha'})] \qquad \ldots 7$$

This expression gives the contribution of weak collisions to $W\alpha$ and $d\alpha$.

As a rough estimation for the contribution of the strong collisions ($\rho < \rho_{min}$) to the width, we use the Lorentz-Weisskopf expression :-

$$W_\alpha^{strong} \approx N \int dv\, f(v)\, \pi v \rho^2_{min} \qquad \ldots 8$$

Using equations 4 and 8 :-

$$W_\alpha^{strong} \approx (4\pi/3) N(\hbar/m)^2 \int \tfrac{1}{2}(dv/v) f(v) \left| \sum_{\alpha'} R\alpha' [A(Z^{min}_{\alpha\alpha'}) + i\, B(Z^{min}_{\alpha\alpha'})] \right| \qquad \ldots 9$$

Adding this term to (7) we get :-

$$W\alpha - id\alpha \approx (4\pi N/3)(\hbar/m)^2 \int (dv/v) f(v) \left\{ \tfrac{1}{2} \left| \sum_{\alpha'} R\alpha' \left[A(Z^{min}_{\alpha\alpha'}) + iB(Z^{min}_{\alpha\alpha'}) \right] \right| + \sum_{\alpha'} R\alpha' \left[a(Z^{min}_{\alpha\alpha'}) + i\, b(Z^{min}_{\alpha\alpha'}) \right] \right\} \quad \ldots 10$$

Which is equation 4.79, Griem.

This expression can be simplified for computational purposes by inserting a Maxwellian velocity distribution into (10), i.e.

$$f(v)dv = 4\pi (m/2\pi kTe)^{3/2} v^2 e^{-mv^2/2kTe} dv \quad \ldots 11$$

We then get an integral containing : $ve^{-mv^2/2kTe}dv$

To simplify put $x = mv^2/ch$ ... 12

Then $W\alpha - id\alpha = (2/3) Ne (h/2m\pi kTe)^{3/2} \int_{x=o}^{\infty} e^{-chx/2kTe} dx \left\{ --- \right\}$ ... 13

$\left\{ --- \right\}$ refers to the bracket in equation 10.

Writing this expression in terms of frequencies, $\nu = w/2\pi$, evaluating the constants and calculating $W\alpha$, $d\alpha$ for $N = 10^{16}$ electrons /cc we get:-

$$W\alpha - id\alpha = 1.318 \times 10^{10} (1/Te^{3/2}) \int_{o}^{\infty} e^{-chx/2kTe} dx \left\{ --- \right\} \quad \ldots 14$$

Thus the only assumption made about the plasma conditions is that the electrons have a Maxwellian distribution. Since $\Delta\nu = -c/\lambda^2 \Delta\lambda$, if we change the sign of $d\alpha'$ a positive shift (evaluated in frequency units)

corresponds to a shift to the red. The final expression is therefore [in sec^{-1}]

$$W\alpha+id\alpha = 1.318 \times 10^{10} Te^{-3/2} \int_{x=o}^{\infty} e^{-chx/2kTe} dx \times \left\{ \tfrac{1}{2} \left| \sum_{\alpha'} R\alpha' [A(Z^{min}_{\alpha\alpha'}) + iB(Z^{min}_{\alpha\alpha'})] \right| + \sum_{\alpha'} R\alpha' [a(Z^{min}_{\alpha\alpha'}) + ib(Z^{min}_{\alpha\alpha'})] \right\}$$

$$= 1.318\ Te^{-3/2} \int_{x=o}^{\infty} \left\{ Re(x) + i\ Im(x) \right\} dx \quad \ldots 15$$

The variable of integration is (from 4, 5 and 12):-

$$x = (2/3)^{\frac{1}{2}} (E\alpha' - E\alpha / Z^{min}_{\alpha\alpha'}) \left| \sum_{\alpha'} R\alpha' [A(Z^{min}_{\alpha\alpha'}) + iB(Z^{min}_{\alpha\alpha'})] \right|^{\frac{1}{2}} \quad \ldots 16$$

Where $E\alpha$, $E\alpha'$ are in wavenumbers.

The quantities A(Z), B(Z), a(Z), b(Z) have been calculated by Griem for a wide range of Z[ref.2].

(2) Evaluation of integral (equation 15)

In the expression for x, $(E\alpha' - E\alpha / Z^{min}_{\alpha\alpha'}$ is independent of α', the perturbing level, from (5). Hence an arbitary value of $Z^{min}_{\alpha\alpha'}$ is chosen for the nearest perturbing level (negative if $E\alpha' < E\alpha$ so that x remains positive). Thus x can be evaluated by doing the sum in (16) over all perturbing levels, and similarly the integrand in (15), knowing $Z^{min}_{\alpha\alpha'}$ for all the other perturbing levels from

$$(E\alpha'' - E\alpha / Z^{min}_{\alpha\alpha''} = \text{const.} = (E\alpha' - E\alpha / Z^{min}_{\alpha\alpha'}$$

Where α'' refers to another perturbing level.

Initially complete L-S coupling is assumed so the perturbing levels to α are found using the dipole selection rules:-

$\Delta J = 0, \pm 1, \quad J = 0 \not\rightarrow J = 0$

$\Delta S = 0$

$\Delta L = 0, \pm 1$

$\Delta l = \pm 1$ (l refers to jumping electron)

Odd $\rightleftharpoons$ even level

Two electron jumps are forbidden.

The matrix elements $R\alpha'$ are then calculated using the Bates and Damgaard approximation, [ref.31] :-

$$R\alpha' = |\langle\alpha|Ra|\alpha'\rangle|^2 = \begin{matrix} l_> (2l_> -1)\sigma^2 & \text{for } l = l-1 \\ l_> (2l_> +1)\sigma^2 & \text{for } l = l+1 \end{matrix}$$

where $l_>$ is the greater of the orbital quatum numbers of $E\alpha$ or the particular perturbing level $E\alpha'$. σ evaluated on Bates and Damgaard's method is given by :-

$$\sigma = \left(c / \sqrt{4l^2-1}\right) x\ (2/n^{*\prime})^{n^{*\prime}} / [n^{*\prime 2}\,\Gamma(n^{*\prime}+l'-1)\,\Gamma(n^{*\prime}-l')]^{\frac{1}{2}}$$

$$x\ (2/n^{*\prime\prime})^{n^{*\prime\prime}} / [n^{*\prime\prime 2}\,\Gamma(*''+l''-1)\,\Gamma(n^{*\prime\prime}-l'')]^{\frac{1}{2}}$$

$$x \sum_{p'=o}^{\infty} \sum_{p''=o}^{\infty} \left\{ Cp'(n^{*\prime},l')\,Cp''(n^{*\prime\prime},l'')\,(n^{*\prime}n^{*\prime\prime}/(n^{*\prime}+n^{*\prime\prime}))^{n^{*\prime}+n^{*\prime\prime}+2-p'-p''} \right.$$

$$\left. \Gamma(n^{*\prime}+n^{*\prime\prime}+2-p'-p'') \right\} \qquad \ldots 8$$

where $Co = 1$

$$Cp = Cp-1\ (n^*/2p)[l(l+1)-(n^*-p)(n^*-p+1)] \qquad \ldots 9$$

n^* = effective principle quantum number of level $\alpha = 2\sqrt{R/(E\infty - E\alpha)}$

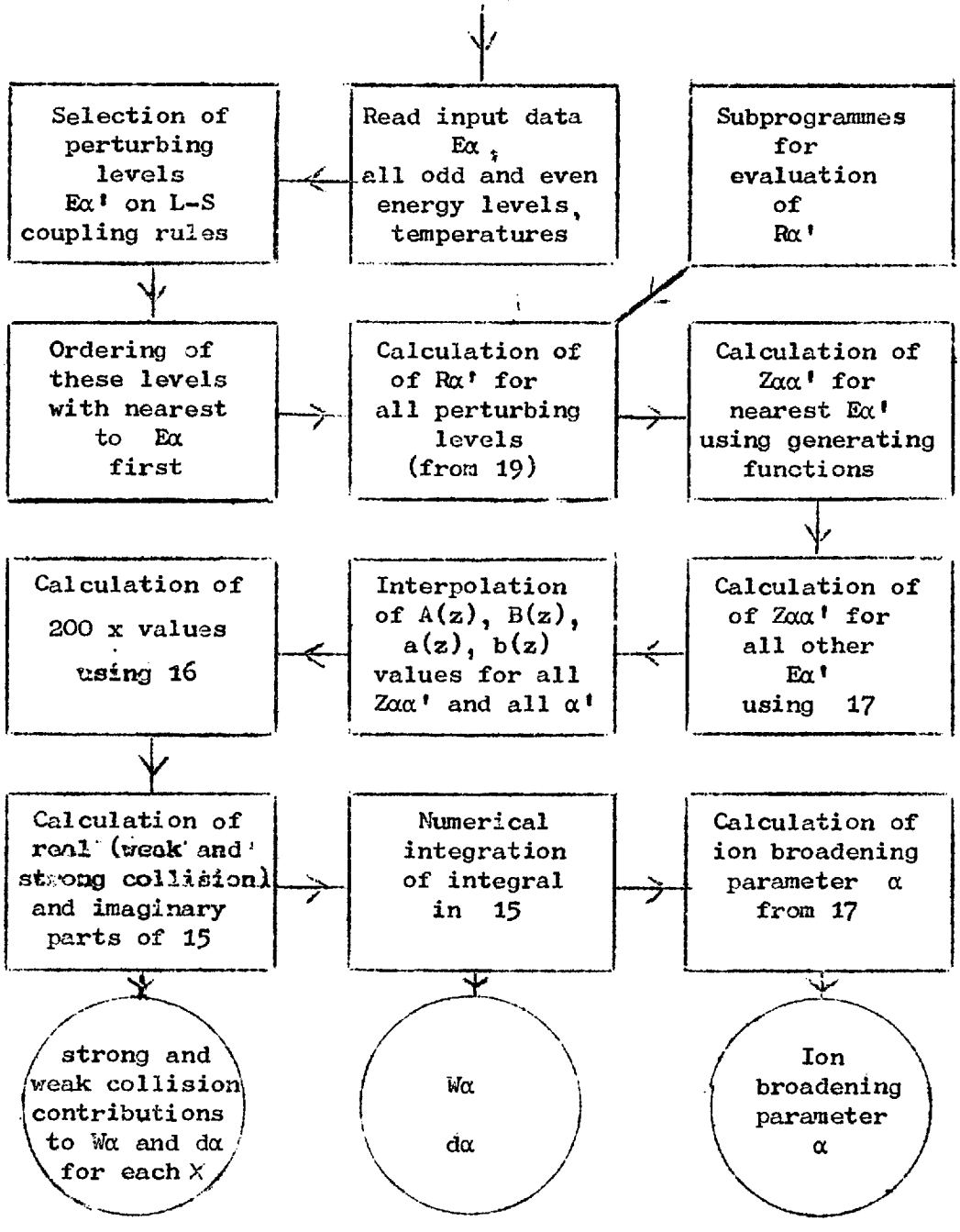
l = orbital quantum number of valence electron.

For n^* and l the subscript ' refers to $E\alpha$ and '' to $E\alpha'$.

The calculation procedure is shown in the flow diagram.

FLOW DIAGRAM FOR CALCULATION

OF $W\alpha$, $d\alpha$ and α



(3) Details of programme (Fortran II)

Values of $W\alpha$, $d\alpha$ and α can be calculated at 7 temperatures for up to 10 levels in each run. In addition the strong and weak collision contributions to the width, and weak collision contribution to the shift, are obtained as a function of x for each level and temperature.

The programme can readily be modified to deal with any charge state of the emitting species. Provision can be made to evaluate $W\alpha$ etc on inclusion of increasing numbers of perturbing levels in the calculations. A total of 50 perturbing levels can be handled.

In cases where array (1) splitting is appreciable matrix elements,

$$\frac{R^2_{mult}\ 1,\ (\Delta l^2_{>} - 1)^{\ 2}}{2L + 1}$$

must be used to couple each perturbing multiplet to the state considered. R^2_{mult} can be obtained from ref. 94.

If multiplet splitting is also negligible matrix elements,

$$f_{\alpha\alpha'}$$

must be used to couple each perturbing level to the state considered.

APPENDIX II

COMPUTER PROGRAMME FOR CALCULATING THE STARK PROFILE EMITTED BY AN OPTICALLY THIN, INHOMOGENEOUS BUT CYLINDRICALLY SYMMETRIC PLASMA

(Simplified version for $N_1 = N_e$ written for an Elliot 803A)

For $N_1 = N_e$ the relations 8.1 to 8.5 simplify to :-

$$I_{OBS}(\lambda) = K \sum_{x'=0}^{25\Delta x'} e^{-Wm/kT_e(x')} \Big/ \left\{1 + \left[\frac{\lambda}{[T_e(x')]N_e(x')} - F[T_e(x')]\right]^2\right\}$$

$$= K \sum_{x=0}^{25\Delta x'} \Lambda(x',\lambda)$$

$$\text{While } I_{CENTRE}(\lambda) = Ke^{-Wm/kT_e(x'=0)} \Big/ \left\{1 + \left[\frac{\lambda}{[T_e(x'=0)]N_e(x'=0)} - F[T_e(x'=0)]\right]^2\right\}$$

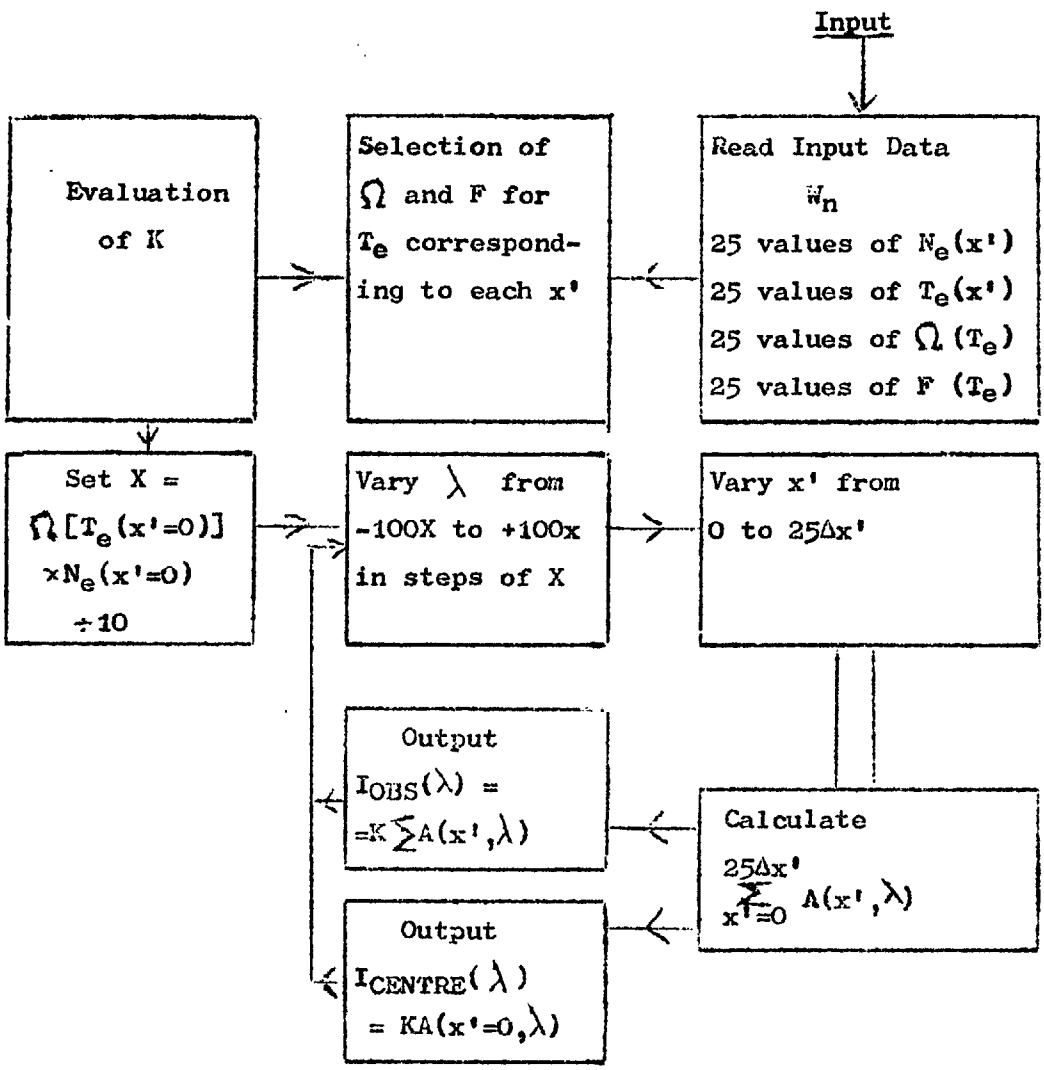
$$= KA(x'=0,\lambda)$$

$$\text{Where } K = \left[1+(F[T_e(x'=0)])^2\right]e^{+Wm/kT_e(x'=0)}$$

These profiles are normalised to the same peak intensity.

Input consists of N_e and T_e for 25 values of x' in equal increments Δx, Ω and F for 25 values of T_e in equal increments from 10,000°K to 25,000°K and Wm the upper state energy of the line considered.

A block diagram of the calculating procedure is given below:-


Input
Read Input Data
W_n
25 values of $N_e(x')$
25 values of $T_e(x')$
25 values of $\Omega(T_e)$
25 values of $F(T_e)$
Selection of
Ω and F for
T_e corresponding to each x'
Evaluation
of K
Set X =
$\Omega[T_e(x'=0)]$
$\times N_e(x'=0)$
$\div 10$
Vary λ from
$-100X$ to $+100x$
in steps of X
Vary x' from
0 to $25\Delta x'$
Output
$I_{OBS}(\lambda) =$
$=K\sum A(x',\lambda)$
Calculate
$\sum_{x'=0}^{25\Delta x'} A(x',\lambda)$
Output
$I_{CENTRE}(\lambda)$
$= KA(x'=0,\lambda)$

APPENDIX III

FURTHER LASER MEASUREMENTS ON AN UNSTABILISED Z-PINCH

In Chapter 6 measurements of N_e at two initial conditions only were presented. Here further measurements are described. These were carried out to investigate the versitility of the Z-pinch as a light source suitable for a detailed study of Stark broadening.

For this purpose it is desirable that N_e can be varied and conveniently measured over as wide a range as possible; the achievement of a given N_e should, ideally, be readily predictable from known initial conditions of filling pressure and bank voltage. In addition the radial distribution of N_e should be closely rectangular.

To achieve a given N_e at peak compression two parameters can be varied, i.e. P and V.

The measured variation with P of $\int N_e \, dl$ through the tube centre is shown in Fig.1. Measurements at 0.75 kv and 1.0 kv were made with the tube in a Fabry-Pérot cavity as in Chapter 6 but the laser was operated at $\lambda 3.39\mu$. Measurements at higher voltages were made at $\lambda 6328\text{Å}$.

The curves of $\int N_e \, dl$ versus P show a distinct maximum at each of three bank voltages. Since framing camera photographs on a basically similar discharge [Chapter 3] had shown the plasma diameter to increase monotonically with filling pressure we should expect a maximum in the axial N_e versus P variation. A similar peaking, which is in contradiction with the existing models of linear pinch dynamics, has been reported previously

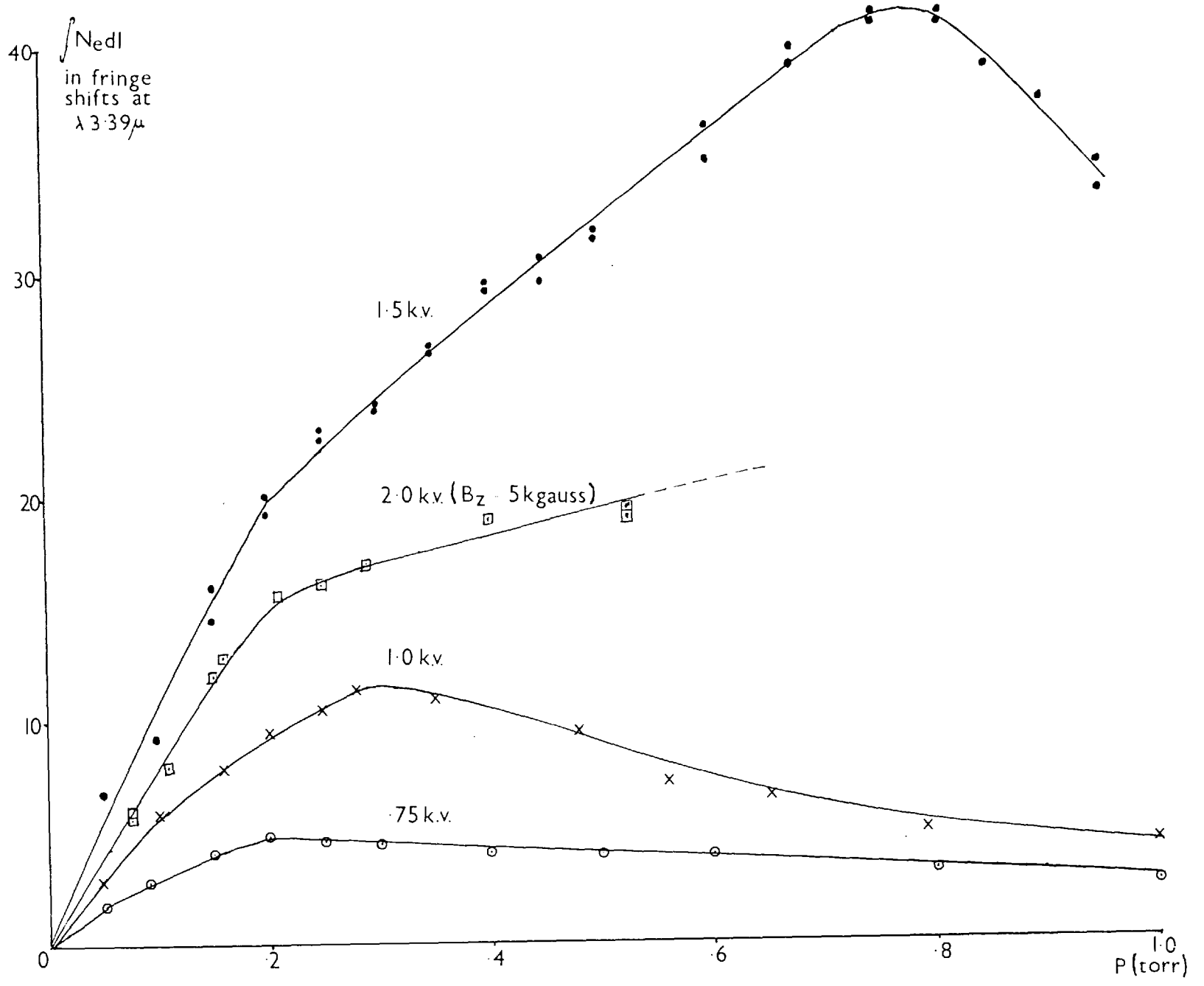


Fig 1. $\int N_e dl$ through tube centre versus pressure. (measurements at 'pinch')

by Burgess [ref.11], Zwicker and Shumacher [ref.103] and Burgess et al [ref.104] on pinches with widely differing parameters.

Peaking was also observed here with an applied B_z field, measuring the axial N_e directly by end on observation [see fig.1]. However refraction of the laser beam out of the plasma prohibited a quantitative determination of P_m.

Further phenomena, which have not previously been reported, can be noted from these results. Firstly, there is an appreciable change in slope of the $\int N_e\,dl$ versus P curves at some pressure $P_c < P_m$. Again this was also observed with an applied B_z [fig.1]. Secondly, both P_c and P_m have a pronounced voltage dependance. Thirdly, the peaking of $\int N_e\,dl$ is accompanied by increasing development of a 'knee' in the $\int N_e\,dl$ versus time curves as P is raised. The time history of $\int N_e\,dl$ at different pressures and two voltages is shown in fig.2.

In an attempt to ascertain the causes of these phenomena time resolved measurements of $\int N_e\,dl$ were made at different heights across the plasma at one bank voltage (1.5 kv). Results at the 'pinch' are shown in fig.3. Abel inversion of these results gave the variation with P of axial N_e shown in fig.4. This variation was very similar to that shown in fig.1 for the same voltage. Correspondingly we might expect the pressure, P_m, at which $\int N_e\,dl$ maximises to be similar to that at which the axial N_e maximises for all bank voltages.

The complete radial distributions of N_e at different times up to the pinch, and at three pressures encompassing P_m, are shown in fig.5. Since these distributions were not the monotonic functions of r expected of existing theories of pinch dynamics the 'pinch time' or time to maximum compression has hitherto been taken as the time at which $\int N_e\,dl$ (through the tube centre)

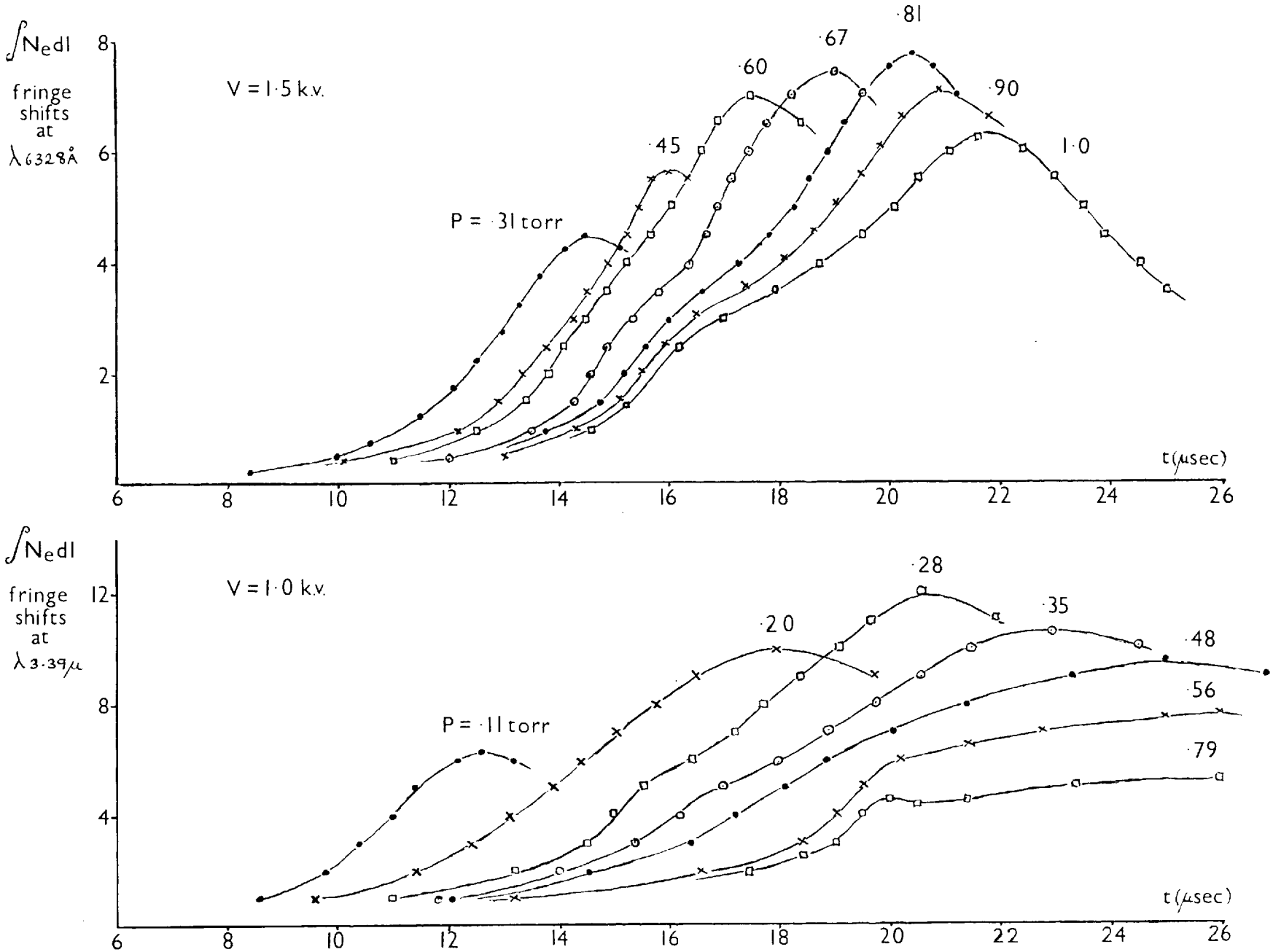


Fig 2. $\int N_e dl$ through tube centre versus time from zero current.

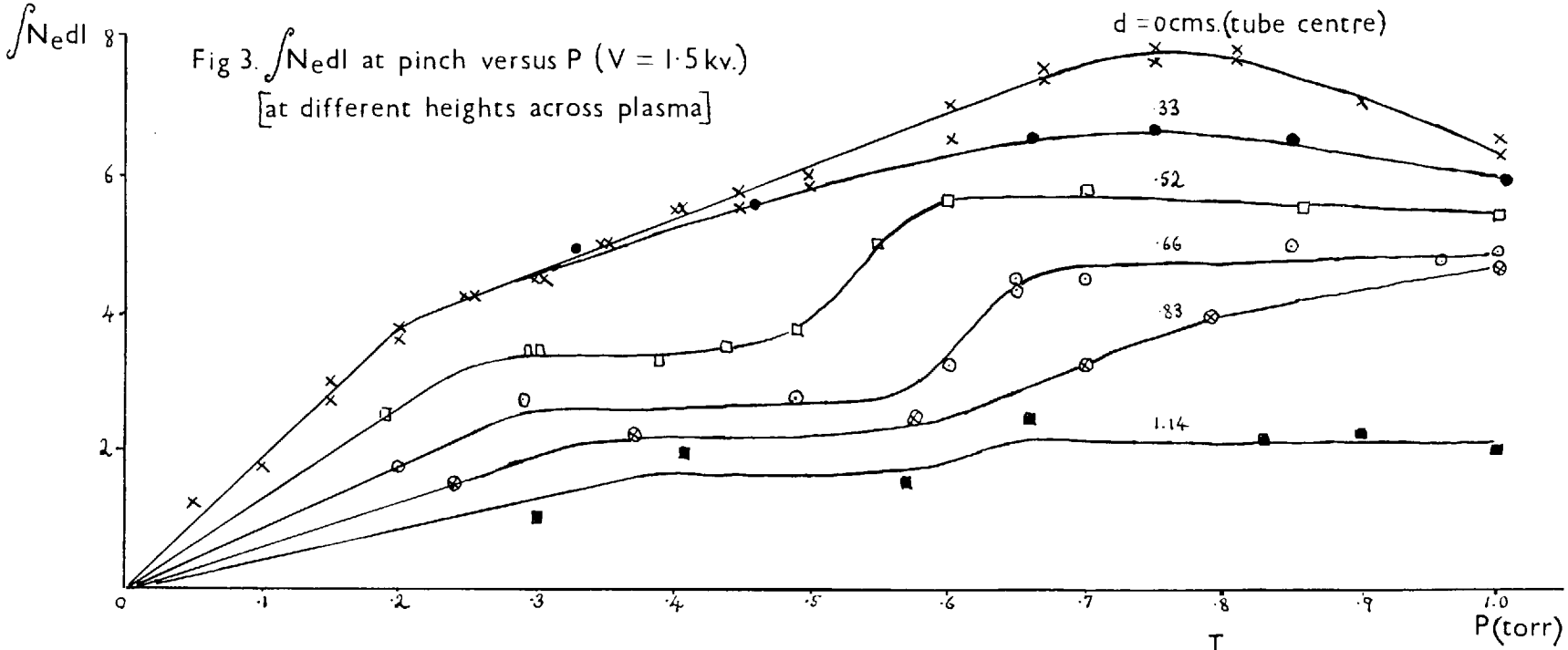


Fig 3. $\int N_e dl$ at pinch versus P (V = 1·5kv.)
[at different heights across plasma]

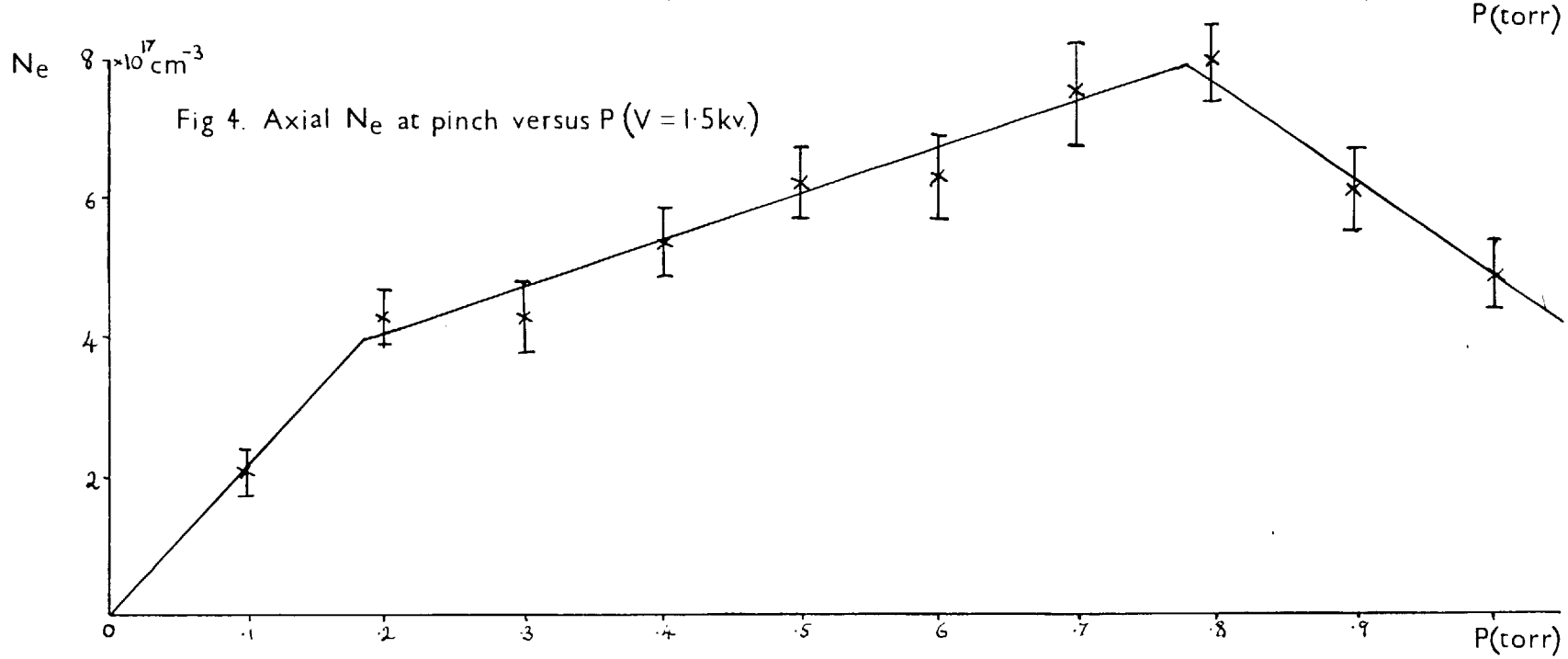


Fig 4. Axial N_e at pinch versus P (V = 1·5kv.)

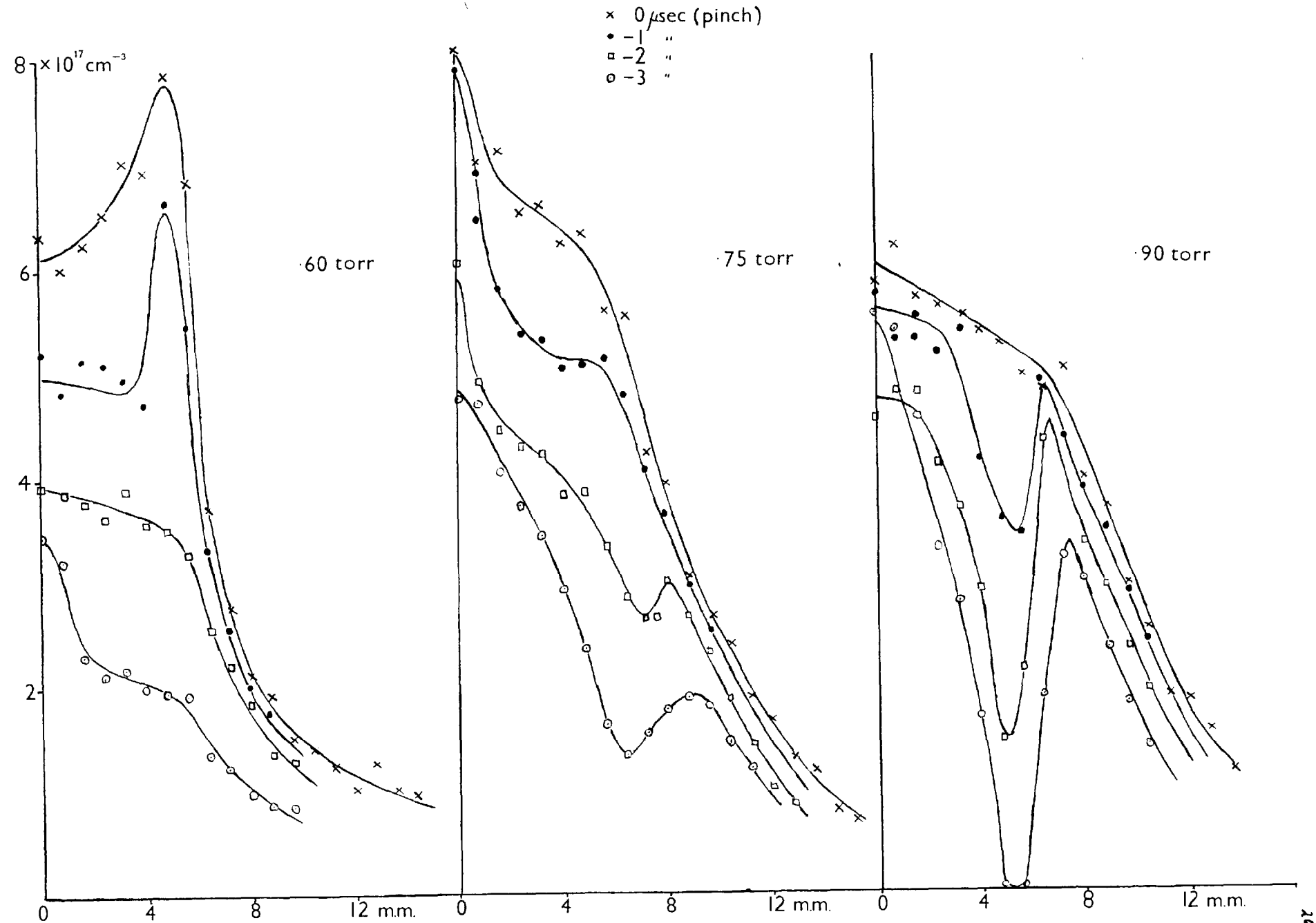


Fig 5. Radial distributions of N_e. (1·5k.v.)

maximises. Generally (see for e.g. fig.5) this appears to be the same as the time at which axial N_e maximises. At each time the radial N_e distributions in fig.5 show a distinct change in character as P is varied through P_m. At lower pressures the distributions at the pinch are similar to that at 0.6 torr though the plasma diameters are smaller and the axial dip in N_e less pronounced.

In attempting to explain the observed phenomena we shall consider, seperately, three pressure regions :-

(1) $\underline{P < P_c}$

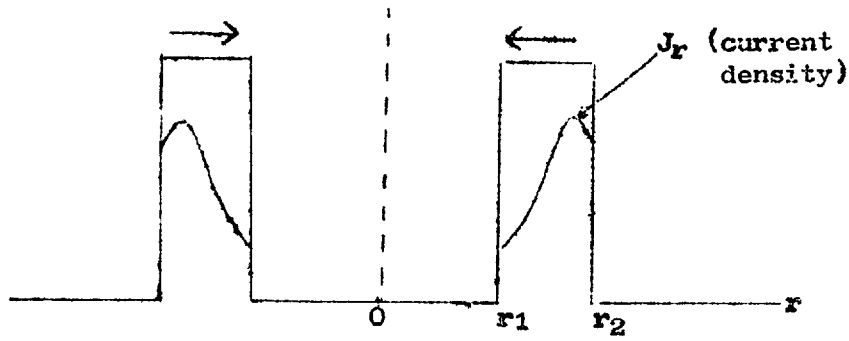
The linear rise of N_e with increasing P in this region is in agreement with a snow-plough model of the pinch [ref.105] assuming complete particle trapping and ionisation and (as observed) comparatively small variations in the plasma radius.

(2) $\underline{P_c < P < P_m}$

As P is increased from P_c we should expect T_e to fall and consequently increasing penetration of current into the collapsing sheath. Haines gives the characteristic penetration time as $t_{pen} \sim \mu \sigma l^2 / 15$ where l is the radius and σ the conductivity of the sheath.

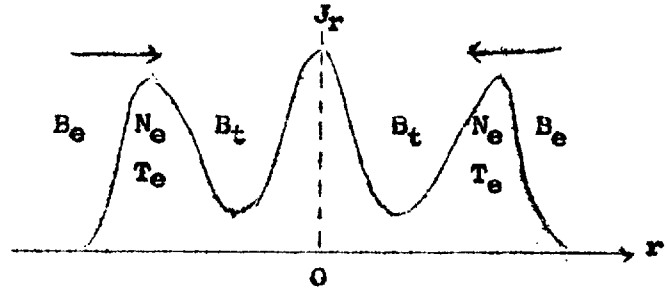
For $P = P_c$, $T_e \sim 30{,}000^{\circ}K$ (from time resolved measurements as in chapter 7) and $l \sim 4$ cms, i.e. $t_{pen} \sim$ 2 μsec. while $t_p \sim 12\mu s$.

Consequently a model of an infinitely thin current carrying layer is no longer applicable. After sufficient time the current density maximum may no longer be at the surface of the sheath. In this case the magnetic driving force on a plasma element (r, dr), $F_r \propto J_r \int_{r_1}^{r} J_r \, 2\pi r \, dr$ (see fig.below), may be a maximum for $r_1 < r < r_2$:-



Collapsing current sheets

Thus the current sheet would become increasingly diffuse and could eventually separate into two regions. The plasma striking the axis first could carry an appreciable part of the current due to its high conductivity leading to a situation :-



The inward pressure on the remaining shell is, assuming high conductivity, $\sim B_e^2/8\pi - B_t^2/8\pi - N_e kT_e$. If the trapped flux is constant $B_t \propto 1/r^2$ whereas $B_e \propto 1/r$. Thus for decreasing r the inward pressure can go to zero leading to an equilibrium situation of a plasma with a hot core surrounded by a cooler, denser layer, the kinetic pressure being uniform over the whole plasma.

(3) $\underline{p \gtrsim p_m}$

As the pressure is increased the conductivity of the plasma should fall and the trapped field B_t be more easily penetrated leading to a rather diffuse plasma at equilibrium. In

addition incomplete particle trapping could be a contributory factor to the observed fall off in N_e. A mechanism by which this could occur is the inverse skin effect, studied theoretically by Haines [ref.106]. Thus if the total discharge current decays after current diffusion into the plasma has occurred, the current density maximum will no longer be at the surface of the plasma as noted in (2) above. Eventually the current may become reversed at the surface. In this case the $\underline{J} \wedge \underline{B}$ force would tend to drive the plasma carrying reverse current away from the axis.

We can obtain an estimate of the time at which this should occur from the expression quoted by Haines for the current density at radius r and time t in a cylindrical conductor of radius a carrying a total axial current $\propto \sin w't$.

If we neglect the transient terms, which decay with a time constant $\tau_{pen} \sim 2\mu s$, the current density is zero at r, t when :-

$$\tan (w\ y) = \left(\frac{ber_o(w^{\frac{1}{2}} x)\, ber_o'w^{\frac{1}{2}} + bei_o(w^{\frac{1}{2}} x)\, bei_o'w^{\frac{1}{2}}}{bei_o(w^{\frac{1}{2}} x)\, ber_o'w^{\frac{1}{2}} - ber_o(w^{\frac{1}{2}} x)\, bei_o'w^{\frac{1}{2}}} \right)$$

where $w = \mu\sigma a^2 w'$, $y = t/\mu\sigma a^2$,

$x = r/a$

The discharge current waveform in the present case is critically damped with a single dip due to inductive effects of the plasma. Up to this dip the current waveform is nearly sinusoidal with,

$$w' \sim 10^5 \text{sec}^{-1}$$

Taking the same value of σ as before,

$$w \sim 3$$

Solving the above relation we get zero current density at r = a

after a time,

$$t \sim 28\mu \text{ sec}$$

The observed time to pinch at P_m was,

$$t_p = 21\mu \text{ sec}$$

A simple model of the inverse skin effect therefore gives reasonable agreement with the observed times. A more quantitative treatment would be computationally rather lengthy as the variation of sheath thickness, radius and conductivity with time would have to be considered. However, we can make one quantitative prediction from this model, i.e. we should expect t_p at P_m to be constant, independent of voltage. This follows because at a given pinch time and therefore collapse time the relevant temperatures and sheath thicknesses should be independent of voltage. In fact t_p for $P = P_m$ was experimentally observed to be independent of voltage [fig.2].

The voltage dependance of P_m, if the snowplough model of the pinch were valid up to this pressure, could be derived from:-

$$t_p^{\text{snowplough}} \propto (P/V^2)^{\frac{1}{4}} = \text{const for } P = P_m$$

i.e. $P_m \propto V^2$

Similarly we should expect,

$$P_c \propto V^2$$

The experimental observations are in good agreement with these relations as seen in fig.6. This agreement seems surprising in view of the marked divergencies from the Snowplough theory for $P > P_c$. Nevertheless both the pressure and voltage dependence of t_p are the same as given on this model as seen in figs. 7 and 8.

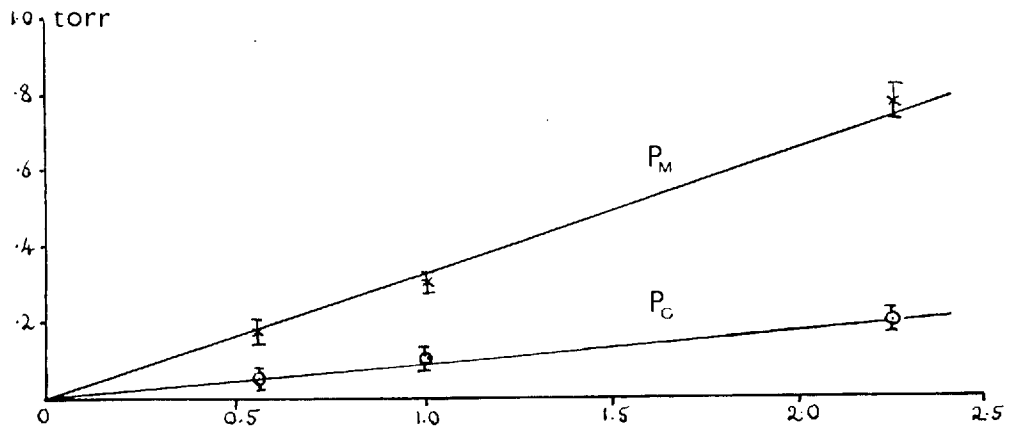


Fig 6. P_M and P_C versus V^2.

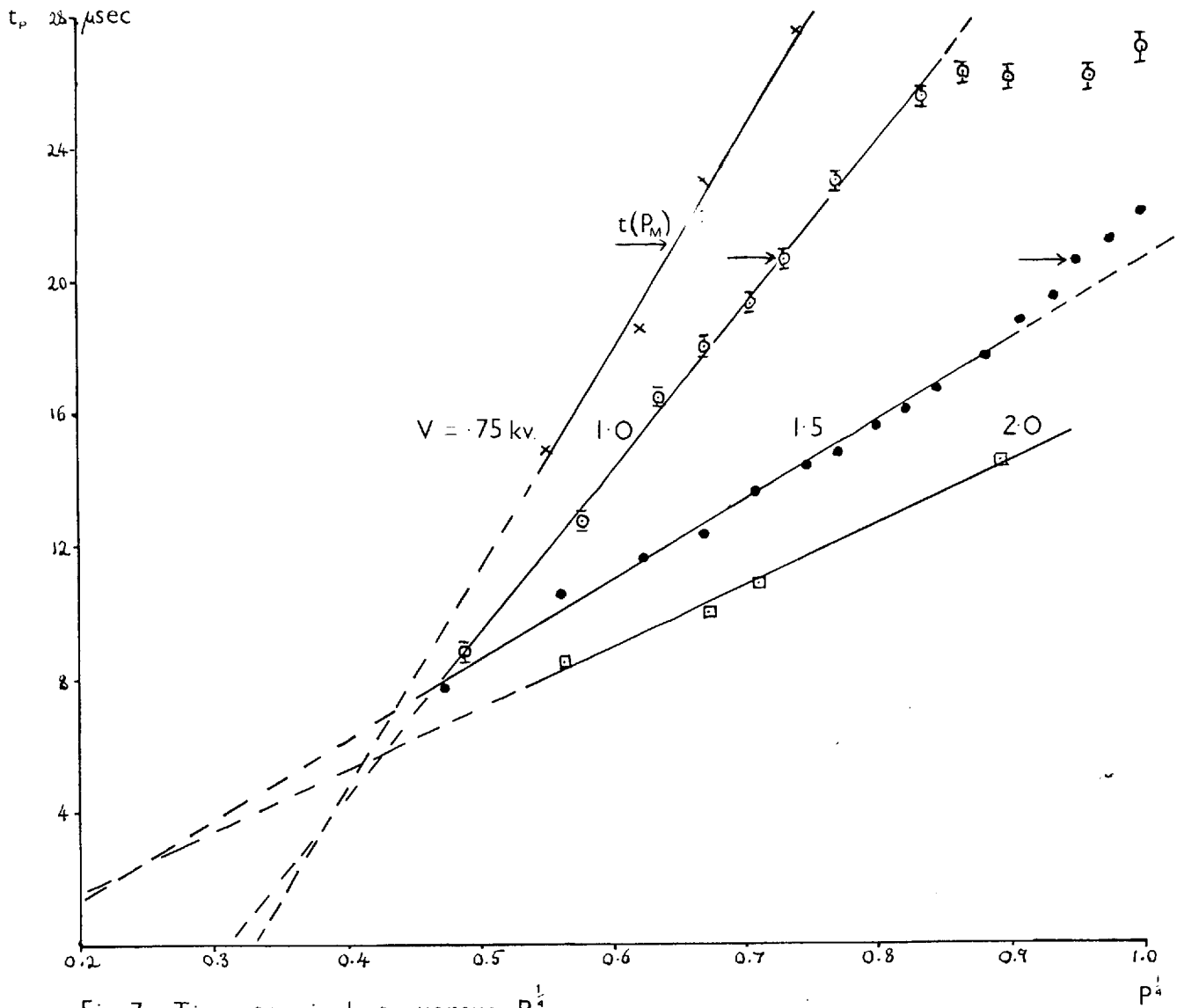


Fig 7. Time to pinch, t_p, versus $P^{\frac{1}{4}}$.

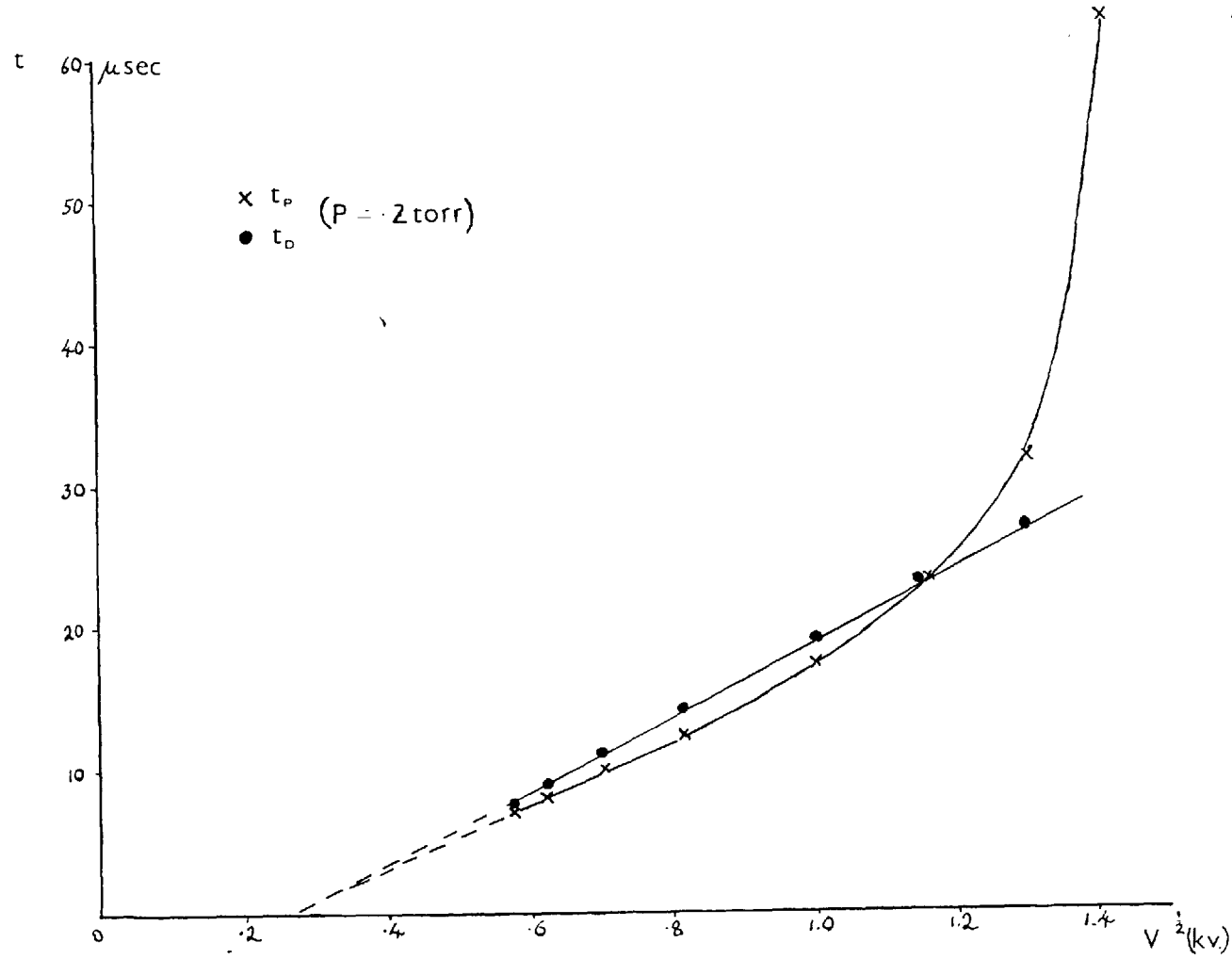


Fig 8. t_P and t_D versus $V^{\frac{1}{2}}$

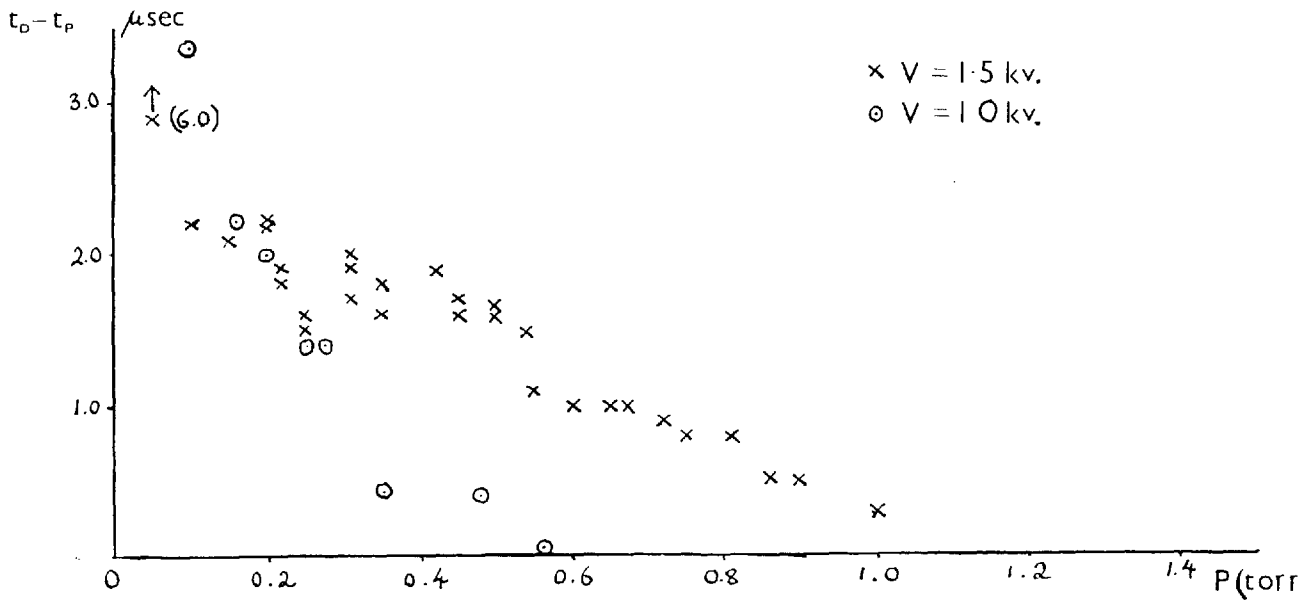


Fig 9. Time to current dip — time to pinch, versus P.

The $t_p \propto P^{\frac{1}{4}}$ curves intersect the origin at a positive pressure which decreases with voltage from $P \sim .01$ torr at 0.75 kv. This is presumably due to poor trapping at very low pressures. Divergences from linearity also occur at high pressures ($> P_m$). For example at 1.0 kv the pinch time appears to become independent of pressure. However in these cases the plasma practically fills the whole tube even at peak compression so the concept of a pinch is not well defined. Again the t_p versus $V^{-\frac{1}{2}}$ curve diverges appreciably from linearity at low voltages, but at 0.5 kv the plasma again practically fills the tube and also $\int N_e \, dl$ (through the tube centre) and the total discharge current are constant to $\sim 10\%$ for 50 μsec so again there is no pronounced 'pinch'.

It should be noted that t_p does not correspond to the time, t_D, of the dip in the current waveform but approaches this as either P or V is increased [fig. 8 and 9]. The t_D-t_p curve appears to show changes at P_c and P_m but these are more or less within experimental error.

The voltage dependence of axial N_e at t_p follows the trend we would expect from the previous results. N_e versus V^2 for $P = 0.2$ torr is shown in fig.10. The relationship is closely linear at high voltages as predicted by a snowplough model of the pinch. However when V is less than that value for which $P_c = 0.2$ torr the axial N_e becomes increasingly less than the value expected on this model, the discrepancy being most appreciable when $V = V(P_m = 0.2 \text{ torr})$.

The importance of the inverse skin effect in inhibiting pinching at high pressures is supported by current density measurements of Frayne [ref.107]. At high P the current sheath becomes increasingly diffuse and appreciable current flows on

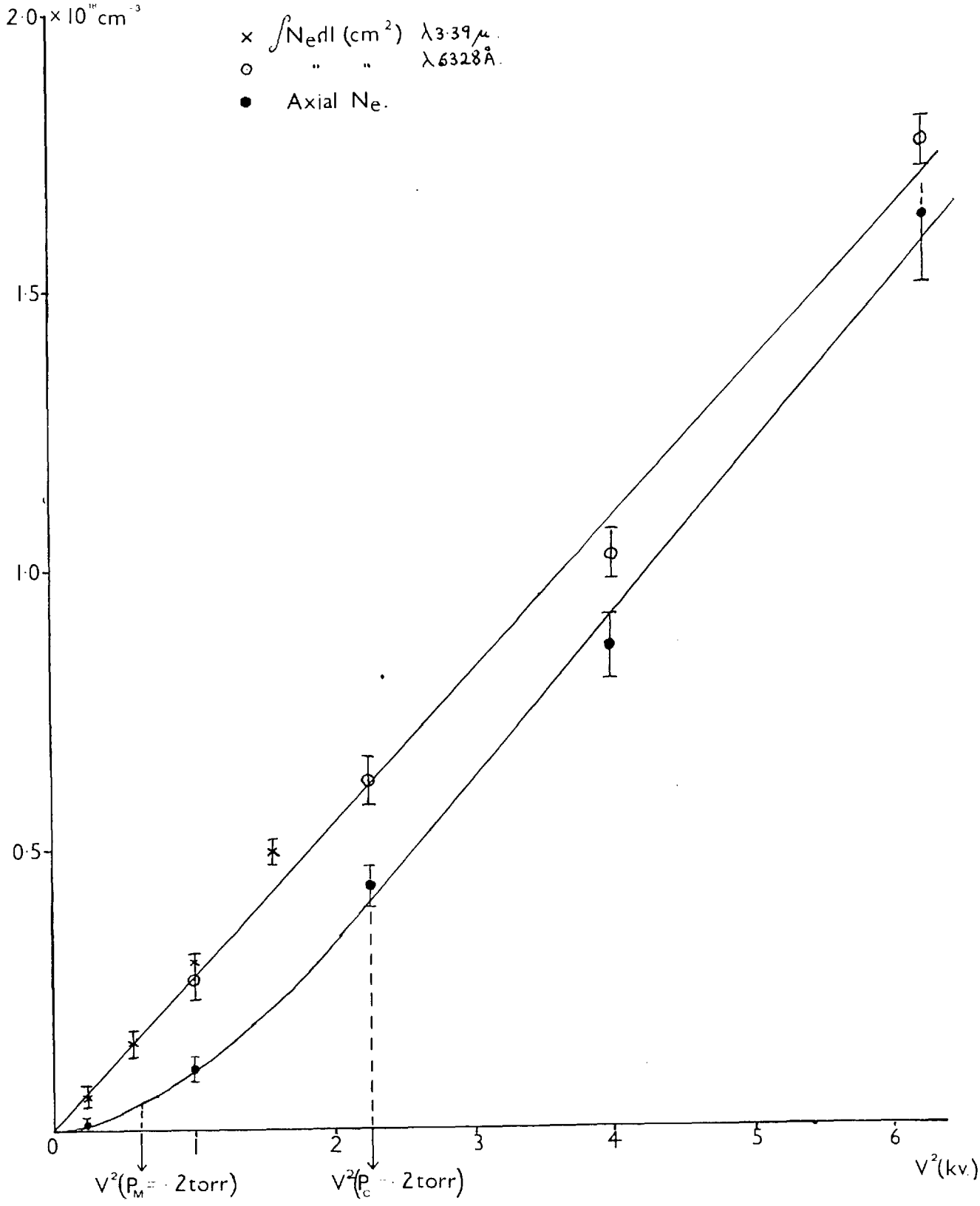


Fig 10. Axial N_e and $\int N_e dl$ at pinch versus V^2.

the axis before peak compression. Eventually the current flows mainly in two regions similar to the N_e regions in fig.5, i.e. axially and in a coaxial sheath. (It is the axial region of N_e which gives rise to the pronounced knee in the curves of fig.2.) The coaxial sheath is prevented from reaching the axis and later expands as a hollow shell (see ref.107) as we would expect for the model for $P_c < P < P_m$. In addition appreciable reverse current was detected at the outer edge of this sheath well before peak compression.

A similar situation was found by Zwicker and Shumacker. However their explanation of the peaking, that at P_m the time to pinch becomes greater than the time to peak (total) current, does not hold in these experiments where t_p is always greater than the time to peak current. Nevertheless it would seem that a model of the inverse skin effect could explain their results.

In Burgess' results [ref.11], on a rather similar discharge to the one used here, P_m appeared to show no voltage dependence. In this case N_e was measured from the width of a Stark broadened AII line. The substantial inhomogeneity of the plasma at high pressure would tend to give a lower line width than that corresponding to the axial N_e (c.f. Chapter 8) and P_m would appear shifted to lower pressures. It seems likely, in this case, that a V^2 dependence, as found in these results, could be accounted for within the limits of experimental error.

Burgess et al [ref.104] made measurements of P_m using different filling gases. They found P_m = .02, .28, .28 torr respectively in argon, helium and hydrogen. On the above results we should expect t_p to be a constant for a given $\rho \propto P_m$ and therefore $P_m \propto 1/M$. This is in rough agreement with

experiment since for these gases 1/M is in the ratio 1:10:20.

The results of spectroscopic importance can now be summarised. Assuming $P < P_c$ or P_m the radial distribution of N_e at the pinch is reasonably rectangular. Furthermore, at least for this discharge, the time to pinch and peak N_e can be accurately predicted, as a function of P or V, from simple relations once normalisation to one or two conditions has been made. Again P_m can be predicted roughly after it has been found for one condition. The quantitative measurements of N_e recorded here cover a range from $10^{16}cm^{-3}$ to $1.7 \times 10^{18}cm^{-3}$ The only other source widely used for similar studies, the electromagnetic T-tube cannot produce plasma with $N_e \gtrsim 5 \times 10^{17}cm^{-3}$ and neither can T_e be varied over as wide a range as with the Z-pinch.

REFERENCES

1. J. Cooper and J.R. Grieg (1963), J.S.I., 40, 433
2. H.R.Griem (1964). Chapter 4 'Plasma Spectroscopy' McGraw-Hill Book Co., New York
3. J.Cooper (1966). 'A review of plasma spectroscopy' Reports of progress in Physics. Vol.1
4. P.W.Anderson (1949). Phys.Rev., 76, 647
5. C.W.Allen (1963). 'Astrophysical Quantities' Athlone Press, London
6. W.L.Wiese (1966), Chapter 6 'Plasma Diagnostic Techniques' Academic Press, London
7. H.R.Griem, A.C.Kolb and K.Y.Shen (1962). Astrophys.J., 135, No.1, 272
8. A.C.Kolb and H.R.Griem (1958). Phys.Rev., 111, 514
9. M.Baranger (1958). Phys.Rev., 111, 494 and 112, 855
10. H.R.Griem, M.Baranger, A.C.Kolb and G.Oertel (1962). Phys.Rev., 125, 177
11. D.D.Burgess (1965). Ph.D.Thesis, University of London
12. H.Statz, F.A.Horrigan, S.H.Koozekanani, C.L.Tang and G.F.Koster (1965). J.A.P., 36, No.7, 2278
13. H.F.Berg, A.W.Ali, R.Linke, H.R.Griem (1962). Phys.Rev., 125, 199
14. W.E.Gericke (1961). Z.Astrophys., 53, 68
15. H.R.Griem (1962). Phys.Rev., 128, No.2, 515
16. P.M.Stone and L.Agnew (1962). Phys.Rev., 127, 1157
17. W.L.Wiese and P.W.Murphy (1963). Phys.Rev., 129, 1225
18. M.Jung (1963). Z.Astrophys., 58, 93
19. A.Stampa (1963). Z.Astrophys., 58, 82
20. R.Chabbal (1957). A.E.R.E. Library translation No.778

21. J.R.Grieg (1965). Ph.D. Thesis, University of London

22. S.Tolansky (1948). 'Multiple beam interferometry' Pergammon Press.

23. E.M.Cherry and D.E.Hooper (1963). Proc.I.E.E., 110, No.2,375

24. F.L.Curzon (1959). Ph.D.Thesis, University of London

25. D.D.Burgess and J.Cooper (1965). J.Sc.I., 42, 829

26. R.M.Measures (1964). Ph.D.Thesis, University of London

27. D.D.Burgess and J.Cooper (1965). Proc.Phys.Soc., 85, 85

28. E.U.Condon and G.H.Shortley (1951). 'The Theory of Atomic Spectra' Cambridge University Press

29. B.D.Adcock and W.E.G.Plumtree (1964). J.Q.S.R.T., 4, 29

30. L.Holland (1963). 'Vacuum Deposition of thin Films' Chapman and Hall Ltd., London

31. D.R.Bates and A.Damgaard (1949). Phil.Trans.Roy.Soc., A.242, 101

32. A.E.Dangor and C.B.Wheeler (1966). Plasma Physics Dept., Imperial College (Internal Report)

33. R.A.Alpher and D.R.White (1959). Phys.Fluids, 2, No.2, 162

34. L.Minnhagen (1963). Arkiv.För Fysik, 25, 203

35. C.E.Moore (1945). 'A Multiplet Table of Astrophysical Interest' (pt.2) Princeton, New Jersey

36. W.J.Pearce (1961). 'Optical Spectrometric Measurements of High Temperatures' (p.125) University of Chicago Press

37. M.H.Key (1966). Ph.D. Thesis, University of London

38. W.B.Bridges and A.N.Chester (1964). Nerem Record p.106

39. J.Troughton, Ph.D.Thesis, to be published

40. A.G.Hearn (1963). Proc.Phys.Soc., 81, 648

41. G.J.Pert (1966). Ph.D.Thesis, University of London

42. D.D.Burgess (1965). 'Tables of Argon Plasma Composition' Internal Report, Imperial College

43. C.B.Wheeler (1963). Proc.6th Int.Conf.Ion.Phen.in Gases (Paris) Vol.1, 247

44. D.D.Burgess and J.Cooper (1965). Proc.Phys.Soc., 86, 1333

45. W.B.Brooks and G.E.Reis (1963). Aero Thermodynamics, SC-4938(RR)

46. Chapter 2 of Reference 2

47. C.E.Moore (1950). 'An ultra violet multiplet table' N.B.S.circular 488, Section 1

48. Chapter 14 of Reference 2.

49. D.E.T.F. Ashby and D.F.Jephcott (1963). Appl.Phys.Lett., 3, 13

50. Chapter 13 of Reference 2.

51. H.R.Griem (1962). Phys.Rev., 128, No.3, 997

52. R.Wilson (1962). J.Q.S.R.T., 2, 477

53. L.Spitzer (1956). 'Physics of Fully Ionised Gases' Interscience, New York

54. R.P.W. McWhirter (1966). Chapter 5 of Reference 6

55. Proceedings of Workshop Conference on the Lowering of the Ionisation Potential and Related Problems of the Equilibrium Plasma (1965). Ed.by J. Cooper JILA Report No.79, Colorado

56. H.W.Drawin and P.Felenbock (1965). 'Data for Plasmas in L.T.E.' Gauthier-Villars, Paris

57. M.J.Seaton (1962). in 'Atomic and Molecular Processes' Academic Press, New York

58. H.N.Olsen (1963). J.Q.S.R.T., 3, 305

59. H.W.Drawin (1956). Z.Phys., 146, 295

60. H.N.Olsen (1961). Phys.Rev., 124, 1703

61. H.N.Olsen (1965), J.Q.S.R.T.

62. J.Bakos, J.Szigeti and L.Varga (1966). Phys.Lett., 20, No.5, 503

63. P.D.Johnson (1966). Phys.Lett., 20, No.5, 499

64. B.M.Dymshits and Y.P.Koretskii (1965). Sov.Phys.Tech.Phys. 9, No.9

65. T.B.Reed (1961). J.A.P., 32, No.5, 821

66. O.H.Nestor and H.N.Olsen (1960). Siam.Rev., 2, 200

67. P.B.Coates and A.G.Gaydon (1965). Proc.Roy.Soc., A283, 18

68. P.B.Coates and A.G.Gaydon(1966). Proc.Roy.Soc., A, 293, 452

69. S.S.Penner (1959). 'Quantitative Molecular spectroscopy and Gas Emissivities' Reading (U.S.A.), Addison-Wesley

70. W.F. Koehler (1955). J.O.S.A., 45, 1011

71. R.A.Day and H.R.Griem (1965). Phys.Rev., 140, No.4A, A1129

72. H.R.Griem (1965). Paper 4.5.2.(3) 7th Int.Conf.on Ion. Phen.in Gases. Belgrade, Yugoslavia

73. M.G.Haines (1965). Adv.in Phys., 14, No.54, 167

74. N.Rostoker and A.C.Kolb (1961). Phys.Rev., 124, 965

75. H.R.Griem, A.C.Kolb, W.H.Lupton and D.T.Philips (1962). Nuc.Fus., Suppl.II, 543

76. H.A.B.Bodin and A.A.Newton (1963), Phys.Fluids, 6, 1338

77. C.Breton, M.Carpet and F.Waelbroeck (1961). Proc.5th Int.Conf.on Ion.Phen.in Gases (Munich) Vol.II, 1913 (North Holland, Amsterdam)

78. K.L.Vander Sluis and J.R.McNally, Jr. (1956). J.O.S.A., 46, No.1, 39

79. M.J.Forrest (1966). Culham Laboratory preprint, CLM-P116

80. H.A.B.Bodin, T.S.Green, G.B.F.Niblett, N.J.Peacock, J.M.P.Quinn and J.A.Reynolds (1962). Nuclear Fusion, Suppl.2, 521

81. K.M.Baird (1959). N.P.L.Symposium 11, Paper 2.2, 51 H.M.S.O., London

82. T.S.Green (1962). Nucl.Fusion, 2, 92

83. J.A.Reynolds, E.E.Aldridge, M.Keilhacker and G.B.F.Niblett (1964). U.K.A.E.A. Culham report, CLM-P46

84. H.A.B.Bodin, T.S.Green, G.B.F.Niblett, N.J.Peacock, J.M.P.Quinn, J.A.Reynolds and J.B.Taylor (1962). Nucl.Fusion, Suppl.2, 511

85. J.Cooper, H.Herold, M.Keilhacker and D.E.Roberts (1966). Paper CN21/54

86. P.Jaquinot (1954). J.O.S.A., 44, 761

87. H.A.B.Bodin, T.S.Green, A.A.Newton, G.B.F.Niblett and J.A.Reynolds (1965). Conference proceedings, Culham Vol.I, 193. Int.Atomic Energy Agency, Vienna 1966

88. W.H.Bostick and D.R.Wells (1963). Phys.Fluids, 6, 1325

89. E.P.Velikhov (1964). J.N.E.C., 6, 203

90. P.C.Thonemann and A.C.Kolb (1964). Phys.Fluids, 7, 1455

91. C.E.Moore (1958). N.B.S. Circular 467, Vol.1 U.S.Dept. of Commerce

92. M.Baranger (1962). Chapter 13 of Reference 57

93. E.U.Condon and G.H.Shortley (1935). Theory of Atomic Spectra (C.U.P.)

94. B.W.Shore and D.H.Menzel (1965). Astrophys.J.Suppl. Series.Vol.XII, No.106, 187

95. R.A.Day (1965). Ph.D. thesis, University of Maryland

96. H.R.Griem and C.S.Shen (1962). Phys.Rev., 125, No.1, 196

97. L.A.Vainshtein and I.I.Sobel'man (1959). Opt.Spectr. (U.S.S.R.), 6, 440

98. M.A.Hazing (1959). Dissertation, Lebedev Institute of Physics, Academy of Sciences, U.S.S.R.

99. N.W.Jalufka, G.K.Oertel and G.S.Ofelt (1966). Phys.Rev.Lett., 16, 1073

100. H.R.Griem (1966). Phys.Rev.Lett.

101. M.Yamamoto (1966). Phys.Rev., 146, 137

102. J.Davis (1967). Proc.Phys.Soc., 90, 283

103. H.Zwicker and V.Schumacher (1965). Z.fur Physik, 183, 453

104. D.D.Burgess, A.E.Dangor and J.E.Jenkins (1966). Imperial College Internal Report (to be published)

105. O.A.Anderson, W.R.Baker, S.R.Colgate, J.Ise, Jr. and R.V.Pyle (1958). Phys.Rev., 110, 1375

106. M.G.Haines (1960). Ph.D. Thesis, University of London

107. P.G.Frayne (1963). Ph.D.Thesis, University of London

108. H. R. Griem and K. Y. Shen (1961). Phys.Rev., 122, No.5 1490

109. H. R. Griem, A.C.Kolb and K.Y.Shen (1959). Phys.Rev., 116, 4

110. D. E. Roberts (1966). Phys.Lett., 22, No.4, 417

PUBLICATIONS

"Doppler Shift Measurements to Investigate Plasma Rotation in the Theta Pinch". (1966)

"Plasma Physics and Controlled Nuclear Fusion Research" Vol.I, I.A.E.A., Vienna.

[Co-authored with J. Cooper, H. Herold and M. Kielhacker.]

"The Stark Widths of Singly Ionised Argon Lines Emitted by a Plasma" (1966) Phys. Lett. 22, No.4, 417

Reprint from

"PLASMA PHYSICS AND
CONTROLLED NUCLEAR FUSION RESEARCH"

Vol.I

INTERNATIONAL ATOMIC ENERGY AGENCY
VIENNA, 1966

DOPPLER SHIFT MEASUREMENTS TO INVESTIGATE PLASMA ROTATION IN THE THETA PINCH

M. KEILHACKER AND H. HEROLD
INSTITUT FÜR PLASMAPHYSIK,
MUNICH-GARCHING, FEDERAL REPUBLIC OF GERMANY
AND
J. COOPER AND D.E. ROBERTS
IMPERIAL COLLEGE OF SCIENCE AND TECHNOLOGY, LONDON, ENGLAND

Abstract — Résumé — Аннотация — Resumen

DOPPLER SHIFT MEASUREMENTS TO INVESTIGATE PLASMA ROTATION IN THE THETA PINCH. Whereas so far experimental investigation of plasma rotation in the theta pinch has been based on the photographic observation of instabilities associated with this rotation, this paper describes experiments to determine the mass rotational velocity and the related angular momentum from the Doppler shift of impurity lines.

As these shifts can be small compared with the line widths, a Fabry-Perot interferometer was used in the first experiments (carried out at Culham Laboratory on 22.5-kJ theta pinch). A suitable line (C II, 4267 Å) was selected by a 10-Å interference filter and the line profile recorded photoelectrically via an eight-channel fibre bundle array which was crossed with one of the Haidinger fringes produced by the Fabry-Perot. The Doppler shifts measured at different positions across the plasma diameter showed the plasma to rotate as a rigid body. The first detectable shift of the C II line, corresponding to an angular velocity of 5×10^4 rev/s, was measured during the first implosion of the plasma.

As the C II line was burned out after one microsecond the Doppler shifts of the C V 2271 Å line were measured in a second experiment carried out at Garching on a 32.5-kJ theta pinch. The profiles were recorded using a high resolution monochromator and a profile-dividing mirror system. In this experiment rotation was only observed at pressures below 30 mTorr D_2 and was then again in the direction of the ion current. It was possible to induce rotation and instabilities at higher pressures in an otherwise stable plasma by superimposing a stationary transverse magnetic field. In this case rotation seems to start in the direction of the electron current but the instabilities showing up later still rotate in the ion current direction. On the other hand the tendency of the plasma to rotate (at pressures of D_2 below 30 mTorr) can be reduced and rotational instabilities suppressed by superimposing a transverse field of the same polarity that causes "opposite" rotation for a usually non-rotating plasma. The results are discussed in the light of existing theories on the origin of rotation and on instabilities.

MESURES DU DEPLACEMENT DU A L'EFFET DOPPLER APPLIQUEES A L'ETUDE DE LA ROTATION DU PLASMA DANS LA STRICTION AZIMUTALE. Alors que l'étude expérimentale de la rotation du plasma dans la striction azimutale reposait jusqu'à présent sur l'observation photographique des instabilités associées à cette rotation, le mémoire décrit des expériences visant à déterminer, à partir du déplacement des raies des impuretés dû à l'effet Doppler, la vitesse de rotation des masses et le moment cinétique correspondant.

Etant donné que ces déplacements peuvent être faibles par rapport aux largeurs des raies, les auteurs ont utilisé un interféromètre Fabry-Pérot pour les premières expériences, effectuées au Laboratoire de Culham sur une striction azimutale de 22,5 kJ. Ils ont isolé, au moyen d'un filtre d'interférences de 10 Å, une raie adéquate (C II, 4267 Å) et ont enregistré photoélectriquement le profil de cette raie au moyen d'un dispositif en faisceau à huit canaux traversé par l'une des franges de Haidinger produites par l'interféromètre de Fabry-Pérot. D'après des mesures des déplacements dus à l'effet Doppler effectuées en différents points du diamètre du plasma, ils ont constaté que la rotation du plasma est semblable à celle d'un corps rigide. Le premier déplacement de la raie C II qu'il a été possible de détecter, déplacement qui correspondait à une vitesse angulaire de 5.10^4 tours/s, a été mesuré pendant la première implosion du plasma.

Etant donné que la raie C II a disparu en 1 μs, les auteurs ont mesuré les déplacements Doppler de la raie C V de 2271 Å dans une deuxième expérience effectuée à Garching avec un appareil à striction azimutale de 32,5 kJ. Ils ont enregistré les profils au moyen d'un monochromateur à fort pouvoir de résolution et d'un système de miroirs qui sépare les profils. Dans cette expérience, une rotation n'a été observée qu'à des pres-

sions inférieures à 30 m Torr de deutérium et l'a été également dans la direction du courant d'ions. Il a été possible de provoquer une rotation et des instabilités à des pressions plus élevées dans un plasma normalement stable, en superposant transversalement un champ magnétique stationnaire. Dans ce cas, la rotation semble démarrer dans la direction du courant des électrons, mais les instabilités qui se manifestent ultérieurement tournent encore dans la direction du courant des ions. Par ailleurs, on peut diminuer la tendance du plasma à subir une rotation (aux pressions inférieures à 30 m Torr de deutérium) et on peut supprimer les instabilités rotationnelles en superposant transversalement un champ ayant la même polarité que celui qui entraîne une rotation «opposée» pour un plasma normalement non tournant. Les auteurs discutent les résultats obtenus, en fonction des théories actuelles sur l'origine de la rotation et sur les instabilités.

ИЗМЕРЕНИЯ ДОППЛЕРОВСКОГО СМЕЩЕНИЯ ДЛЯ ИССЛЕДОВАНИЯ ВРАЩЕНИЯ ПЛАЗМЫ В ТЕТА-ПИНЧЕ. До сих пор экспериментальные исследования вращения плазмы в тета-пинче основывались на фотографическом наблюдении неустойчивостей, связанных с этим вращением. В настоящем докладе описываются эксперименты по определению массовой скорости вращения и связанного с ней момента количества движения на основании допплеровского смещения линий примесей.

Поскольку эти смещения могут быть невелики по сравнению с шириной линий, в первых экспернментах, проведенных в Калэмской лаборатории на тета-пинче с энергией в 22,5 кдж использовался нитерферометр Фабри-Перо. Фильтром в 10 Å была выбрана подходящая линия (C II 4267 Å) и профиль линии зарегистрирован фотоэлектрнческим способом с помощью восьмиканальной разделительной системы, которая пересекалась одной из полос Хайдингера с интерферометра Фабрн-Перо. Допплеровские смещения, измеренные в различных положениях по диаметру плазмы, показали, что плазма вращается как твердое тело. Первое обнаруженное смещение линии C II, соответствующей угловой скорости 5×10^4 обор /сек, было измерено в течение первого сжатия плазмы.

Поскольку линия C II перегорала через одну микросекунду, допплеровское смещение линии C V 2271 Å было измерено во втором эксперименте, проведенном в Гархинге на тета-пинче с энергией 32.5 кдж. Профили регистрировались с помощью монохроматора с высокой разрешающей способностью и зеркальной системы, делящей профнль. В данном эксперименте вращение наблюдалось лишь при давлении ниже 30 мтор D_2 и затем вновь в направлении потока ионов. Оказалось возможным вызвать вращение и неустойчивости при более высокнх давлениях в плазме, устойчивой в других отношениях, с помощью наложения постоянного поперечного магнитного поля. В этом случае представляется, что вращение начинается в направлении потока электронов, однако неустойчивости, появляющиеся позднее, все равно вращаются в направлении потока ионов. С другой стороны, тенденция плазмы вращаться (при давлениях ниже 30 мтор D_2) может быть уменьшена и неустойчивости вращения устранены путем наложения поперечного поля той же полярности, которая вызывает "обратное" вращение для обычной не вращающейся плазмы. Результаты рассматриваются в свете существующих теорий происхождения вращения и неустойчивостей.

ESTUDIO DE LA ROTACION DEL PLASMA EN LA CONSTRICCION AZIMUTAL POR MEDICION DEL DESPLAZAMIENTO DOPPLER. Hasta la fecha, el estudio experimental de la rotación del plasma en la constricción azimutal se ha basado en la observación fotográfica de las inestabilidades vinculadas a dicha rotación; la presente memoria describe, en cambio, experimentos destinados a determinar la velocidad de rotación de las masas y el momento angular correspondiente, sobre la base del desplazamiento de las líneas de las impurezas, debido al efecto Doppler.

Como estos desplazamientos pueden se pequeños comparados con el ancho de las líneas correspondientes los autores utilizaron un interferómetro de Fabry-Pérot en los primeros experimentos, realizados en el Laboratorio de Culham con una constricción azimutal de 22,5 kJ. Aislaron una línea adecuada (C II, 4267 Å) mediante un filtro de interferencias de 10 Å y registraron fotoeléctricamente el perfil de la línea con ayuda de un dispositivo de haz de ocho canales, atravesado por una fase de las franjas de Haidinger producidas por el interferómetro de Fabry-Pérot. Los desplazamientos debidos al efecto Doppler, medidos en distintos puntos situados sobre el diámetro del plasma pusieron de manifiesto que éste gira como un cuerpo rígido. El primer desplazamiento observable de la línea C II, que corresponde a una velocidad angular de 5×10^4 rev/s, se midió durante la primera implosión del plasma.

Como la línea C II desapareció al cabo de 1 μs, los desplazamientos de Doppler de la línea C V 2271 Å se midieron en un segundo experimento efectuado en Garching con una constricción azimutal de 32,5 kJ. Los perfiles espectrales se registraron mediante un monocromador de elevado poder de resolución y un sistema de espejos separador de perfiles. En este experimento, la rotación se observó solamente a presiones inferiores a 30 m Torr de D_2, y también tuvo lugar en la dirección de la corriente iónica. Superponiendo un campo

magnético transverso estacionario, fue posible inducir la rotación e inestabilidades a presiones más elevadas en un plasma de por sí estable. En este caso, la rotación parece iniciarse en la dirección de la corriente electrónica, pero las inestabilidades que aparecen más tarde giran en la dirección de la corriente iónica. En cambio, puede atenuarse la tendencia del plasma a girar (a presiones de D_2 inferiores a 30 mTorr) y suprimirse las inestabilidades de rotación superponiendo un campo transverso de la misma polaridad que hace girar en sentido opuesto a un plasma habitualmente carente de rotación. Los resultados se examinan a la luz de las teorías actuales sobre el origen de la rotación y sobre las inestabilidades.

A. Introduction

One of the factors that limit the lifetime of the plasma in theta pinch experiments is rotation and subsequent instability of the plasma. So far experimental investigation of this rotation has been confined mainly to measurements of the rotational velocities of these instabilities by high speed photographic techniques [1-6] , i.e. limited to the later stages of rotation.

This paper describes experiments to determine the azimuthal velocity of the plasma by observing the Doppler shift of radiation emanating from impurity ions in such a plasma. Apart from the fact that this method provides a means of measuring rotational velocities with greater precision than is obtained by photographic observation, it enables the rotation to be detected and measured in its early stages before instabilities set in. It is thus possible to compare the time variation of the rotational velocity with the predictions of several theoretical models postulated to explain the origin of rotation [7-12] . In addition it can be checked whether the rotating plasma, before getting unstable, satisfies the stability criteria put forward by these theories.

The first part of this paper describes the measuring systems that have been used to detect the small Doppler shifts. The second summarizes the results on rotation and instability obtained by the Doppler shift measurements, by high speed photography and magnetic probe measurements made over a wide range of experimental conditions. Finally these results are compared with the predictions of existing theories.

B. Diagnostic Technique for Measuring Small Line Shifts

As the expected shifts are only a few tenths of an Angström and the percentage of impurity ions must be kept to a minimum, the measuring system must have high spectral resolution together with maximum light gathering power and high time resolution.

1. Fabry-Perot Interferometer

For lines in the visible part of the spectrum, emitted while the plasma is only moderately hot, a Fabry-Perot interferometer was used (for the theory of the Fabry-Perot interferometer see [13]). Fig. 1 shows the optical system. A suitable, intense impurity line was isolated by a 10 Å bandwidth interference filter to reject unwanted light in other orders and its profile recorded photoelectrically via an eight channel fibre bundle array which was crossed with one of the off-axis Haidinger fringes produced by the 2-inch diameter Fabry-Perot (see top half of Fig. 1). The whole apparatus was mounted on a table which could be shifted vertically to scan across the plasma diameter. The relative sensitivities of the 8 photomultipliers and associated fibre bundle channels were determined by calibration with a carbon arc or with the C II line itself using the set up shown in Fig. 1 (but with the Fabry-Perot removed. The relative calibration could be assumed accurate to ± 4%. The spatial resolution, defined by the height of the fibre bundle array and the magnification of the two lenses was 0.6 mm.

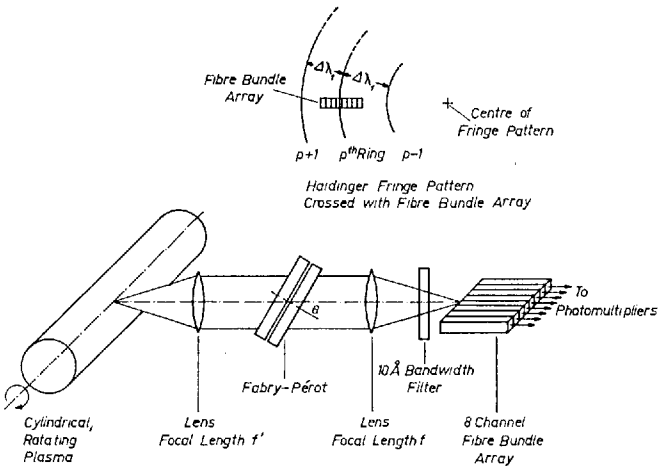


FIG. 1. Experimental arrangement for recording line profiles via an 8 channel fibre bundle array crossed with one of the fringes produced by a Fabry-Perot interferometer.

In order to record a well-defined line profile the free spectral range $\Delta\lambda_f$ of the Fabry-Perot was chosen to be approximately three times the half width of the line to be measured ($\Delta\lambda_f = 2.54 \pm 4\%$ for the C II 4267 line).

In addition, to obtain the maximum dispersion, the lengths of the 8 channel fibre bundle array should correspond to one free spectral range, so that the line profile covers most of the 8 channels. This leads to the following condition (see Fig. 1)

$$s = f\,(\theta_{p+1} - \theta_p) = \frac{f\lambda}{2\,d\,\theta_p} \quad \text{(for small } \theta_p\text{)}$$

where d is the separation of the Fabry-Perot plates. Since s is proportional to the focal length f of the focussing lens this condition can be satisfied for any ring p of the pattern by means of varying f and rotating the Fabry-Perot about a vertical axis until this ring is focussed on the centre channel of the fibre bundle.

The Fabry-Perot plates were coated with Ag. The reflection finesse at the wavelength used was $12.5 \pm 12\%$ and the etalon transmission 53%. The plates were flat to $\lambda/40$ at this wavelength giving an associated finesse of approximately 20. Thus the overall finesse was > 8. It was not important in this experiment to have a finesse of much greater than 8 since we were limited by the fibre bundle channels to 8 resolution elements. It is worth pointing out that the instrument width limits the accuracy of line profile measurements but is less important for the measurement of line shifts.

2. Monochromator with Profile-Dividing Mirror System

During the later stages of theta pinch discharges the intense line radiation is due to high stages of ionization and is emitted in the UV part of the spectrum. Since with the Fabry-Perot interferometer observation was confined to the visible range by the use of glass etalons and of glass fibre bundles, a mirror system (developed by M.J. Bernstein [14]) was used together with a high resolution, high optical speed monochromator (f/12, 8.3 Å/mm) for channeling off spectral profiles in the ultraviolet range.

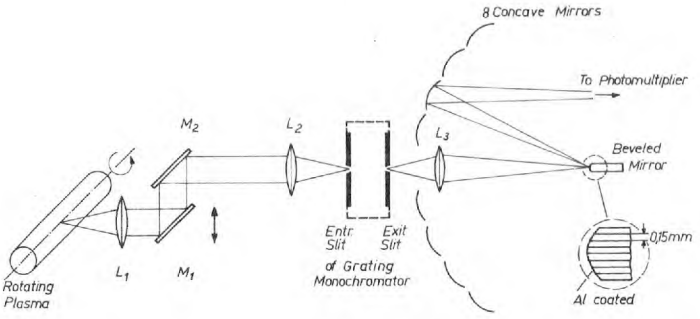


FIG. 2. Experimental arrangement for recording line profiles using a monochromator and a profile-dividing mirror system. L_3 profile-magnifying lens, M_3 profile-dividing mirror.

Fig. 2 shows the optical system. The plasma which is in the focal plane of lens L_1 is imaged on the entrance slit of the monochromator via two mirrors M_1, M_2 and a second lens L_2. By moving L_1 and M_1 vertically, plasma light emitted along different chords can be focussed on the entrance slit, which was normally set to 40 μ. The line profile which appears at the exit slit of the monochromator is magnified by a quartz lens L_3 and imaged on a set of very narrow, beveled mirrors. These profile-dividing mirrors then reflect the various parts of the line profile on to a set of photomultipliers. For a relative calibration of the different channels the line under investigation itself was used by opening the monochromator slits sufficiently to illuminate each channel with the entire line intensity. The spatial resolution was 1.5 mm.

All mirrors were Al-coated. The channel width chosen was about 0.25 Å/photomultiplier. Asymmetric line shifts of about 0.05 Å could be detected with this system. The reliability of the mirror system was checked by recording line profiles emitted by a stationary Hg-Cd lamp.

C. Experimental Results

Fig. 3 shows the time behaviour of the intensities of a C III, C IV and C V line emitted by the plasma in the Garching theta pinch experiment, in which the maximum electron temperature is in the 100 eV range. In order to detect line profiles during the whole half cycle of the discharge radiation from different stages of ionization had to be used.

1. Investigation of Early Rotation Using a C II Line

In the first experiment carried out at the Culham Laboratory the early stages of rotation were investigated by measuring the Doppler shifts of the C II 4267 line using the Fabry-Perot interferometer described before. In this theta pinch experiment (see first column of Tab. I for technical data) axial streak and framing photographs showed a rotation of the plasma throughout the operating range of initial pressures, i.e. from 45 μ to 120 μ D_2. The C II 4267 line burnt out before rotation became visible on the streak photographs. Therefore, in order to make the best comparison between the angular velocity observed from Doppler shifts and that observed on streak photographs, an initial pressure was chosen such that the rotation showed up earliest. This was at a filling pressure of 60 μ D_2 when the gas broke down just before the 3rd half cycle (no pre-ionization was applied) and the plasma trapped a small amount of reverse flux.

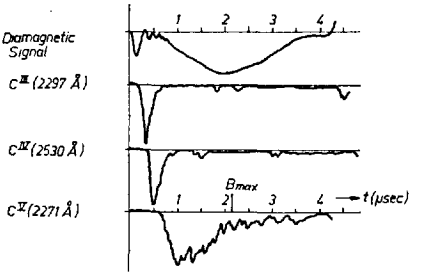


FIG. 3. Time behaviour of diamagnetic signal and intensities of C III, C IV and C V lines. Initial pressure 20 mTorr D_2. Reverse bias field $B_{ZO} = -1$ kG.

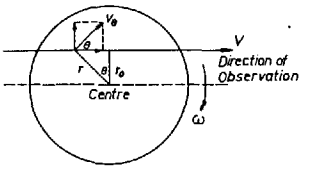


FIG. 4. Plasma rotating rigidly with angular velocity ω.

Provision was made for introducing known quantities of CH_4 impurity into the plasma via a gas mixer. It was found that 1% atomic C impurity was sufficient to give suitable signals with the C II 4267 line.

In order for the Doppler shift measurements to give unambiguous results in terms of rotational velocities all regions of the plasma have to rotate with constant angular velocity ω, i.e. the plasma has to rotate as a rigid body. In this case we have (see Fig. 4)

$$v_\theta = r\,\omega$$

$$v = r\,\omega\cos\theta = r_o\,\omega$$

i.e. at a particular chord distance r_o from the centre, all the ions of a particular species will be travelling with the same velocity v along the line of observation and the radiation is therefore subject to a constant Doppler shift.

The magnitude of this Doppler shift is given by

$$\Delta\lambda = \lambda\,\frac{v}{c} = \lambda\,\frac{r_o\,\omega}{c} \qquad (1)$$

Thus on scanning across the plasma in the direction of r_o one would expect to see a Doppler shift varying linearly with r_o and in opposite directions on either side of the centre.

Fig. 5 shows the shifts of the C II 4267 line at various distances across the plasma diameter for three points of time (t_1: during initial implosion, t_2: 1st max. compression, t_3: 2nd max. compression). The result is consistent with the interpretation that the plasma rotates as a rigid body. The direction of rotation is that of a positive ion in the driving magnetic field B_z. The angular velocities of the plasma Ω, found from the gradients of the lines through the measured shifts by resorting to eq.(1) are indicated in the diagram. Rotation is already detectable during the initial implosion. Its angular velocity is 5.3×10^4 rev/s and increases slightly with time. The rotational velocity of the

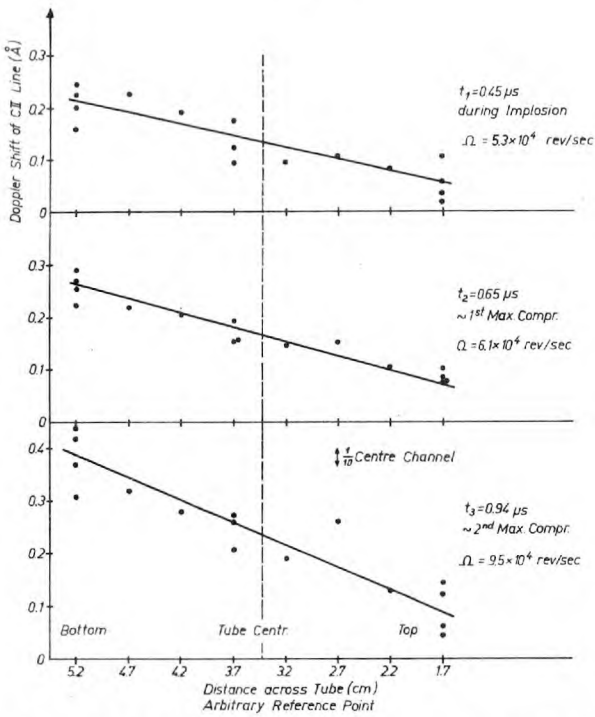


FIG. 5. Doppler shift Δλ of C II 4267 line at various distances across tube. Arbitrary reference point for Δλ and distance across tube. 60 mTorr D_2. Small reverse bias field B_{zo}.

Table I Technical data of theta pinch experiments

	Culham θ-Pinch	Garching θ-Pinch
Bank Energy (kJ)	22.5	32.5
Bank Voltage (kV)	15	36
Max. B_z Field (kG)	40 (3rd h.c.)	57 (1st h.c.)
Half Period (μsec)	7.2	4.2
Coil Length (cm)	21	30
Coil Diameter (cm)	5.5	7
Preionization	1st and 2nd half cycle of main discharge	high frequency theta pinch

m = 2 instabilities as detected from streak photographs at the earliest possible time (at 2.25 μsec) is 1.9 x 10^6 rev/s. This corresponds to an increase in angular momentum per particle by a factor 3 (taking into account the measured change in plasma diameter).

2. Investigation of Rotation over an Extended Time Scale Using a C V Line

To investigate the later stages of rotation the Doppler shift measurements were continued at Garching on the C III 2297 and, in particular, on the C V 2271 line using the profile-dividing mirror system described before. These measurements cover the time period up to 2 μsec when rotational instabilities start to show up on streak photographs.

The second column of Tab. I summarizes the technical data of the theta pinch. Initial pressure was in the range 2o - 1oo μ D_2. Usually 1 - 2% atomic C were added to give reasonable line intensities. In all experiments reported here a reverse bias field B_{zo} of 1 kG was superimposed.

Streak photographs showed that in this experiment rotational instabilities developed only at a pressure below 3o μ D_2. Thus it was possible to induce rotation and instabilities at higher pressures in an otherwise non-rotating and stable plasma by superimposing a transverse magnetic field B_{tr} and to study its influence on rotation.

2.1 Measurements without superimposed Transverse Field

These measurements were carried out at an initial pressure of 2o μ D_2. The diamagnetic signal, B_θ -signal and streak photograph in Fig. 6 show the characteristic behaviour of such a discharge. The m = 2 instabilities showing up on the streak photograph in the last third of the half cycle rotate at an angular velocity in the range 1 - 2 x 10^6 rev/s. The time variation of the B_θ -field was measured by a probe which was placed between theta pinch coil and discharge tube and oriented and balanced to maximize the $\dot{B}_\theta / B_z$ signal. The $\dot{B}_\theta$ signal shows two regions of relatively well defined oscillations, one in the first and one in the last third of the half cycle. The oscillations at the beginning correspond according to ref. [15] to the frequency of the azimuthally rotating electrons transporting B_r-fields (e.g. small stray fields) for times which are short compared with the characteristic field diffusion time. The frequency of the oscillations in the last third of the half cycle agrees with the frequency of the m = 2 instabilities as observed on streak photographs, thus indicating that the B_r-field is now distorted by the m = 2 instabilities.

Doppler shift measurements show rotation of the plasma column long before it is detectable on photographs. Fig. 7 shows two C V line profiles measured at radial distances r_o = + 4 and - 4 mm at time o.85 μsec. They show a line shift of approximately o.4 Å corresponding to a rotational velocity of 1 x 10^6 rev/s. The direction of rotation determined from such Doppler shift measurements as well as from stereoscopic side-on streak photographs is again that of the ion current.

Fig. 8 shows the time behaviour of the rotational velocity as determined from Doppler shift measurements, B_θ probe signals and streak photographs. Before discussing the results in detail two general remarks concerning these measurements should be made. First it is important to point out that the three diagnostic techniques measure three different types of rotational velocity: During the early stages of rotation the B_θ probes measure the rotational velocity of the electrons, whereas the Doppler shifts give the one of the C-ions. After instabilities have set in both the streak photographs and B_θ probes give the rotational velocity ω/m of an instability of mode m. Secondly with respect to the question as to whether the measured velocities of the C-ions are representative for the plasma as a whole, i.e. of the deuterons, it can be shown that the difference in the two velocities becomes less than 1o% of the absolute velocity of the deuterons in a characteristic time t_c which is approximately $1o(m_C/m_D - Z_C)\ t_D$, where t_D is the

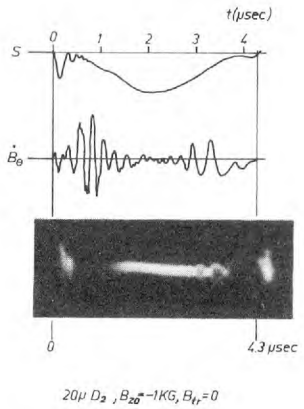


FIG. 6. Diamagnetic signal S, $\dot{B}_\theta$ probe signal and streak photograph of a discharge at 20 mTorr D_2. $B_{ZO} = -1$ kG, $B_{tr} = 0$.

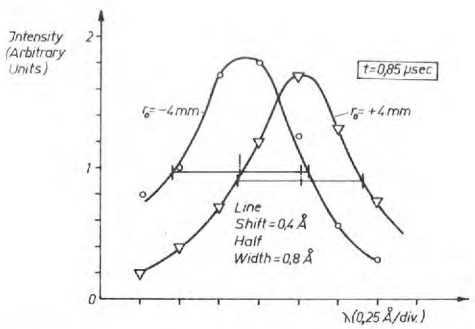


FIG. 7. Line profiles of C V 2271 line taken at two radial positions ($r_O = +4$ mm and -4 mm) across tube. 20 mTorr D_2. $B_{ZO} = -1$ kG.

"deflection time" calculated by Spitzer [16]. Since the factor $(m_C/m_D - Z_C)$ is 5 for C II and 2 for C V and t_D is of the order 10^{-8} sec for our experimental conditions, t_c is of the order 10^{-7} sec which is approximately equal to the time in which the velocity changes, i.e. the Doppler shifts give the rotational velocity of the plasma column to within 10%, which is within the experimental error.

Qualitatively the angular velocities obtained from Doppler shifts and those from $\dot{B}_\theta$ signals show a similar time dependence. The difference in the absolute values is a measure for the percentage of I_θ current carried by the ions and electrons respectively. Rotation is detectable at the second maximum compression (t = 0.5 μsec), increases to a maximum at 1.2 - 1.4 μsec and then decreases rapidly to an almost constant (usually slowly decreasing) value. The rapid decrease in angular velocity coincides with the time when the plasma contracts axially and is partly due to an increase in plasma diameter. The rotational velocity ω of the m = 2 instabilities is about a factor 3 higher than the angular velocity of the plasma. This will be discussed in part D.

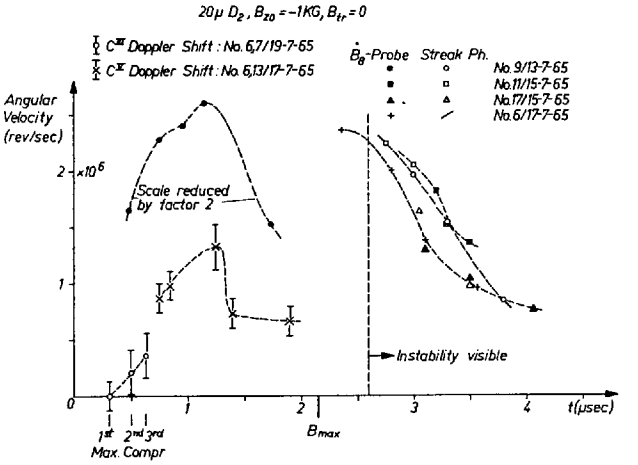


FIG. 8. Time behaviour of angular velocities as determined from Doppler shifts of C III and C V line, $\dot{B}_\theta$ probe signals and streak photographs. Note that Doppler shift measurements give the mass rotational velocity Ω, whereas the streak photographs and the $\dot{B}_\theta$ signals in the last third of the half cycle give the rotational velocity of an instability wave ω. The $\dot{B}_\theta$ signals at the beginning of the half wave give the rotational velocity of the electrons. Initial pressure 20 mTorr D_2, $B_{ZO} = -1$ kG, $B_{tr} = 0$.

2.2 Measurements with Superimposed transverse Field

A stationary magnetic field B_{tr} transverse to the axis and to the plane through axis and feed point of the thetapinch coil was superimposed by means of two coils in Helmholtz geometry. The field was homogeneous to within 1o%. Its amplitude could be varied from 0 to 1ooo G.

This transverse field changes the character of the discharges considerably. At initial pressures of 4o μ D_2 and 8o μ D_2 transverse fields of >3oo and >7oo G respectively cause rotation of an otherwise non-rotating plasma. Fig. 9 shows that with increasing amplitude of the transverse field the onset time for the m = 2 instabilities is reduced, the plasma diameter decreases and the frequency of the first detectable m = 2 instability increases linearly as shown in Fig. 1o. End losses and irreproducible plasma drift are greatly enhanced under these conditions, the trapped reverse flux already dissipates during the early stages of the discharge and no axial contraction can be observed.

The Doppler shifts of the C V line at various distances across the tube (Fig. 11) seem to indicate that in discharges with transverse field the plasma region emitting the C V line also rotates rigidly before instabilities set in. Fig. 12 shows the time behaviour of the angular velocity for a discharge at 4o μ D_2 with a superimposed transverse field of 56o G. In contrast to the "naturally" rotating plasma at 2o μ D_2 rotation becomes detectable later (at ~ 1 μsec) and is then in "opposite" direction, i.e. in the direction of the electron current. On the other hand the m = 2 instabilities which start to show up on streak photographs at ~1.6 μsec rotate in the direction of the ion current. This might indicate that the plasma does not rotate rigidly at later times, but that rather the inner region of the plasma, which emits the C V line, rotates with different velocity compared to the plasma surface from which the instabilities develop. It must also be considered that the accuracy of the Doppler shift measurements is greatly reduced under these conditions due

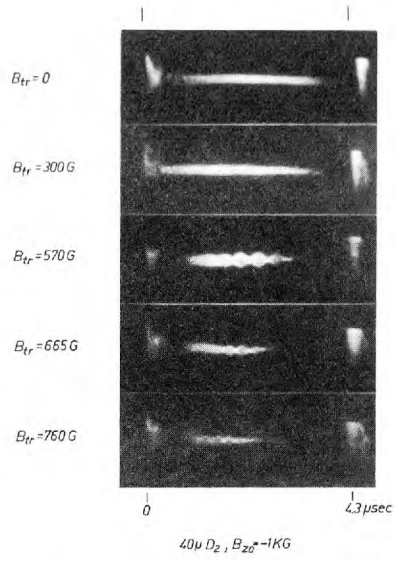


FIG. 9. Streak photographs of discharges at 40 mTorr D_2 showing the influence of a superimposed transverse field B_{tr} on the rotation. B_{ZO} = - 1 kG.

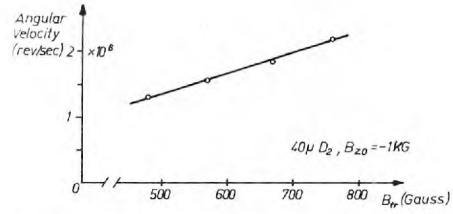


FIG. 10. Angular velocity as determined from streak photographs as a function of superimposed transverse field B_{tl}. Initial pressure 40 mTorr D_2, B_{ZO} = - 1 kG.

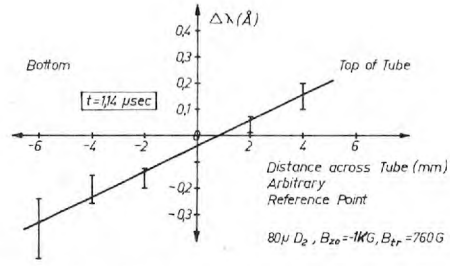


FIG. 11. Doppler shift of C V 2271 line at various distances across tube. 80 mTorr, B_{ZO} = - 1 kG, B_{tr} = 760 G.

to irreproducible plasma drift. "Induced" rotation at 80 μ D_2 shows qualitatively the same behaviour, especially it also starts in "opposite" direction.

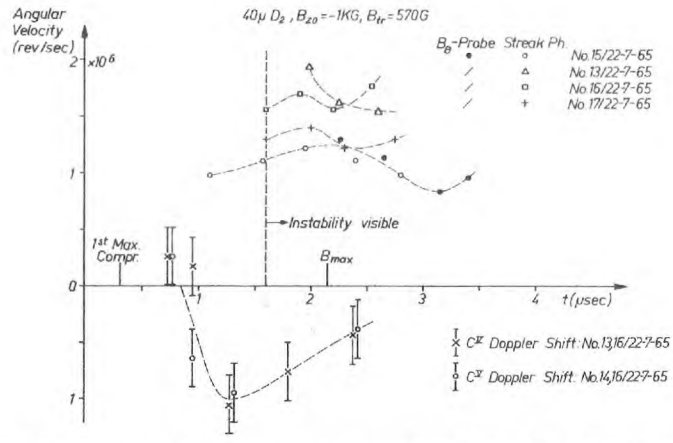


FIG. 12. Time behaviour of angular velocities as determined from Doppler shifts of C V 2271 line, $\dot{B}_\theta$ probe signals and streak photographs for discharges with a superimposed transverse field of 570 G. See note at Fig. 8 for explanation of results. Initial pressure 40 mTorr D_2, $B_{ZO} = -1$ kG.

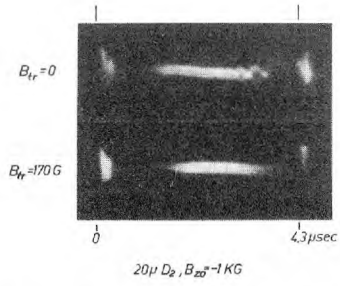


FIG. 13. Streak photographs of two discharges at 20 mTorr D_2 showing that rotational instabilities can be suppressed by superposition of a transverse field B_{tr}. $B_{ZO} = -1$ kG.

The fact that "induced" rotation starts in "opposite" direction should be viewed in conjunction with another experimental result which is shown in Fig. 13. In discharges where the plasma rotates "naturally", i.e. where no superimposed transverse field is needed for rotation (e.g. at 20 μ D_2), this rotation can be reduced by a superimposed transverse field of the same polarity that causes "opposite" rotation for a usually non-rotating plasma. If the magnitude of this field is properly chosen (e.g. 170 ± 10 G) at 20 μ D_2), rotational instabilities can be suppressed.

D. Discussion of the Results

For a comparison of the experimental results with the predictions of various theories on plasma rotation the following experimental findings seem to be important:

a) The tendency of the plasma to rotate increases with temperature, i.e. it is higher at low initial pressure and with low impurity concentration. In our experiments rotation occurred only if a reverse B_z field was initially trapped in the plasma.

b) Rotation, if present, is already detectable during the very early stages of the discharge (an angular velocity of 5 x 10^4 rev/s

was measured during the initial implosion) and reaches its maximum angular velocity (approximately 1 x 10^6 rev/s) after 1 - 1.5 μs.

c) In the early stages of the discharge, i.e. before instabilities set in, the plasma seems to rotate as a rigid body.

d) By superimposing a stationary transverse field rotation can be imposed on an otherwise non-rotation plasma. The angular velocity increases linearly with the magnitude of this transverse field, while the onset time of the instabilities is reduced.

e) The direction of rotation without superimposed transverse field is that of an ion in the driving B_z field. With superimposed B_{tr} field rotation starts in "opposite" direction but instabilities which show up later on photographs still rotate in the direction of the ion current.

f) The tendency of the plasma to rotate and become unstable can be reduced by a superimposed transverse field of the same polarity which causes "opposite" rotation for a usually non-rotating plasma. If the magnitude of the field is properly chosen rotational instabilities can be suppressed.

Various theoretical models have been postulated to explain the origin of rotation, i.e. how the plasma acquires its angular momentum. An excellent review of these theories was recently given by Haines [17] . One can distinguish between three basic models, according to where the mechanical reaction is transferred:

a) Reaction on the wall of the discharge tube, either by radial currents circulating between the plasma and conducting walls thereby shorting out the radial electric sheath field [8,9] (in the following refered to as model A) or by collisions during the initial stage of contact between plasma and wall [17] (model A').

b) Reaction on external conductors which generate magnetic fields with azimuthally varying B_r-components via magnetic stress [10] (model B). In this case, angular momentum is generated in the plasma by the interaction of the B_r field with the plasma I_θ current to produce axial Hall currents I_z which in turn react with the B_r field to give a force $I_z \cdot B_r$, proportional to B_r^2, in the azimuthal direction.

c) Separation of the plasma either radially [12] (model C) or axially [11] (model C') into two or more parts which rotate in opposite direction.

As far as our experiments are concerned model C' can be excluded, since end-on streak photographs show the plasma to rotate uniformly along its length. The fact that Doppler shift measurements show the plasma at least during early stages to rotate as a rigid body does not rule out model C since radiation from a particular stage of ionization is emitted by a particular plasma region, but makes it appear unlikely.

Since model A and B yield roughly the same range of predicted terminal angular velocities (10^6 - 10^7 rev/s) and acceleration times (1 - 10 μsec) it cannot yet be decided on the basis of our experimental results which mechanism plays the dominant part. But our experimental results on the influence of superimposed transverse fields and earlier results of Kolb [6,15] on the influence of Joffe bars show that the model involving B_r fields, which to some extent are always present in a theta pinch, describes at least one of the effects that cause rotation. Therefore we are now going to estimate the acceleration time and maximum angular velocity predicted by this model.

Under various simplifying assumptions (constant external magnetic field, incompressibility of the plasma a.o.) Thoneman and Kolb [18] derive the following expression for the rotational velocity for times $t \ll T_d$:

$$(2) \qquad v_\theta \approx v_o \left(\frac{T_v}{T_A}\right)^2 \cdot \frac{1}{T_D} \left(T_d + t\right)$$

with $v_o = I_{\theta o}/ne \equiv$ drift velocity of electrons at time $t = o$, $T_v \equiv$ drift time of electrons around the plasma column, $T_A \equiv$ transit-time of Alfven-wave through B_r-field, $T_D \equiv$ resistive decay time of the I_θ current.

In a time of the order T_v the rotational velocity jumps to a finite value

$$(v_\theta)_{T_v} \approx v_o \left(\frac{T_v}{T_A}\right)^2$$

and increases to twice that value within time T_D. Numerical calculations [18] for conditions which were rather similar to ours show that the rotational velocity reaches its maximum value $(v_\theta)_{max}$ of approximately 10 times $(v_\theta)_{T_v}$ after about $2 \cdot T_D$ and then decays exponentially due to field diffusion.

For the conditions of the Garching theta pinch $V_\theta \approx 1.4 \times 10^7$ cm/s $T_v \approx 6 \times 10^{-8}$ sec, $T_A \approx 7 \times 10^{-7}$ sec and $T_D \approx 2.5 \times 10^{-6}$ sec and we find that a maximum velocity of 1×10^6 cm/s should be reached within about 5 μsec. The maximum velocity agrees very well with our experimental result whereas the predicted time scale is too slow by about a factor 4.

Finally the stability of the plasma shall be considered using the theoretical condition for stability against an m = 2 instability which is the fastest growing mode [17]

$$-0.4 < \frac{2\Omega}{W_i} < 2.4$$

where Ω is the angular velocity of the plasma and W_i the angular velocity associated with the ion diamagnetic current. Since the angular velocity ω of an m = 2 instability wave is given by [17]

$$-\mathcal{R}\,\omega = \Omega - \frac{W_i}{2}$$

W_i can be estimated from the measured rotational velocities Ω and ω at later times when the instabilities show up on photographs. On the other hand it follows from the definition of $W_i = \frac{1}{\varrho r} \cdot \frac{\partial}{\partial r}\left(\frac{P_{i\perp}}{\Omega_i}\right)$ that it is negative in sign if $\partial B_z/\partial r > 0$ and $\partial P_{i\perp}/\partial r < 0$, which are likely conditions ($P_{i\perp}$ is the transverse ion pressure). This shows qualitatively that the "naturally" rotating plasma, where Ω is in the direction of ion motion, i.e. negative, is less liable to instability than the plasma where rotation is "induced" and starts in the direction of electron motion. A crude estimate shows that for our experimental conditions W_i is approximately 10^6 rev/s which means that the "naturally" rotating plasma should be stable until it reaches approximately that velocity.

Acknowledgments

The authors are indebted to Dr.H.A.B. Bodin and Dr. G.B.F. Niblett and to Prof. E. Fünfer and Prof. A. Schlüter for their interest and support during the course of these experiments and to Dr. M.G. Haines and D. Düchs for many valuable discussions.

References

[1] Rostocker, N., and Kolb, A.C., Phys. Rev. 124 (1961) 965

[2] Little, E.M. et al., Nucl. Fusion, Suppl 2 (1962) 497

[3] Bodin, H.A.B. et al., Nucl. Fusion, Suppl. 2 (1962) 521

[4] Bodin, H.A.B., and Newton, A.A., Phys. Fluids 6, 9 (1963) 1338
[5] Kvartskhava, I.F., et al.,Nucl. Fusion 3 (1963) 285
[6] Hintz, E., and Kolb, A.C., Phys. Fluids 8, 7 (1965) 1347
[7] Rosenbluth, M.N. et al., Nucl. Fusion, Suppl 1 (1962) 143
[8] Roberts, K.V. discussed in Ref. [3]
[9] Taylor, J.B., J.nucl.Energy C, 4, (1962) 401
[10] Haines, M.G., Phys. Letters 6 (1963) 313
[11] Bostick, W.H. and Wells, D.R., Phys. Fluids 6 (1963) 1325
[12] Velikhov, E.P., J.nucl. Energy, C, 6 (1964) 203
[13] Tolansky, W., "High Resolution Spectroscopy", Methuen and Co., London (1947)
[14] Bernstein, M.J., Appl. Optics, (to be published)
[15] Kolb. A.C. et al., Phys. Fluids 8, 5 (1965) 1005
[16] Spitzer, L., "Physics of Fully Ionized Gases", Interscience Publ. Inc., New York (1965)
[17] Haines, M.G., Advances in Physics 14 (1965) 167
[18] Thoneman, P.C., and Kolb. A.C. Phys. Fluids 7 (1964) 1455

This work was performed as part of the joint research program of the Institut für Plasmaphysik GmbH, Garching and Euratom.

DISCUSSION

A. C. KOLB: According to your paper, you have repeated some of our theta-pinch experiments with a steady transverse field. There seem to be certain fundamental differences, however. For example, we found that the tendency to rotate was greater with decreasing electron temperature (which could be varied by adding impurities). Could you comment on this?

M. KEILHACKER: We have indeed found that the tendency for the plasma to rotate is higher at lower pressures and with small impurity concentrations, that is with higher electron temperatures. This result is in agreement with theory, according to which the acceleration time decreases with increasing electric conductivity.

A. C. KOLB: Could you discuss the difference between probe signals with and without a superimposed steady transverse field?

M. KEILHACKER: Within the limits of reproducibility the $\dot{B}_\theta$ signals are similar in discharges with and without a superimposed transverse field.

A. C. KOLB: Finally, is there any relation at all between the $\dot{B}_\theta$ frequency and the hydromagnetic oscillation frequency during the early phases of the discharge?

M. KEILHACKER: During the dynamic phase of the discharge the two frequencies are close together and the periodic structure of the signals cannot be correlated unambiguously with the rotation of the electrons. Therefore, we started the evaluation of the signals at a time when the amplitude of the hydrodynamic oscillations was very small (as can be seen from the diamagnetic signal in Fig. 6).

E. HINTZ: What do you think of the possibility that the angular momentum of the plasma (in the direction of the electron current) in the case of the superimposed transverse field may be acquired during the preheating discharge?

M. KEILHACKER: This cannot be ruled out on the basis of our measurements so far. But there are other explanations for the rotation in the direction of the electron current in discharges with superimposed transverse field that in our opinion are more likely. For example, gain of angular momentum by collisions between plasma particles and the wall of the discharge vessel during the initial stage of the discharge, which according to a private communication of M. G. Haines can be in the direction of the electron current. Another explanation may be given by model C mentioned in our paper; radial separation of the plasma column into two or more parts which rotate in opposite directions.

THE STARK WIDTHS OF SINGLY IONISED ARGON LINES EMITTED BY A PLASMA

D. E. ROBERTS
Physics Department, Imperial College, London

Received 19 July 1966

The Stark broadened widths of some lines emitted by A II have been measured. These widths were more than a factor of two larger than the theoretical widths of Griem. A computer programme, written to recalculate the widths, partially accounts for the discrepancies.

Profiles of A II lines emitted by a plasma have been studied at Imperial College. The widths of these lines were more than a factor of two larger than the theoretically calculated widths of Griem [1]. Similar discrepancies have been found independantly by Oertel et al. [2]. The results for the one line measured in common (4806Å), agree within experimental error. Such discrepancies are in direct contrast with the good [$\lesssim$ 20%] experimental agreement with the Stark broadening theory as applied to isolated lines emitted by A I, Cs I, O I, N I, [1] and N II [3].

The results on A II transitions at Imperial College were obtained using a critically damped Z-pinch as a plasma source.

In these measurements the independent determination of electron density, N_e, was made using a helium-neon laser, operated at 6328 Å, side on to the plasma column so that the latter was in a Fabry-Pérot cavity. A scan across the plasma and subsequent Abel inversion enabled the radial distribution of N_e to be obtained.

The electron temperature was determined from the ratio of the total intensities of the A III line 3344.7 Å and the A II line at 3350.9 Å, viewed side on to the plasma.

The Stark broadened line profiles were obtained with a scanning Fabry-Pérot interferometer [4] again viewing the plasma side on.

The experimentally measured widths of some A II lines, together with Griem's calculated values, are shown in table 1.

In view of such large discrepancies a computer programme was written to see whether these could be accounted for within the structure of modern Stark broadening theory. The electron impact broadened widths of the upper states of lines of A II were calculated following the basic prescription of Griem [1], but allowing the inclusion of up to 50 perturbing levels. In all cases the widths obtained were larger than those of Griem (table 1). The reasons for this are twofold.

Firstly, Griem used the tables of Moore [5] to obtain the perturbing energy levels. The use, in this program, of the energy levels given by Minnhagen [6] provides, in some cases, perturbing levels to the upper state of the line which were not given by Moore.

Secondly, Griem used only five perturbing levels in most of his calculations (private communication).

Table 1
Experimental and theoretical line $\frac{1}{2}$-$\frac{1}{2}$ widths, ω, for some A II lines
(Widths in Å units). $N_e = (4.4 \pm 0.4) \times 10^{17}/cm^3$, $T_e = 31\,000^oK \times 1\,500^oK$

λ (Å)	Transition	ω exp.	ω* theor. Griem	ω* theor. Roberts	ω* with mixed L–S wavefunctions	strong collision contribution to ω (%)	ω* theoretical (lower level)
4806	$4s^4P_{2\frac{1}{2}}$-$4p^4P^0_{2\frac{1}{2}}$	0.89 ± 0.13	0.36 ± 0.04	0.47 ± 0.05	0.47 ± 0.05	48	0.33 ± 0.03
5062	$4s^4P_{\frac{1}{2}}$ -$4p^4P^0_{1\frac{1}{2}}$	0.97 ± 0.10	0.40 ± 0.04	0.60 ± 0.06	0.61 ± 0.06	48	0.35 ± 0.04
4880	$4s^2P_{1\frac{1}{2}}$-$4p^2D^0_{2\frac{1}{2}}$	1.08 ± 0.15	0.34 ± 0.03	0.92 ± 0.09	0.87 ± 0.09	41	0.38 ± 0.04
4266	$4s^4P_{2\frac{1}{2}}$-$4p^4D^0_{2\frac{1}{2}}$	0.74 ± 0.10	0.20 ± 0.02	0.42 ± 0.04	0.47 ± 0.05	60	0.28 ± 0.03
3351	$4p^2F^0_{2\frac{1}{2}}$-$4d^2F_{2\frac{1}{2}}$	1.30 ± 0.09		1.41 ± 0.14		36	0.51 ± 0.05

* Quoted errors due to uncertainties in Ne and Te.

Table 2
Experimental and theoretical total line widths, 2ω, for some N II lines
(Widths in Å units)

λ (Å)	Transition	2ω exp. (day)	2ω Theor. (Griem)	2ω Theor. (Roberts)	Strong collision contribution to ω (%)
5495	$3p^3D$ -$3d^3P^0$	1.2 ± 0.15	1.09	1.89	53
5045	$3s^3P^0$-$3p^3S$	1.0 ± 0.15	0.85	1.00	57
4614	$3s^3P^0$-$3p^3P$	0.9 ± 0.15	0.81	1.04	66
3006	$3p^1P$-$4s^1P^0$	1.65 ± 0.15	1.69	1.69	54
3838	$3p^3P$-$4s^3P^0$	1.9 ± 0.2	1.68	1.95	64

Often considerably more are required for convergence of the width to near its asymptotic value. (e.g. 15 for 4880 Å). The use of distant perturbing levels, however, throws considerable doubt on the validity of the "no back reaction" and "classical path" approximations made in the theory [1].

It is also seen in table 1 that the percentage width due to strong collisions is large. This importance of strong collisions is confirmed by the use of the larger strong cut-off used for He I [7]. The strong collision contribution to the width is increased by about 50% but the weak collision contribution reduced, keeping the total width approximately the same.

This indicates that much of the contribution from weak collisions in fact comes from the regime where ρ, the electron perturber impact parameter, is not much larger than ρ_{min}, the strong collision cut-off parameter.

Thus the assumption in the theory that strong and weak collisions rarely overlap in time is suspect, and the weak collision contribution is therefore probably overestimated [1].

The large size of the strong collision contribution to the width was also found in the case of N II lines (table 2).

If anything the present calculations for N II yielded, with one exception, even better agreement with experimental results [3] than obtained by Griem (see table 2). Since this indicates that the Lorentz-Weisskopf treatment of strong collisions, through crude, may be sufficient, two other sets of calculations were performed in the case of A II.

To account for the partial breakdown of L-S coupling in A II each upper state wavefunction was taken as a linear sum of L-S coupled wavefunctions. The coefficients in the sum were obtained from Statz et al. [8]. The line widths recalculated on this basis were not altered by, typically, more than 15% (table 1).

Separate calculation of the width of the lower state of each line shows that in many cases for

Ar II this is not negligible compared with the width of the upper state (table 1). However, incoherent addition of the widths of the upper and lower states of a line is liable to give a gross overestimation of the resultant widths. Nevertheless the assumption that lower state broadening is negligible [1] would see m to be suspect.

The calculations described bring the theoretical widths of Griem more into agreement with experiment. However serious doubt has been thrown on many of the assumptions made in the theory. This can be expected to be true of all heavy element emitters.

Further results, including coherent addition of the lower state width, are to be published.

I should like to thank Dr. R. Latham who supervised this work and Dr. D. D. Burgess for much helpful discussion.

1. H. R. Griem, Plasma spectroscopy (McGraw-Hill Book Company, New York).
2. N. W. Jalufka and G. K. Oertel, Paper AA-11 (1965), Division of Plasma Physics of American Physical Society Conf. San Francisco.
3. R. A. Day and H. R. Griem, Phys. Rev. 140 (1965) A1129.
4. J. Cooper and J. R. Grieg, J. Sci. Inst. 40 (1963) 433.
5. C. Moore, N. B. S. circular number 467 (US Goverment Printing Office, Washington, 1949, 1958).
6. L. Minnhagen, Arkiv Fysik 25 (1963) 19.
7. H. R. Griem, M. Baranger, A. C. Kolb and G. Oertel, Phys. Rev. 125 (1962) 177.
8. Statz et al., J. Appl. Phys. 36 (1965) 2278.

* * * * *